UNIVERSITY OF NOTTINGHAM

DEPARTMENT OF CIVIL ENGINEERING

A theoretical analysis of welded steel joints in rectangular hollow sections

by

Jeffrey Alan Packer, B.E., M.Sc.

Thesis submitted to the University of Nottingham for the degree of Doctor of Philosophy.

CONTENTS

ABSTRACT

In this thesis a theoretical analysis is presented for statically loaded structural hollow section (SHS) lattice girder joints having one compression bracing member and one tension bracing member welded to a rectangular hollow section chord member. A set of joint failure modes are established for gapped and overlapped bracings and the research is aimed towards establishing the yield and ultimate loads of such joints with the yield line method as the main analytical tool. The results of 150 joint tests, conducted both in isolation and in complete trusses at testing centres in three different countries, have been used to verify the theories proposed.

A study of the parameters which are believed to influence the strength and behaviour of rectangular hollow section joints has also been made. Finally, a computer program has been written in Fortran to provide an automatic assessment of the strength of welded lattice girder joints having a rectangular hollow section chord member and either rectangular or circular bracing members.

ACKNOWLEDGEMENTS

The author is most grateful for the considerable advice and encouragement given to him by Dr. G. Davies and Dr. M.G. Coutie under whose supervision this research work has been carried out, and for the support of the Head of Department, Professor R.C. Coates.

This research project has been sponsored by the British Steel Corporation Tubes Division, Corby, Northamptonshire, and the Comité International pour le Developpement et l'Etude de la Construction Tubulaire (CIDECT), who have both provided considerable financial support and technical information. Particular thanks are extended to Mr. T. Giddings and Dr. A.S. Haleem of the B.S.C. Tubes Division Research Centre, Mr. J. Wardenier of Delft University of Technology, Netherlands and Mr. W. Rose, CIDECT Technical Secretary, for their continual assistance and liaison.

Finally the author wishes to thank Miss A. Griffin and Miss J. Clerbaut for their careful and skilful typing of this thesis.

LIST OF FIGURES

LIST OF TABLES

NOTATION

A_i	=	Sectional area of member
b_i	=	width of member (90^o to plane of truss)
b_i'	=	$b_i - t_i$
CHS	=	Circular Hollow Section
CIDECT	=	Comité International pour le Developpement et l'Etude de la Construction Tubulaire
d_i	=	diameter of member
e	=	eccentricity - positive being towards the outside of the girder when related to joint noding.
E	=	Modulus of elasticity
E_{sh}	=	Strain - hardening modulus
F	=	axial load in chord at a joint in addition to the horizontal reaction from bracings. (i.e. force in chord on the compression bracing side of the joint). Positive F represents tension.
Fp	=	squash load of chord
F_{purl}	=	compressive purlin load acting normal to the chord
g*	=	nominal gap between bracing members on the chord face
g	=	actual gap between bracing members on the chord face
g'	=	actual gap between bracing members on the chord face divided by b_o'
h_i	=	depth of member (in plane of truss)
h_i'	=	$h_i - t_i$
H	=	length of the strut member measured along its centre line from the chord face. In the case of a truss the length is half the centre-line distance between the inside faces of the two chord members.
mp_i	=	plastic moment of resistance per unit length
mp_i'	=	reduced plastic moment of resistance per unit length due to axial load

Mp_i = plastic moment capacity

Mp_i' = reduced plastic moment capacity due to axial load

N, Np = axial load in strut and squash load of strut respectively.

N_{ult} = ultimate joint load measured as a force in the strut

N_y = joint yield load measured as a force in the strut.

P = $N\sin\theta_1$

q = amount of overlap

RHS = Rectangular Hollow Section

S,Sp = membrane force in joint crotch, and yield load of membrane

T = axial load in tension bracing member

t_i = thickness of member

t_p = length of bearing of purlin

t_s = thickness of stiffening plate

w = maximum deflection of buckle dimple

Z_i = elastic modulus of member

δ = deflection

ε_{yi} = yield strain of member

θ_i = angle between bracing member and chord

λ_i = b_i/b_o or d_i/b_o

λ_i' = $(b_i + 2 \times \text{Weld leg length})/b_o'$

λ_{av} = $(\lambda_1 + \lambda_2)/2$

ν = poissons ratio

σ_{crit} = critical elastic buckling stress

σ_i = stress in member

σd_i = limit state design strength of a member

σe_i = yield stress of a member

The subscripts i = 0, 1, 2 refer to the chord, strut and tie respectively.

CHAPTER 1

INTRODUCTION

Since the first structural hollow sections (SHS) were produced by Stewarts and Lloyds, (now a part of the British Steel Corporation), in 1952, their popularity has increased considerably worldwide, largely due to the increased publicity and knowledge about their structural behaviour and design, until at present, for example, tubular steel products account for 28% of total steel production in Japan.[19]

A popular application of structural hollow sections is in lattice trusses or girders for reasons of pleasing aesthetics, structural efficiency and also economy. Tubes are often much stronger than open section members of the same weight, but the economic advantage gained from this may be offset by the connection costs which can be high. The cost of joint fabrication is minimized if the number of joints is minimal and so initial economy in tubular trusses can be achieved by designing as a Warren truss rather than a Pratt or 'N' truss. Furthermore, to avoid profile-shaping circular hollow section (CHS) members, which is a facility restricted to only some fabricators, rectangular hollow sections (RHS) which only require straight cutting can be chosen. RHS joints are thus simpler to fabricate which offsets the disadvantage of RHS tube being generally more expensive than CHS tube.

Most research on welded tubular joints has been confined to circular tubes[73], and until recently little test evidence has been available for joints made of RHS.[68] The aim of the research described in this thesis has been to further the study and understanding of hot-rolled RHS joints which are used in two dimensional lattice girders and which are predominantly statically loaded. The types of joint configurations which could be encountered in such girders are shown in fig. 1.1, but this study is limited to joints having one compression bracing member and one tension bracing member only, such as joint k (without purlin or applied load) or joint ℓ (with purlin or applied load) in fig. 1.1. The bracing members of such joints can have any angle of inclination to the chord member and can be overlapped, (also referred to as lapped), or gapped at the connection to the chord face.

Bracing members may be either fillet or butt welded to the chord member with typical weld details shown in fig. 1.2 for RHS chord joints.[11, 14, 15, 63 and 71] Fillet welding is more common than butt welding and has been used for all the test joints listed in Appendix 1. In the few cases where butt welds were made they were overlaid by fillet welds.

General Terminology

(i) Overlap

Overlap joints, formed when the bracing members of a truss or isolated joint intersect, necessitate the double shaping of either one or both of the bracing members as shown in fig. 1.3. When bracing members of lapped joints are of the same width and thickness, it has been suggested that either bracing member be double-shaped[11], although it is probably more common to double mitre the strut (fig. 1.3(b)) in this case because of the belief that the tie is restrained better if connected directly to the chord face. Stelco[63] however recommends that both bracing members be double-shaped at the intersection (fig. 1.3(c)).

If the widths of the bracing members vary considerably it is better to double cut the smaller branch member, regardless of whether it is the strut or tie, but if the widths of the bracing members are the same yet they have substantially different thicknesses it is more common to weld the thicker web member directly on to the chord. This recommendation is borne out in the recent German draft standard.[46] For Warren girders with bracing members of the same outside dimensions this will probably mean welding the compression bracing member directly on to the chord face. No significant difference in behaviour has been detected[9, 10] between overlap joints which have the compression member double mitred and those with the tension member double mitred.

Authors in different countries have used different methods for defining the amount of overlap at a joint. With regard to fig. 1.4 the British percentage overlap is expressed as (CD/AC) x 100.[33] In France and Canada the lap tends to be expressed by the length DC[63], whereas the Dutch employ the definition (CD/AB) x 100%.[71] The German definition[45] coincides with the British, and as this is the recommended CIDECT definition too[60], it is this expression for lap which is adopted for this thesis. It has been generally agreed[17] that it is not necessary to weld the hidden bracing member toe in a lapped joint (e.g. if the tension bracing member was double shaped in fig. 1.4 then point c is the hidden toe). Generally the toe would be tack welded in position only whilst the joint or truss was being fabricated, and this was the procedure for all joints listed in Appendix 1.

(ii) Eccentricity

For simplicity of design, members are usually arranged so that all centre-lines are noding but if a specific gap or lap of the bracing members is preferred then a moment on the joint is likely to be produced by the noding eccentricity. If the eccentricity from the chord centre-line towards the outside of the truss or girder is termed positive, then gapped joints will generally have a positive noding eccentricity and lapped joints will generally have a negative noding eccentricity (see fig. 1.4(a)).

Research at Sheffield University[31, 32] has indicated that moments produced by noding eccentricities do not significantly affect the joint strength, although they can affect the strength of the chord member on either side of the joint, as the chord member may be assumed to resist all of this moment. Since the chord member is usually continuous through the joint, it is permissible then to divide the moment equally between the chord member on either side of the joint, provided that the chord stiffness on one side of the joint is less than, or equal to, 1.5 times the chord stiffness on the other side. In cases where this ratio is exceeded, the secondary bending moment should be divided in proportion to the stiffness on either side of the joint (i.e. the moment of inertia of the chord divided by its length).[31, 32]

For the theoretical analysis of joint strength in this thesis, the secondary moments produced by noding eccentricity are treated in this manner and are assumed to only cause an increase or decrease in the maximum stresses in the chord on either side of the joint. The joint eccentricity, however, is dependent upon the member sizes, bracing member angles and the amount of lap or gap on the chord face, and as these parameters have been found to affect the joint behaviour and strength, the noding eccentricity indirectly also becomes a parameter for the behaviour of a joint.

(iii) Gap

For joints which have a gap between the bracing members on the chord face, the nominal gap (g^*) as shown in fig. 1.5 is reduced to a smaller actual weld gap (g) because of the fillet welds around the bracing members. If either bracing angle θ_i is less than or equal to 60^o then the fillet weld, for the research in this thesis, is taken to be included in the intersection length of the bracing member at the toe adjoining the gap, (see detail C fig. 1.2), as this was the nature of the welding on RHS gap joints at Corby.[9] The relative gap (g') is then defined by the actual weld gap (AB in fig. 1.5) divided by b_o', the distance between the centres of the chord walls.

Typical load-deflection characteristics for welded tubular joints are shown in fig. 1.6. After an initial elastic deformation the joint reaches a yield load provided local buckling does not occur during the elastic load range (curve d). At this yield load the joint may deform at almost constant load (curve b), show an increase in load capacity with increasing deformations (curve a) or show a reduction in load capacity with increasing deformations (curve c). The ultimate load of the joint is then defined by the maximum load which the joint achieved. A recent trend in European structural design philosophy has been to interpret structural behaviour in terms of limit state solutions and so the yield load and ultimate load of a joint are important factors for assessing the strength of a tubular joint.

In this thesis the theoretical analysis has been directed towards a means of calculating the yield and ultimate strengths of welded tubular joints between RHS members. The analytical tool used for the study was the yield line method which Johansen[40] originally developed for reinforced concrete slabs. Calladine[13], although pointing out that reinforced concrete slabs differed from metal plates only in their respective yield loci, found Johansen's yield line theory suitable for metal plates and others such as Wood[79] have found good agreement with test results. The yield line theory uses a mechanism or geometry approach in which the energy balance is calculated and this produces a collapse load without considering the equilibrium equations at all. This collapse load, although an upper bound solution and hence always 'unsafe', usually gives a 'close' bound and consequently the upper bound method has been widely used in practice in preference to complex lower bound methods because the latter are generally not only safe but over-conservative.[13]

In this thesis the yield line theory, valid for small deflections which are necessary to form a mechanism, is extended to joints in the large deflection range. The post-yield load-deflection behaviour of curve a in fig. 1.6, which also corresponds to the large deflection behaviour of a transversely loaded plate[13], can be obtained by introducing membrane action, whereas the behaviour of a joint which deforms according to curve c in fig. 1.6 can be studied by monitoring the unloading of the joint with increasing deflections. Curves a and c on fig. 1.6 are the most common modes of deformation for gapped and overlapped joints respectively.

Apart from strain hardening due to tensile membrane action in gapped joints, the joint material is considered to be rigid-perfectly plastic and residual stresses are ignored as these will have no effect on the attainment of a plastic collapse mechanism.[13] Some residual stresses will be present in tubes due to the hot forming operation and considerable residual stresses will be introduced by the welding of the joint. Residual stresses receive further consideration in Chapter 5 part 2 because of their influence upon the stiffness and buckling load of a compression member.

Yield line theory was first applied to tubular joints by Jubb and Redwood[42] who investigated the yield loads of T joints between RHS members, then by Davies and Roper[23, 24, 59] for Pratt truss (N) gapped joints and by Mouty[51] for Warren joints. All of these investigations were concerned with the transverse loading of a plate, (the connecting face of the chord member), by bracing members whose width was less than that of the chord member and reasonable agreement with the joint yield loads was obtained.

Jubb and Redwood used yield line fans around the extreme corners of the yield pattern as did Davies and Roper, but the latter showed that straight yield lines give only a very slightly higher yield load than patterns with yield line fans[23], over the practical range of joint sizes. Hence rectilinear yield line patterns have been chosen by the author and these have the additional advantage of being more easily adapted to calculations involving large changes in geometry. The yield lines are assumed to be located at the centres of tube walls and where bracing members are fillet welded to the chord member the yield hinge is taken to occur at the edge of the connecting weld as shown in fig. 1.7, which Mouty[51] had also done.

Rectangular hollow section members, which actually have small corner radii, have been simplified to rectangles as shown in fig. 1.7 and the sides of an RHS member are then considered as connected plates. As these plates are relatively thin, when they are subjected to transverse loading the load is resisted mainly by bending stresses and the shearing or compressive stresses are small.[13]

As the dominant mode of failure is likely to be different for a joint when the bracings are overlapped rather than gapped, the theoretical analysis of gap joint failure modes is treated in Chapters 3 and 4 whereas the theoretical analysis of lap joint failure modes is covered by Chapter 5. The behaviour of both joint types when an applied load acts on the connection, or with variation in one or more of the recognised joint strength parameters, is discussed in Chapters 6 and 7. Although the research presented in this thesis is entirely theoretical, extensive comparison has been made with experimental work conducted in England[9], Italy[10] and the Netherlands[28, 71] on both isolated and truss joints. A total of 110 RHS to RHS joints have been consulted along with 40 CHS to RHS joints for use in Chapter 7 part 8. The data for all these tests is given in Appendix 1.

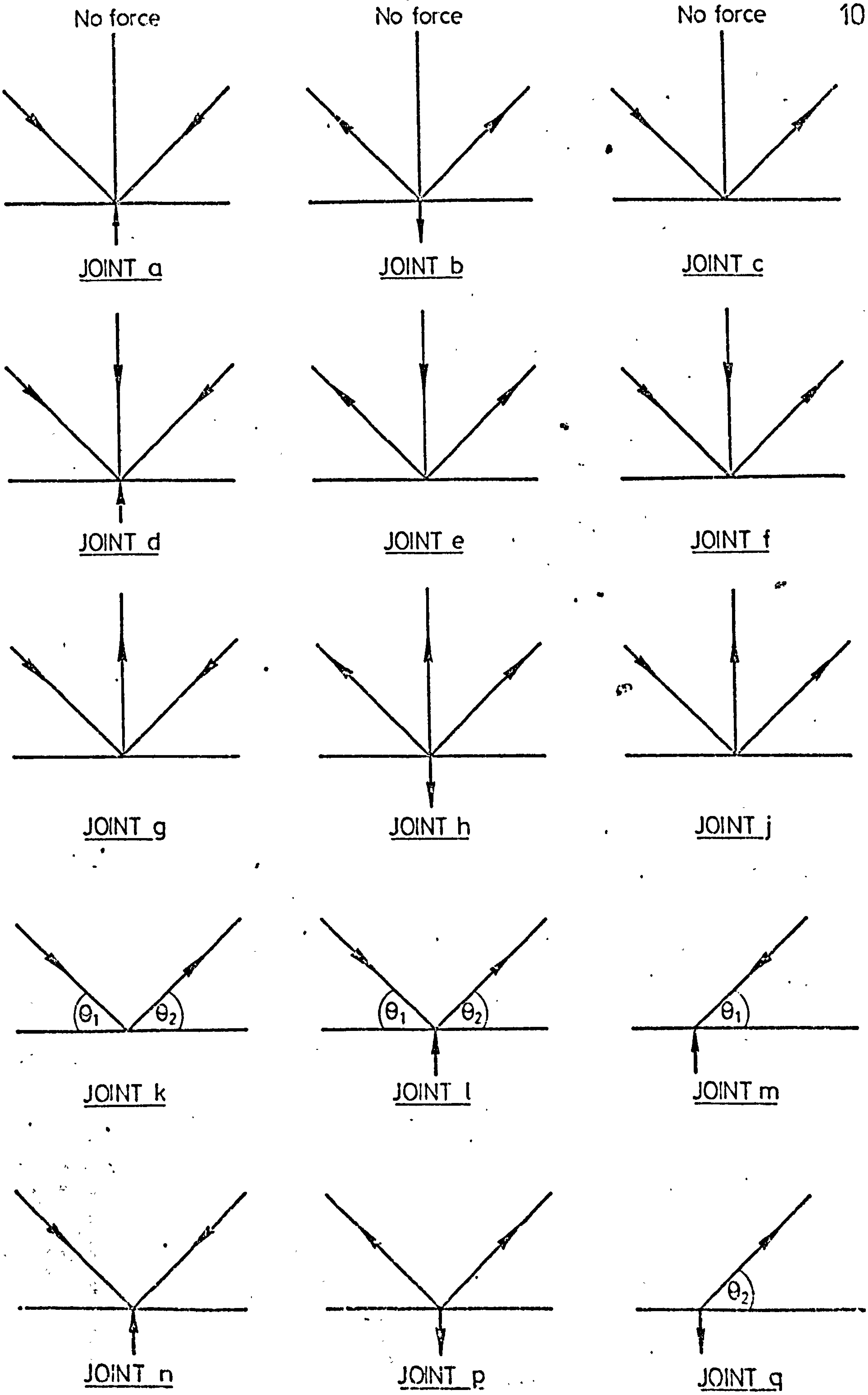

Fig. 1.1 Joints encountered in Warren or Pratt trusses

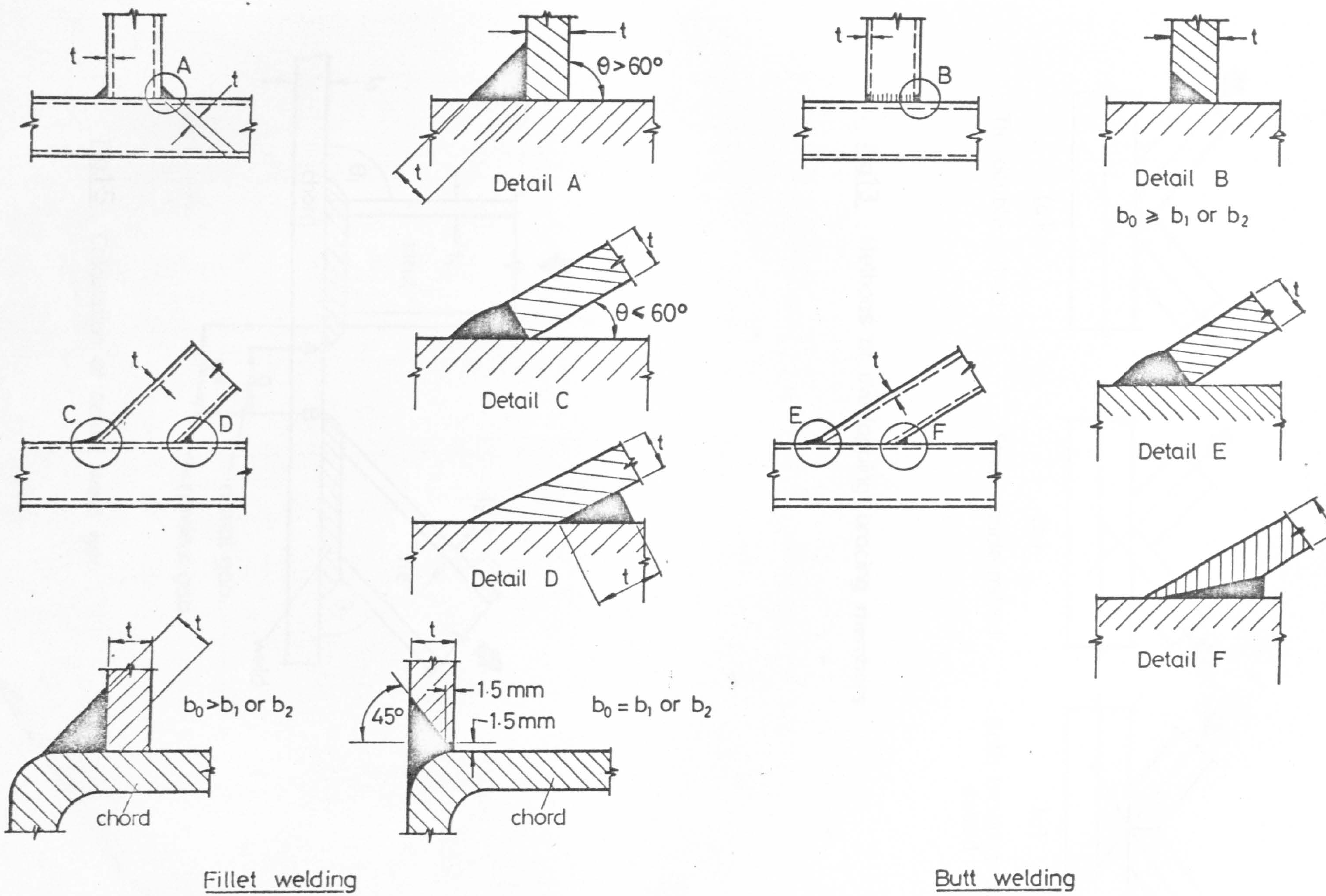

Fig.1·2 Typical welding details

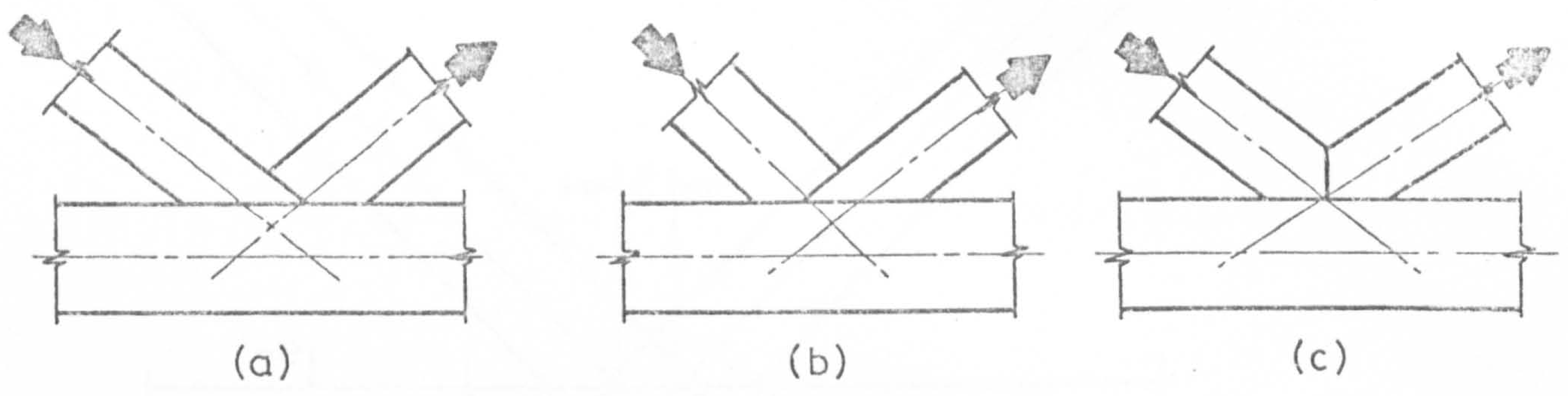

Fig.1.3 Methods of overlapping bracing members

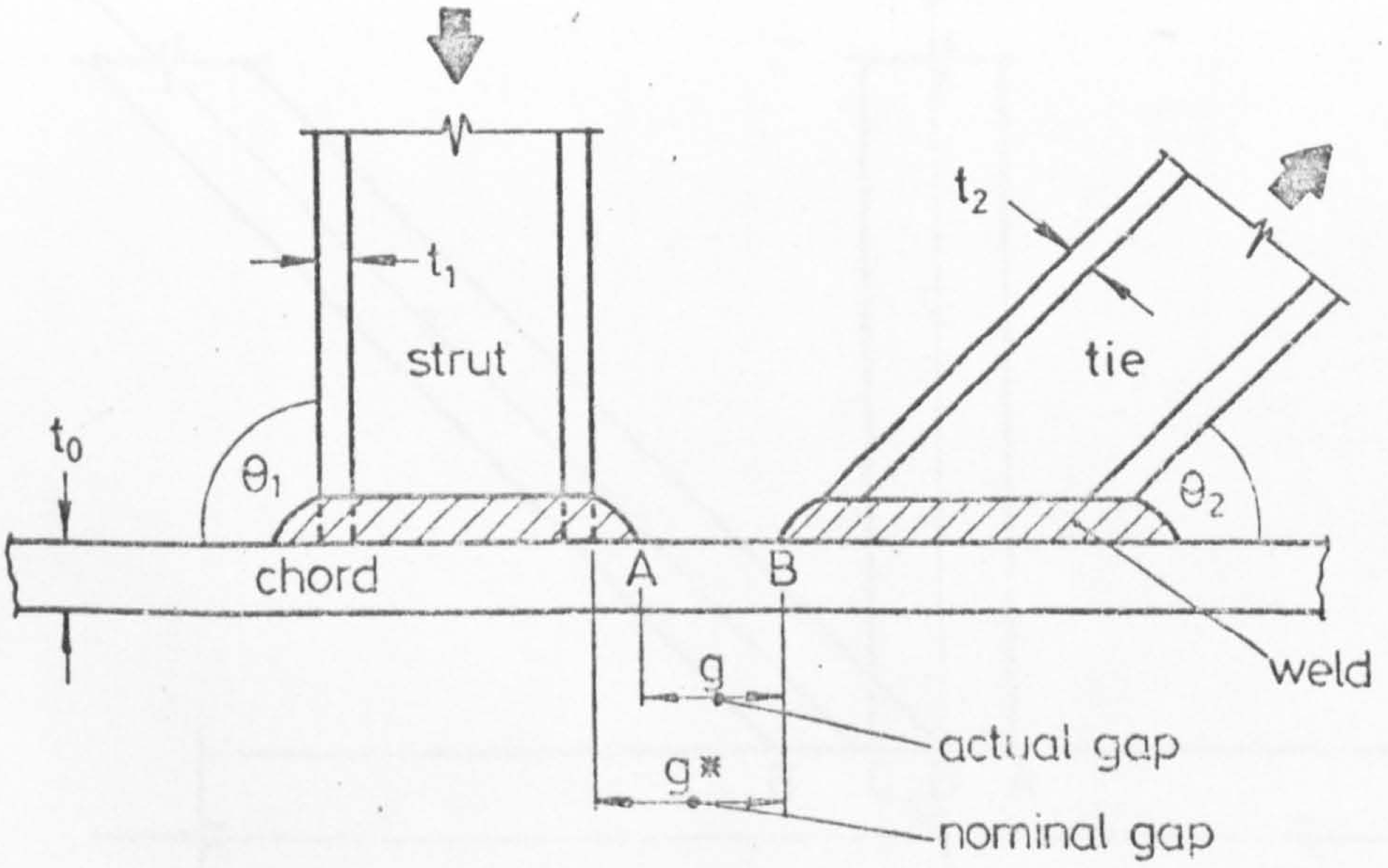

Fig.1.5 Calculation of actual weld gap

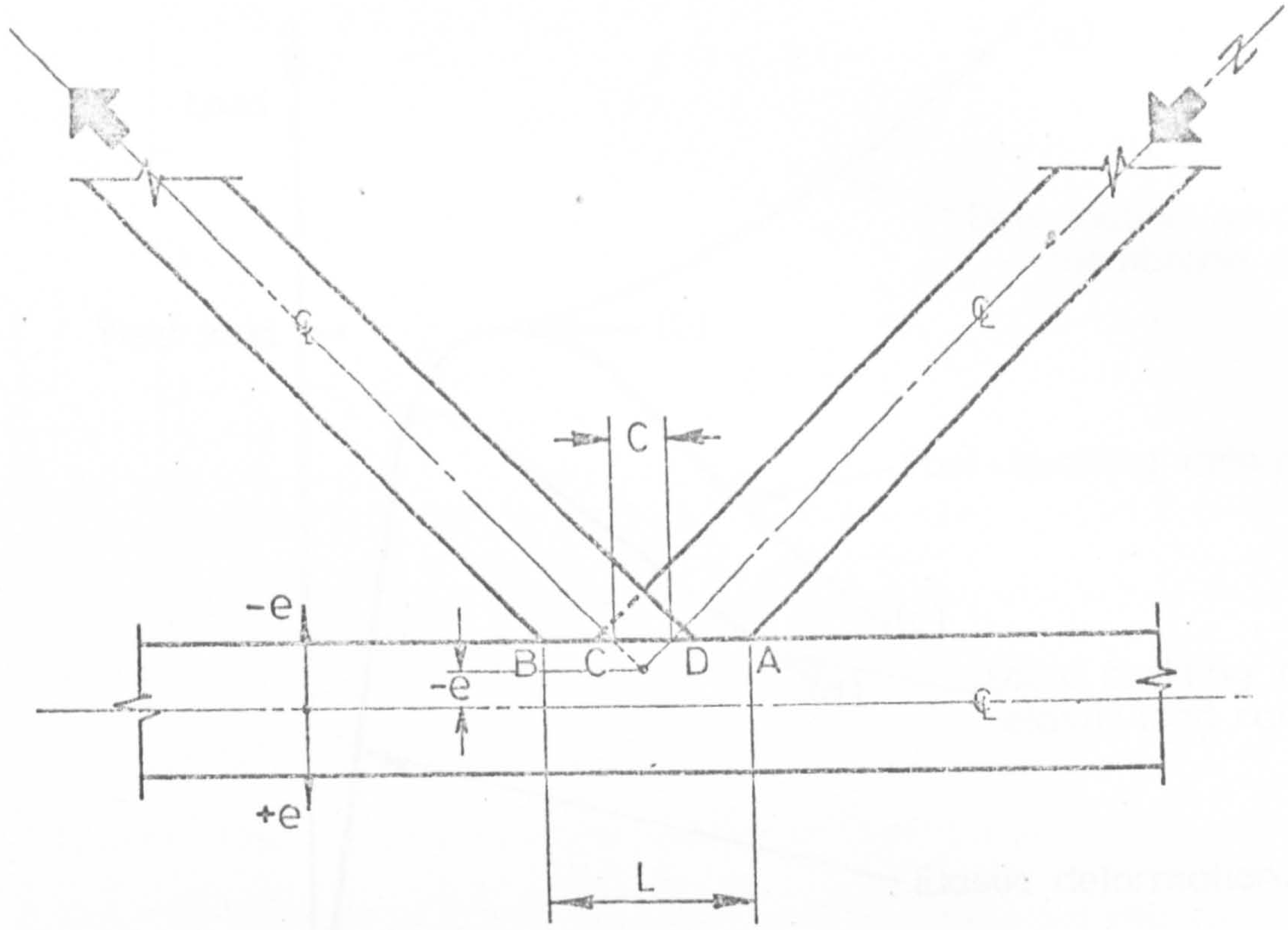

(a) Warren joint with negative eccentricity

$$\text{Percentage overlap} = \frac{CD}{CA} \times 100\%$$

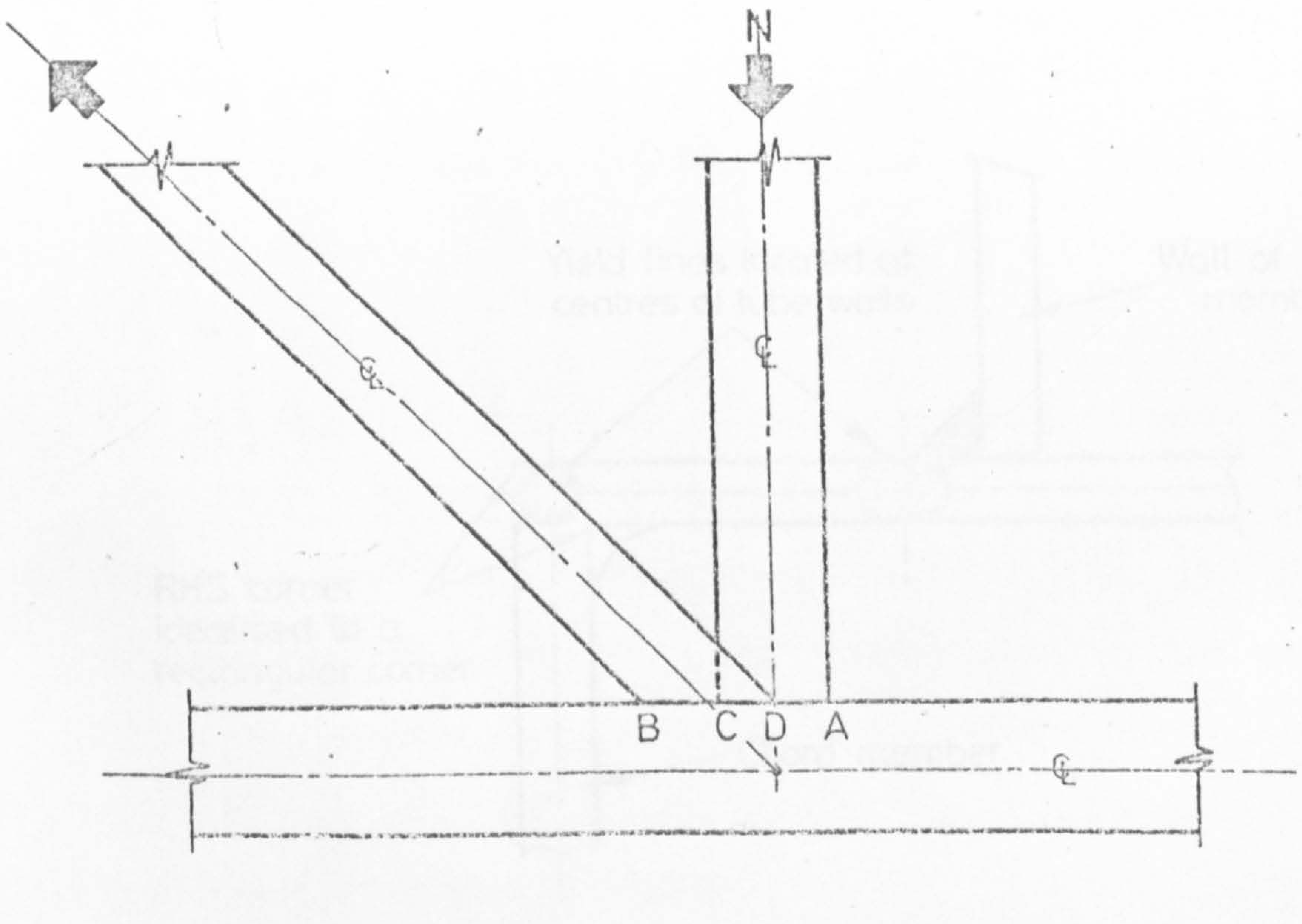

(b) Pratt joint with no eccentricity

Fig.1·4 Definition of overlap

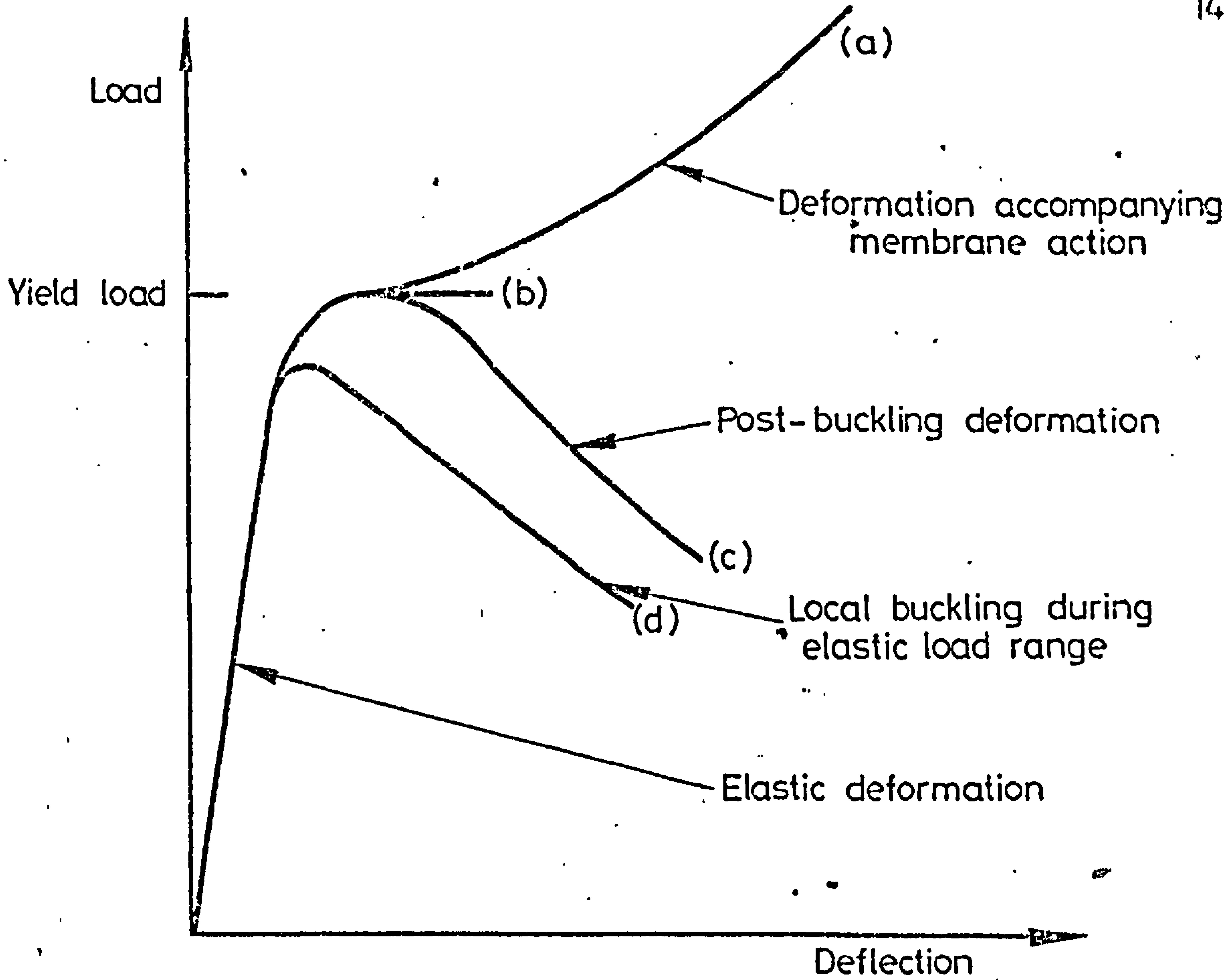

Fig1·6 Load v. deflection characteristics of tubular joints

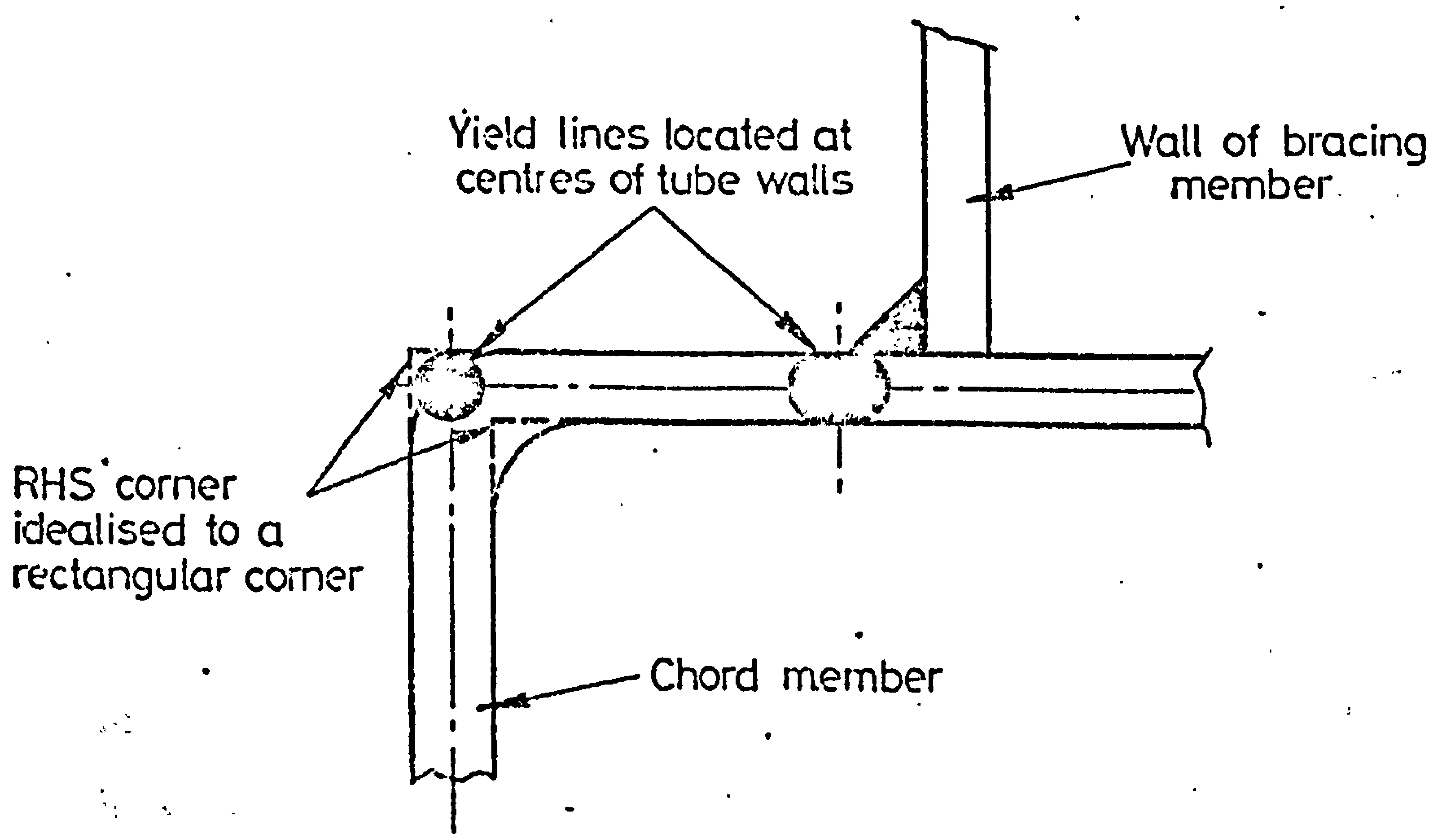

Fig.1·7 Location of yield lines and simplification of rounded corners

CHAPTER 2

REVIEW OF LITERATURE ON RHS JOINTS

The advent of RHS tubes solved the jointing difficulties which fabricators found with CHS joints but concern grew over the strength and behaviour of joints with RHS chords, both in the static state or under fatigue loading. Research in Great Britain into the behaviour of welded lattice girder joints with RHS chords began at Sheffield University and more recently investigations have also been conducted at the British Steel Corporation Tubes Division, Corby, and Nottingham University.

At Sheffield University, five predominantly experimental projects were carried out by Blockley[5, 6], Babiker[2], Shinouda[61], Mee[48] and Chandrakeerthy.[16] All experimental work was performed with isolated joint specimens of 'N' configuration between RHS chord members and CHS or RHS bracing members, with the diagonal (tension) bracing member always at 45° to the chord.

Blockley[5] conducted static tests on 60 mild steel joints with CHS bracing members with a varying gap or overlap and covering a wide range of member sizes. Blockley found that the ultimate strength of gap joints was significantly less than if the bracing members were lapped, and if the chord face was relatively thin then large local deformations occurred at loads below the working load of the specimen, for gap joints. Local deformations encountered in lap joints, on the other hand, were much lower. Blockley claimed that as the joint stiffness was low, secondary bending stresses caused by joint eccentricities do not affect the ultimate joint strength and may often be neglected, but it was suggested that the concept of joint eccentricity be considered together with the amount of weld gap or overlap of the bracing members.

Babiker[(2)] studied the effect of cyclic loading upon 55 mild steel joints with CHS branch members and found that although a joint may be considered sufficiently strong for static purposes, its life under fatigue conditions could be so low that it would be unacceptable as a B.S.153 Class F joint. Joints with 100% overlap were fully satisfactory and the bending stresses caused by the eccentricity with such joints could be neglected as they are small compared with the direct stress. Babiker found that partially intersecting joints were slightly lower than the B.S.153 curve for Class F joints, and because this type of joint has intersecting weld beads which can cause stress concentrations, this type of joint was not recommended. Weld gap joints fell considerably below the B.S.153 curve and were quite unsafe, so Babiker recommended a new category of B.S. Class H for such joints. The width to thickness ratio for both the chord or bracing members had some effect on fatigue performance but this was insignificant compared with the effect of joint geometry. It was also found that no increase in the fatigue endurance limit could be gained by using a gusset plate or stiffening rings to connect the members at a joint.

Joints are most easily reinforced either by putting gusset plates across the bracing members and in the plane of the lattice girder, or by welding a stiffening plate under the bracing members to the loaded face of the chord, as shown in fig. 2.1.

Shinouda[61] investigated the latter type of stiffened joint with a series of 61 tests on CHS to RHS weld gap joints and his conclusions are the best available guide for the reinforcement of joints at present. For CHS to RHS gap joints with $b_o/t_o < 14.3$ no stiffening of the joint was necessary. If $b_o/t_o > 14.3$ the joint could be stiffened according to the following recommendations.

(i) The minimum thickness of the stiffening plate (t_s) is determined by interpolation from:

$$\begin{aligned} &\text{for } d_1/b_o = 0.25, \ t_s = 0.0464\, b_o^{2/3} \sqrt[3]{c.t_1} \\ &\text{for } d_1/b_o = 0.50, \ t_s = 0.0582\, b_o^{2/3} \sqrt[3]{c.t_1} \\ \text{and } &\text{for } d_1/b_o \doteq 0.75, \ t_s = 0.0591\, b_o^{2/3} \sqrt[3]{c.t_1} \end{aligned} \tag{2.01}$$

where c in this case is the ratio of b_o to the desired local chord deflection, which Shinouda took to be 100.

(ii) The plate and chord wall thicknesses should also satisfy the following:

$$\begin{aligned} &\text{for } d_1/b_o = 0.3839 \ , \ s > 75 \times 10^{-4} \ , \\ &\text{for } d_1/b_o = 0.5446 \ , \ s > 100 \times 10^{-4}, \\ \text{and } &\text{for } d_1/b_o = 0.6786 \ , \ s > 100 \times 10^{-4} \end{aligned} \tag{2.02}$$

where $s = (t_o^3 + t_s^3)/b_o^2 t_1$. In the formulae above, d_1 and t_1 could also be replaced by d_2 and t_2 if the branch members are not identical.

Mee[48] undertook research at Sheffield University on the static strength of RHS to RHS joints with 57 tests on specimens having varying weld gap or lap and different chord preloads. The chord compression preload was applied by means of prestressing bars through the chord section whereas all subsequent joint testing rigs used hydraulic jacks. Mee confirmed Blockley's findings that the joint strength and stiffness increased as the weld gap decreased or lap increased, and at a 100% overlap the connection approximated to a rigid joint. The results also showed that there was little advantage in having 100% overlap rather than 50% overlap. The behaviour of RHS joints was again found to depend mainly upon the joint geometry, and the ultimate strength increased with increasing λ or t_o. For large b_o/t_o ratios RHS branch member joints tended to be slightly stronger than CHS branch member joints, but when b_o/t_o was small the reverse was true. Mee found that there was little difference between various joints which had the same geometry but varying prestressing forces. All subsequent researchers have found that an increasing compression preload causes a continual reduction in ultimate joint strength, and the different conclusions about the effect of compression preload may be due to the different way in which Mee applied it.

Mee carried out a theoretical analysis of the elastic load deformation characteristics of the connecting chord face of a gap joint by treating it as a laterally loaded plate and analysing it by means of the "Theory of Thin Plates" using a finite difference technique. The elastic behaviour of the joint was well predicted, so an analysis was then carried out to solve for the secondary moments in a plane framework by taking account of the joint flexibility.

The work of Blockley[5, 6], Babiker[2], Shinouda[61] and Mee[48] has also been reported in references 3, 4, 31, 32, 58 and 62. Eastwood and Wood[32] summarized the work done at Sheffield University up to 1970 by proposing a set of tentative design rules for hot-rolled CHS or RHS bracing members framing on to an RHS chord, which are listed below:

(i) Lap Joints. These should have an overlap of not less than 50% of the mean diameter of the web members, and the greater the degree of overlap, the smaller the deflections in the connecting face of the chord member and the greater the fatigue resistance. When there is at least 50% overlap the normal load transmitted to the chord by the bracing members is unlikely to be a limiting factor, and the chord face deflections will be small.

(ii) Gap Joints. Where the weld gap is small there will be less distortion of the face of the rectangular section than with a wide gap, but the joint will be more prone to fatigue failure. With no stiffening, the vertical component of the working load normal to the chord should not exceed:

$$1.2t_o\sigma e_o \qquad \text{for} \qquad \lambda_{av} \leq 0.5$$

$$\text{or} \qquad 1.2t_o\sigma e_o \left[1 + 3(2\lambda_{av} - 1) \right] \text{ for } 0.5 < \lambda_{av} \leq 0.89 \tag{2.03}$$

$$\text{or} \qquad 4t_o\sigma e_o \qquad \text{for} \qquad 0.89 \leq \lambda_{av} \leq 1.00$$

(iii) Eccentricity. For a compression chord the secondary moment produced by noding eccentricity may be divided equally between the chord member lengths on either side of the joint, provided that the chord member is effectively continuous and that the moment of inertia of either chord member section, divided by its actual length, does not exceed 1.5 times the corresponding value for the other length. In cases where this ratio is exceeded, the bending moment shall be divided in proportion to the moments of inertia of the chord member sections, divided by their respective actual lengths. The bending moments so calculated shall then be assumed to be inoperative at the neighbouring chord member joints.

For a tension chord, the secondary moment produced by noding eccentricity may be divided between the two chord members intersecting at the joint in any proportion provided that the resulting total tensile stress shall not exceed the permissible stress in direct tension in either member.

(iv) Fatigue. Joints in which the bracing members overlap by 50 to 100% of the larger web member can be designed for fatigue loading according to Class F in B.S.153. The fatigue life of gap joints is seriously reduced and should be taken as 10% of that for Class F members in B.S.153.

These recommendations resulting from work at Sheffield University received particular acceptance in Canada, and are used by Stelco[63] and the C.I.S.C.[14, 15] A further research project at Sheffield University was undertaken by Chandrakeerthy[16, 78] who tested 47 RHS to RHS 45^{O}N joints made from cold-formed sections, with test specimens covering gap and lap (50% and 100%) joints. The aim was to study the influence of typical joint parameters, identified from tests on hot-rolled sections, on cold-formed RHS joints. Initial steps were also taken to set up an elasto-plastic finite element programme for the analysis of tubular joints.

At Nottingham University, complete trusses, for which the joint design was based upon certain isolated joint tests at Sheffield, were tested by Dasgupta.[21] These trusses, 11 in all, were of 20 foot span and CHS to RHS with small weld gaps. Truss joint failure loads were found to be up to 30% lower than the equivalent isolated joint failure loads which was thought to be due to additional moments imposed on the joints when acting as a part of a complete structure, as well as some inadequately fabricated joints. Dasgupta also wrote a computer program using the matrix equilibrium method to analyse trusses with joint eccentricity, joint flexibility and with the effects of axial forces also taken into consideration. The actual joint flexibility was calculated by a finite element analysis. It was found that the secondary moments increase considerably with the increase in axial flexibility, and the latter increases at a faster rate when λ decreases. The elastic rotational flexibility of the joint was also small which caused high secondary moments in the bracing members. These secondary moments in turn cause high stress concentrations at the crotch of the gapped joint if there is a positive noding eccentricity, or conversely relieve the stresses at the crotch if there is a negative eccentricity.

To complement the research done at Sheffield and Nottingham Universities, further testing was undertaken by the British Steel Corporation[22] at Corby to investigate larger sections and to provide direct correlation between the testing rigs at the different establishments. The test specimens were comprised of 30 N-type joints, one having 30^{o} bracing and all others 45^{o}, and one Warren joint. Of these joints five were RHS to RHS nominal weld gap joints. In general it was found that the results were in reasonable agreement with the Sheffield or Nottingham tests. No generalizations were able to be made from the one test with the tension bracing member at 30^{o}, which failed at the same load as its 45^{o} equivalent, or from the Warren joint test which failed at 18% less than the 45^{o} N joint equivalent.

From the tests at Sheffield, Nottingham and Corby, a series of ultimate strength curves were empirically derived for both CHS to RHS and RHS to RHS isolated N joints, as shown in fig. 2.2, which were independent of the weld gap parameter and eccentricity. The vertical axis of these graphs is actually not dimensionless but was found to give the best graphical presentation. These graphs, known as 'Corby curves', differentiated between CHS and RHS braced joints which Eastwood and Wood[32] had not done.

In the Netherlands an extensive experimental research programme has been taking place at the TNO Institute and Delft University of Technology, sponsored by the E.C.S.C., CIDECT, the Dutch government and Dutch tube suppliers. About 450 isolated joint specimens have been tested[68] of which many are with RHS members. Apart from some tests on Tee joints, Cross joints and joints between structural hollow section bracing members joined to an open profile (I or U) chord, the bulk of the experiments were with Pratt and Warren truss joints with the aim of studying the following parameters:

(a) the width ratio between bracings (b_1/b_2)

(b) the height to width ratio of the chord (h_o/b_o)

(c) the angle between bracings and chord (θ_1,θ_2)

(d) gap and lap of the bracings

(e) axial load or 'preload' in the chord

(f) additional loads such as purlin loads

(g) grade of material

(h) the thickness ratio between bracings and chord (t_1/t_o or t_2/t_o)

(i) the weld shape: fillet welds and butt welds

(j) scale effects

(k) cold finished hollow section joints as compared with hot-formed ones.

(1) the slenderness of the chord wall (b_o/t_o) and the width ratio between bracings and chord ($(b_1 + b_2)/2b_o$)

Measurements relating to the joint tests were well documented[28] and the results were publicised in a series of reports[26,27,66,67,69,70,71,72,74] by Wardenier et al, leading to the draft version of the Dutch regulations for Tubular Construction[53], which were empirically based. It was concluded that the mean ultimate static strength, (expressed as a force in the compression bracing member), of Pratt and Warren type joints in RHS members and with a weld gap, is given by:

$$N_{ult} = 9\sigma e_o t_o^{1.5} b_o^{0.5} \cdot \lambda_{av} \cdot \left(\frac{h_o}{b_o}\right) \left(\frac{1+\sin\theta_1}{2\sin\theta_1}\right) \cdot f(F/Fp) \qquad (2.04)$$

The influence of the chord force, $f(F/Fp)$, was to cause a reduction in joint strength for both tension and compression chords according to:

$$f(F/Fp) = 1.3 - \frac{0.4}{\lambda_{av}} \left| \frac{\sigma_{o\,max}}{\sigma e_o} \right| , \text{ but } \ngtr 1.0 \qquad (2.05)$$

These formulae were only valid within the following range of application:

(i) $0.4 \le b_i/b_o \le 1.0$ (ii) $h_o/t_o \le 40$

(iii) $15 \le b_o/t_o \le 35$ (iv) $0.5 \le h_i/b_i \le 1.5$

(v) $30^o \le \theta_i \le 90^o$ (vi) $0.1 \le g^*/b_o \le 1.2 - \lambda_{av}$

(vii) $|e| \le 0.5h_o$

Equation (2.04) was then subject to the following checks:

(i) For member strength, $N \leq \sigma e_1 t_1 \ (2h_1 - 4t_1 + b_m)$

$$\text{and} \quad T \leq \sigma e_2 t_2 \ (2h_2 - 4t_2 + b_m) \tag{2.06}$$

(ii) For chord shearing, $N \leq \dfrac{\sigma e_o t_o}{\sqrt{3}} \ (2h_1/\mathrm{Sin}\theta_1 + b_m) \cdot \dfrac{1}{\mathrm{Sin}\theta_1}$

$$\text{and} \quad T \leq \frac{\sigma e_o t_o}{\sqrt{3}} \ (2h_2/\mathrm{Sin}\theta_2 + b_m) \cdot \frac{1}{\mathrm{Sin}\theta_2} \tag{2.07}$$

whenever $\lambda_1 \leq 0.85$, $h_i/b_i \leq 1.0$ or $\dfrac{\sigma e_i t_i}{\sigma e_o t_o} \geq 0.58$

$b_m = b_i + \dfrac{kt_o}{\lambda_{av}}$ providing $b_m \leq 2b_i$, and the values of k are given below.

Values of k			
	Fe360	Fe430	Fe510
Tension member	7	7	6
Compression member	9	9	8

(iii) Tension bracing members must also comply with $b_2/t_2 \leq 35$ and compression bracing members must have $b_1/t_1 \leq 5 + 30\ (b_1/b_o)$.

No recommendations were given for the ultimate static strength of lapped joints, but as these were found to be generally stiffer and stronger than gap joints, it was suggested that equation (2.04), subject to its checks, could be used for a conservative estimate of lap joint strength. Equation (2.04) represented the line of best fit for the Dutch gap joint tests only, based upon assumed joint parameters, and which had no chord preload ($F = 0$). The reduction factor (equation (2.05)) for the chord force was then added as a reasonable lower bound on a large scatter of test results which had chord preloads. A tensile chord preload was actually found to slightly increase the strength of an isolated gap joint, but the reduction factor of equation (2.05) was still applied to tension chords as limited results from truss tests elsewhere[10] had indicated that truss joints probably suffered a loss in strength due to tensile preloads even if isolated joints generally did not. Although the size of the gap appeared to have some influence upon the ultimate joint strength depending upon b_o/t_o and λ_{av}, the gap parameter is not included in equation (2.04) as the results were inconclusive as to its effect. No difference in behaviour regarding the ultimate static strength was evident between cold formed and hot formed section joints, providing the yield stresses were based upon stub column tests. The initiation of cracks in cold-formed section joints started earlier, however, which may seriously reduce the fatigue strength.

It is interesting to compare the format of equation (2.04) with an empirically derived formula for the ultimate load of CHS to CHS Warren gap joints by Washio, Togo and Mitsui[75] given below:

$$N_{ult} = \sigma e_o \left(\frac{b_o 2}{4}\right) \left(\frac{2t_o}{b_o}\right)^{1.5} . (1+6.52\lambda_{av}) . \left[\frac{1-0.26Cos^2\theta_1}{Sin\theta_1}\right] . f(g^*) \qquad (2.08)$$

where $f(g^*) = 1.75 - 2.65g^*/b_o$ for $g^*/b_o \leq 0.2$

or $f(g^*) = 1.15 - 0.06g^*/b_o$ for $g^*/b_o > 0.2$

The ultimate load of the joint in this case is dependent upon $b_o^{0.5} t_o^{1.5}$, which is the same as proposed by researchers at Delft, but the factors for the influence of the bracing angles and gap differ. Washio et al[76] later changed the bracing angle influence function from $(1-0.26Cos^2\theta_1)/Sin\theta_1$ to $(1+Sin\theta_1)/2Sin\theta_1$ which was also later adopted by Wardenier et al in equation (2.04). Washio et al also found that while the strength of an isolated Warren joint was not influenced appreciably by tensile chord preloads, it was reduced significantly by compressive force in the chord. Considerably more research has been done on joints having CHS chords rather than RHS chords, particularly in Japan and the U.S.A., and the reader may refer to the bibliography compiled by Wardenier and Verheul[73] for further references to CHS/CHS joints.

As part of CIDECT programme 5F, 8 Pratt trusses with RHS chords and spans of between 14 and 16 metres have been fabricated in England[33] and then tested at Pisa University, Italy.[10] These girders were all designed such that the bays of one half of each girder had noding joints whilst the bays of the other half of the girder had nominal gap joints. Five girders had CHS bracings and three had RHS bracings. In association with these girder tests, some of the joints being investigated in the girders were reproduced as isolated joint specimens for testing at Corby[9], to give further correlation, if possible, between the behaviour of isolated joints and similar ones in complete girders. Many of the isolated joint tests failed by local buckling of the chord but this did not occur in any of the girder tests, and the latter also showed no appreciable difference between the strength of joints on the compression chord and the similar joints on the tension chord.[35]

From the results of these tests at Pisa[10] and Corby[9], as well as from those in the Netherlands[28, 71, 72], it has been shown by Coutie, Davies, Packer and Haleem[18, 36] that the mean ultimate static strength of RHS or CHS to RHS <u>gap</u> joints can be expressed by:

$$N_{ult} = \sigma e_o b_o^{0.3} t_o^{1.7} \left[3.8+10.75 \left(\frac{b_1+b_2+h_1+h_2}{4(b_o-2t_o)} \right)^2 \right] \cdot \frac{1}{\sin\theta_1} \cdot \sqrt{1-|F/Fp|} \tag{2.09}$$

As with equations (2.04) and (2.08), the ultimate joint strength again depends on $b_o^{\alpha}.t_o^{(2-\alpha)}$ so that the equation is dimensionally correct, but in this case the angle function $1/\sin\theta_1$ gave acceptable agreement with test results, and a simpler function for the influence of the chord preload was adopted. For gaps greater than

$$g^* = 1.25\sqrt{b_1+b_2+h_1+h_2}\text{ , with dimensions in mm,} \tag{2.10}$$

the limit state of excessive local deflections becomes operative. Equation (2.09) is also subject to a check for chord shear (see fig. 3.1 mode G3) failure:

$$N\mathrm{Sin}\theta_1 \text{ or } T\mathrm{Sin}\theta_2 \le \frac{2\sigma e_o t_o}{\sqrt{3}} (h_o+0.2b_o)\sqrt{\frac{b_1+b_2+h_1+h_2}{4h_o}} \cdot \sqrt{1-|F/Fp|} \tag{2.11}$$

The mean ultimate static strength of RHS or CHS to RHS <u>lap</u> joints is given by the equation[18, 36]:

$$N_{ult} = 1.25\sigma e_1 A_1 \sqrt{1-|F/Fp|} \cdot \left[\left({}^{b_1{}^*}/_{b_o}\right)\left({}^{b_o}/_{t_o}\right)\left({}^{t_1}/_{t_o}\right)^2\right]^{-0.25} \tag{2.12}$$

$$\text{where } b_1{}^* = (b_1 + h_1)/2 \tag{2.13}$$

The ultimate strength of lap joints is thus considered to be independent of the bracing angles, and the strut area A_1 indicates that the ultimate lap joint strength is less for CHS bracing members than for RHS bracing members of the same width, thickness and grade of steel, when connected to the same chord member. Equations (2.09) to (2.13) apply to both CHS or RHS bracings, but for CHS bracings the terms b_1,h_1 and b_2,h_2 are replaced by d_1,d_1 and d_2,d_2 respectively. Equation (2.12) is also subject to a check for chord shear failure similar to that for gap joints (equation (2.11)) but the shear area will be slightly increased when the bracings lap one another. Equations (2.09) to (2.13) are applicable within the following range:

(i) $t_i/t_o \geq 0.4$ (ii) $30^o \leq \theta_i \leq 90^o$

(iii) $0.2 \leq b_i/b_o \leq 1.0$ (iv) $0.5 \leq h_i/b_i \leq 2.0$.

In West Germany, research on rectangular hollow section joints has taken place recently at Karlsruhe University of Technology and the Mannesmann Research Institute, Düsseldorf. A total of 43 joints had been tested at M.R.I. up until September 1973, which were CHS or RHS to RHS Warren braced, and these are reported by Mang.[43] He found that different curve characteristics were obtained for Warren joints compared to the 'Corby curves' presented by Davie and Giddings[22] for N joints.

In 1974 six large size RHS to RHS Warren joints were tested at Mannesmann[37] (CIDECT Prog. 5M Series 1) of which three were gapped and three lapped, with all being fabricated from mild steel. Hohl's[37] experimental results included the joint yield load which he defined as the load producing 0.2% strain at the joint. This strain is measured as the total deflection of the joint intersection, (using a Williot diagram analysis), in the direction of the compression bracing member, divided by the length of the compression bracing member. This concept could be adapted to different joint test rigs to allow for member restraint conditions, but is restricted to joints with equal member lengths.[37] Hohl also found that a compressive chord preload of up to 70-80% of the difference between the chord ultimate and working loads had no effect on the 'loaded behaviour of the joint', but could substantially lower the failure load. Hohl's test results were much higher than predicted by the 'Corby curves' of Davie and Giddings.[22]

In sequel to these tests a further six RHS to RHS Warren joints were tested[38, 44]. (CIDECT Prog. 5M Series 2) but using all higher yield steel for three tests, and mild steel bracing members with higher yield steel chord members for the other three tests. For these joints, all of which were lapped, it was found that using a higher yield steel chord member generally produced a 15 to 30% stronger joint, yet there seemed little additional joint strength obtained by using higher yield steel bracing members as well, except for small λ_{av} values.

From these tests on isolated RHS joint specimens in West Germany and also those in the Netherlands by Wardenier et al[28, 71, 72], proposals for the German standard DIN4116 on statically loaded SHS connections, have been drafted by Mang and Striebel.[46] The recommendations make use of the joint parameters t_o/t_1 or t_o/t_2, b_o/t_o, λ_{av} and σe_o. Using these variables four design charts are given for four different b_o/t_o ranges; viz. $b_o/t_o \leq 20$, $b_o/t_o = 25$, $b_o/t_o = 30$ and $b_o/t_o = 35$. These design charts are similar in format, a typical one being given in fig. 2.3. For a particular t_o/t_1, b_o/t_o, λ_{av} and steel grade, the maximum axial chord stress can be read off the ordinate axis for the design cases with wind loading and without wind loading (as these have different load factors). It is interesting to note that these comprehensive design charts apply to CHS/CHS, CHS/RHS and RHS/RHS joints, and for both gap or lap joints too.

Theoretical analyses of RHS to RHS lattice girder joints, or even joints with RHS chord and CHS bracings are less numerous than experimental research projects. Elastic analyses were made by Blockley[5], based on the elastic theory of thin plates with a finite difference method; Mee[48], continuing the same analytical approach; Chandrakeerthy[16], using the finite element method; Dasgupta[21] and Roper[59], again using a finite element method but of the complete joint, and Mansour[47] using a finite difference method. Mang and Striebel[45] have developed a novel approach for the elastic analysis of RHS to RHS gap joints using a spring simulation model but certain joint parameters to be used in the theory still had to be found or calculated by measurements from test specimens.

These elastic analyses showed that parts of a joint, such as the crotch area in a gapped joint, are stressed to the yield point at well below the joint working load. These severe stress concentrations in the crotch of a gapped joint are reflected by the low fatigue strength of the gap joint crotch. Extending an analysis such as the finite element technique into the plastic range is likely to be very expensive because the lack of symmetry of a typical joint would involve considerable computer time and storage. Hence the analysis of a joint in the post-elastic range has been approached using the yield-line method. As mentioned in the previous chapter, Jubb and Redwood[42] first applied the simple yield line theory to T joints between RHS members and then Patel[56] and Wardenier[71] also did the same finding good agreement between the joint yield load and the theory.

Davies and Roper[23, 24, 59] applied the yield line method, as early as 1971, to Pratt truss (N) gapped joints with RHS bracing members of the same size framing on to an RHS chord member. The yield line pattern which was used is shown in fig. 2.4, in which the angle α and the fraction x are both unknown. As the N joint is non-symmetrical, the point of zero deflection of the connecting chord face is no longer necessarily midway between the two bracing members, and so x may not be 0.5. An expression for the yield load of the joint (N_Y) can be obtained which is a function of both α and x. Differentiating to find the minimum solution for N gives $\tan\alpha = \sqrt{1-\lambda}$, and so:

$$N_Y = \frac{2mp_o}{g'} + \frac{8mp_o}{\sqrt{1-\lambda'}} + \frac{8mp_o}{1-\lambda'}\left\{ (2x^2-2x+1)g'+\eta(x+(1-x)\text{Cosec}\theta_2)\right\} \tag{2.14}$$

$$\text{where } x = \frac{\eta(\text{Cosec}\theta_2-1)}{4g'} + \frac{1}{2} \text{ and } mp_o = \frac{t_o^2 . \sigma e_o}{4} \tag{2.15}$$

Davies and Roper[24] showed that the value of x varies between 0.5 and 1.0 depending upon the angle θ_2, the size of gap and the value of η. When x = 1.0 the point of zero chord deflection is adjacent to the toe of the sloping tension bracing member and so all joint deformation is caused by the strut pushing into the chord. As the weld gap decreases the shear in the joint crotch increases, until the shear yield of the chord face is reached before the yield failure pattern along the hinges is developed. Hence there will be a minimum weld gap (g'_{cs}) below which no increase in yield load can be obtained because of shear failure in the crotch. For the N joint in fig. 2.4, this was found[24] to be given by:

$$g'_{cs} = \frac{\sqrt{3}t_o}{(1+\lambda')b_o'} \qquad (2.16)$$

This yield line model for gapped N joints was tested by comparison with the results of experiments by Mee[48] and Davie and Giddings[22], and acceptable correlation was obtained providing allowance was made for the fillet welds around the bracing members, except at large λ values. At the large width ratios Davies and Roper[24] recognised that other failure modes needed to be considered, and also pointed out that allowance for the effect of combined stress on the yield criterion could be made.

Mouty[51, 52] extended the yield line pattern of Davies and Roper to cover Warren and unsymmetrical gapped joints, and applied yield line theory to RHS to RHS lapped joints too. Mouty considered that lapped joints failed by means of a rotational mechanism of the connecting chord face, which was represented by the yield line pattern shown in fig. 2.5. By considering the virtual work done by the mechanism and minimising this with respect to the unknown angle α, (see fig. 2.5), the following expression for the yield load of a symmetrical Warren lapped joint was obtained:

$$N_y = \frac{t_o^2 \sigma e_o}{\sin\theta_1} \cdot \frac{L}{c} \left\{ \frac{L}{b_o'(1-\lambda')} + \frac{b_o'}{2L} + \frac{2}{\sqrt{1-\lambda'}} \right\} \qquad (2.17)$$

where L and c for this equation are shown on fig. 1.4(a). This equation, however, implies that the strength of a lap joint becomes infinite as the lap approaches 100% (i.e. as c tends towards zero on fig. 1.4(a)).

Mouty[51] also considered the effect which axial load has upon the plastic moment of resistance of a yield line pattern. It is well known[39] that an axial load F which is less than the squash load Fp of a steel member causes a reduction in the plastic moment of resistance of yield lines normal to the direction of the force F such that:

$$mp' = mp(1 - (F/Fp)^2) \tag{2.18}$$

Now consider a yield line which is inclined to the direction of the force F, such as yield line AB in fig. 2.5 when there is an axial load (F) in the chord member. The axial load parallel to the chord which is applied to this hinge AB is equal to

$$\sigma_o . t_o (b_o' - \lambda' b_o')/2 \quad .$$

By resolving this force into components parallel and perpendicular to the hinge AB, the force perpendicular to the yield line is given by

$$\sigma_o t_o b_o' (1 - \lambda') \mathrm{Cos}\mu/2$$

where μ is shown on fig. 2.5. This force is applied to a section of area equal to

$$t_o b_o' (1 - \lambda')/(2\mathrm{Cos}\mu) \quad ,$$

and so the stress normal to the hinge is $\sigma_o \text{Cos}^2\mu$. Substituting this into a form of equation (2.18) one obtains:

$$mp' = mp\left(1 - \left(\frac{\sigma_o \text{Cos}^2\mu}{\sigma e_o}\right)^2\right)$$

$$\text{i.e.}\quad mp' = mp\,(1 - (F/Fp)^2.\text{Cos}^4\mu). \qquad (2.19)$$

The derivation of this relationship assumed that the presence of a transverse shear has a negligible effect upon the value of mp, and that an axial force parallel to a yield line also has negligible effect upon the value of mp. The latter assumption also checks with the resulting equation (2.19) when $\mu = \pi/2$.

Mouty[51] noted that further strength beyond the yield load was obtained for a T joint, Warren or Pratt truss gap joint because of a membrane tension field forming in the connecting face of the chord. Although the membrane action manifests itself in directions parallel and transverse to the chord member, Mouty found that the transverse stiffness of the chord member was generally so small that membrane effects in this direction could be neglected.

In subsequent chapters of this thesis the author uses the yield line method for the yield and ultimate load analysis of gap and lap joints between RHS members[54, 55] as part of an overall study of their behaviour and modes of failure.

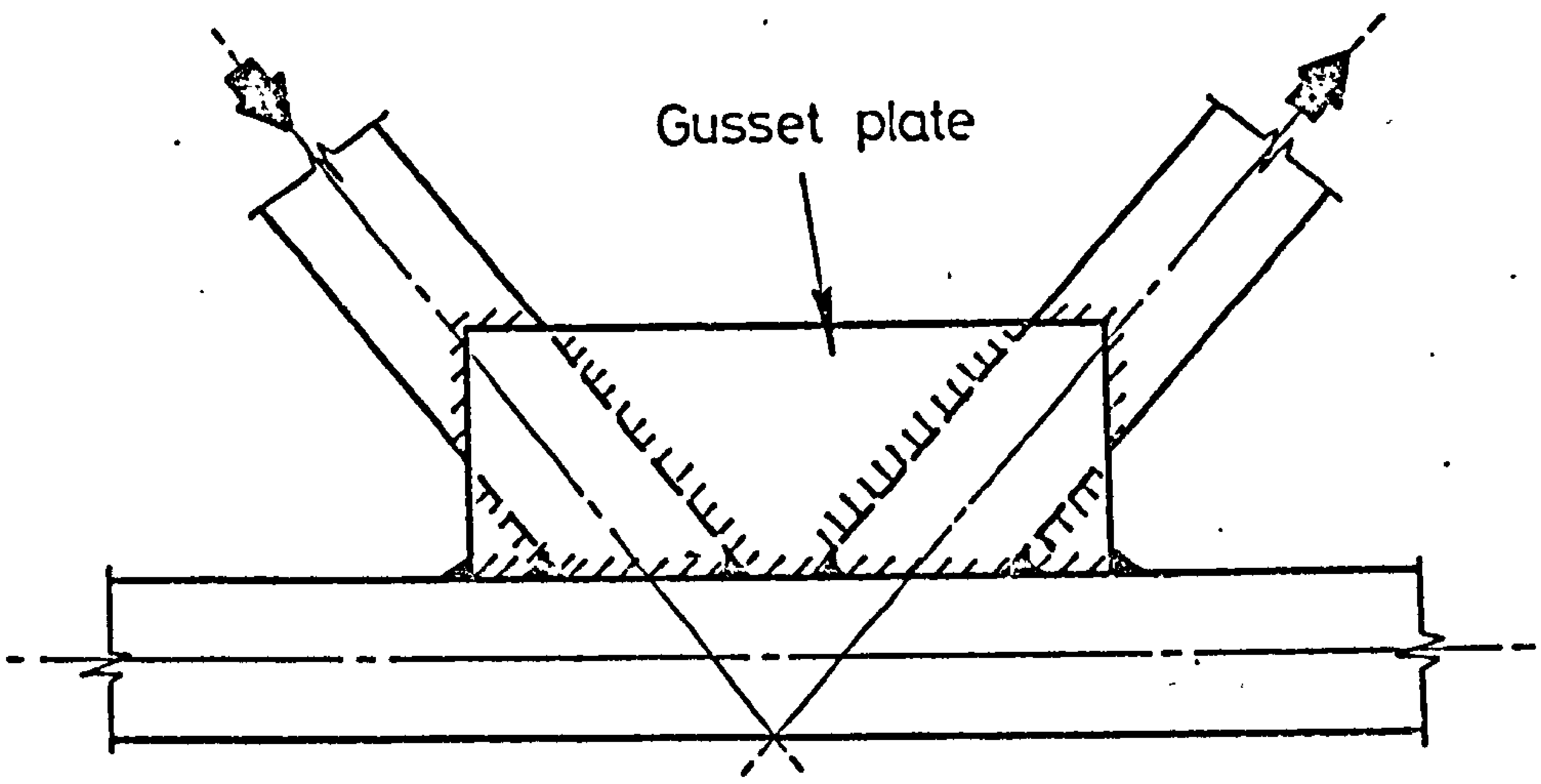

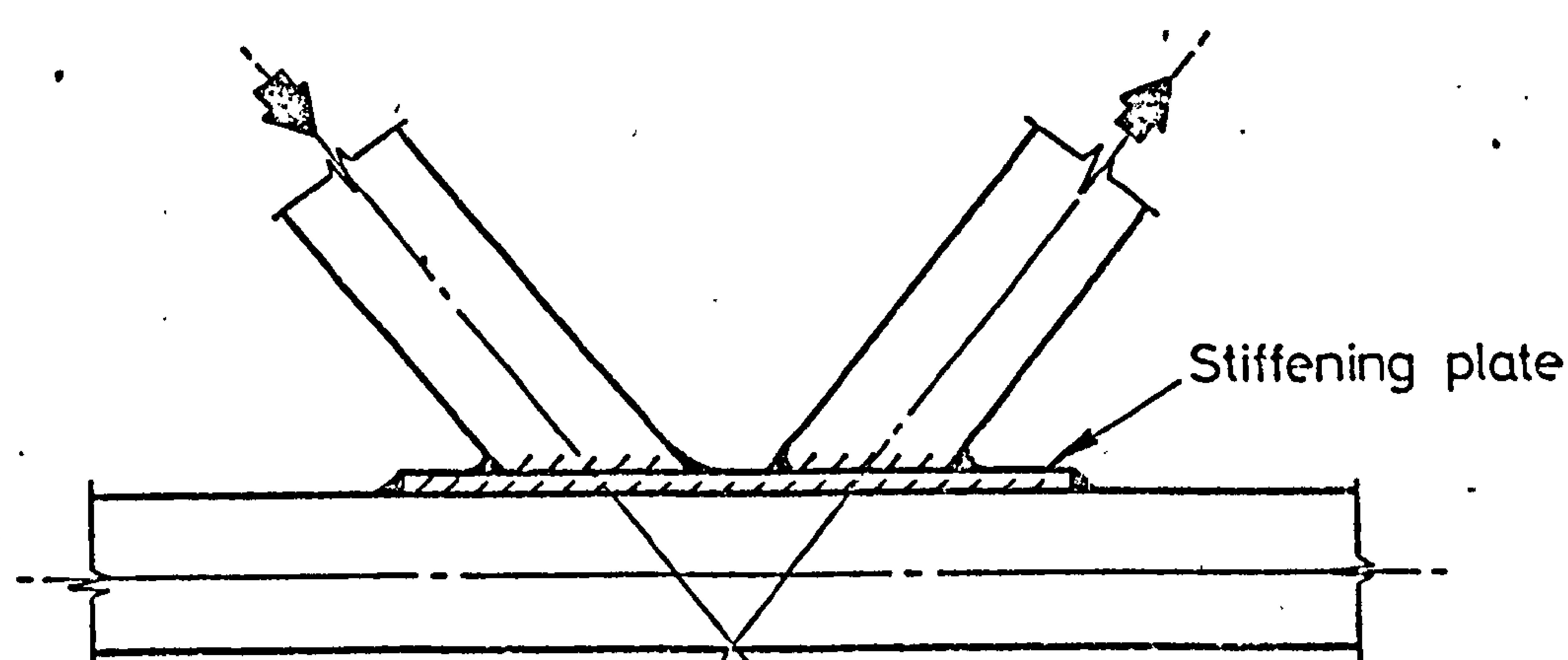

Fig 2·1 Methods of reinforcing tubular joints

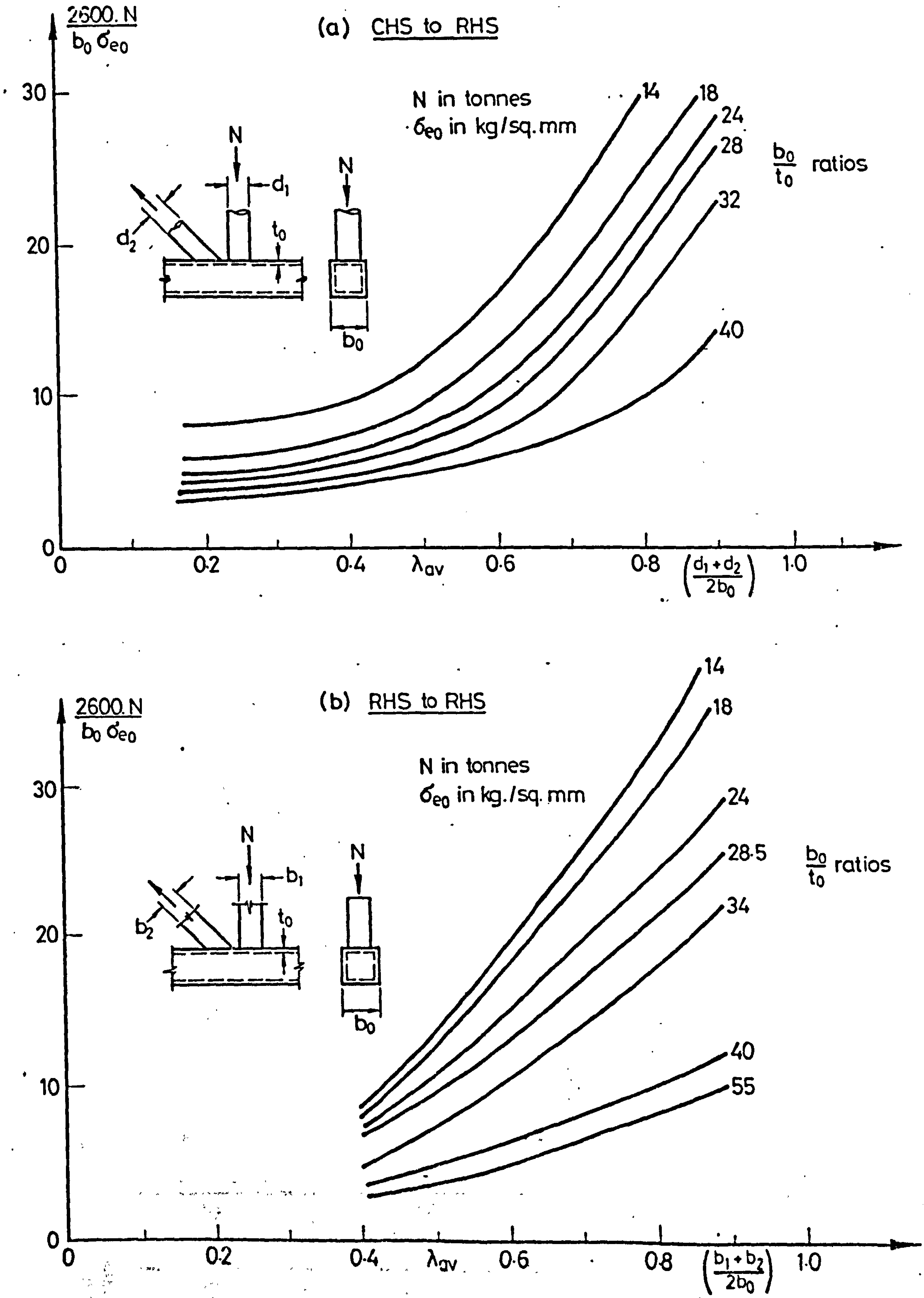

Fig.2.2 Corby ultimate load curves for 45° N joints

Fig.2·3 DIN 4116 (Static strength of SHS Connections) - Typical design chart

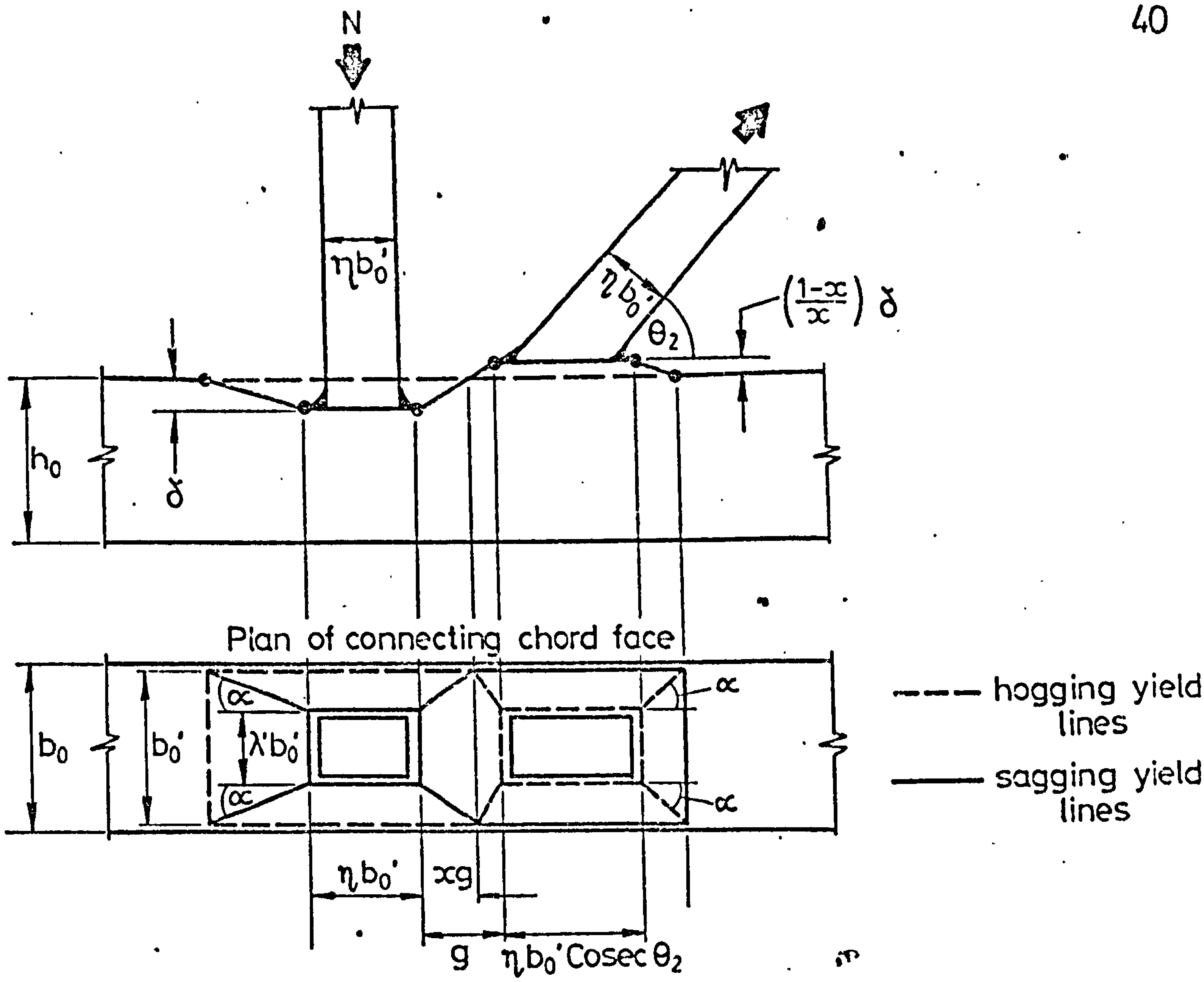

Fig.2.4 Yield line pattern for RHS to RHS N-braced gap joints by Davies and Roper (23)

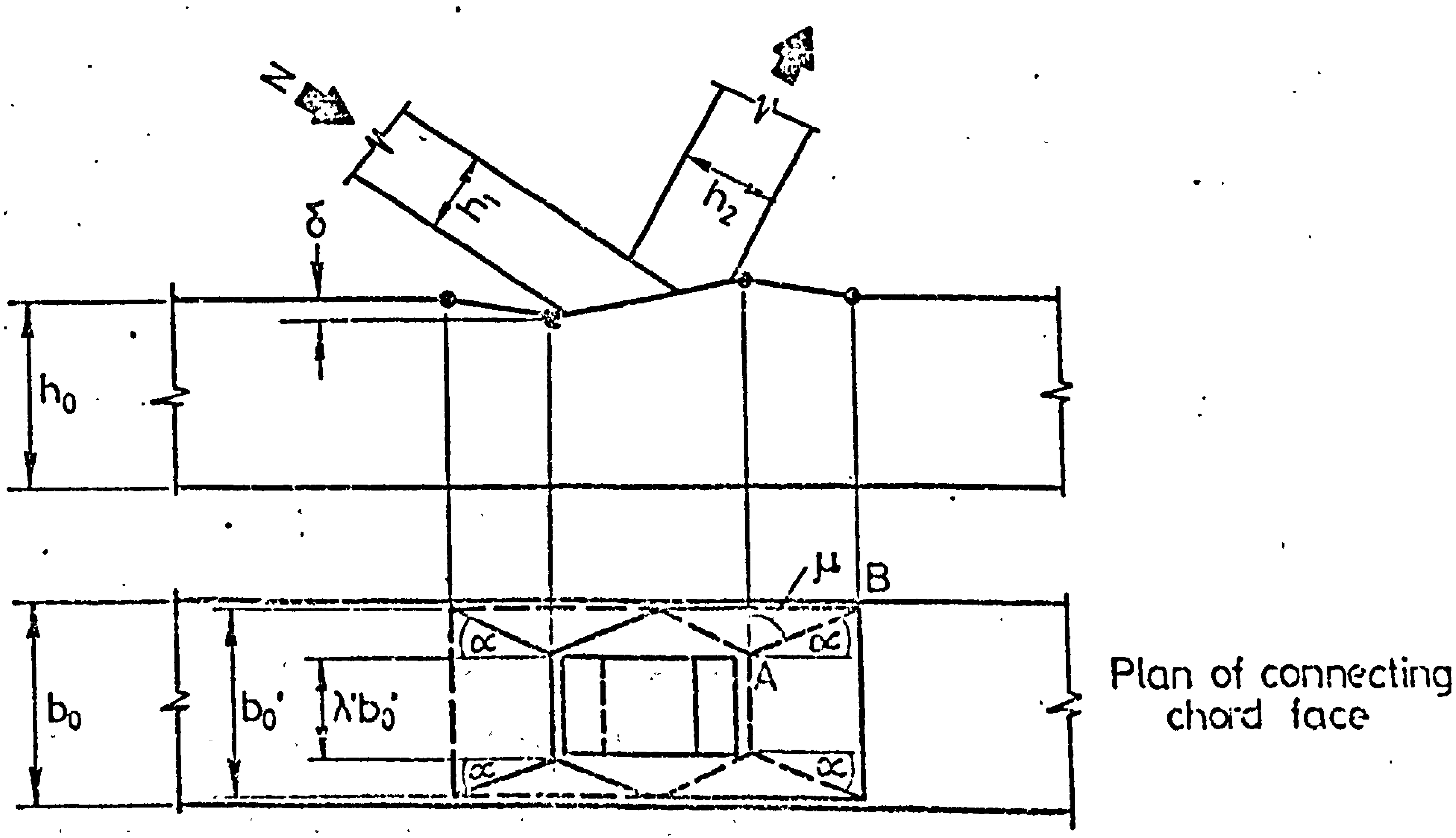

Fig.2.5 Yield line pattern for RHS to RHS Lap joints by Mouty (51)

CHAPTER 3

YIELD STRENGTH OF GAP JOINTS

3.1 Introduction to gap joints

The possible failure modes which have been identified in previous experimental research[9, 10, 71] for RHS gap joints are shown in fig. 3.1, and these are:

(i) Failure of the connecting chord face with little deformation of the chord side walls (G1)

(ii) Failure of the connecting chord face and chord walls around the joint with cracking (G2)

(iii) Chord shear failure (G3)

(iv) Failure of the connecting chord face and chord walls around the joint without cracking (G4)

(v) Cracking leading to failure of the tension bracing member (G5)

(vi) Local buckling of the compression bracing (G6)

(vii) Local buckling of the chord behind the heel of the tension bracing (G7)

(viii) Chord face and chord wall failure around the tension bracing only (G8)

(ix) Chord wall buckling (G9)

The strength of a gap joint may be limited by other failure modes which do not strictly represent joint failures, such as elastic local buckling of any compression member due to axial load only, overall buckling of the strut or attainment of its yield load, or yielding being attained throughout the tie. The failure modes of joints listed in Appendix 1 are described by the notation above. These descriptions are based upon the appearance of a distorted joint specimen at ultimate load, as observed by a particular researcher, but the mode of failure which is noted may not always be the cause of the failure. For example, chord shear failure (G3) is a common cause of failure for gap joints with $\lambda = 1.0$ but this is often reported as chord wall buckling (G9), so not too much emphasis should be placed on the 'observed' failure mode.

3.2 Push-pull mechanisms

For RHS to RHS gap joints with width ratios (λ) less than about 0.8, the most common failure mode is one in which the strut force pushes the chord face inwards and the tie force pulls the chord face outwards, which usually results in cracking of the chord face (G2) but modes G1, G4, G5, G8 and even G9 are all associated with this type of deformation (see fig. 3.1). Figure 3.2 shows the typical appearance of a deformed gap joint in which fracture of the chord face initiated in the joint crotch between the bracing members. This deformation of the connecting chord face is idealized by the yield line mechanism of fig. 3.3(b), in which all the deflection of the chord face is caused by the vertical components of the bracing member forces only. This model is hence known as a 'push-pull' mechanism. In this instance no external loading is applied to the joint, such as a purlin load, and so the vertical components of the bracing member forces (P) will be equal. The area of contact between the bracing members, the chord face and the connecting welds is assumed to remain rigid during deformation.

With regard to the yield line pattern in fig. 3.3, the internal virtual work done by the yield lines for a small deflection δ beneath the compression bracing member can be calculated in a manner similar to Appendix 3 and is given by

$$\frac{8mp_o\delta}{b_o'(1-\lambda_1')}\left\{\frac{b_o'(1-\lambda_1')}{2\mathrm{Tan}\alpha}+\eta_1 b_o'+xg\right\}+\frac{2mp_o b_o'\delta\left[1-(F/Fp)^2\right]}{xg}$$

$$+\frac{8mp_o\delta(1-x)}{b_o'(1-\lambda_2')x}\left\{\frac{b_o'(1-\lambda_2')}{2\mathrm{Tan}\beta}+\eta_2 b_o'+g(1-x)\right\} \qquad (3.01)$$

$$+\frac{4mp_o b_o'\delta\mathrm{Tan}\alpha}{b_o'(1-\lambda_1')}\left[1-(F/Fp)^2\right]+\frac{4mp_o b_o'\ \delta(1-x)\mathrm{Tan}\beta\left[1-(F/Fp)^2\right]}{x.b_o'(1-\lambda_2')}$$

which can be equated to the total external work done of $P\delta/x$.

$$\therefore\ P = 8mp_o\left[\frac{x}{2\mathrm{Tan}\alpha}+\frac{\eta_1 x}{1-\lambda_1'}+\frac{x^2 g}{b_o'(1-\lambda_1')}+\frac{(1-x)}{2\mathrm{Tan}\beta}+\frac{(1-x)\eta_2}{1-\lambda_2'}+\frac{g(1-x)^2}{b_o'(1-\lambda_2')}\right]$$

$$+\ 4mp_o\left[1-(F/Fp)^2\right]\left[\frac{x\mathrm{Tan}\alpha}{1-\lambda_1'}+\frac{(1-x)\mathrm{Tan}\beta}{1-\lambda_2'}+\frac{b_o'}{2g}\right] \qquad (3.02)$$

As P is an upper bound solution, the minimum value is required, and this will occur when $\dfrac{\partial P}{\partial \alpha}=0$, $\dfrac{\partial P}{\partial \beta}=0$ and $\dfrac{\partial P}{\partial x}=0$.

i.e. when
$$\text{Tan}\,\alpha = \frac{\sqrt{1-\lambda_1'}}{\sqrt{1-(F/Fp)^2}}, \tag{3.03}$$

$$\text{Tan}\,\beta = \frac{\sqrt{1-\lambda_2'}}{\sqrt{1-(F/Fp)^2}}, \tag{3.04}$$

and
$$x = \frac{b_o'}{4g\left[\frac{1}{1-\lambda_1'} + \frac{1}{1-\lambda_2'}\right]}\left\{\text{Cot}\,\beta - \text{Cot}\,\alpha + \frac{2\eta_2}{1-\lambda_2'} - \frac{2\eta_1}{1-\lambda_1'} + \frac{4g}{b_o'(1-\lambda_2')}\right.$$
$$\left. - \left[1-(F/Fp)^2\right]\left[\frac{\text{Tan}\,\alpha}{1-\lambda_1'} - \frac{\text{Tan}\,\beta}{1-\lambda_2'}\right]\right\} \tag{3.05}$$

If $F/Fp = 0$, $\lambda_1' = \lambda_2'$ and $\eta_2 = \text{Cosec}\theta_2.\eta_1$ then equation (3.05) simplifies to equation (2.15). Equations (3.03) and (3.04) show that as $|F/Fp|$ increases, Tan α and Tan β increase, which means that the yield pattern on the chord face reduces in size, (see fig. 3.3(c)), and so the joint yield load is slightly reduced by this effect. $|F/Fp|$ similarly has a small influence on the value of x, (equation (3.05)), providing the joint is non-symmetrical. Although this expression for x is the theoretical minimum, the value given by equation (3.05) may not satisfy the assumed yield pattern and therefore be invalid. For example, if a joint has $\lambda_1' = \lambda_2'$ and $\eta_2 = 2\eta_1$ then equation (3.05) gives:

$$x = \frac{\eta_1 b_o'}{4g} + 0.5 ,$$

which may easily be greater than 1.0. In such a case the value of P is monotonically decreasing as x approaches 1.0 giving a minimum value of P at the extreme permissible value of x. So as Davies and Roper[24] have observed that the value of x lies between 0.5 and 1.0, two separate mechanisms will be analysed - one having $x = 0.5$ and the other having $x = 1.0$, which are likely to be the two bounds on the real behaviour.

3.3 The effect of branch member yielding upon the push-pull mechanism yield load.

High concentrations of stress around the toes of the bracing members adjacent to the joint crotch have been identified by previous elastic analyses, so there is the possibility that the toes of the bracing members may yield and cause a different yield line pattern to form in the chord face at perhaps a lower joint yield load. This idea is now investigated to check on the validity of the assumption in §3.2 that the contact area between the chord and bracings remains rigid.

For RHS to RHS gap joints with width ratios (λ) less than about 0.8, which is the range in which the push-pull failure mechanism is likely to occur, the easiest and most common way of welding the bracings to the chord is to use fillet welding rather than butt welding. However, let us assume that there are no fillet welds around the bracing members and that the joint is butt welded which would result in yield lines forming immediately adjacent to the edges of the bracing members as shown in fig.3.4(b).

Yielding at the toe of a bracing member would effectively increase the actual weld gap, g, to g + a, g + b or g + a + b where a is the horizontal length of yielded strut member and b is the horizontal length of yielded tie member. Figure 3.4 shows the case where yielding at the toes of both bracing members increases the effective gap size to g + a + b.

As the effective gap size increases due to yielding of a bracing member toe, the angle of rotation of the two inner hinges at each end of the effective gap decreases, and so less internal virtual work is done in forming the yield-line pattern in the chord face. To counteract this decrease in internal virtual work done, additional virtual work is done in yielding the toes of either of the bracing members and this can be calculated from the approximate extension or compression of a bracing member toe as shown in fig.3.4(c) and (d). Consequently, if the extra virtual work done by the applied loads in yielding the toes of either bracing member is less than the loss in virtual work expended in yielding the chord face, then the externally applied load needed to cause yield failure of the joint may be less than the load without yielding of the bracing members. This will most likely occur if the thickness of the bracing members is small relative to the chord thickness.

Considering fig.3.4, the internal work done in forming the yield line pattern is given by:

$$\frac{8mp_o\ \delta}{b_o'-b_1}\left\{\frac{b_o' - b_1}{2\text{Tan}\ \alpha} + n_1 b_o' + xg\right\}$$

$$+\frac{8mp_o\ \delta(g-xg+b)}{(xg+a)(b_o' - b_2)}\left\{\frac{b_o' - b_2}{2\text{Tan}\ \beta} + n_2 b_o' + g(1-x)\right\} \tag{3.06}$$

$$+ 4b_o'\delta mp_o(1-(F/Fp)^2)\left\{\frac{\text{Tan}\ \alpha}{b_o'-b_1} + \frac{(g-xg+b)\text{Tan}\ \beta}{(xg+a)(b_o'-b_2)} + \frac{1}{2(xg+a)}\right\}$$

The total internal virtual work needed to yield the compression bracing member toe is approximately equal to

$$\frac{\sigma e_1 t_1 \delta a}{xg + a}\left\{b_1 + (a\text{Sin}\theta_1 - t_1)\right\} \tag{3.07}$$

and similarly for the tension bracing member:

$$\frac{\sigma e_2 t_2 \delta b}{xg + a}\left\{b_2 + (b\text{Sin}\theta_2 - t_2)\right\} \tag{3.08}$$

Equating the sum of these three components to the external virtual work done of

$$P\delta + \frac{P\delta(g-xg+b)}{xg + a},$$

gives an expression for the yield load of the joint, P, which will be a minimum when $\frac{\partial P}{\partial \alpha} = 0$, $\frac{\partial P}{\partial \beta} = 0$ and $\frac{\partial P}{\partial x} = 0$.

$$\text{i.e. when Tan}\ \alpha = \sqrt{\frac{b_o' - b_1}{b_o'(1-(F/Fp)^2)}}, \tag{3.09}$$

$$\text{and} \quad \text{Tan}\,\beta = \sqrt{\frac{b_o' - b_2}{b_o'(1-(F/Fp)^2)}}\,, \tag{3.10}$$

$$\text{and} \quad x = \frac{1}{4g\left[\dfrac{1}{b_o'-b_1} + \dfrac{1}{b_o'-b_2}\right]} \left\{ \text{Cot}\,\beta - \text{Cot}\,\alpha + \frac{2\eta_2 b_o'}{b_o'-b_2} - \frac{2\eta_1 b_o'}{b_o'-b_1} + \frac{4g}{b_o'-b_2} \right.$$

$$\left. + \frac{2b}{b_o'-b_2} - \frac{2a}{b_o'-b_1} - \left[1-(F/Fp)^2\right]\left[\frac{\text{Tan}\,\alpha}{b_o'-b_1} - \frac{\text{Tan}\,\beta}{b_o'-b_2}\right]\right\}$$

(3.11)

providing $x \nleq 1.0$.

To assess the significance of the change in yield load of the joint due to yielding in the toes of the bracings, consider a 45^o Warren joint which is entirely symmetrical, made of the same steel grade and having $F = 0$. For such a joint,

$$P = 2\sigma e_o t_o^{\,2} \cdot \frac{(xg + a)}{(g+a+b)} \left\{ \frac{1}{2\sqrt{1-b_1/b_o'}} + \frac{\eta_1}{1-b_1/b_o'} + \frac{xg}{b_o'(1-b_1/b_o')} \right\}$$

$$+ 2\sigma e_o t_o^{\,2} \frac{(g-xg+b)}{(g+a+b)} \left\{ \frac{1}{2\sqrt{1-b_1/b_o'}} + \frac{\eta_2}{1-b_1/b_o'} + \frac{g(1-x)}{b_o'(1-b_1/b_o')} \right\}$$

$$+ \frac{\sigma e_o t_o^{\,2}}{(g+a+b)} \left\{ \frac{xg+a}{\sqrt{1-b_1/b_o'}} + \frac{(g-xg+b)}{\sqrt{1-b_1/b_o'}} + 0.5b_o' \right\}$$

(3.12)

$$+ \frac{\sigma e_o t_1}{(g+a+b)} \left\{ b_1 \ (a+b) + 0.707 \ (a^2+b^2) - t_1 \ (a+b) \right\}$$

with $x = 0.5 + (b-a)/4g$ (3.13)

which implies that $-2g \leq (b-a) \leq 2g$ (3.14)

If a reduction in the joint yield load is possible, then the work done in the chord face must be high compared to the work done in the bracings, so take t_1/t_o to be 0.4 which is a lower practical limit and assume a value for b_1/b_o' of 0.4. With $\eta_1 = 0.5$, $b_o' = 100$ and $t_o = 4$, for example, equation (3.12) then reduces to:

$$\frac{P}{\sigma e_o t_o^2} = \frac{(xg + a)}{(g+a+b)} \left\{ 2.957 + 0.0333 \ xg \right\} + \frac{(g-xg+b)}{(g+a+b)} \left\{ 2.957 + 0.0333 \ g \ (1-x) \right\} + \frac{1}{(g+a+b)} \left\{ 3.84(a+b) + 0.0707(a^2+b^2) + 50 \right\} + 1.291. \tag{3.15}$$

The reduction in joint yield strength due to yielding of the bracing member toes which results is shown in fig. 3.5 for various gap sizes. The minimum yield load has been obtained by considering a whole range of values for a and b within the limits of equation (3.14), and the case in which a = b = 0 corresponds to the yield load of the joint without any yielding in the toes of the bracing members. It can be seen that even for this extreme thickness ratio between the bracings and chord, there is no possibility of a lower yield load for the joint except at very small gap sizes. (With hybrid trusses in which the chord member is of a higher steel grade than the bracing members, an effective reduction in the thickness ratio t_1/t_o will also be caused). At such a gap size shear failure would normally occur in the joint gap and pre-empt the formation of a yield line mechanism.

Hence it can be concluded that for butt welded joints, yielding of the bracing member toes is unlikely to ever cause a yield load which is lower than that calculated by considering the ends of the bracing members as being rigid. Normally all gap joints which are less than full width ($\lambda < 1.0$) would be fillet welded, in which case additional internal virtual work would need to be done to cause the connecting welds to yield at point e on fig. 3.4(c) and (d), making the possibility of a reduction in yield load even more remote for fillet welded joints. Thus the assumption of §3.2 that the contact area between the chord and bracings remains rigid, is permissible, and gap joints of less than full width will tend to develop the yield line pattern around the bracings shown in fig.3.3, which also assumes that fillet welding is the normal practice.

3.4 Comparison of push-pull mechanism yield loads with test results.

There is no agreement at present on how to define the yield load of a lattice girder joint in structural hollow sections from the experimental load-deflection characteristics. Load-deflection curves for the connecting chord face vary from curve a to curve b in fig. 3.6, so the joint yield load is not necessarily distinct and the trend has been to relate experimental results and empirical deductions to the ultimate joint load, which is simply the maximum load attained. In Chapter 2 a method by Hohl[37] for determining the joint yield load has been mentioned, based upon calculating the total deflection of the joint intersection using a Williot diagram analysis, but this method is dependent upon the member sizes and the testing rig used.

Mouty[51] took the load corresponding to a local deflection of 1% of the chord width (b_o) as the joint yield load whereas the traditional method has been to interpret the yield load from the load v. deflection diagram of the connecting chord face, where possible, in the manner shown for curve b in fig. 3.6. All of these methods are only approximate and the latter has been used in this case as it is more generally accepted. Gap joints are more typical of the deformation given by curve b than curve a in fig. 3.6 but the determination of the yield load is still subjective by this method. For the isolated Warren joint illustrated in fig. 3.6 (curve b) it can be seen that the load given by a deformation of 1% of the chord width is slightly higher, but similar, to the yield load obtained by the method chosen.

To calculate the theoretical yield load of a gapped joint the push-pull mechanism outlined in §3.2, which corresponds to fig. 3.3, has been used, with the assumption that the ends of the bracing members remain rigid at the connection to the chord face. The joint yield load is hence given by equations (3.02), (3.03) and (3.04) with two cases considered for each joint; one having $x = 0.5$ and the other having $x = 1.0$. The yield load of the joint is then taken as the lower yield load predicted by each of these two cases, although in general the two values are very close to each other.

Of the RHS to RHS gap joints listed in Appendix 1, some tests included measurements for the load v. deflection of the chord face beneath the compression bracing member, and so the joint yield load could usually be ascertained for such tests in the manner described above. Correlation between the actual and theoretical joint yield loads for 41 RHS to RHS gap joints with width ratios less than 1.0 is shown in fig. 3.7. The agreement obtained is resonably good for most joints, with theoretical predictions of the joint yield load usually erring on the conservative (safe) side. The interpretation of the experimental yield load is probably the cause of poor correlation for joint P6BI (fig. 3.7) as good agreement is achieved for the ultimate load prediction of this joint (Chapter 4).

3.5 Other modes of deformation for gap joints

At the start of this chapter the possible failure modes for gapped joints were introduced and these are shown diagramatically in fig. 3.1. Those which are not a result of the push-pull action of the bracing members on the connecting chord face are:

(i) Local buckling of the compression bracing (G6)

(ii) Local buckling of the chord behind the heel of the tension bracing (G7), and

(iii) Chord shear failure (G3)

Failure modes (i) and (ii) above are unstable forms of deformation as unloading of the joint would take place once the yield load was reached. i.e. the yield load also corresponds to the ultimate load of the failure 'mechanism'. Local buckling of the compression bracing and local buckling of the chord are hence discussed in the next chapter which deals with the ultimate strength of gapped joints.

A joint which fails by shearing of the chord, on the other hand, does have a small reserve of strength after attaining the shear yield load of the chord side walls as shown in fig. 3.8. This type of failure can occur when joints have a width ratio near 1.0. Assuming a chord shear area of $2h_o t_o$ and a Von Mises shear yield criterion with reduction due to axial loading[39] in the chord, the chord shear yield load is given by:

$$P \cong \frac{2h_o t_o \sigma e_o}{\sqrt{3}} \cdot \sqrt{1-(F/Fp)^2} \tag{3.16}$$

This expression does not include the horizontal component of the compression bracing member force in the axial chord load, as the effect of the compression bracing member force is complex. Equation (3.16) tends to be conservative in the estimation of the shear yield strength.

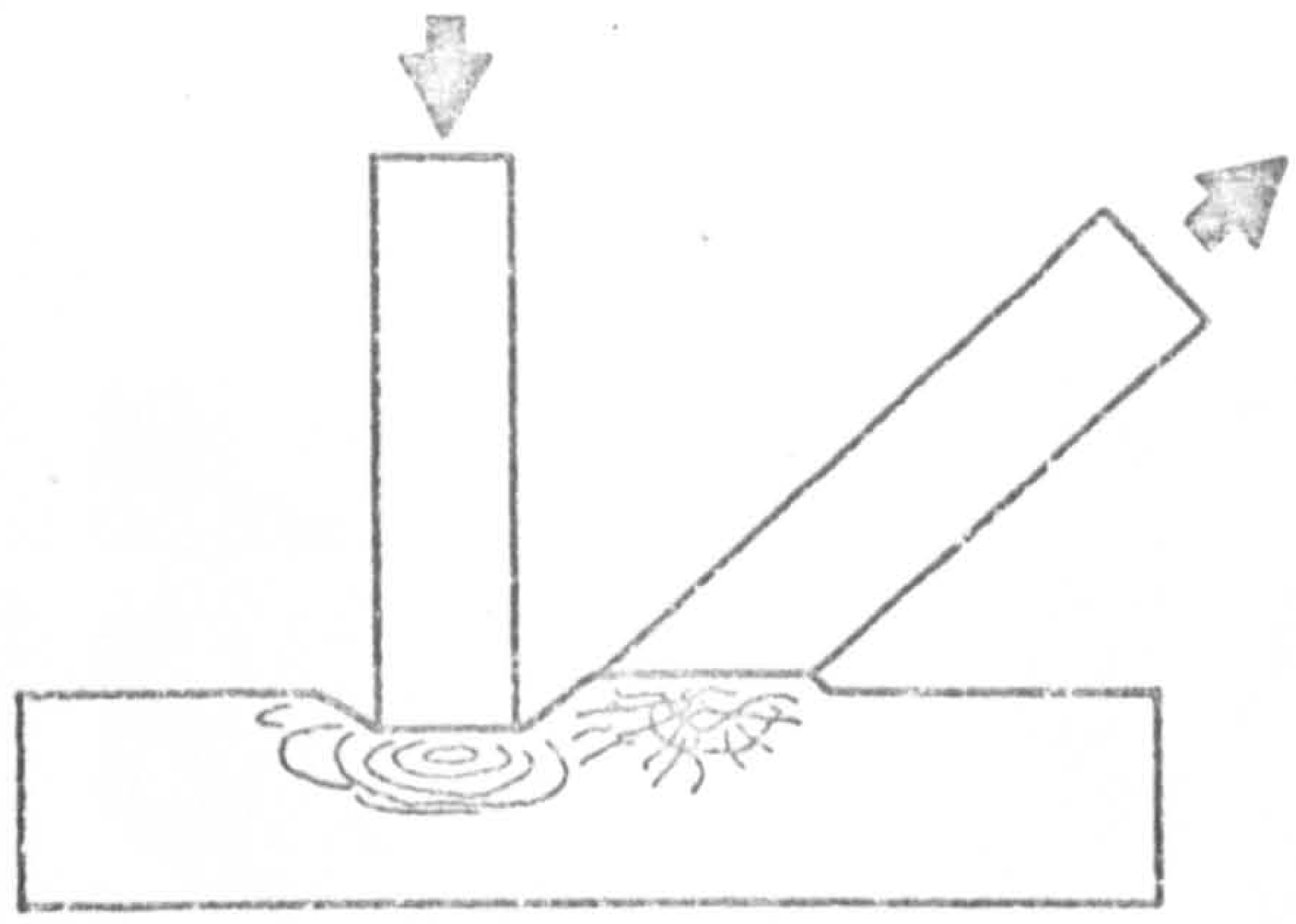

Chord face failure with little deformation of the chord side walls (G1)

Chord face and chord wall failure around the joint with cracking (G2)

Chord face and chord wall failure around the joint without cracking (G4)

Cracking leading to tie failure (G5)

Chord face and chord wall failure around tension bracing only (G8)

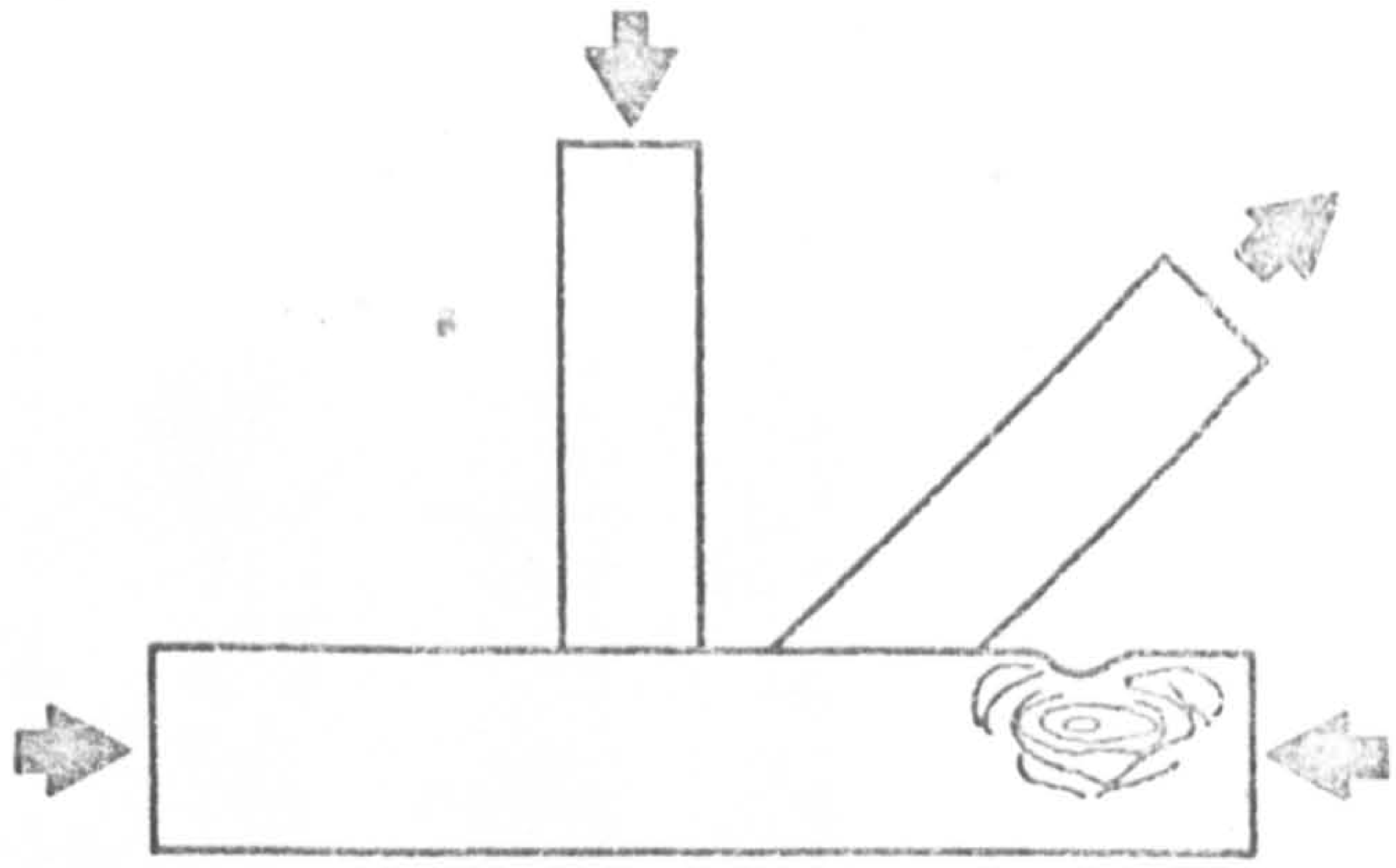

Local buckling of the chord behind the heel of the tension bracing (G7)

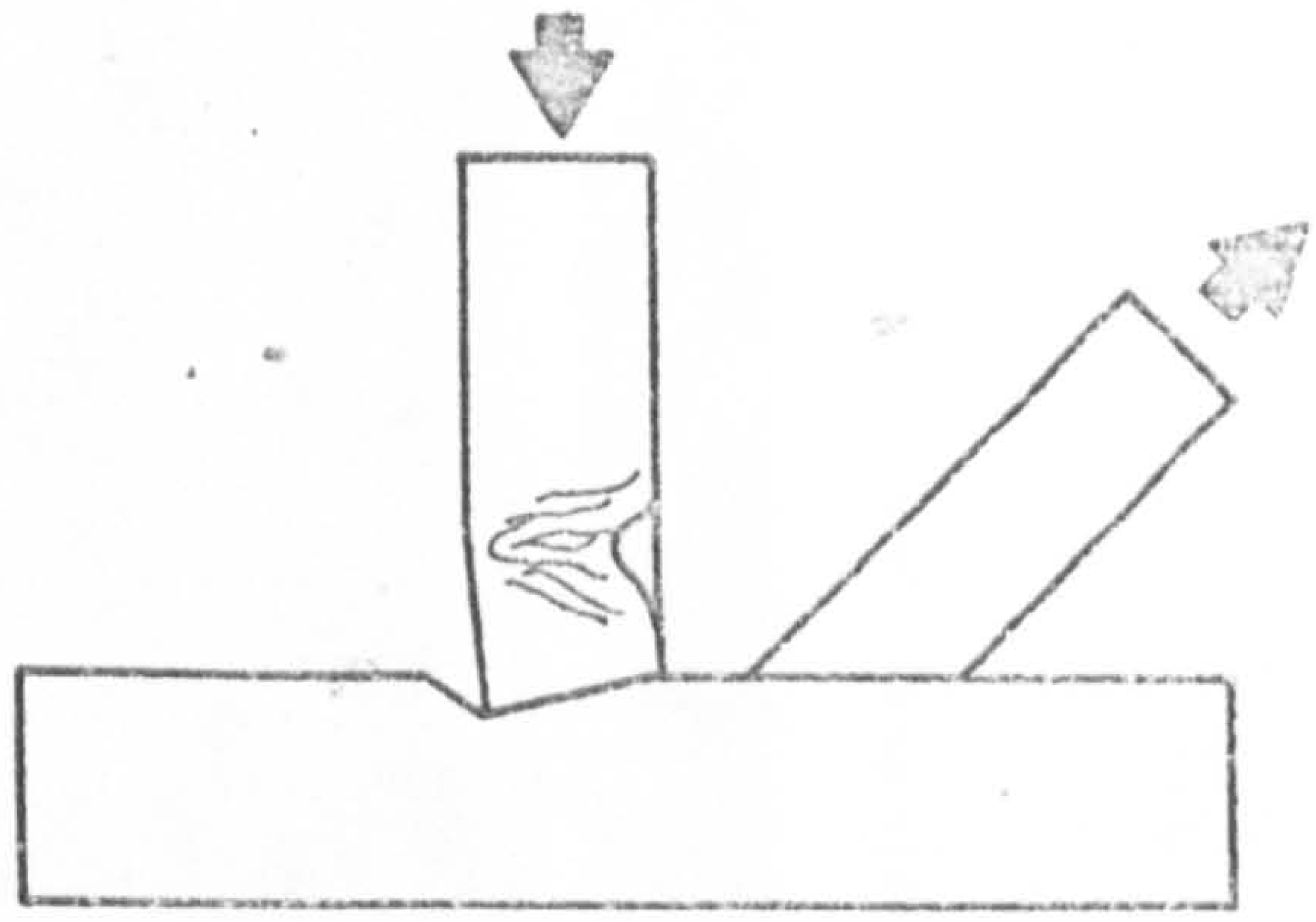

Local buckling of the compression bracing (G6)

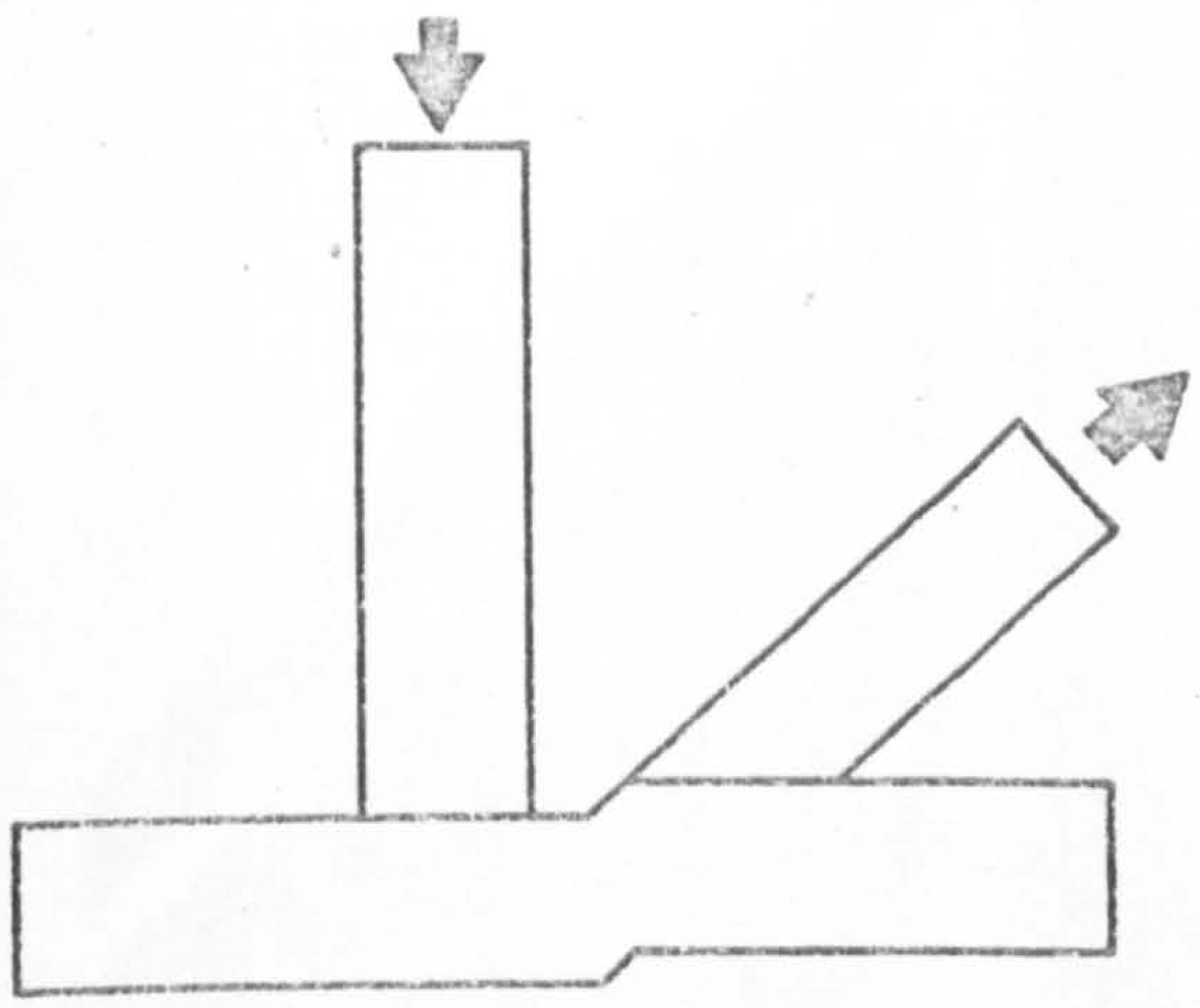

Chord shear failure (G3)

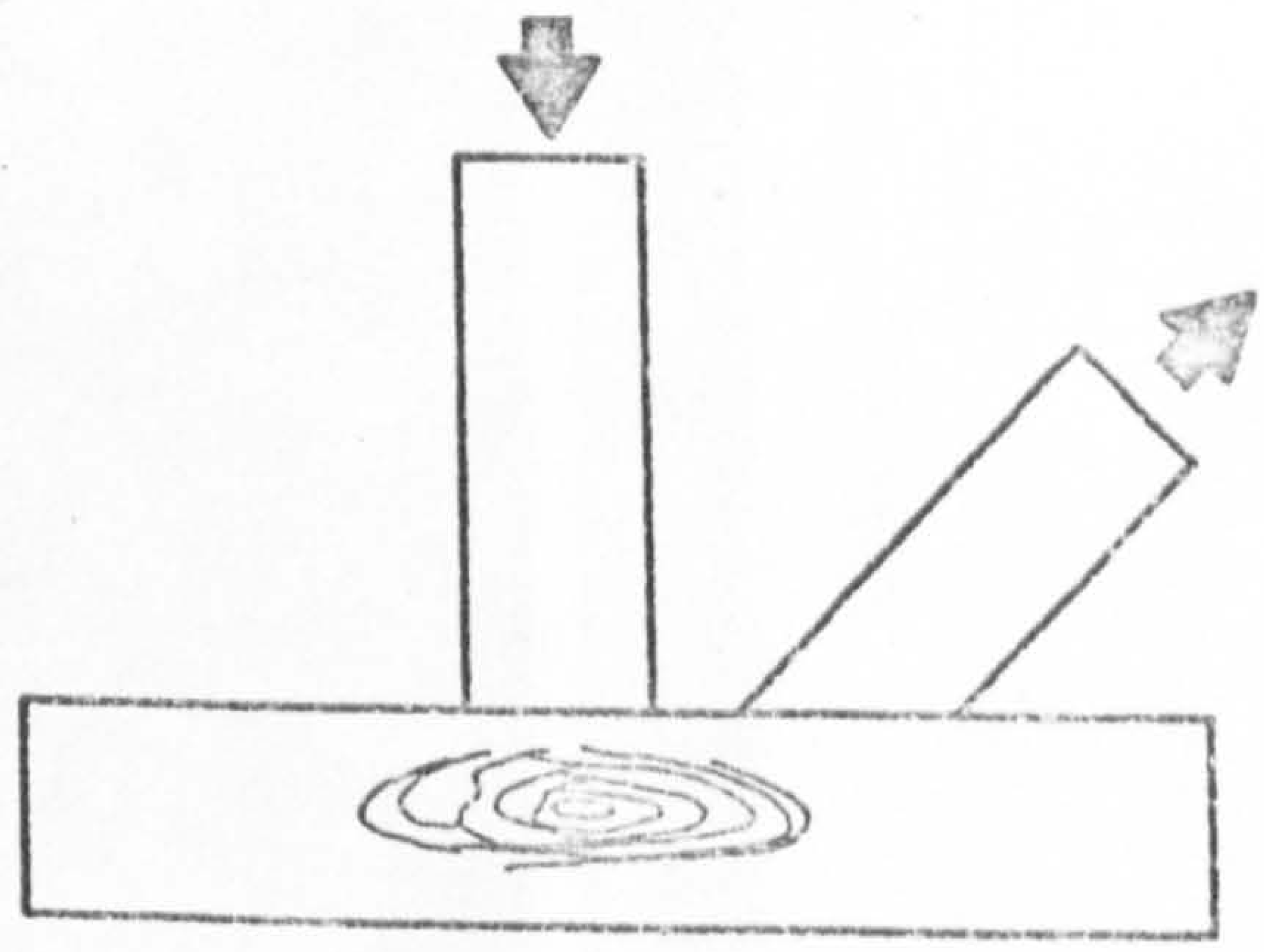

Chord wall buckling (G9)

Fig.3·1 Gap joint failure modes

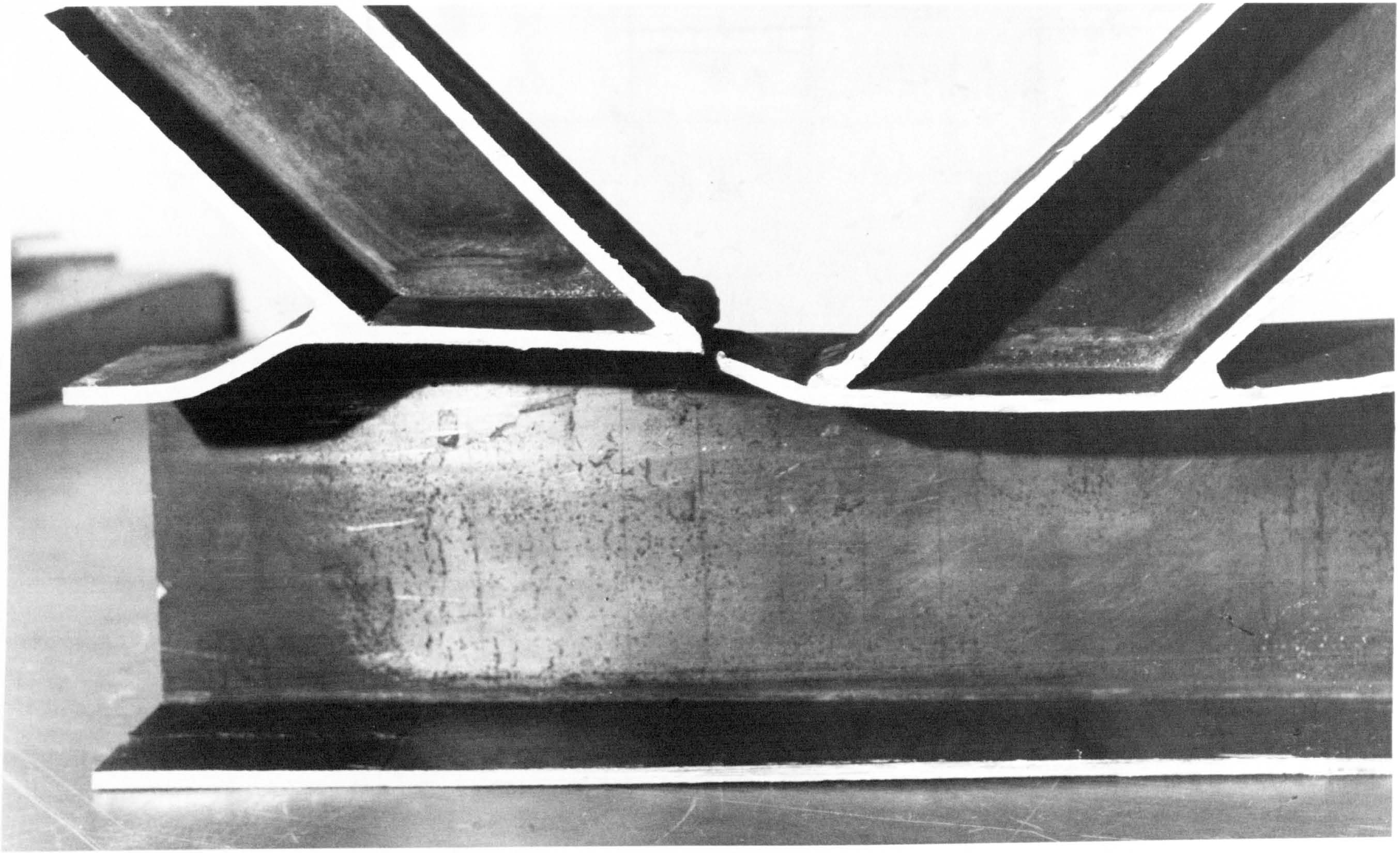

Fig. 3.2 Typical appearance of a deformed gap joint (section view)

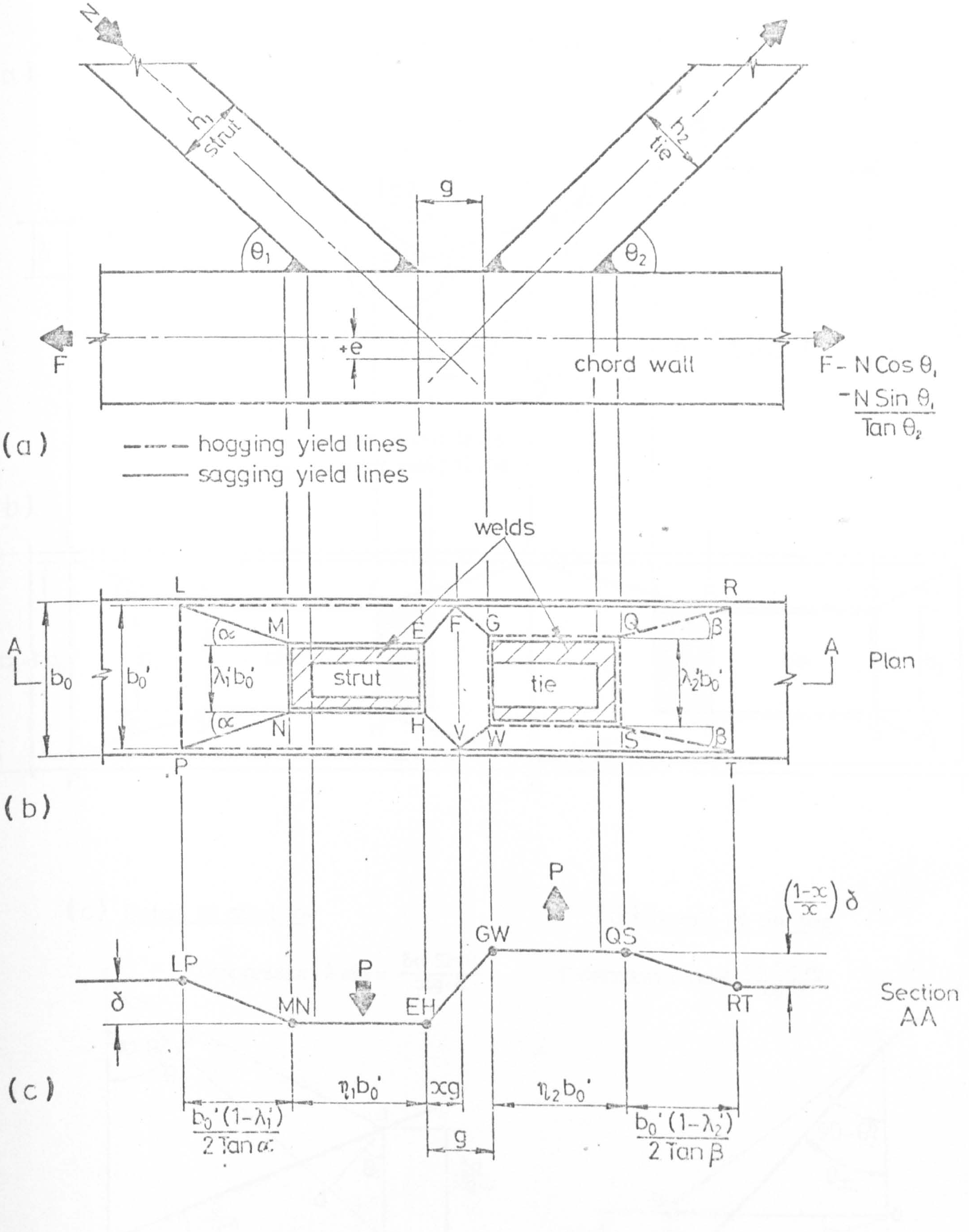

Fig.3·3 Yield line pattern for small deflections of chord face

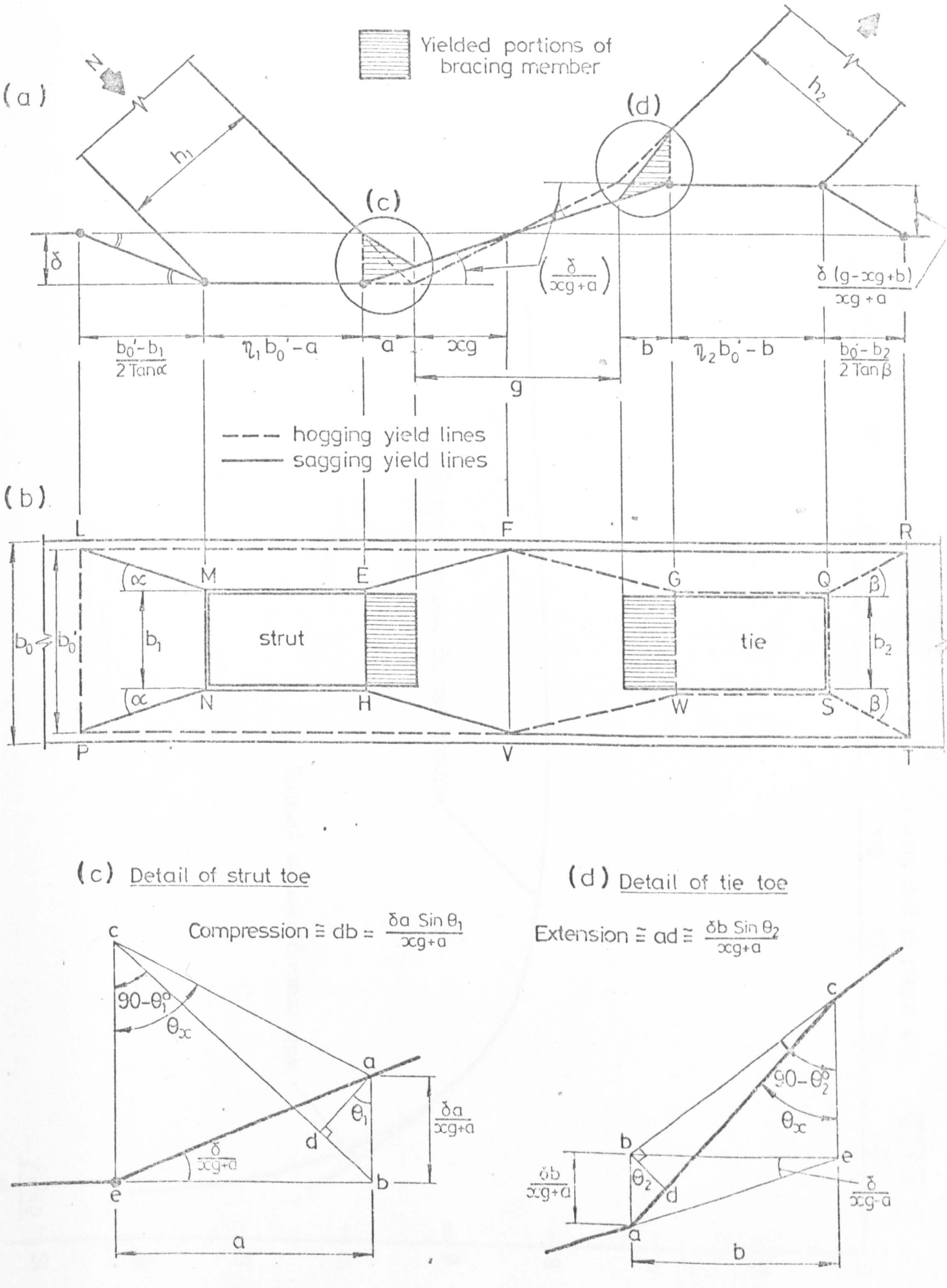

Fig.3.4 The effect of branch member yielding upon the push-pull mechanism

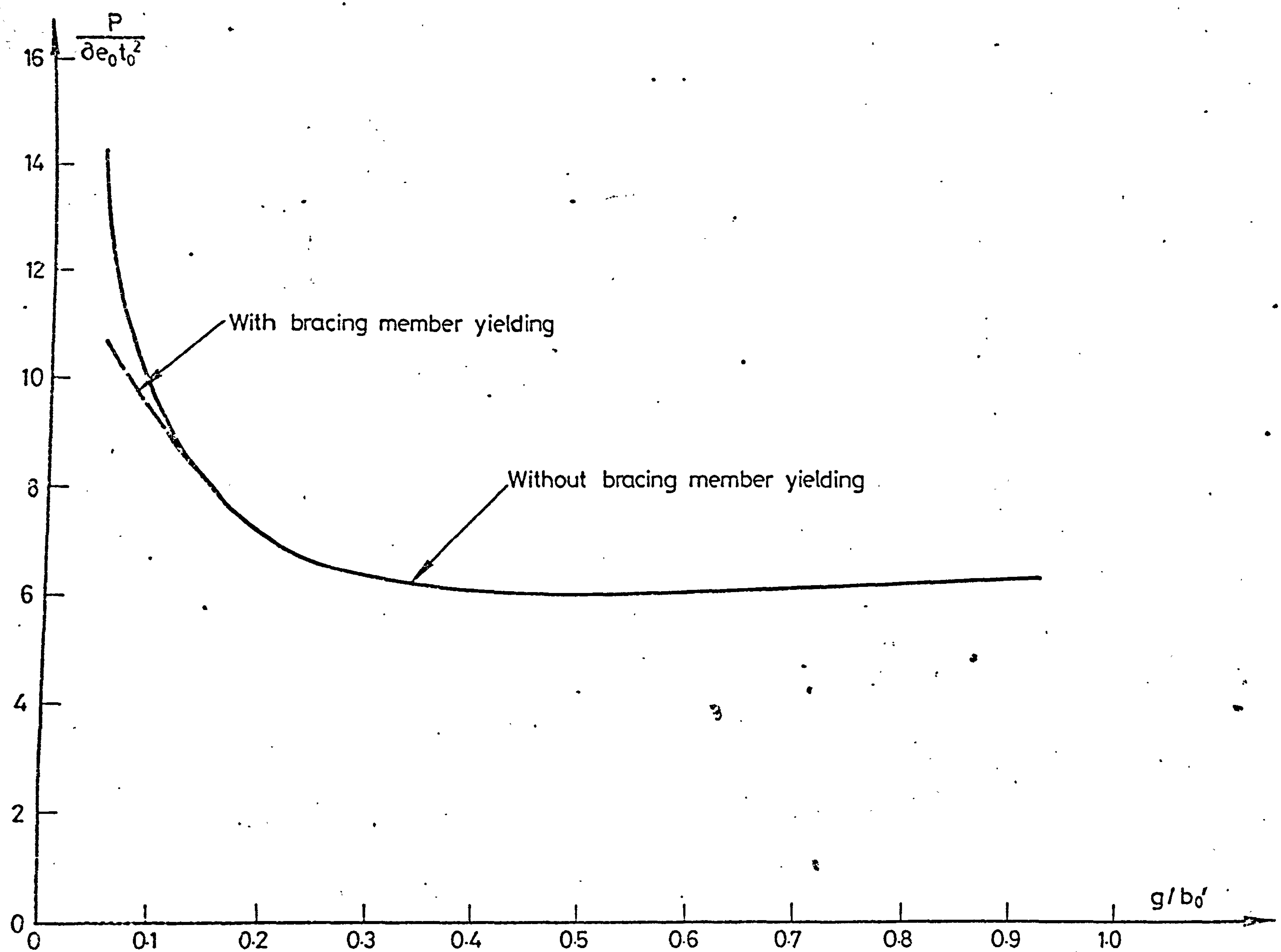

Fig.3·5 The effect of gap size upon the joint yield strength with yielding at the toes of the bracing members

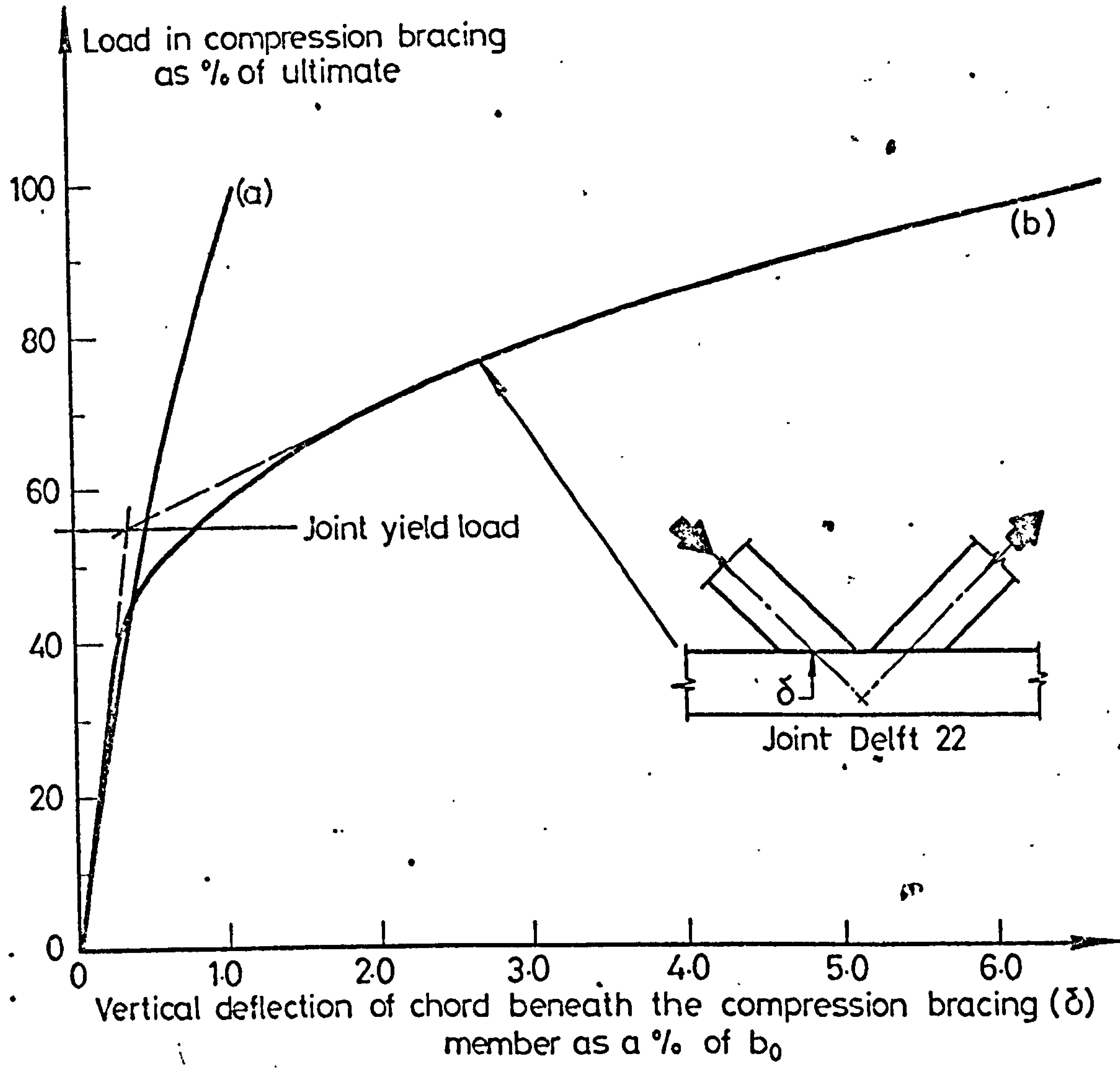

Fig.3·6 Definition of joint yield load

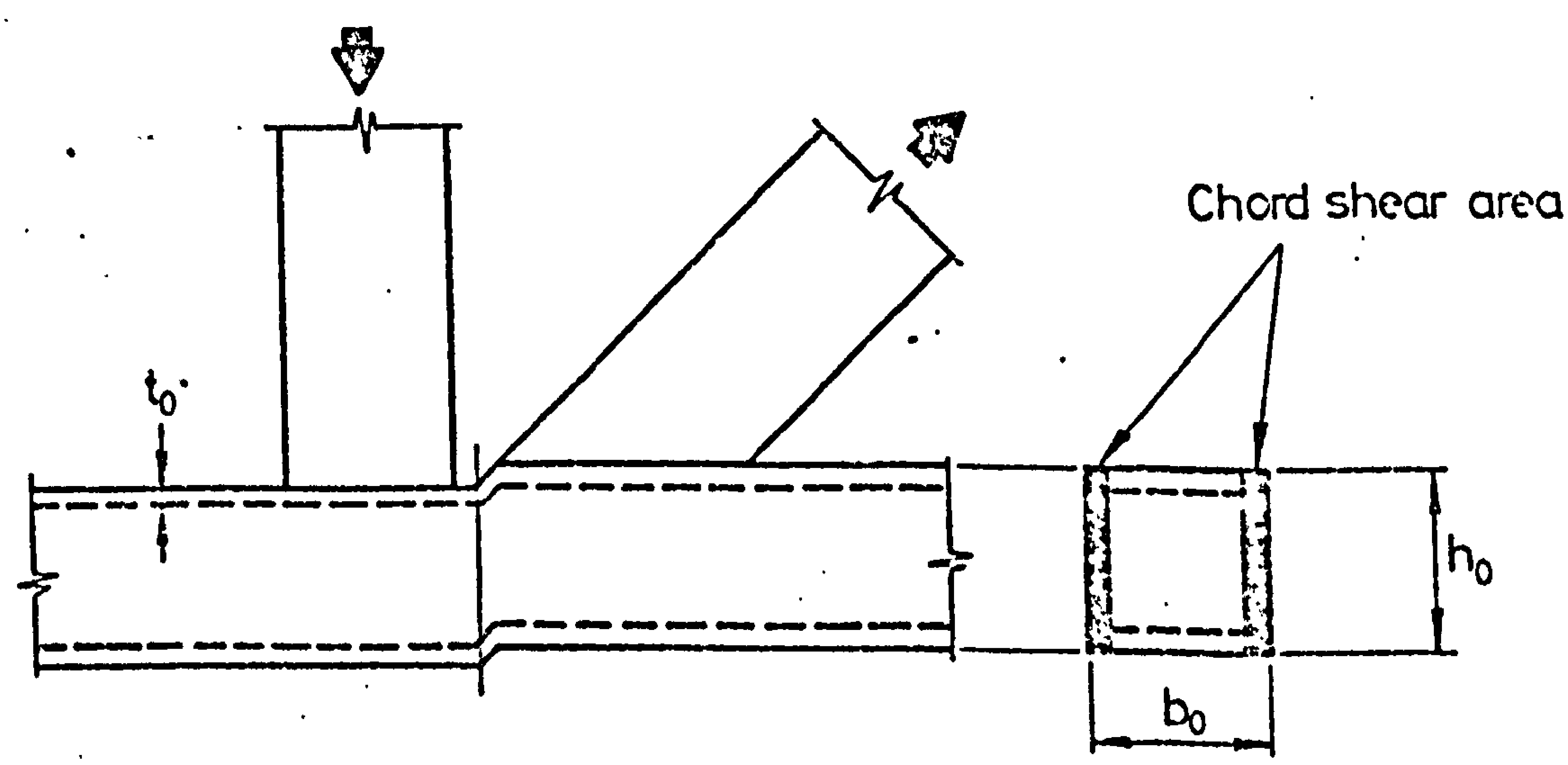

Fig.3·8 Chord shear yielding for RHS chord gap joint

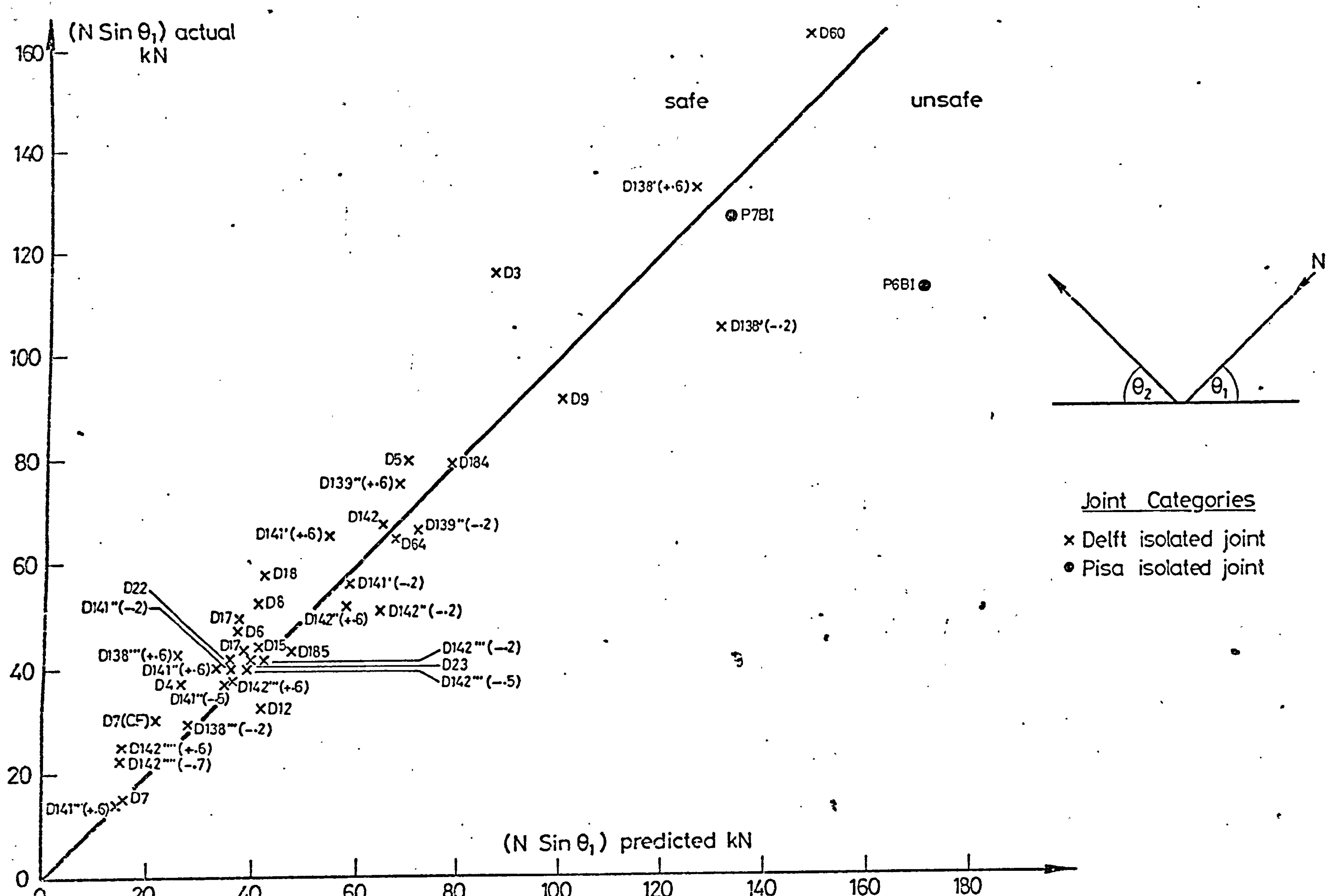

Fig.3·7 Actual v. predicted yield loads for RHS to RHS gap joints

CHAPTER 4

ULTIMATE STRENGTH OF GAP JOINTS

4.1 Large deflection push-pull mechanisms

The two yield line patterns which may form in the chord face around the bracing members of a gapped joint at the yield load are shown in figs 4.1(b), (for the case in which the point of zero deflection of the chord face is in the middle of the clear weld gap), and fig. 4.2(b), (for the case in which the point of zero deflection of the chord face is adjacent to the toe of the tension bracing member). As the yield line patterns undergo large deformations above the yield load and up to the ultimate load, it is assumed that the bracing members maintain their horizontal distance apart and only move vertically up or down, which causes stretching of the panel EFGWVH, (figs 4.1(b) and 4.2(b)), and hence membrane forces in the joint crotch. The chord side walls are considered to be flexible, which Mouty[51] also believes to be valid (Chapter 2), and capable of moving towards each other, hence producing very little membrane action transverse to the chord.

As the mechanisms deform it has been assumed that the ends of the yield line pattern LP and RT in fig. 4.1(b), or LP in fig. 4.2(b), maintain their position on the chord member, yet no membrane action is considered to be formed by stretching of the panels LMNP and QRTS in fig. 4.1(b), or panel LMNP in fig. 4.2(b). It is thought that the yield lines LP and RT readjust themselves to reduce the force in these membranes, probably by developing an extensive yielded area around the lines LP and RT. In practice it seems that any membrane action developed in these ends is relatively low, and this observation is supported by Mouty[51]. The lengths J_i on figs 4.1(c) and 4.2(c) are taken to be the same as for the small deflection yield line pattern.

i.e. $$J_i = 0.5b_o'\sqrt{1-\lambda_1'}.\sqrt{1-(F/Fp)^2} \qquad (4.01)$$

For both yield line mechanisms it is assumed that there is no purlin or applied load on the joint and the vertical components of the bracing member forces are then equal. The load-deflection relationship is found by means of a simple rigid-plastic geometrical folding of the plates accompanied by membrane action in the crotch. The plastic moment of resistance (mp_i) of all yield lines is reduced by the effect of the axial chord force according to equation (2.19) by Mouty[51]. The membrane force in the crotch is calculated from the change in distance between the yield lines EH and GW, (figs 4.1(b) and 4.2(b)), based upon an assumed effective crotch width and an assumed strain-hardening modulus. As the vertical deflection of the bracing members (δ) in the yield line mechanisms of fig. 4.1 or fig. 4.2 increases by an increment $\Delta\delta$, the rotation of each yield line in the chord face and the strain in the crotch produce an incremental change in the internal virtual work done by the mechanism.

4.1.1 Mechanism with x = 0.5

Referring to fig. 4.1 and letting $\Delta\ell$ be the incremental extension of the inner crotch panel as the mechanism deflects from δ to $\delta + \Delta\delta$, then

$$\Delta \ell = g\text{Sec}(\theta+\Delta\theta) - g\text{Sec}\theta \tag{4.02}$$

$$\delta = g\text{Tan}\theta/2 \text{ , so}$$

$$\Delta\delta = g\text{Tan}(\theta+\Delta\theta)/2 - g\text{Tan}\theta/2 \tag{4.03}$$

where θ = rotation of yield lines EH and GW. Letting the rotation of yield lines LP and MN be ϕ_1 and the rotation of lines QS and RT be ϕ_2,

$$\phi_1 = \text{Tan}^{-1}(g\text{Tan}\theta/2J_1)$$

$$\therefore \quad \Delta\phi_1 = \text{Tan}^{-1}(g\text{Tan}(\theta+\Delta\theta)/2J_1) - \text{Tan}^{-1}(g\text{Tan}\theta/2J_1) \tag{4.04}$$

Similarly,

$$\Delta\phi_2 = \text{Tan}^{-1}(g\text{Tan}(\theta+\Delta\theta)/2J_2) - \text{Tan}^{-1}(g\text{Tan}\theta/2J_2) \tag{4.05}$$

Letting the rotation of yield lines LF, ME, NH and PV be γ_1, and the rotation of lines FR, GQ, WS and VT be γ_2, then

$$\delta = b_o'(1-\lambda_1')\text{Sin}\gamma_1/2 \text{ and so } \gamma_1 = \text{Sin}^{-1}\frac{g\text{Tan}\theta}{b_o'(1-\lambda_1')}$$

$$\therefore \quad \Delta\gamma_1 = \text{Sin}^{-1}\left(\frac{g\text{Tan}(\theta+\Delta\theta)}{b_o'(1-\lambda_1')}\right) - \text{Sin}^{-1}\left(\frac{g\text{Tan}\theta}{b_o'(1-\lambda_1')}\right) \tag{4.06}$$

Similarly,

$$\Delta\gamma_2 = \text{Sin}^{-1}\left(\frac{g\text{Tan}(\theta+\Delta\theta)}{b_o'(1-\lambda_2')}\right) - \text{Sin}^{-1}\left(\frac{g\text{Tan}\theta}{b_o'(1-\lambda_2')}\right) \tag{4.07}$$

Letting the rotation of yield lines LM and NP be β_1, and the rotation of lines QR and ST be β_2, then

$$\Delta\beta_1 = \sin^{-1}\left(\frac{g\tan(\theta+\Delta\theta).J_1}{b_o'(1-\lambda_1').LM}\right) - \sin^{-1}\left(\frac{g\tan\theta.J_1}{b_o'(1-\lambda_1').LM}\right) \quad (4.08)$$

$$+ \tan^{-1}\left(\frac{g\tan(\theta+\Delta\theta).b_o'(1-\lambda_1')}{2J_1.2LM}\right) - \tan^{-1}\left(\frac{g\tan\theta.b_o'(1-\lambda_1')}{2J_1.2LM}\right)$$

where $LM = \sqrt{(b_o'(1-\lambda_1')/2)^2 + J_1^2}$ (4.09)

Similarly,

$$\Delta\beta_2 = \sin^{-1}\left(\frac{g\tan(\theta+\Delta\theta).J_2}{b_o'(1-\lambda_2').QR}\right) - \sin^{-1}\left(\frac{g\tan\theta.J_2}{b_o'(1-\lambda_2').QR}\right) \quad (4.10)$$

$$+ \tan^{-1}\left(\frac{g\tan(\theta+\Delta\theta).b_o'(1-\lambda_2')}{2J_2.2QR}\right) - \tan^{-1}\left(\frac{g\tan\theta.b_o'(1-\lambda_2')}{2J_2.2QR}\right)$$

where $QR = \sqrt{(b_o'(1-\lambda_2')/2)^2 + J_2^2}$ (4.11)

Letting the rotation of yield lines EF and HV be α_1, and the rotation of lines FG and VW be α_2, then

$$\Delta\alpha_1 = \sin^{-1}\left(\frac{g\tan(\theta+\Delta\theta).g}{b_o'(1-\lambda_1').2EF}\right) - \sin^{-1}\left(\frac{g\tan\theta.g}{b_o'(1-\lambda_1').2EF}\right)$$

$$+ \tan^{-1}\left(\frac{\tan(\theta+\Delta\theta).b_o'(1-\lambda_1')}{2EF}\right) - \tan^{-1}\left(\frac{\tan\theta.b_o'(1-\lambda_1')}{2EF}\right)$$

(4.12)

where $EF = \sqrt{(g/2)^2 + (b_o'(1-\lambda_1')/2)^2}$ (4.13)

Similarly,

$$\Delta\alpha_2 = \sin^{-1}\left(\frac{g\tan(\theta+\Delta\theta).g}{b_o'(1-\lambda_2').2FG}\right) - \sin^{-1}\left(\frac{g\tan\theta.g}{b_o'(1-\lambda_2').2FG}\right)$$

$$+ \tan^{-1}\left(\frac{\tan(\theta+\Delta\theta).b_o'(1-\lambda_2')}{2FG}\right) - \tan^{-1}\left(\frac{\tan\theta.b_o'(1-\lambda_2')}{2FG}\right)$$

(4.14)

where $FG = \sqrt{(g/2)^2 + (b_o'(1-\lambda_1')/2)^2}$ (4.15)

For any deflection, the total extension of the membrane is $gSec\theta-g$ which represents a total strain of $Sec\theta-1$. The membrane force in the crotch will act between the bracing members and is hence assumed to be distributed over a width of $(b_1+b_2)/2$. If a linear strain-hardening slope is chosen for the crotch material, then the stress/strain line can only coincide with the real stress/strain curve of the crotch material at one particular point beyond yield. The main point of interest is the average ultimate strain in the crotch material and so a bilinear stress-strain model with a strain hardening modulus of $E_{sh} = E/300$ would be suitable, as shown in fig. 4.3. Using the guaranteed mechanical properties for hollow sections[7], the difference between the yield and ultimate stresses and the amount of elongation at failure vary between the different steel grades, but a value of $E_{sh} = E/300$ will produce an ultimate strain which is near the minimum average elongation of the various steels (20%).

By using a value of $E_{sh} = E/300$ one would also only expect the load-deflection behaviour to coincide with that of a real joint near failure in the crotch, and to model the load-deflection curve of a joint accurately a strain-hardening modulus which varies with strain would be needed. For the value of E, the ECCS recommends 210 kN/mm^2[34], whereas British Standards are proposing a value of 206 kN/mm^2[8].

Hence, if $Sec\theta-1 \leq \varepsilon y_o$, $S = (b_1+b_2)t_oE(Sec\theta-1)/2$

and if $Sec\theta-1 > \varepsilon y_o$, $S = (b_1+b_2)t_o\sigma e_o/2$

$$+ (b_1+b_2)t_o(Sec\theta-1-\varepsilon y_o)E_{sh}/2 \quad (4.16)$$

So as the vertical deflection of the bracing members increases by an increment $\Delta\delta$, the rotation of each yield line in the chord face and the strain in the crotch produce an incremental change in the internal virtual work done by the mechanism, which can be equated to the incremental change in external work done by the applied forces.

$\therefore$ $2P\Delta\delta$

$$\begin{aligned}
&\simeq (1+\lambda_1')b_o'mp_o\Delta\phi_1(1-(F/Fp)^2) + (1+\lambda_2')b_o'mp_o\Delta\phi_2(1-(F/Fp)^2) \\
&+ (\lambda_1'+\lambda_2')b_o'mp_o(1-(S/Sp)^2)\Delta\theta, \text{ subject to } S = Sp \text{ if } S > Sp, \\
&+ (4\eta_1 b_o'+g+2J_1)mp_o\Delta\gamma_1 + (4\eta_2 b_o'+g+2J_2)mp_o\Delta\gamma_2 \qquad (4.17) \\
&+ 2LMmp_o\Delta\beta_1(1-(F/Fp)^2.\text{Cos}^4\chi_1) + 2QRmp_o\Delta\beta_2(1-(F/Fp)^2.\text{Cos}^4\chi_2) \\
&+ 2EFmp_o\Delta\alpha_1(1-(F/Fp)^2.\text{Cos}^4 Z_1) + 2FGmp_o\Delta\alpha_2(1-(F/Fp)^2.\text{Cos}^4 Z_2) \\
&+ S.\Delta\ell
\end{aligned}$$

where $\text{Cos}\chi_1 = b_o'(1-\lambda_1')/2LM$, $\text{Cos}\chi_2 = b_o'(1-\lambda_2')/2QR$,

$\text{Cos}Z_1 = b_o'(1-\lambda_1')/2EF$ and $\text{Cos}Z_2 = b_o'(1-\lambda_2')/2FG$.

From equation (4.17) the P v. δ relationship can then be calculated for any particular value of F.

4.1.2 Mechanism with x = 1.0

The mechanism having x = 1.0, in which all deformation is caused by the pushing-in of the strut member, is shown in fig. 4.2. By using the same notation for yield line rotations as in §4.1.1 (with x = 0.5), it can be found that:

$$\Delta\delta = g\text{Tan}(\theta+\Delta\theta) - g\text{Tan}\theta \tag{4.18}$$

and

$$\Delta\ell = g\text{Sec}(\theta+\Delta\theta) - g\text{Sec}\theta \tag{4.19}$$

$$\Delta\phi_1 = \text{Tan}^{-1}(g\text{Tan}(\theta+\Delta\theta)/J_1) - \text{Tan}^{-1}(g\text{Tan}\theta/J_1) \tag{4.20}$$

$$\Delta\gamma_1 = \text{Sin}^{-1}\left(\frac{2g\text{Tan}(\theta+\Delta\theta)}{b_o'(1-\lambda_1')}\right) - \text{Sin}^{-1}\left(\frac{2g\text{Tan}\theta}{b_o'(1-\lambda_1')}\right) \tag{4.21}$$

$$\Delta\beta_1 = \text{Sin}^{-1}\left(\frac{2g\text{Tan}(\theta+\Delta\theta).J_1}{b_o'(1-\lambda_1').LM}\right) - \text{Sin}^{-1}\left(\frac{2g\text{Tan}\theta.J_1}{b_o'(1-\lambda_1').LM}\right) \tag{4.22}$$

$$+ \text{Tan}^{-1}\left(\frac{g\text{Tan}(\theta+\Delta\theta).b_o'(1-\lambda_1')}{J_1.2LM}\right) - \text{Tan}^{-1}\left(\frac{g\text{Tan}\theta.b_o'(1-\lambda_1')}{J_1.2LM}\right)$$

where $LM = \sqrt{(b_o'(1-\lambda_1')/2)^2 + J_1^2}$ (4.23)

$$\Delta\alpha_1 = \text{Sin}^{-1}\left(\frac{2g\text{Tan}(\theta+\Delta\theta).g}{b_o'(1-\lambda_1')EF}\right) - \text{Sin}^{-1}\left(\frac{2g\text{Tan}\theta.g}{b_o'(1-\lambda_1')EF}\right) \tag{4.24}$$

$$+ \text{Tan}^{-1}\left(\frac{\text{Tan}(\theta+\Delta\theta).b_o'(1-\lambda_1')}{2EF}\right) - \text{Tan}^{-1}\left(\frac{\text{Tan}\theta.b_o'(1-\lambda_1')}{2EF}\right)$$

where $EF = \sqrt{g^2 + (b_o'(1-\lambda_1')/2)^2}$ (4.25)

The total strain in the crotch is again given by $\text{Sec}\theta-1$ and the membrane force now acts over a width of b_1. The same assumptions for strain-hardening of the crotch material in §4.1.1 (with x = 0.5) are again used. Hence,

$$\text{If } \text{Sec}\theta-1 \leq \varepsilon y_o,\ S = b_1 t_o E(\text{Sec}\theta-1)$$

$$\text{and if } \text{Sec}\theta-1 > \varepsilon y_o,\ S = b_1 t_o \sigma e_o + b_1 t_o(\text{Sec}\theta-1-\varepsilon y_o)E_{sh} \tag{4.26}$$

Equating the internal virtual work done to the external work done, gives:

$$P\Delta\delta \cong (1+\lambda_1{}')b_o{}'mp_o\Delta\phi_1(1-(F/Fp)^2)$$

$$+ (1+\lambda_1{}')b_o{}'mp_o(1-(S/Sp)^2)\Delta\theta, \text{ subject to } S = Sp \text{ if } S > Sp,$$

$$+ (4\eta_1 b_o{}'+2g+2J_1)mp_o\Delta\gamma_1 \tag{4.27}$$

$$+ 2LMmp_o\Delta\beta_1(1-(F/Fp)^2.\mathrm{Cos}^4\chi_1)$$

$$+ 2EFmp_o\Delta\alpha_1(1-(F/Fp)^2.\mathrm{Cos}^4\Xi_1) + S\Delta\ell$$

where $\mathrm{Cos}\chi_1$ is given in §4.1.1 and $\mathrm{Cos}\Xi_1 = b_o{}'(1-\lambda_1{}')/2EF$.

From equation (4.27) the P v. δ relationship can then be calculated for this mechanism at any particular value of F.

For both of these push-pull mechanisms now, ultimate load in the joint will be reached if either:

(a) the membrane stress in the crotch reaches the ultimate stress of the chord material, or

(b) the entire chord section is stressed to yield because of the combination of forces and moments acting around the crotch section (i.e. An upper limit on the tensile force across the gap is provided by the ability of the remaining chord section to withstand and react to this force without exceeding the yield stress.)

The former type of failure can be anticipated by monitoring the membrane force, S, with each increment of chord face deflection, and the latter will now receive further consideration. The chord section is likely to be most highly stressed around the crotch area because of the high local tension force in the membrane, which only acts over part of the full chord width. The other forces acting on the chord member around the gap, as well as the membrane tension, S, are shown in fig. 4.4. Taking a section through the crotch at the point of zero chord displacement, (AA for $x = 0.5$ or BB for $x = 1.0$ with regard to fig. 4.4), gives a stress distribution over the remaining part of the chord section, excepting the crotch width, as shown in figs 4.5(a), (b) and (c) at full plasticity of the chord, which will be the limiting load capacity of the section. A joint which failed in this manner would form buckles in the side walls of the chord member (mode G9 in fig. 3.1).

The total axial force on the section AA or BB (fig. 4.4) is given by:

$$L = N\cos\theta_1 - F + S\cos\theta, \qquad (4.28)$$

and the moment on section AA about the equal area axis is:

$$M = S\cos\theta . x_{ea} + N\cos\theta_1 . x_{ea} - N\sin\theta_1 . d - F(x_{ea} - h_o/2) \qquad (4.29)$$

x_{ea} is the distance to the chord equal area axis as shown in fig. 4.5, and d is replaced by d' for the moment on Section BB ($x = 1.0$). To locate the equal area axis

$$2(b_o - \lambda_{av}' . b_o')t_o/2 + 2(x_{ea} - t_o)t_o = 2(h_o - x_{ea} - t_o)t_o + b_o t_o$$

$$\therefore \quad x_{ea} = (2h_o + \lambda_{av}' . b_o')/4 \qquad (4.30)$$

<u>Neutral Axis in Flange</u>

For the cases shown in figs 4.5(a) and (b) with $y > h_o - t_o$,

$$L = 2(h_o-2t_o)t_o\sigma e_o+(b_o-\lambda_{av}'b_o')t_o\sigma e_o+(y-h_o+t_o)b_o\sigma e_o-b_o(h_o-y)\sigma e_o$$

$$\therefore \quad y = \left\{ \frac{L}{2\sigma e_o b_o} - \frac{(h_o t_o-h_o b_o+b_o t_o-2t_o^2-\lambda_{av}'b_o't_o/2)}{b_o} \right\} \qquad (4.31)$$

If $v \geq t_o$, $(b_o-\lambda_{av}'b_o')t_o + 2(v-t_o)t_o = (h_o-y)b_o$

$$\text{and so } v = \left\{ \frac{(h_o-y)b_o - (b_o\lambda_{av}'b_o')t_o + 2t_o^2}{2t_o} \right\} \qquad (4.32)$$

If $v \leq t_o$, $(b_o-\lambda_{av}'b_o')v = (h_o-y)b_o$

$$\text{and so } v = \frac{(h_o-y)b_o}{b_o-\lambda_{av}'b_o'} \qquad (4.33)$$

Hence if $v \geq t_o$,

$$M = \sigma e_o(h_o-y)b_o(y-x_{ea}+h_o/2-y/2)+(b_o-\lambda_{av}'b_o')t_o\sigma e_o(x_{ea}-t_o/2)$$
$$+ 2(v-t_o)t_o\sigma e_o(x-t_o-(v-t_o)/2) \qquad (4.34)$$

which upon substitution becomes:

$$M = -y^2 \left\{ \frac{\sigma e_o b_o}{2} + \frac{\sigma e_o b_o^2}{4t_o} \right\} \qquad (4.35)$$
$$+ y \left\{ \sigma e_o b_o x_{ea} - \frac{\sigma e_o b_o}{4t_o} \left[-2h_o b_o+2(b_o-\lambda_{av}'b_o')t_o+4t_o x_{ea}-4t_o^2 \right] \right\}$$
$$+ \left\{ \frac{\sigma e_o b_o h_o^2}{2} - \sigma e_o b_o h_o x_{ea}+\sigma e_o t_o(x_{ea}-t_o/2).(b_o-\lambda_{av}'b_o') \right.$$
$$\left. + \frac{\sigma e_o}{4t_o}(h_o b_o-\left[b_o-\lambda_{av}'b_o'\right] t_o)(4t_o x_{ea}-h_o b_o+\left[b_o-\lambda_{av}'b_o'\right] t_o-4t_o^2) \right\}$$

Alternatively, if $v \leq t_o$,

$$M = \sigma e_o(h_o-y)b_o(y-x_{ea}+h_o/2-y/2) + (b_o-\lambda_{av}'b_o')v(x-v/2)\sigma e_o \qquad (4.36)$$

Which upon substitution becomes:

$$M = -y^2\{\frac{\sigma e_o b_o}{2} + \frac{\sigma e_o b_o^2}{2(b_o-\lambda_{av}'b_o')}\}$$

$$+ y\{\frac{\sigma e_o b_o^2 h_o}{(b_o-\lambda_{av}' b_o')}\} + \{\frac{\sigma e_o b_o h_o^2}{2} - \frac{\sigma e_o b_o^2 h_o^2}{2(b_o-\lambda_{av}'b_o')}\} \tag{4.37}$$

Equations (4.35) and (4.37) can now be solved for N by substituting M for the expression in equation (4.29) and y for the equation (4.31) which is also a function of N. Hence the maximum permissible value of N can be obtained for a particular value of the chord 'preload' (F) on the joint, and a particular S.

<u>Neutral Axis in Web</u>

For the case shown in fig. 4.5(c) with $y < h_o - t_o$,

$$L = \sigma e_o(4yt_o - \lambda_{av}'b_o t_o - 2h_o t_o) \tag{4.38}$$

$$\therefore y = \{\frac{L}{4\sigma e_o t_o} + \frac{\lambda_{av}'b_o'+2h_o}{4}\} \tag{4.39}$$

$$v = h_o - y + \lambda_{av}'b_o'/2 \tag{4.40}$$

$$M = \sigma e_o(b_o-\lambda_{av}'.b_o')t_o(x_{ea}-t_o/2)$$

$$+2(v-t_o)t_o(x_{ea}-v+(v-t_o)/2)\sigma e_o \tag{4.41}$$

$$+\sigma e_o b_o t_o(h_o-x_{ea}-t_o/2)+2\sigma e_o(h_o-y-t_o)t_o(y-x+h_o/2-y/2-t_o/2)$$

which upon substitution becomes:

$$M = -y^2\{2\sigma e_o t_o\}$$

$$+y\{2\sigma e_o t_o h_o+\sigma e_o t_o\lambda_{av}'b_o'\} \tag{4.42}$$

$$+\{2\sigma e_o t_o^3 - \sigma e_o b_o t_o^2 + \sigma e_o \lambda_{av}' b_o' t_o^2/2 + \sigma e_o b_o h_o t_o$$

$$+\sigma e_o b_o h_o^2 - 2\sigma e_o t_o h_o - \sigma e_o t_o h_o^2 - \sigma e_o t_o h_o \lambda_{av}' b_o'$$

$$-\sigma e_o \lambda_{av}'^2 . b_o'^2 . t_o/4\}$$

The equation above can now be solved for N by substituting M for the expression in (4.29) and y for the equation (4.39) which is also a function of N. Thus the maximum permissible value of N can again be found for particular values of F and S.

So in summarizing, the procedure which has been adopted for calculating the ultimate strength of the push-pull mechanisms is to give each mechanism a series of small increments of deflection, calculating the tensile stress in the crotch membrane and the strut load which the mechanism can sustain, each time. The mechanism is allowed to deform until:

(a) the stress in the crotch membrane reaches the ultimate stress of the chord, or

(b) the combination of the particular strut load, (which the mechanism could sustain at that deflection), and the membrane force, produces yielding of the whole chord section around the gap. These calculations are carried out by computer using the program listed in Appendix 2.

4.2 Comparison of large deflection push-pull mechanisms with test results

55 RHS to RHS gap joints predicted to fail in the chord connecting face or side walls, (failure modes G1, G2, G4, G5, G8

and G9 in fig. 3.1), and for which the joint data is given in Appendix 1, have been analysed by the two push-pull mechanism approaches. The correlation between the theoretical and actual ultimate loads of these joints is shown in figs 4.6 and 4.7, with a reasonable prediction of the ultimate joint strength being obtained. The analysis becomes conservative for Warren joints having a compressive chord 'preload', which accounts for many test results clustered on the left hand side (safe side) of the diagonal line in fig. 4.6.

By referring to fig. 4.4 one can see that the total axial compression force in the chord at the gap reduces if the joint is a Pratt (N) truss joint as $N\cos\theta_1 = 0$ and similarly the moment on the gap section becomes less severe, which means that N joints are not likely to fail by yielding of the whole chord section around the crotch and should always fail by ultimate stress being attained in the crotch. For Warren joints, on the other hand, the chord may fail by either manner. The presence of a tension chord 'preload' on a Warren joint makes the joint unlikely to fail by yielding of the whole chord section at the gap, and it should always reach failure by fracture of the crotch, because the tension 'preload' will reduce the chord axial compressive stress and relieve the moment on the section too.

Figure 4.8 shows a predicted load-deflection behaviour of the chord connecting face for an RHS to RHS Warren joint having λ less than 1.0, by the two push-pull mechanisms. The theoretical load v. deflection curves only bound the real joint load v. deflection curve around ultimate load, which is to be expected because of the choice of a linear, and hence unrealistic, strain-hardening modulus. Using this strain-hardening modulus the theoretical post-yield joint deflection cannot be expected to correlate well with the actual joint load-deflection behaviour and a constantly varying value of E_{sh} would be necessary to model the joint deflections more accurately between the yield and ultimate loads. The push-pull yield line mechanisms will, of course, only give a post-yield deflection curve and other techniques must be used to calculate the elastic joint deformations, such as the finite difference method, finite element analysis or beam on an elastic foundation concept which have all been applied to tubular joints before (see Chapter 2). This would then provide an elastic load line for the joint deformation from which a complete joint load-deflection behaviour could be formed.

Although the theoretical load v. deflection curves in fig. 4.8 have a constantly increasing gradient, whereas the actual deflection curve of a joint has a constantly decreasing gradient, the theoretical push-pull mechanism curves have the same shape as the theoretical load v. large deflection curve of a laterally loaded longitudinally restrained steel plate[13].

4.3 Other gap joint failure modes

Failure modes for a gap joint which are not a result of the push-pull action of the bracing members on the connecting chord face have been mentioned in §3.5 and these are:

(i) Local buckling of the compression bracing (G6),

(ii) Local buckling of the chord behind the heel of the tension bracing (G7), and

(iii) Chord shear failure (G3).

4.3.1 Local buckling of the compression bracing

As this is the principal failure mode for lap joints, theoretical analyses for this type of failure which are applicable to both gap and lap joints, and based upon two strut buckling mechanisms, are presented in Chapter 5.

4.3.2 Local buckling of the chord behind the heel of the tension bracing

Chord local buckling is caused by a concentration of compressive stress in the connecting face of the chord member behind the heel of the tension bracing. A typical chord local buckle in an isolated joint is shown in fig. 4.9. This compressive stress is a result of the horizontal components of the bracing member forces, any bending stress in the chord caused by the moment produced by the noding eccentricity of the member centre-lines and the chord axial 'preload'.

There are two ways in which a prediction of the chord local buckling load can be calculated. As the connection of the bracing members to the chord is made on one face only, the horizontal components of the bracing member forces are largely transmitted through the chord connecting face near the joint. From strain gauged test specimens, Haleem[35] has observed that the horizontal components of the bracing member forces cause a distribution of stress through the chord section which is triangular behind the tension bracing member as shown in fig. 4.10(a) regardless of the joint eccentricity. This implies that for a square hollow section chord, one half of the horizontal force components are borne by the connecting chord face. This is only slightly more than the "approximately one third" suggested by Eastwood and Wood[32] previously. However the triangular stress distribution observed by Haleem was only for width ratios up to $\lambda = 0.7$ and for greater width ratios the stress distribution was uniform. Local buckling of the chord then occurs when the total compressive stress at the critical, (most heavily stressed), chord face equals the critical buckling stress, which is generally the chord yield stress for hot rolled rectangular hollow sections. As this distribution of stress through the chord is caused by the connection to only one face of the chord rather than the noding eccentricity, it applies to both gapped or lapped joints having $\lambda \leq 0.7$.

An alternative view of the horizontal force component transfer is to consider the extra stress built up on the connecting chord face being due to the bending moment in the chord produced by the noding eccentricity of the joint centre-lines. Hence a bending moment distribution as shown in fig. 4.10(b) is produced in the chord member, and the bending stress in the connecting chord face is

$$e(N\cos\theta_1 + T\cos\theta_2)/(kZ_o) \qquad (4.43)$$

For isolated joints in which the bending moment is taken on one side of the joint, $k = 1$, but for truss joints in which the chord member is continuous on both sides of the joint and is the same length on either side of the joint to a neighbouring joint, k = 2. Gapped joints will usually have a positive noding eccentricity as shown in fig. 4.11 which would produce a tensile bending stress behind the tension bracing member tending to relieve the local stress concentration. In this case the greatest compressive stress would occur on the outside of the chord member furthest from the joint, (for a compression chord), initiating local buckling at this position but this has never been observed in any joint tests.

Applying the triangular stress distribution observed by Haleem for $\lambda \leq 0.7$ can still be unsafe for many lapped joints and often overestimates the chord local buckling load, whereas calculating the local buckling load by this latter method gives reasonable predictions for joints with positive eccentricity, such as lapped joints. Hence it is suggested that the joint local buckling load be calculated by both methods and the lower estimate be taken, but if the noding eccentricity is positive then the likelihood of local chord buckling starting on the outside of a girder is remote.

The incidence of chord local buckling in trusses will be much less than in isolated joint tests because:

(i) The compression chord of a truss will deflect such that the inside (connecting) face of the chord member is under less compressive stress than the outside chord face, and so the build up of stress behind the heel of the tie member will be slightly relieved.

(ii) The position of maximum chord axial compressive stress is usually in the middle of the girder and coincides with the position of the lowest forces in the bracing members. Similarly the position of the maximum bracing member forces is usually at the ends of the girder which coincides with the position of the lowest axial chord loads.

(iii) The bending moment produced by the noding eccentricity will usually be taken by the chord member on both sides of the joint in a truss whereas isolated joint tests are one-sided and all the bending stress is resisted by the chord member on one side of the joint.

In fact in tests on trusses(10) which corresponded to isolated joints which had failed by chord local buckling(9), no chord local buckling failures occurred. Fig. 4.11 shows a comparison between the predicted and the actual chord local buckling loads for 8 RHS to RHS gapped <u>and</u> lapped joints, with the agreement obtained between predictions and test results being reasonably good by taking the lower of the two failure predictions as recommended.

4.3.3 Chord shear failure

For large width ratios (λ) and also for rectangular chord members with the larger side of the rectangle as the connecting chord face ($h_o < b_o$), there is a likelihood that the chord section may fail in shear due to the vertical components of the bracing member forces acting on the chord walls. Taking the chord shear area at ultimate load as $2(h_o+2t_o)t_o$ according to Wardenier and

De Koning[71], and assuming a Von Mises shear yield criterion with reduction due to axial loading in the chord, the ultimate shear resistance of the chord section is given by:

$$P \approx 2(h_o+2t_o)t_o \frac{\sigma e_o}{\sqrt{3}} \cdot \sqrt{1-(F/Fp)^2} \qquad (4.44)$$

An alternative (equation 2.11) has also been proposed but equation (4.44) is used for the calculation of the ultimate shear strength of an RHS chord.

The theoretical formulae which have been presented in Chapter 4 to enable one to predict the ultimate strength of an RHS to RHS gap joint by a series of recognised failure modes, have been incorporated into a computer program, which is listed in Appendix 2, for the analysis of such joints. By this means, 84 RHS to RHS gap joints from Appendix 1 have been studied with the resulting correlation between the predicted and actual ultimate joint loads shown graphically in figs 4.12 and 4.13.

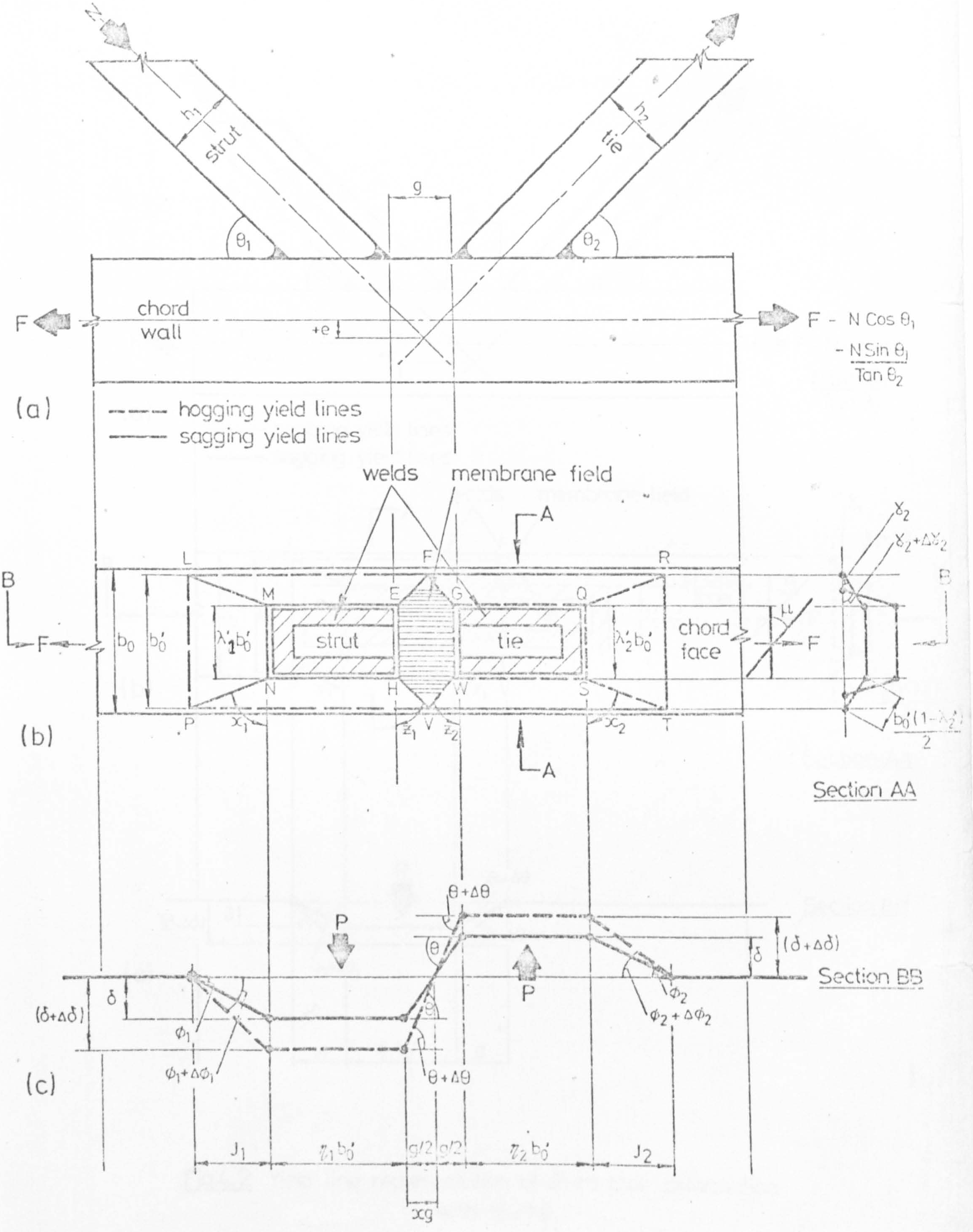

Fig.4.1 Yield line representation of chord face deformation with $x = 0.5$

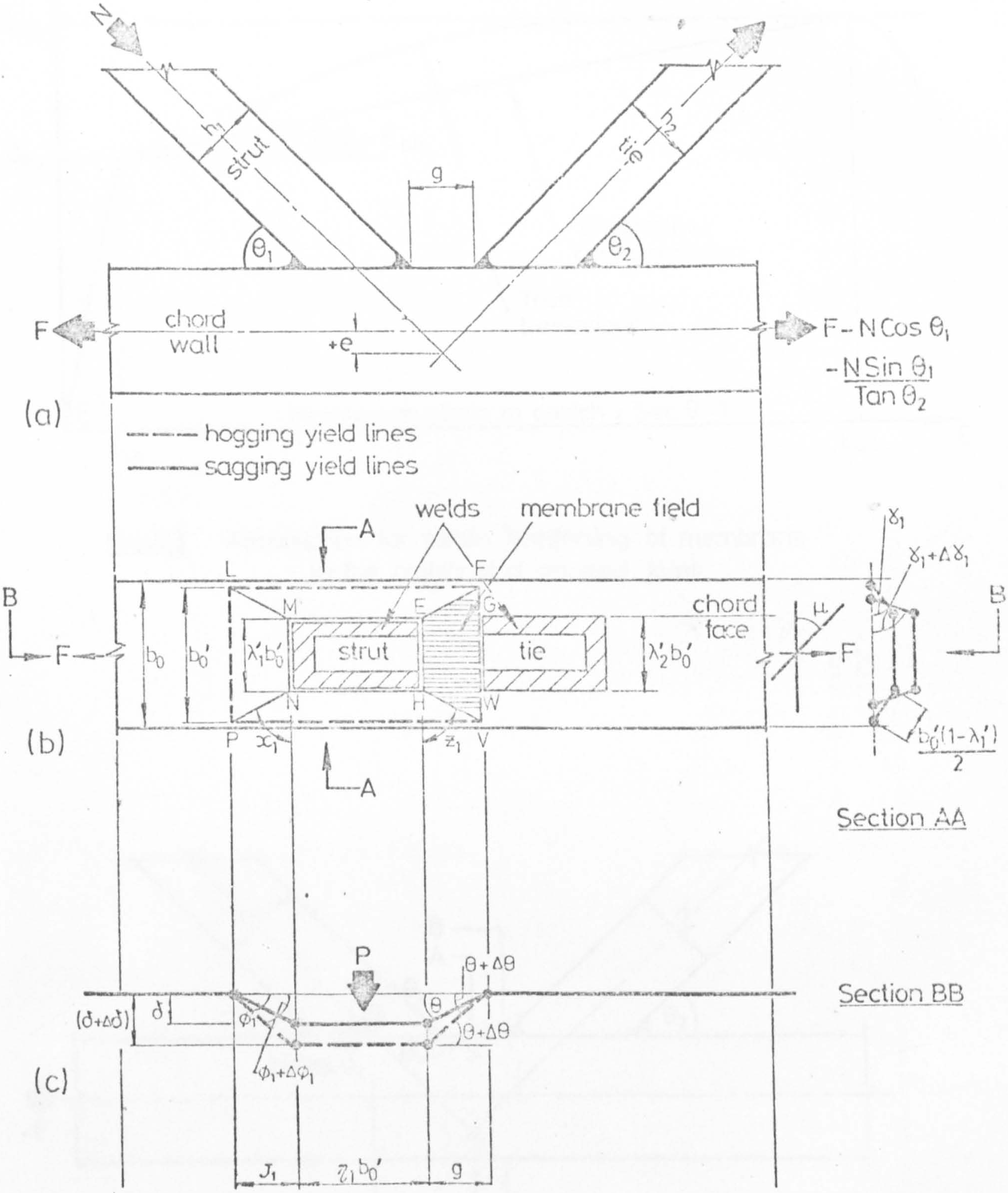

Fig.4.2 Yield line representation of chord face deformation with $x = 1{\cdot}0$

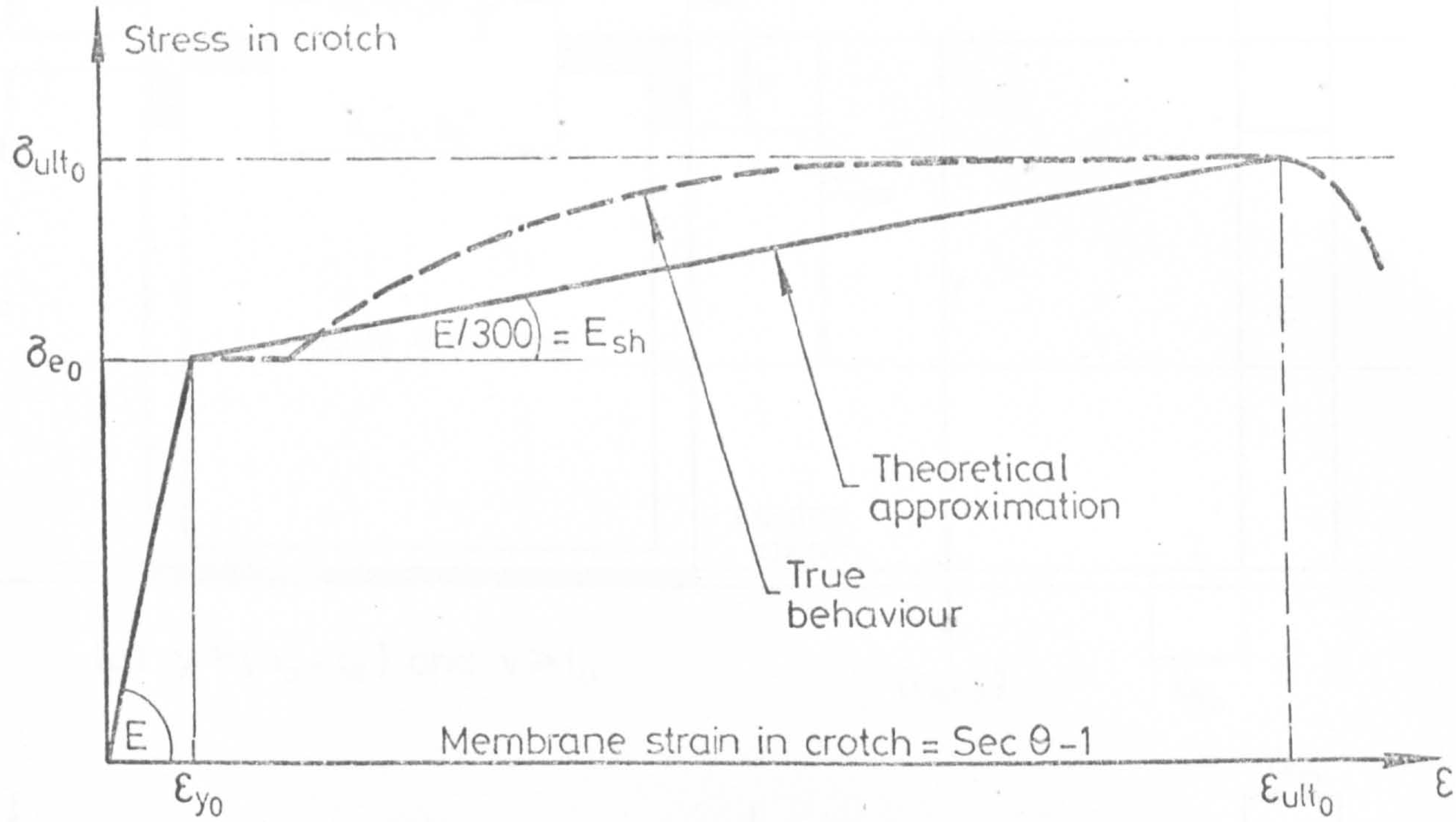

Fig.43 Assumption for strain hardening of membrane in the crotch of a gapped joint

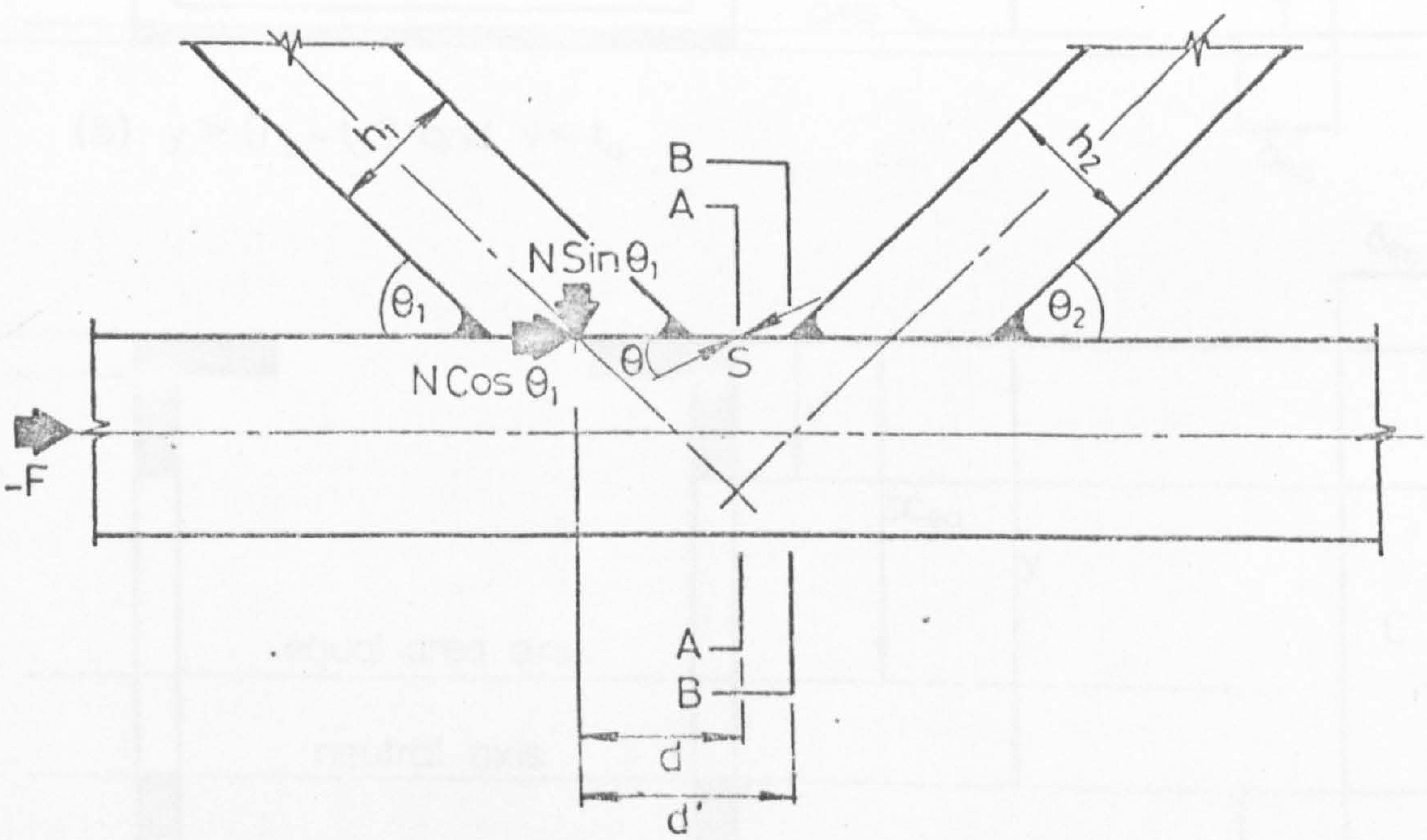

Fig.44 Forces acting on one side of a gapped joint

Fig.4.5 Stress distribution through chord section at crotch for full plasticity

Fig.4·6 Actual v. predicted ultimate loads by push-pull mechanisms for RHS to RHS gap joints

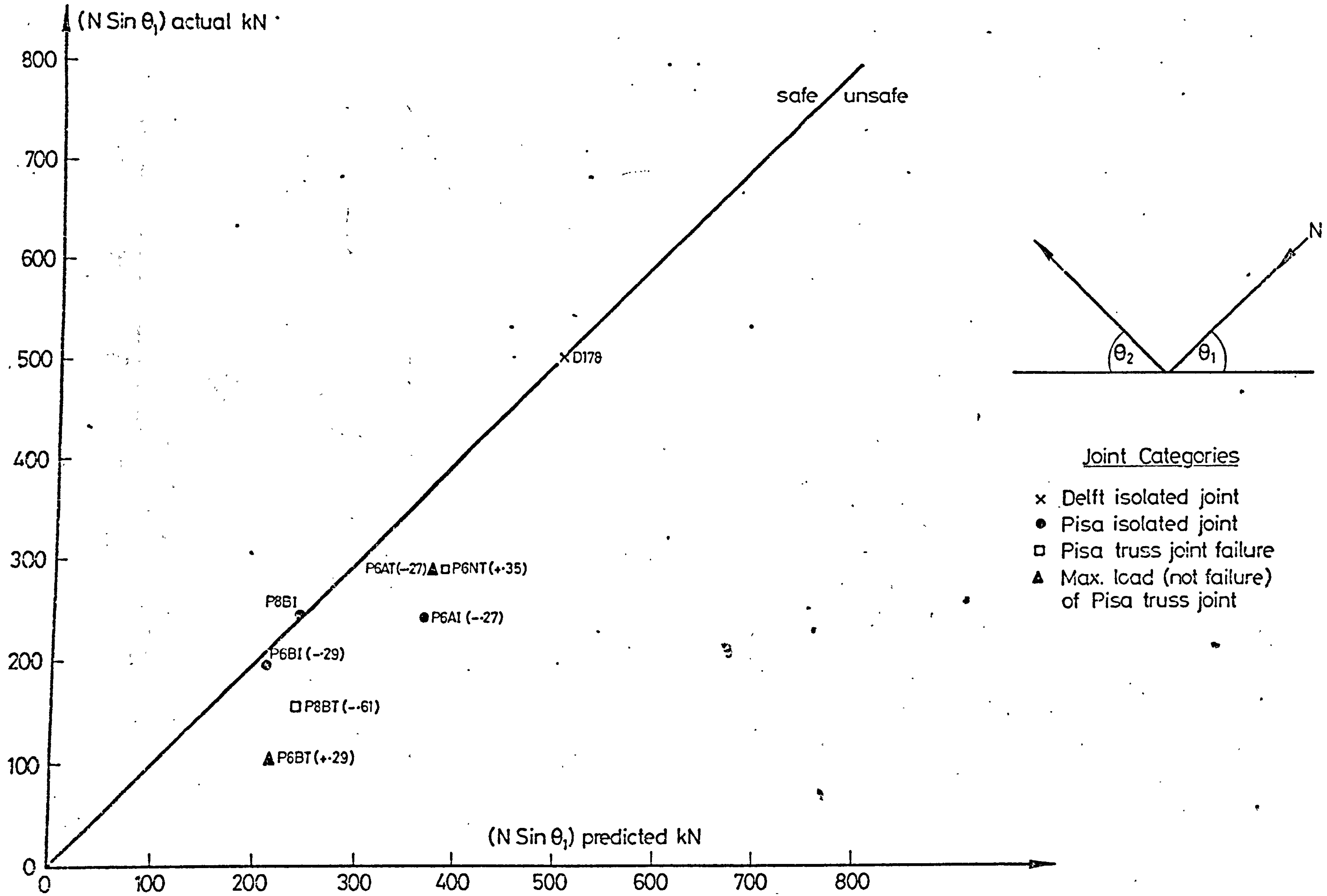

Fig.4·7 Actual v. predicted ultimate loads by push-pull mechanisms for RHS to RHS gap joints

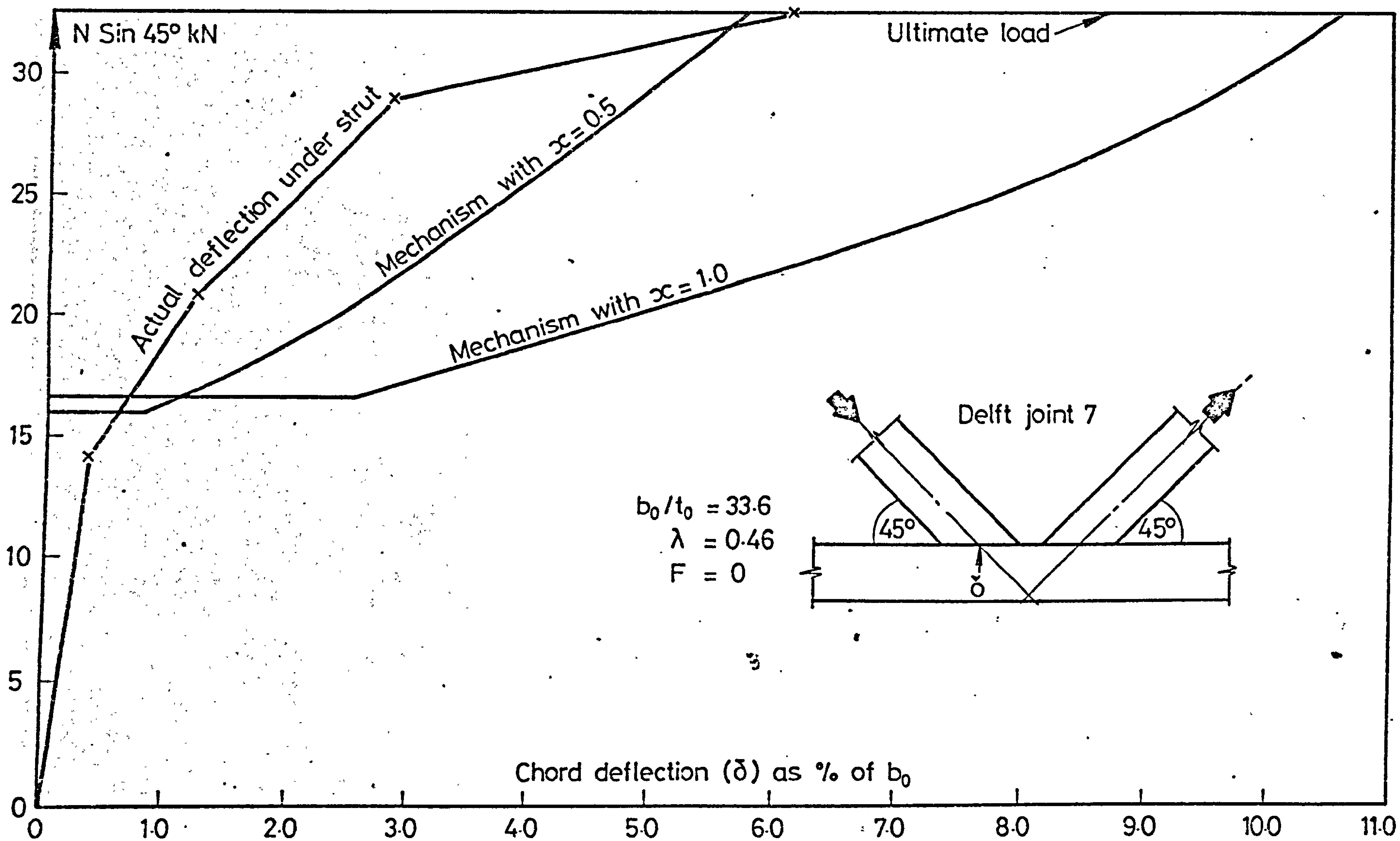

Fig.4.8 Theoretical load v. deflection behaviour of a gapped joint with $\lambda < 1.0$

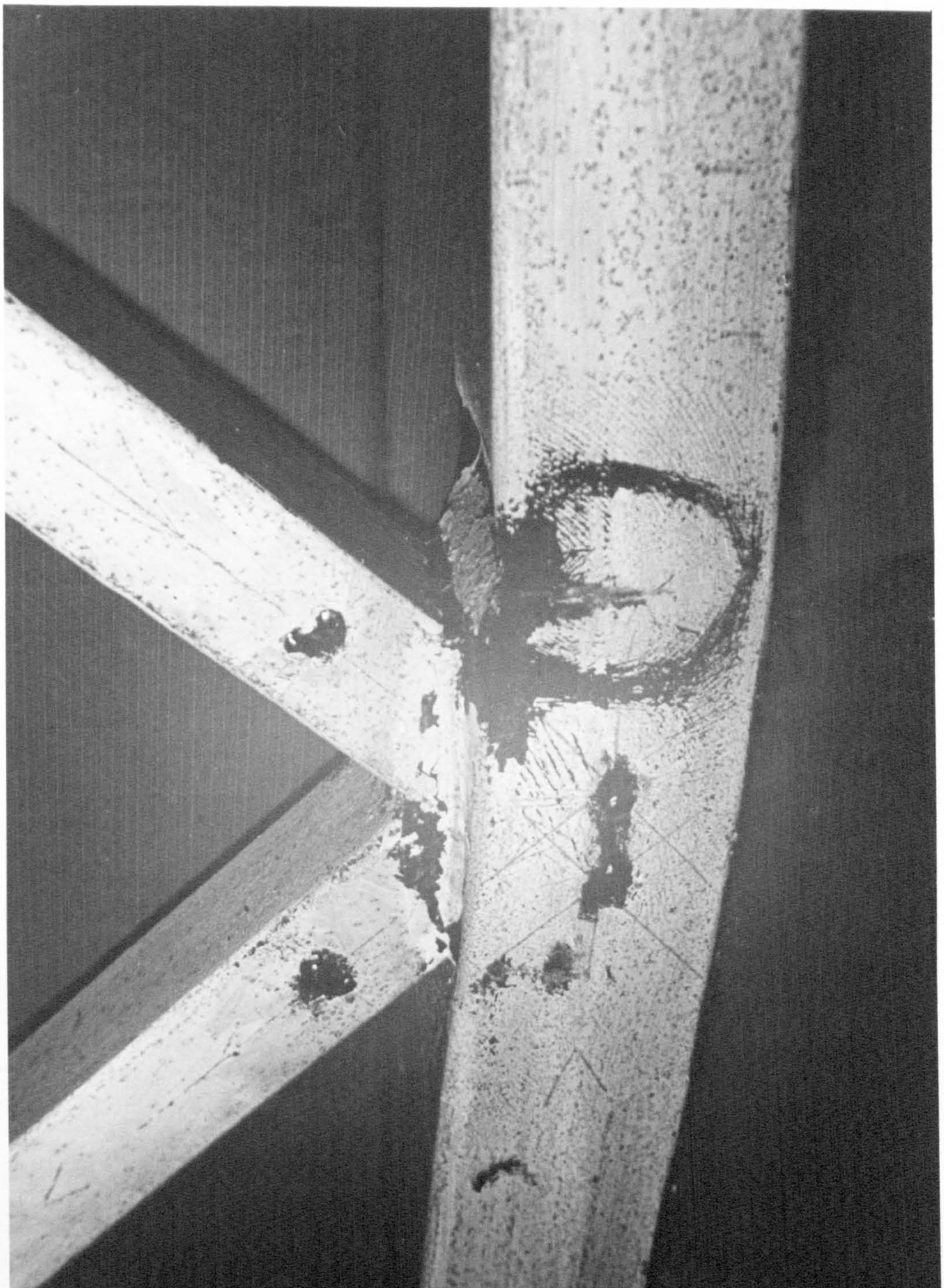

Fig. 4.9 Typical chord local buckle in an isolated joint

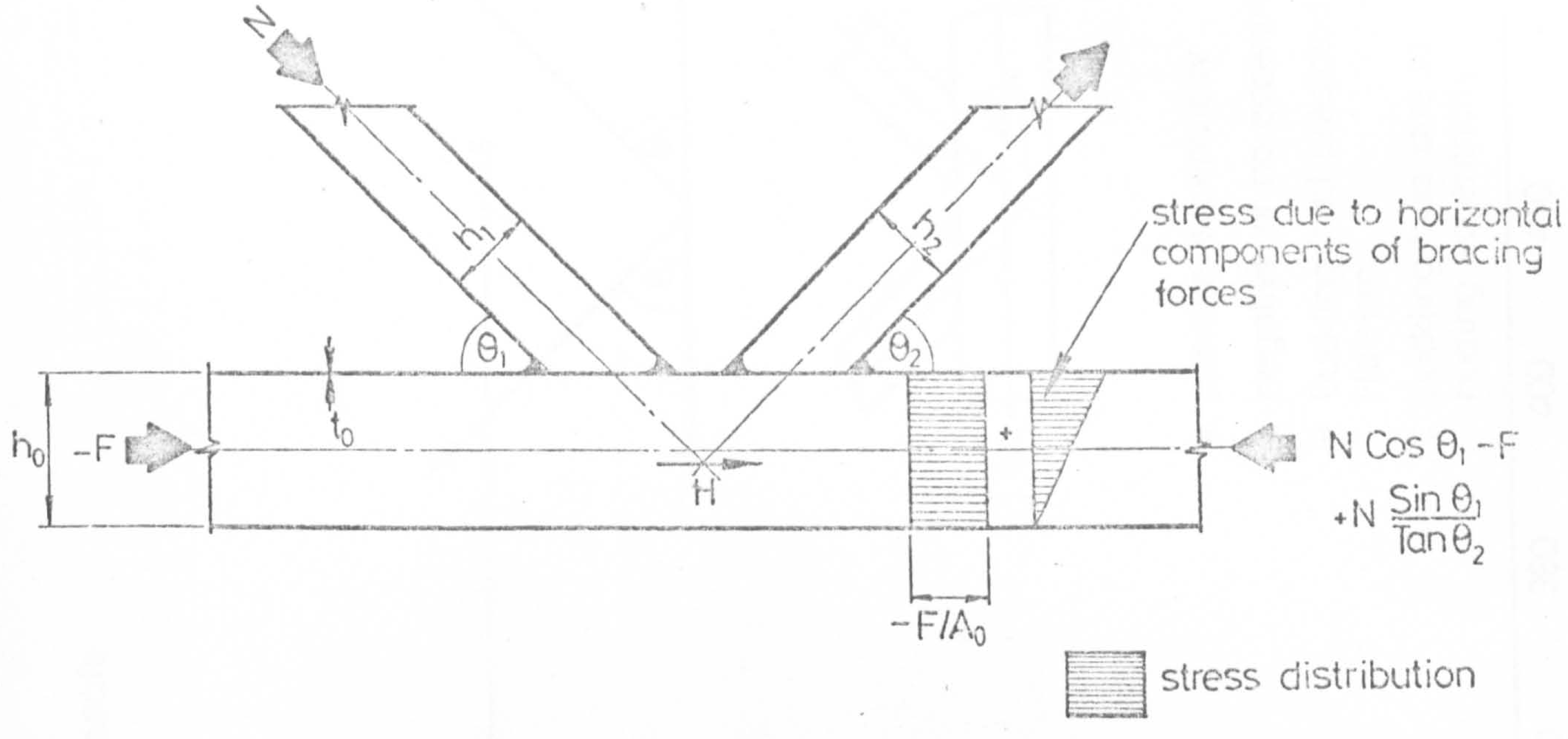

Fig.4.10(a) Stress concentration causing chord local buckling according to Haleem (35) for $\lambda \leq 0.7$

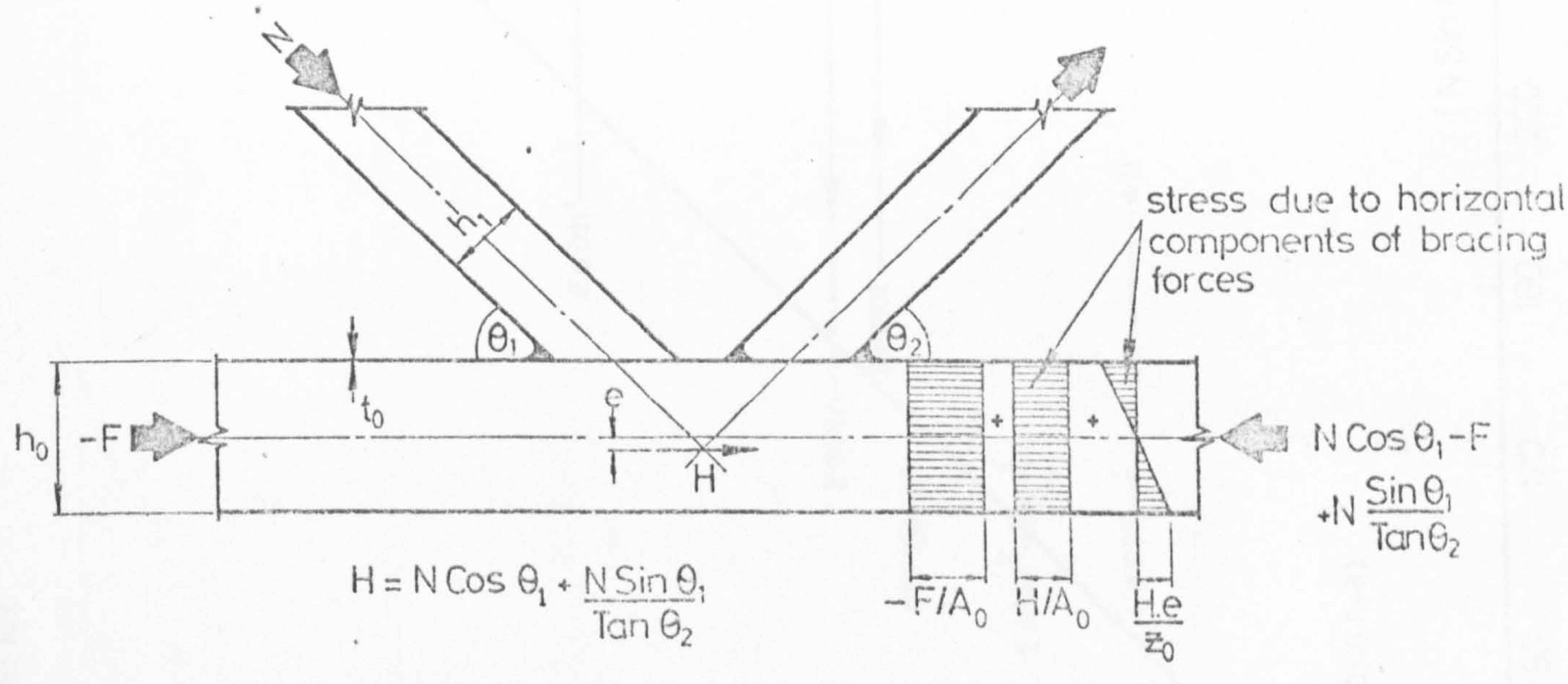

Fig.4.10(b) Stress concentration causing chord local buckling because of noding eccentricity

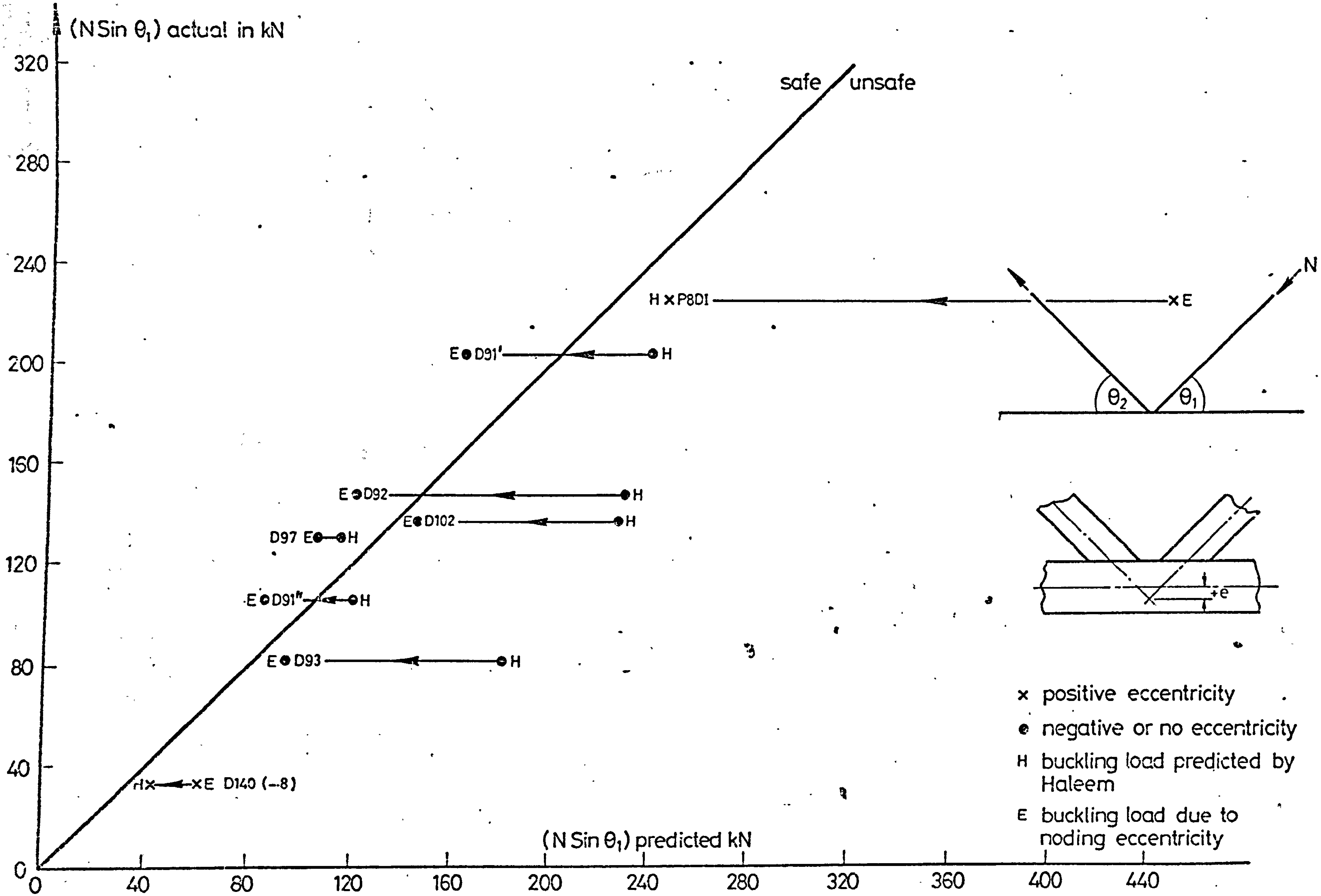

Fig.4.11 Actual v. predicted chord local buckling loads for RHS to RHS gap and lap joints

Fig.4·12 Actual v. predicted ultimate loads for RHS to RHS gap joints

Fig.4·13 Actual v. predicted ultimate loads for RHS to RHS gap joints

CHAPTER 5

ULTIMATE STRENGTH OF LAPPED JOINTS

5.1 Introduction to lapped joints

The failure modes for overlapped joints which have been identified by previous experimental research on RHS joints [9,10,71] are as follows:

(i) Chord face and wall failure around the joint (L4). This is usually associated with shearing of the chord section for large width ratios.

(ii) Local buckling of the compression bracing accompanied by some deformation of the chord face (L6).

(iii) Chord local buckling behind the heel of the tension bracing member (L7).

These types of joint failure are shown in fig. 5.1 along with a further failure mode in which the compression bracing member punches into the tension bracing member (L10). It is thought that this failure mode may occur for overlapped joints in which the compression bracing member has a smaller width than the tension bracing member, but all tests on overlapped joints have hitherto had bracing members of the same width and this type of failure has never actually been observed.

As with gapped joints, the strength of an overlapped joint may be limited by other failure modes which do not strictly represent joint failures. These have been described in §3.1. In this chapter the failure of overlapped joints by modes L4, L6 and L7 is considered with the emphasis on the ultimate strength of the joint as this coincides with the 'yield strength' for the unstable buckling failure modes and is very close to the yield strength for chord shear failure.

5.2 Local buckling of RHS members under axial compression

For the purpose of axial compression, Timoshenko[64], Johnston[41] and Watson and Babb[77] have considered that a rectangular hollow section can be idealized as four simply supported plates. Experimental studies on box sections and plates under uniaxial compression at Cambridge University have shown that some restraint between the sides does exist. In fact the elastic buckling load of the wider sides is increased by rotational restraint from the more narrow sides by up to 30% over a square section if the sides are such that $h_i = 0.5\ b_i$ (the limit for British sections), but the maximum load sustained by the wider sides is not increased. The result has been that Dwight[30] too has concluded that a reasonable design approach is to consider the four sides of a rectangular hollow section as being simply supported plates.

Apart from the edge restraint, plate buckling strength will also be influenced by the stress/strain curve of the material, residual stresses and the initial out of flatness. Very little is known about the latter two effects for RHS members, but it is thought likely[30] that some moderate mid-width residual compression stress exists on each side of rectangular hollow sections. For a uniaxially loaded steel plate which is initially flat and stress free, the elastic critical buckling stress is given by the classical plate buckling formula,

$$\sigma_{crit} = \frac{k\pi^2 E t^2}{12(1-\nu^2)b^2} \qquad (5.01)$$

For large aspect ratios and simply supported edges, k is very close to 4[41]. Hence with $\nu = 0.3$ and $E = 206$ kN/mm^2,[8] equation (5.01) simplifies to:

$$\sigma_{crit} = \frac{744.7}{(b/t)^2} \text{ kN/mm}^2 \qquad (5.02)$$

In this case b is the effective width of the plate, which for the side of an RHS is not well defined because of the rounded corners. In light gauge codes the effective plate width is simply taken as the flat width (b_f on fig. 5.2), but Dwight[30] considers that this is rather optimistic and suggests the effective plate width be taken as $(b_f+b_{in})/2$. However if a safe estimate is to be taken for the effective plate width, b' from fig. 5.2 could be chosen. The range of currently produced rectangular hollow sections in Great Britain[12] has a maximum b'/t value of 46.6, which means that the lowest elastic critical buckling stress for any face of an RHS tube is 343 N/mm^2. Consequently no Grade 43 RHS sections are liable to elastic local buckling and only a few will be liable in the higher steel grades.

At low to moderate b'/t values of the tube side walls, rectangular hollow sections in higher grades of steel will be 'compact'. The term 'compact'[8] means that the member can reach the compressive yield load and also has enough strain capacity while holding yield to enable redistribution of stress to take place. At moderate to high b'/t values, the tube walls may reach the compressive yield load but have only a limited or zero plastic plateau, and so the member is termed 'semi-compact'. For very high b'/t values of the tube side walls in higher grades of steel the yield stress may not be reached because of elastic local buckling, and such sections are called 'slender'[8]. Slender sections will buckle initially at σ_{crit} but then exhibit a post-buckled reserve of strength with a final collapse stress above σ_{crit}, with a greater reserve of strength being obtained for higher b/t values. The maximum stress attained by a slender section (σ_{max}) can be calculated[65] by:

$$\frac{\sigma_{max}}{\sigma_e} = 0.36 + 0.83\left(\frac{\sigma_{crit}}{\sigma_e}\right) - 0.19\,\frac{(\sigma_{max}/\sigma_e)^2}{(\sigma_{crit}/\sigma_e)} \qquad (5.03)$$

which of course is subject to σ_{crit} being less than σ_e.

Instead of quoting plate strength in terms of σ_{max} an alternative procedure is to use the effective width concept whereby the load is assumed to be carried by yielding edge strips, each of half the effective width, while the central portion of the plate is assumed ineffective. For the purposes of checking the liability of an RHS member to local buckling under a particular load, the maximum stress idea would be easier to use than the latter concept.

Considerable experimental research has been done at Cambridge[30] on welded box-columns by Harrison, Chin, Moxham and Little, by Jubb at Cranfield, and on individual plates by Ratcliffe and Moxham at Cambridge which have revealed how the parameters such as b/t, residual stress, out of flatness, etc., affect the buckling strength and load-deformation characteristics. The theoretical prediction of the ultimate strength of plate elements in compression is a formidible task and has been attempted by Ratcliffe, Moxham, Crisfield, Frieze, Harding and Little[30] with the aim of taking account of large deflection behaviour, gradual spread of plasticity, out-of-flatness and residual stress. These complex analyses, as well as providing the maximum stress (σ_{max}) which a plate is capable of taking, provide the complete load v. end shortening characteristic, but they involve considerable computer time and their application to hot rolled rectangular hollow sections is still being debated.

A simpler approach to the calculation of plate buckling strength has been made by Davies, Kemp and Walker[25] using a yield line method to construct a plastic unloading curve for the plate. The ultimate load is then found by the intersection of this curve with an elastic loading line. The yield line pattern of the folded plate is shown in fig. 5.3. The optimum value of β was shown to be 35.5^{o} and the length of the central yield line JK was found to be half the plate width on actual test specimens, thus making the length of the buckle pattern (ℓ) equal to 0.7 of the plate width. Rawlings and Shapland[57] tested five thin walled square box sections in axial compression and presented a collapse theory also based upon the yield line concept with folding assumed to occur along straight lines. However the buckling of the box sections included a kinking mechanism in the corner edges which does not occur for hot-rolled RHS members. The ultimate load for the box section in their case was again determined by the intersection of the post-buckling unloading line with an elastic load line, using an effective width method from B.S. 153.

With axially loaded RHS members, to check for local buckling one merely requires to know if the section will be either semi-compact or compact and reach the yield stress before buckling, for the particular slenderness ratio of the tube walls, and if the section is slender then the maximum axial compressive stress which the tube can take is required. Knowing the specific guaranteed yield stress of each steel grade, many countries have hence given maximum slenderness limits for plates or tube walls to avoid slender sections, but there is vast discrepancy between various national codes. Based upon suggestions by Dwight[30], British Standards draft regulations[8] are now proposing that to avoid slender sections,

$$b_f/t \ngtr 45\sqrt{\frac{240}{\sigma_d}}, \tag{5.04}$$

where σ_d is in N/mm^2, and b_f is shown on fig. 5.2. This can be rewritten as

$$\sigma_d \leq \frac{486}{(b_f/t)^2} \text{ kN/mm}^2 \tag{5.05}$$

Recent Dutch recommendations for tubular structures[53] give a limitation of a similar nature but use the whole section width (b) to calculate the wall slenderness ratio, as given below:

$$\sigma_{max} \leq \frac{100\sigma_r}{(b/t)^2}, \tag{5.06}$$

where σ_r is a reference stress given by the Dutch code NEN 3851.

In the absence of suitable experimental evidence on the local buckling of hot rolled RHS, a simple approach for the calculation of the maximum compressive stress will be taken according to equations (5.02) and (5.03), with the effective plate width being $b' = b-t$ and neglecting the effects of residual stress and out of flatness. The maximum compressive stress (σ_{max}) for any tube wall can then be easily calculated, subject to $\sigma_{max} \leq \sigma_e$. Thus, when checking for local buckling of the chord member behind the heel of the tension bracing as described in §4.3.2, the maximum compressive stress, (due to both axial loading and the moment produced by noding eccentricity), which the chord connecting face can transmit before locally buckling will be given by σ_{max} and this will then restrict the load which can be applied through the bracings to a joint. This check is incorporated into the computer program for joint analysis given in Appendix 2, along with an automatic check to ensure that the load in the compression bracing of a joint does not produce a compressive stress in any wall of the strut which exceeds the local buckling stress of that wall.

If circular hollow section members are used for the bracings of a joint then there are no hot rolled CHS sections produced in Britain which are slender [8,30] and so local buckling due to axial compression is not a problem. Dutch recommendations [53] also confirm this, as they give a limiting tube slenderness of

$$d/t \nless \frac{E}{8.75\sigma_e}, \tag{5.07}$$

which is outside the range of British hot rolled CHS for all steel grades.

5.3 Strut buckling mechanism 1

Of the failure modes for overlapped joints described in §5.1, the most common is local buckling of the compression bracing (L6) near the joint. The typical shape of such a local buckle is shown in fig. 5.4. This type of local buckling differs from the elastic local buckling considered in the previous section because this buckle involves deformation of the connecting chord face and often the tension bracing member as well, hence making it a joint failure rather than a member failure. It can be seen in fig. 5.4 that the buckle is non-symmetrical around the strut and that the largest buckle dimple occurs on the inside connecting face due to a moment acting on the base of the strut within the plane of the truss. The magnitude of this moment depends on the properties and geometry of the joint. The inside (adjacent to tie) face of the strut is the most heavily stressed and so begins to buckle elastically or yield first, but in order for the strut section to collapse adjacent to the connection, plasticity must spread sufficiently for the joint as a whole to form a failure mechanism. Hence this type of local buckling adjacent to a joint could be called 'plastic buckling'.

As the compression bracing is subject to axial load and a moment at the joint, consider the case of an eccentrically compressed rectangular hollow section as shown in fig. 5.5(a). With the neutral axis within the tube web, the yield stress distribution is as shown in fig. 5.5(b), and hence

$$N = 2a(2t_1)\sigma e_1 \quad \text{and} \quad Np = 2(b_1'+h_1')t_1\sigma e_1$$

$$Mp' = b_1h_1^2\sigma e_1/4 - (b_1-2t_1)(h_1-2t_1)^2\sigma e_1/4 - 2t_1(2a)^2\sigma e_1/4$$

$$= Mp - 2t_1(2a)^2\sigma e_1/4$$

$$\therefore Mp' = Mp - 2t_1\sigma e_1\left\{\frac{N}{4t_1\sigma e_1}\right\}^2$$

$$\therefore \frac{Mp'}{Mp} = 1.0 - \left\{\frac{2t_1(b_1'+h_1')^2.(N/Np)^2}{b_1h_1^2 - (b_1-2t\ )(h_1-2t_1)^2}\right\} \qquad (5.08)$$

i.e. $$\frac{Mp'}{Mp} = 1.0 - f_1(N/Np)^2$$

With the neutral axis within the tube flange, the yield stress distribution is as shown in fig. 5.5(c), and hence

$$N = 2(h_1-2t_1)t_1\sigma e_1 + (2a-h_1+2t_1)b_1\sigma e_1$$

$$Mp' = b_1h_1^2\sigma e_1/4 - b_1(2a)^2\sigma e_1/4$$

Np and Mp are as above, and so

$$Mp' = Mp + \sigma e_1\{(b_1-2t_1)(h_1-2t_1)^2 - b_1(2a)^2\}/4$$

$$\therefore \frac{Mp'}{Mp} = 1.0 - \frac{\left[b_1\left[\frac{2t_1(N/Np)(b_1'+h_1')-(h_1-2t_1)2t_1}{b_1} + (h_1-2t_1)\right]^2 - A\right]}{b_1h_1^2 - A}$$

(5.09)

where $A = (b_1-2t_1)(h_1-2t_1)^2$

i.e. $\frac{Mp'}{Mp} = 1.0 - f_2(N/Np)^2$

The relationship between the moment and axial load at the end of the member which produces yielding across the whole section is given by equations (5.08) and (5.09), and the interaction is shown graphically in fig. 5.6 for square hollow sections with

b_1/t_1 equal to 20 and 30. It can be seen that the neutral axis of rotation lies within the tube flange for compressive loads greater than 50% of the tube squash load (Np), and can even be assumed to be within the flange for as low as N/Np = 0.4 with negligible error. As test results indicate that this level of compression is always reached in the strut member before local buckling, it is assumed for a theoretical buckling model that rotation of the strut section occurs about a point within the flange. In fact if a square tubular strut did buckle locally due to a combination of axial load and end moment, then the strut ultimate load could reach a minimum of 48% of the squash load, for a tube with $b_1/t_1 \approx 30$. However, the local buckling load of a strut in a tubular joint will generally be higher because of the restraint provided by the members to which the end of the strut is connected.

A typical joint local buckle, as shown in fig. 5.4, is represented by the yield line mechanism of fig. 5.7. In this mechanism rotation of the strut is assumed to take place about the point A which is where the strut member meets the chord face (if the tie is double mitred), or the projection of the inside face of the strut (if the strut is double mitred). If the tie and chord members do not suffer plastic deformations to the left of point J, (see fig. 5.7), then point J is effectively restrained in position by the constraints at the ends of the tie and chord members. For this mechanism it is also assumed that JA remains rigid. Under loading from N, the point D rotates to D' and B elongates plastically to B' within the tie section, whilst the base of the strut remains rigid. E is the point of contraflexure occurring at the mid-length of a strut in a truss situation, or for an isolated joint test it represents the position of the lateral restraint on the strut.

The assumed yield line pattern for the strut buckle is shown in fig. 5.8. For this mechanism it is assumed that the angle $\varepsilon_2 = 35.5^o$ and also that the line CD = $0.5b_1'$, which Davies, Kemp and Walker[25] observed for their tests on simply supported steel plates under uniaxial compression (see §5.2 and fig. 5.3). Dowling[29] also showed that an angle of $\varepsilon_2 = 35^o$ produced a lower limit for the simply supported plate mechanism under uniaxial compression. Hence the length of the buckle on the most critical tube face is $0.7b_1'$, which compares well with test observations[10]. It is also assumed that the angle $\varepsilon_1 = \varepsilon_2$ on fig. 5.8. The load/deflection relationship for this mechanism is found by means of a rigid-plastic geometrical folding of the plates accompanied by squashing in the tube corners AE and BF (fig. 5.8) ignoring axial strains in the yielded portions elsewhere.

The plastic moment of resistance (mp) of all yield lines is reduced by the effect of the axial strut load (N) according to equation (2.19) by Mouty[51]. The presence or distribution of residual stresses is ignored, as the collapse load of a plastic mechanism is independent of residual stresses and of the path by which it was achieved. Whilst this is justified in studying the ultimate strength of the joint, it may not be when considering the elastic deformation[13].

As the maximum deflection of the buckle dimple w (see fig. 5.8) undergoes an incremental increase to $w + \Delta w$, the rotation of each yield line and of the chord face, or displacement of the load, can be related to w. The incremental rotation of the yield line GG is denoted $2\Delta\psi$, $\Delta\xi$ for GA and GE, $\Delta\tau$ for GH, $(\Delta\phi - \Delta\psi)$ for AB and EF, $2\Delta\phi$ for CD, $\Delta\Sigma$ for AH and HE, ΔX for AJ and JE, and $\Delta\eta$ for AC and CE.

With regard to section XX on fig. 5.8,

$$T = \sin^{-1}(\sqrt{(0.35b_1')^2 - w^2}/GA)$$

$$T-\Delta\psi = \sin^{-1}(\sqrt{(0.35b_1')^2 - (w+\Delta w)^2}/GA)$$

$$\therefore\ \Delta\psi = \sin^{-1}(\sqrt{(0.35b_1')^2 - w^2}/GA) - \sin^{-1}(\sqrt{(0.35b_1')^2 - (w+\Delta w)^2}/GA) \qquad (5.10)$$

Point H (fig. 5.8) can be located for any deflection knowing that it rotates about the point G with a radius of $h_1' - 0.25b_1'$, and also about the point A with a radius of $0.4301\ b_1'$. Hence H lies on the intersection of the two spheres centred at G (given co-ordinates 0,0,0) and A (GA CosT, GA SinT,0), where the co-ordinate directions are shown on fig. 5.8. Due to symmetry about GH, H has zero y co-ordinate. Therefore,

$$x_H^2 + z_H^2 = GH^2 \qquad (5.11)$$

and

$$(x_H - x_A)^2 + y_A^2 + z_H^2 = AH^2 \qquad (5.12)$$

$$\therefore\quad GH^2 - AH^2 - 2GA\,\mathrm{Cos}T.x_H + (GA\,\mathrm{Cos}T)^2 + (GA\,\mathrm{Sin}T)^2 = 0$$

and

$$GH^2 - AH^2 - 2GA\,\mathrm{Cos}(T-\Delta\psi)x_H' + (GA\,\mathrm{Cos}(T-\Delta\psi))^2 + (GA\,\mathrm{Sin}(T-\Delta\psi))^2 = 0$$

$$x_H = (GA^2 + GH^2 - AH^2)/(2GA\,\mathrm{Cos}T) \qquad (5.13)$$

and $$x_H' = (GA^2 + GH^2 - AH^2)/(2GA\ \mathrm{Cos}(T-\Delta\psi)) \tag{5.14}$$

where $x_H' < x_H$, and substituting into equation (5.11) gives

$$z_H = \sqrt{GH^2 - x_H^2} \tag{5.15}$$

and $$z_H' = \sqrt{GH^2 - (x_H')^2}$$

Hence the point H moves from $(x_H, 0, z_H)$ to H' at $(x_H', 0, z_H')$.

$$\therefore \quad \Delta\xi = \sin^{-1}(z_H'/MH) - \sin^{-1}(z_H/MH) \tag{5.16}$$

where $$MH = 0.35b_1'(h_1' - 0.25b_1')/\sqrt{h_1'^2 + (0.35b_1')^2} \tag{5.17}$$

$$\Delta\tau = 2\mathrm{Sin}^{-1}\left[\frac{z_H'.h_1'}{MH\sqrt{h_1'^2 + (0.35b_1')^2}}\right] - 2\mathrm{Sin}^{-1}\left[\frac{z_H.h_1'}{MH\sqrt{h_1'^2 + (0.35b_1')^2}}\right] \tag{5.18}$$

With regard to fig. 5.8(b),

$$\Delta\phi = \mathrm{Sin}^{-1}((w+\Delta w)/0.35b_1') - \mathrm{Sin}^{-1}(w/0.35b_1') \tag{5.19}$$

As the tube receives a rigid body rotation of $\Delta\psi$ also, the rotation at the hinges AB or EF is actually $\Delta\phi - \Delta\psi$

$$= \mathrm{Sin}^{-1}((w+\Delta w)/0.35b_1') - \mathrm{Sin}^{-1}(w/0.35b_1') - \mathrm{Sin}^{-1}(\sqrt{(0.35b_1')^2 - w^2}/GA)$$
$$+ \mathrm{Sin}^{-1}(\sqrt{(0.35b_1')^2 - (w+ w)^2}/GA) \tag{5.20}$$

Relative to A, (fig. 5.8(a)), point C moves inwards by $0.35b_1'\mathrm{Sin}\phi$, and so the co-ordinates about the origin G are:

$$C: \quad (GA\ \mathrm{Cos}T - 0.35b_1'\mathrm{Sin}\phi,\ 0,\ -0.25b_1')$$

and $$C': \quad (GA\ \mathrm{Cos}(T-\Delta\psi) - 0.35b_1'\mathrm{Sin}\phi,\ 0,\ -0.25b_1')$$

To locate the point J, we know that because of symmetry J lies on the XZ plane as shown on fig. 5.9. It can then be shown that with respect to the origin at G, J has co-ordinates of:

$$(x_H + 0.25b_1'\mathrm{Sin}(j+k),\ 0,\ z_H - 0.25b_1'\mathrm{Cos}(j+k))$$

and

$$J':\quad (x_H' + 0.25b_1'\mathrm{Sin}(j+k)',\ 0,\ z_H' - 0.25b_1'\mathrm{Cos}(j+k)')$$

where $$(j+k) = \mathrm{Cos}^{-1}(\sqrt{(x_C-x_H)^2 + (z_C-z_H)^2}/0.5b_1') + \mathrm{Tan}^{-1}\{|(x_C-x_H)/(z_H-z_C)|\}$$

When point J moves to the position J', the lines AJ and JE overlap at J because J does not have the same x co-ordinate as point C, and the edge of the tube remains less depressed than the centre of the buckle CD. The amount of squashing at J can be calculated from the real and apparent lengths of AJ or JE, as shown in fig. 5.10, and is denoted SQL where

$$SQL = 2(0.35b_1' - \sqrt{(x_A - x_J)^2 + y_A^2 + z_J^2})$$

$$\therefore \quad \Delta SQL = 2\sqrt{(x_A' - x_J')^2 + (y_A')^2 + (z_J')^2} - 2\sqrt{(x_A - x_J)^2 + y_A^2 + z_J^2} \qquad (5.21)$$

It is assumed that the tube is yielded across the whole thickness at J and that the amount of squashing tapers linearly to zero at H and C (see fig. 5.8).

The rotation of yield lines AH and HE (Σ) can be calculated by referring to fig. 5.11.

$$z_S = 0.814\, z_H \sqrt{(x_A - x_J)^2 + y_A^{\,2} + z_J^{\,2}}/(0.4301b_1')$$

and
$$\Sigma = \operatorname{Sin}^{-1}\{|z_S - z_J|/(0.58\sqrt{(x_A - x_J)^2 + y_A^{\,2} + z_J^{\,2}})\}$$
$$+ \operatorname{Sin}^{-1}\{z_H/PH\} \qquad (5.22)$$

The total rotation of lines AJ and JE (χ) at any instant is given by the angle $\alpha_1 + \alpha_2$ in fig. 5.12.

$$\chi = \operatorname{Tan}^{-1}\{(x_C - x_J)/(z_C - z_J)\} + \operatorname{Tan}^{-1}\{(x_H - x_J)/(z_H - z_J)\} \qquad (5.23)$$

To calculate the rotation of the yield lines AC and CE (η), J moves from the position $(x_C,0,0)$ to J at $(x_J,0,z_J)$ by rotation about AC.

$$\text{Hence,}\quad \eta = \operatorname{Sin}^{-1}\{(x_J - x_C)/(JC \operatorname{Cos} 35.5^{\circ})\} \qquad (5.24)$$

The total internal virtual work done in the strut member as it undergoes an incremental rotation is then given by:

$$2b_1'\Delta\psi mp_1(1-(N/Np)^2) + 4CA\Delta\xi mp_1(1-\operatorname{Cos}^4\Phi(N/Np)^2)$$
$$+ 2GH\Delta\tau mp_1(1-(N/Np)^2) + 2b_1'(\Delta\phi-\Delta\psi)mp_1(1-(N/Np)^2)$$
$$+ 2(0.5b_1')\Delta\phi mp_1(1-(N/Np)^2) \qquad (5.25)$$
$$+ 4(0.4301b_1')\Delta\Sigma mp_1(1-\operatorname{Cos}^4(54.5^{\circ})(N/Np)^2)$$
$$+ 4AJ\Delta\chi mp_1 + 4AC\Delta\eta mp_1(1-\operatorname{Cos}^4(54.5^{\circ})(N/Np)^2)$$

To this must be added the internal virtual work done in the corners of the strut, in the chord face and at the base of the tie member. The internal work done in a compressed corner of the strut is determined by the amount of squashing at point J necessary to maintain the mechanism geometry, which reduces linearly to zero squashing at points H and C. Hence the additional amount of virtual work done in the strut corners

$$= 0.5b_1'\Delta SQLt_1\sigma e_1 \qquad (5.26)$$

For a joint with the bracing members inclined at angles θ_1 and θ_2 to the chord, the yielding at the toe of the tie member produces internal virtual work of

$$\sigma e_2 b_2 t_2 (q \operatorname{Sin}\theta_2 - t_2/2)\Delta z + 2\sigma e_2 t_2 \frac{(q \operatorname{Sin}\theta_2 - t_2)^2}{2} \Delta z \qquad (5.27)$$

for lapped connections where z is the rotation of the chord face and q is shown on fig. 5.7. This strut buckling mechanism could also be applied to gapped joints with this component of the internal work done (equation 5.27) being omitted.

The internal virtual work done in the connecting chord face is

$$mp_o\Delta z\left\{2b_o'(1-(F/Fp)^2) + \frac{4h_1\operatorname{Cosec}\theta_1}{\sqrt{1-\lambda_1'}} + 4h_1\operatorname{Cosec}\theta_1\left(\frac{2h_1\operatorname{Cosec}\theta_1}{b_o'(1-\lambda_1')} + \frac{\sqrt{1-(F/Fp)^2}}{\sqrt{1-\lambda_1'}}\right)\right\} \qquad (5.28)$$

Equation (5.28) uses a value for the length DF (see fig. 5.7) of $0.5b_o'\sqrt{1-\lambda_1'}.\sqrt{1-(F/Fp)^2}$ similar to the yield line pattern for the push-pull mechanisms for gapped joints. Membrane action in the chord is also neglected which is possible because the chord rotations sustained before the strut collapses are small. The total internal work done from equations (5.25), (5.26), (5.27) and

(5.28) can then be equated to the total external work done of $Nh_1 \sin(\Delta z)$ where $\Delta z = 2\Delta\psi$. The solution by computer gives a rigid-plastic unloading line for the mechanism, as shown in fig. 5.13 for a particular strut and connection. There is a cut-off at $N/Np = 1.0$ in the graph at an out of plane buckle dimple deflection w/t_1 of about 0.3. This cut-off has also been observed for plates in uniaxial compression, and Dowling[29] attributes this to an in-plane mechanism, or squashing, occurring for very low w/t_1 values.

An approximate ultimate load for the strut by this failure mechanism can be achieved by the intersection of this unloading line with an elastic loading line, a method already tried for the determination of plate buckling loads by Davies et al[25] and Rawlings and Shapland[57]. This elastic load line is calculated conservatively by considering the strut reaction to pass through the face A in fig. 5.7, as represented in fig. 5.14. At any section XX in the strut there is a bending moment of $Nh_1'x/2H$ and an axial stress of N/A_1, where H is the height of the strut member and A_1 is the sectional area of the strut. The total strain at Section XX

$$= \frac{N}{A_1.E} + \frac{Nh_1'x}{2H\,Z_1E}$$

Hence the total compression over the length H for the edge of the tube which is always in maximum compression

$$= \int_0^H (N/A_1E + Nh_1'x/2HZ_1E)\,dx$$

$$= 2(N/Np)\left(\frac{H}{A_1E} + \frac{h_1'}{4Ez_1}\right)(b_1'+h_1')t_1\sigma e_1 \qquad (5.29)$$

The resulting elastic loading line is shown on fig. 5.13, and although the actual ultimate load is theoretically less than the intersection of the elastic and rigid-plastic lines, the conservative selection of the point of load reaction at the base of the strut reduces the significance of this effect.

5.4 Strut buckling mechanism 2

In this section a further failure mechanism is presented in which both the strut and tie sections may achieve full plasticity at less than the strut squash load. For the previous strut buckling mechanism it was shown that the point J (see figs. 5.15 and 5.7) was restrained in position and rotation was assumed to occur about A (fig. 5.7), but in this mechanism which is shown in fig. 5.15, rotation occurs about the point J. Under loading from N, the point D rotates to D' and the part of the connection which is overlapping acts as a rigid body attached to JD. As with mechanism no. 1, point E (fig. 5.15) is the point of contraflexure occurring at the mid length of a strut in a truss situation, or for an isolated joint test it represents the position of the lateral restraint on the strut.

As the chord face undergoes a total rotation of θ, the internal work done in the tie is given by

$$\left(Mp_2' + \frac{NSin\theta_1}{Sin\theta_2}.a_2\right)\theta \qquad (5.30)$$

and in the strut:

$$(Mp_1'+Na_1)\theta(1+LTCos\theta_1/(H-0.5Tan(\pi/2-\theta_1)h_1')) \qquad (5.31)$$

where a_1 and a_2 correspond to the distance a shown in fig. 5.5(c).

The internal virtual work done in the chord face is

$$mp_o\theta(2b_o'\sqrt{1-(F/Fp)^2} + \frac{4LT}{\sqrt{1-\lambda_1'}} + \frac{8LT(LT+0.5b_o'\sqrt{1-\lambda_1'}.\sqrt{1-(F/Fp)^2})}{b_o'(1-\lambda_1')} \quad (5.32)$$

The total internal work done can then be equated to the total external work done, which for the small deflections incurred up to failure, is given by

$$N.LT.\theta.\mathrm{Sin}\theta_1 \quad (5.33)$$

Hence $N.LT.\mathrm{Sin}\theta_1 =$

$$\begin{aligned}
&\frac{b_2'h_2'^2\sigma e_2}{4} - \frac{b_2'\sigma e_2}{4}\left[\frac{N\mathrm{Sin}\theta_1}{\mathrm{Sin}\theta_2.b_2'.\sigma e_2} + (h_2'-2t_2)\left(1-\frac{2t_2}{b_2'}\right)\right]^2 \\
&+ \frac{N\mathrm{Sin}\theta_1}{2\mathrm{Sin}\theta_2}\left[\frac{N\mathrm{Sin}\theta_1}{\mathrm{Sin}\theta_2.b_2'\sigma e_2} + (h_2'-2t_2)\left(1-\frac{2t_2}{b_2'}\right)\right] \\
&+ \left\{\frac{b_1'h_1'^2.\sigma e_1}{4} - \frac{b_1'\sigma e_1}{4}\left[\frac{N}{b_1'\sigma e_1} + (h_1'-2t_1)\left(1-\frac{2t_1}{b_1'}\right)\right]^2\right\}.C_2 \quad (5.34) \\
&+ \frac{N}{2}\left[\frac{N}{b_1'.\sigma e_1} + (h_1'-2t_1)\left(1-\frac{2t_1}{b_1'}\right)\right].C_2 \\
&+ \frac{t_o^2.\sigma e_o}{2}\left\{b_o'\sqrt{1-(F/Fp)^2} + \frac{4LT}{\sqrt{1-\lambda_1'}} + \frac{4LT(LT+0.5b_o'\sqrt{1-\lambda_1'}\sqrt{1-(F/Fp)^2})}{b_o'(1-\lambda_1')}\right\}
\end{aligned}$$

where $C_2 = (1+LT\ \mathrm{Cos}\theta_1/(H-0.5\ \mathrm{Tan}(\pi/2-\theta_1)h_1'))$

Equation (5.34) above uses a value for the length DF (see fig. 5.15) of $0.5b_o'\sqrt{1-\lambda_1'}.\sqrt{1-(F/Fp)^2}$, as for the strut buckling mechanism 1. This equation can then be solved for the strut load, N, by computer using the program listed in Appendix 2. The failure load for this mechanism is usually higher than that predicted by mechanism 1, but may occasionally be the governing failure mode for strut buckling.

5.5 Comparison of strut buckling mechanisms with test results

Both of these strut buckling mechanisms can be applied to the analysis of strut buckling in gapped joints too, as was mentioned in §4.3.1. For the strut buckling mechanism 1, the component of virtual work done in yielding the tie member represented by equation (5.27) becomes zero and the strut is still taken to rotate about the toe at point A on fig. 5.7. Consequently the strut buckling load according to mechanism 1 will be constant for gapped joints which only differ by the size of gap. When mechanism 2 is applied to the problem of strut buckling in gapped joints, the distance LT (see fig. 5.15) is affected by the size of gap, and so the strut buckling mechanism 2 predicts a lower strut buckling load as the gap increases, (provided the failure load is less than the strut and tie yield loads).

For an overlapped joint which was expected to fail by the strut buckling mechanism 1, the theoretically predicted loading and unloading lines are plotted in fig. 5.16 with the actual measured deflection of the joint (P7CI) under the heel of the strut. Very good correlation with the measured deflections was obtained for this joint, which was tested by BSC at Corby[9].

These two strut buckling mechanisms have been tested by comparing the predicted buckling loads of RHS to RHS gap and lap joints from Appendix 1 with the actual ultimate loads obtained.

The correlation between the predicted and actual strut buckling loads is shown in fig. 5.17 with the axes in the non-dimensional form of maximum strut load divided by strut squash load which shows that local buckling of the strut can occur at well below the squash load, and even as low as 53% of it. Some truss tests used in fig. 5.17 correspond to isolated joints which failed by strut buckling and in most instances failure of the same joint in the truss was not achieved due to failure elsewhere in the truss. The slight variations between the predicted failure loads for isolated joints and their identical truss joints are due to the differences in the lengths of the struts when in a truss and then in an isolated joint, as this affects the elastic loading line of mechanism 1.

The correlation between the actual and predicted strut buckling loads shown in fig. 5.17 is poorest for joints P8ATG and P6CIL, bearing in mind that joint P7BTG did not actually fail. These two joints also had long strut members. The length of the strut is most influential in determining the elastic load line for strut buckling mechanism 1 (fig. 5.13) so the simple method used for finding the elastic load line (fig. 5.14) may warrant further improvement in the light of more test evidence on joints having this failure mode.

5.6 Other lap joint failure modes

Aside from local buckling of the compression bracing, other less common modes of failure for RHS to RHS lapped joints which were described in the introduction to this chapter will be also investigated, such as:

(i) Chord wall shear failure (L4).

(ii) Chord local buckling behind the heel of the tension bracing member (L7).

The latter failure mode also occurs in RHS to RHS gapped joints and an analysis of this type of failure, which is applicable to both gapped and lapped joints, has already been presented in §4.3.2. The former failure mode (L4) will be caused by shearing of the whole chord section due to the vertical components of the bracing member forces, and is more likely to occur at large width ratios (λ) or for rectangular chord members with the larger side of the rectangle as the connecting chord face ($h_o < b_o$), particularly when the overlap is small. In tests on lapped joints L4 has sometimes been recorded as the failure mode when λ has been small but in these cases the joints have invariably reached either the strut squash load or the tie yield load and the joint is then being plastically distorted.

Chord shear failure

With reference to fig. 5.18, the strut force could cause shear failure along the path AB_1C_1, the tie force could cause shear failure along AB_3C_3, or alternatively shearing could happen along the line AB_2C_2, depending upon the thickness of the bracing members. Mathematically each path is equivalent to a normal force of $N\sin\theta_1$ shearing along a vertical line AB_2C_2, where the thickness of AB_2 will be the lesser of t_1 and t_2 and will actually determine the real shear path AB_1, AB_2 or AB_3, (providing the strut and tie also have the same yield stress). For a Pratt truss (N) joint the lines AB_1 and AB_2 will of course coincide.

The shear yield stress τ_e along AB_2 will be reduced by the forces in the bracing members, but is neglected at this stage, and the shear yield stress along B_2C_2 (or B_1C_1 or B_3C_3) will be reduced mainly by the axial chord force (F) as discussed in §3.5 by an amount equal to $\sqrt{1-(F/Fp)^2}$. Hence the chord shear load, assuming $\lambda \simeq 1.0$, is given by:

$$N\sin\theta_1 \simeq 2\left(q\,\frac{\sin\theta_1\sin\theta_2}{\sin(\theta_1+\theta_2)} + t_1\right)t_1\frac{\sigma e_1}{\sqrt{3}} + 2(h_o+t_o)t_o\,\frac{\sigma e_o}{\sqrt{3}}\,\sqrt{1-(F/Fp)^2} \tag{5.35}$$

The strut load necessary to cause chord shearing is the minimum of the value N calculated in equation (5.35) above, and the value of N calculated by replacing t_1 with t_2 and σe_1 with σe_2. Equation (5.35) assumes that the corners of the RHS members are also included in the shear area at ultimate load, which Wardenier and De Koning[71] had done for shear failure of gapped joints (equation 4.44). In tests in which RHS to RHS lapped joints have a large width ratio and modest overlap, chord shear may have been anticipated but it was generally preceded by chord local buckling, but in the case of truss joints where the possibility of chord local buckling is diminished, chord shearing may become a likely failure mode.

The interaction between local buckling failure of the strut and chord shear failure for an RHS to RHS lap joint of reasonably large width ratio is shown in fig. 5.19. It can be seen that chord shearing becomes the failure mode for small values of lap whenever the strut and chord thicknesses are approximately equal, but chord shearing becomes influential over a much larger lap range if the strut thickness is greater than the chord thickness.

The theoretical failure mechanisms and formulae which have been developed for RHS to RHS lapped joints in this chapter are part of the computer program for joint analysis which is listed in Appendix 2. With this analytical package, 26 RHS to RHS lap joints from Appendix 1 have been studied, with the resulting correlation between the predicted and actual ultimate joint loads shown graphically in fig. 5.20.

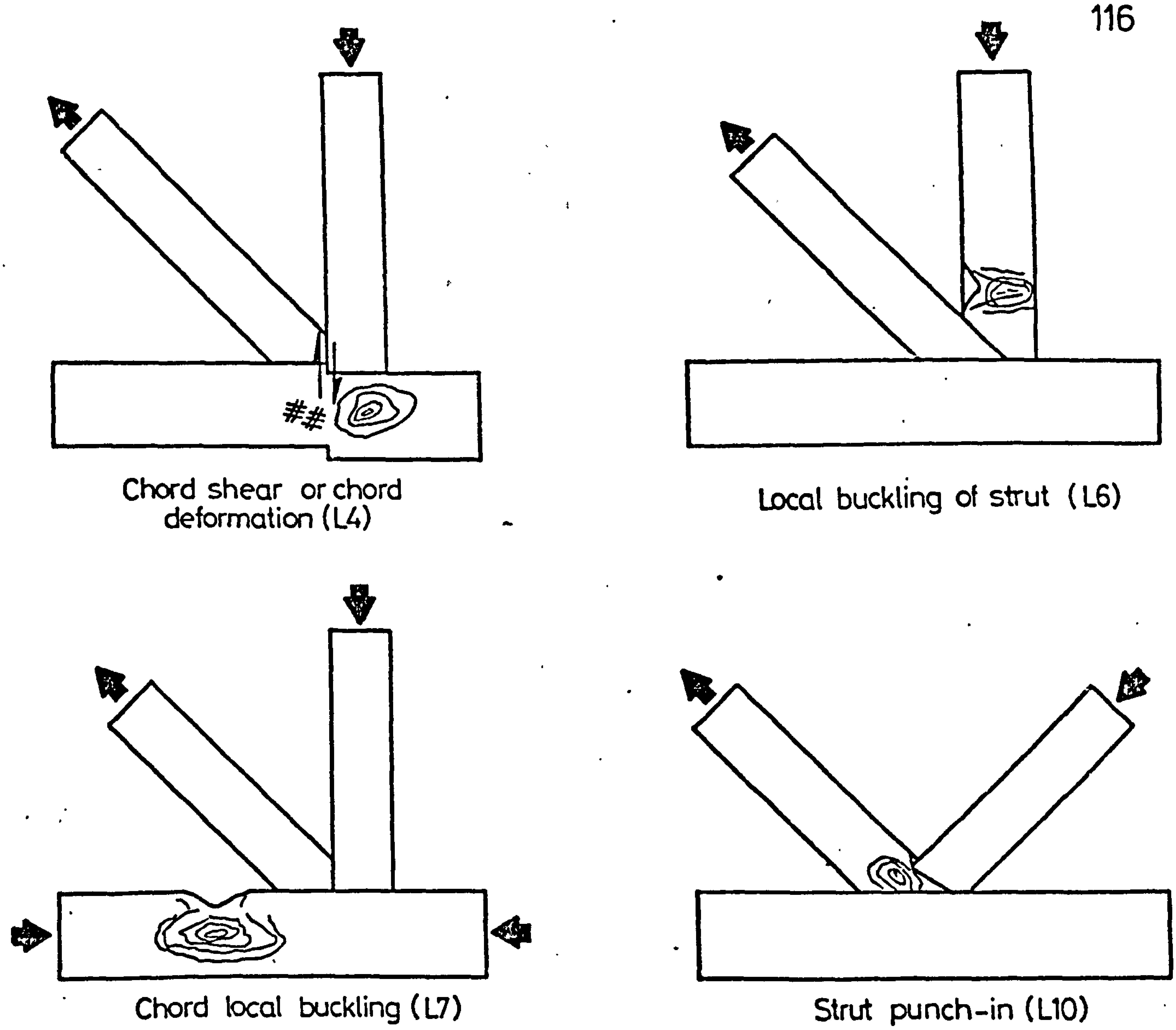

Fig.5·1 Lap joint failure modes

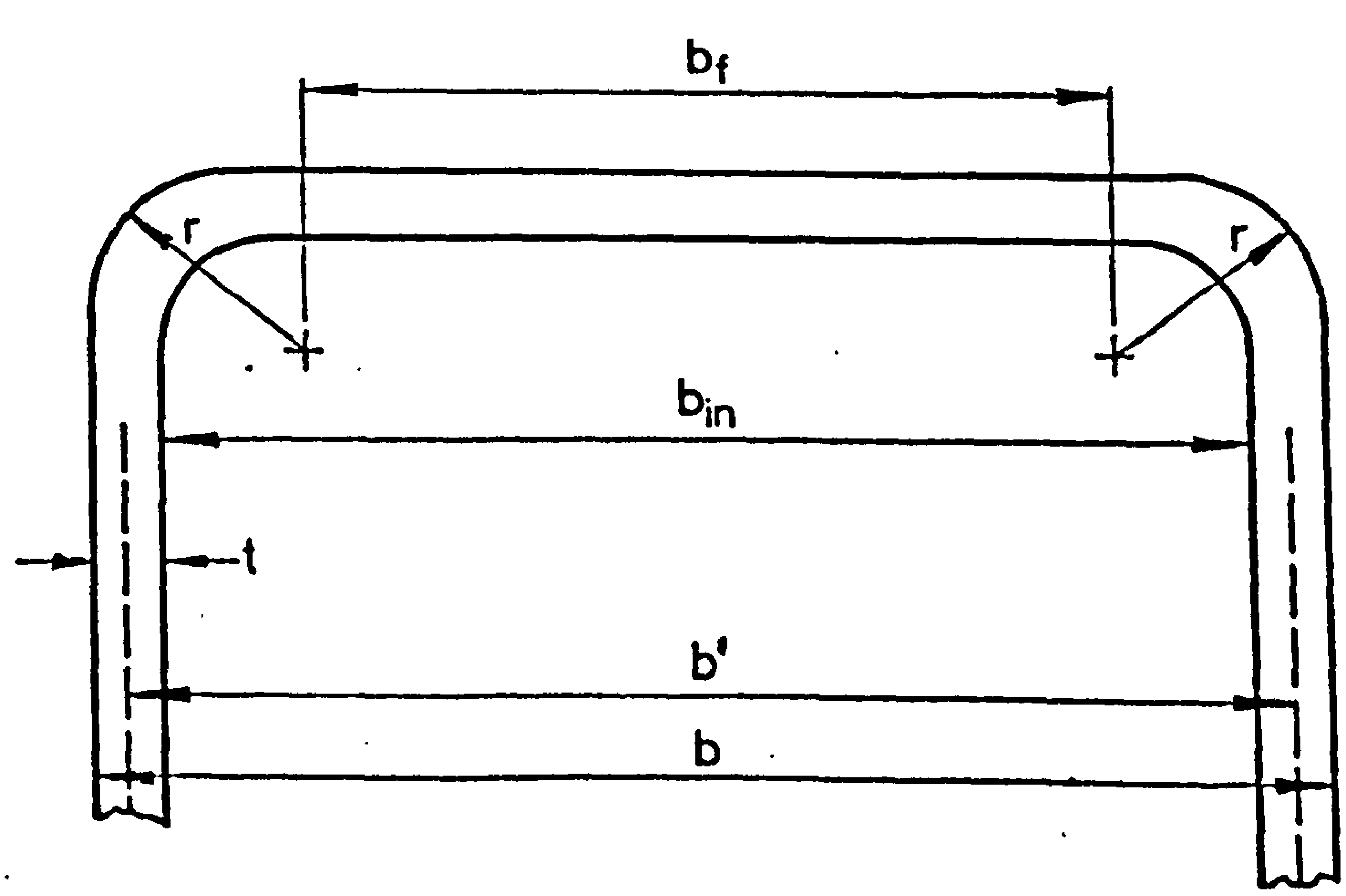

Fig.5·2 Effective widths for a side of an RHS for local buckling

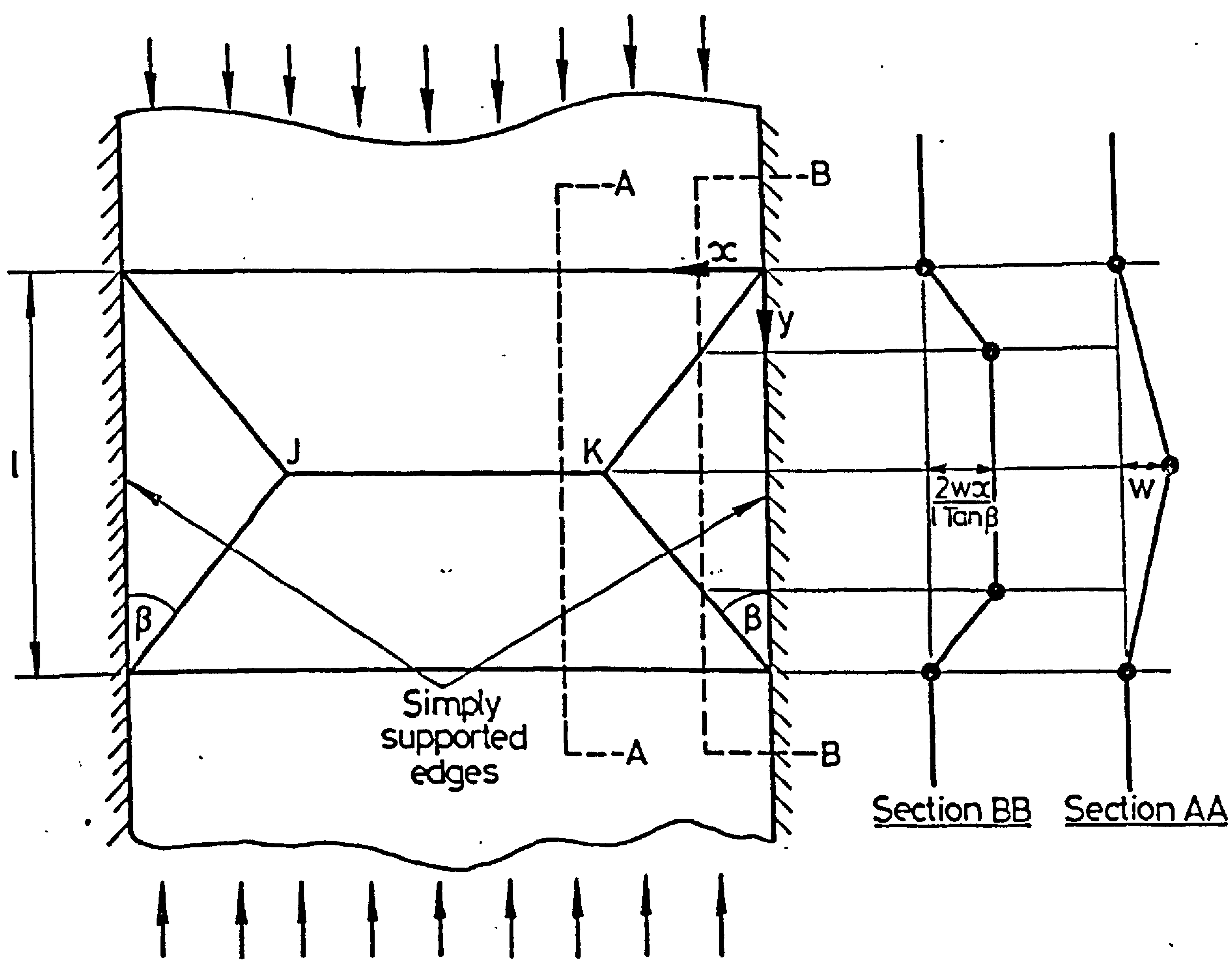

Fig.5·3 Plate buckling mechanism by Davies et al (25)

Fig. 5.4 Local buckling in strut member

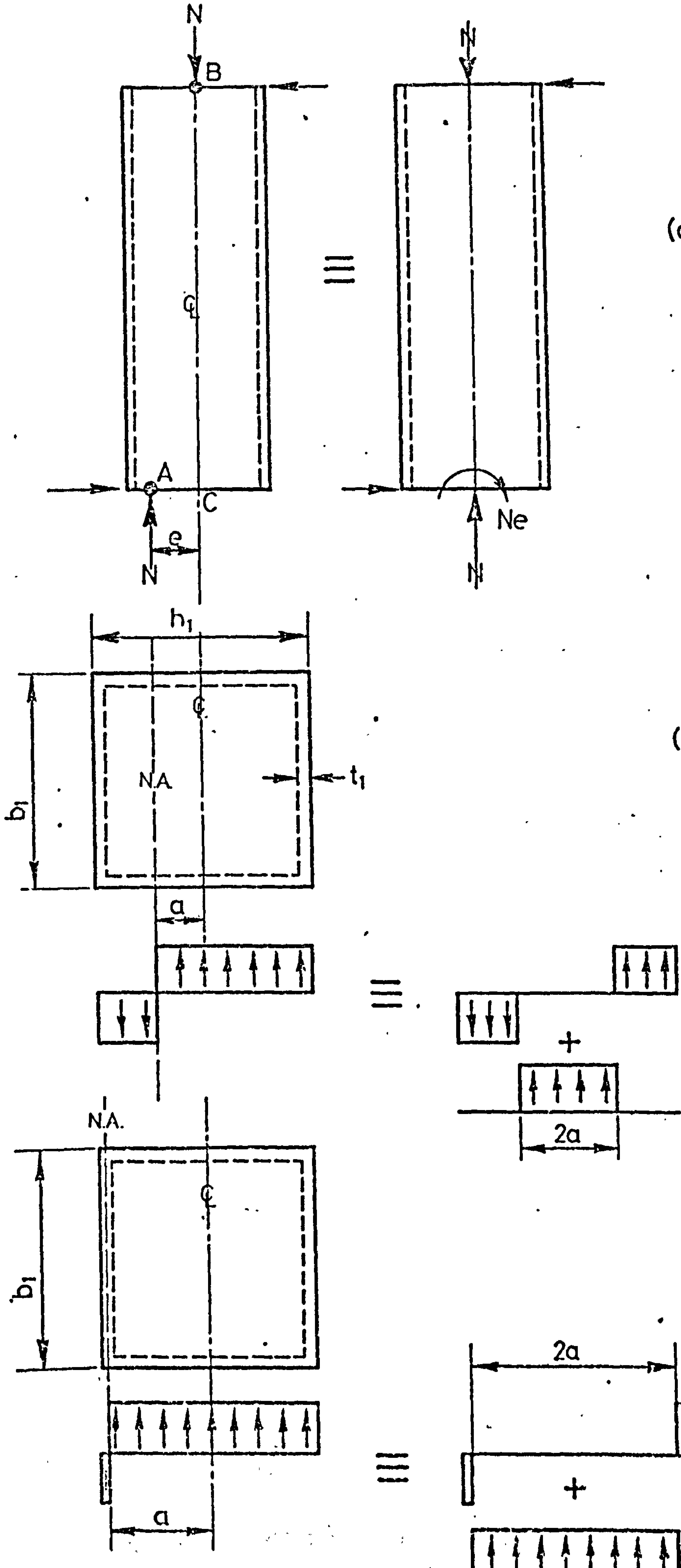

(a) Eccentrically compressed strut

(b) Stress distribution with Neutral axis in tube web

(c) Stress distribution with Neutral axis in tube flange

Fig.5·5 RHS tube under non-axial compression

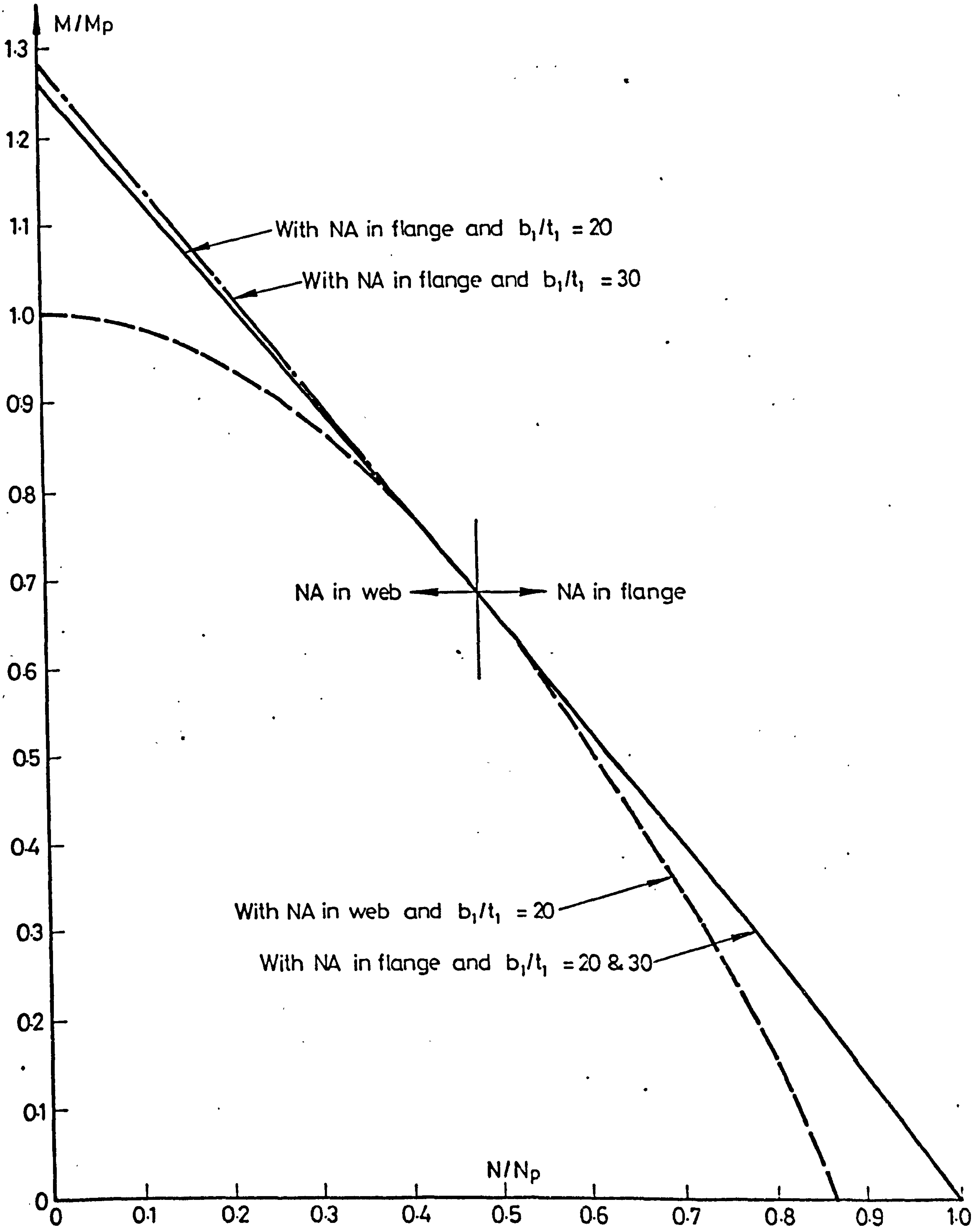

Fig.5·6 Interaction between plastic moment capacity and axial load for a hollow square tube

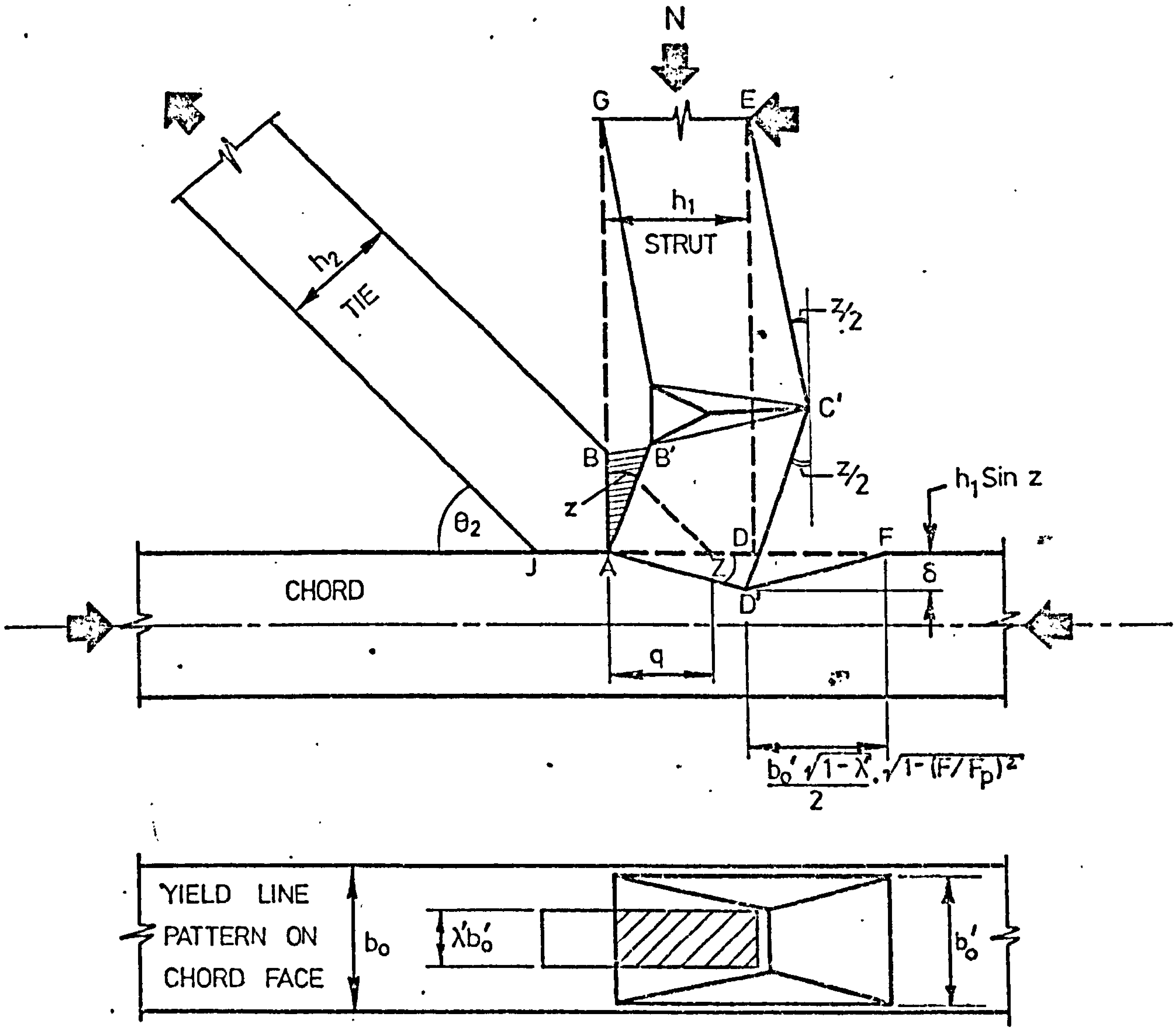

Fig.5·7 Strut local buckling Mechanism N° 1 shown for a Pratt truss lapped joint

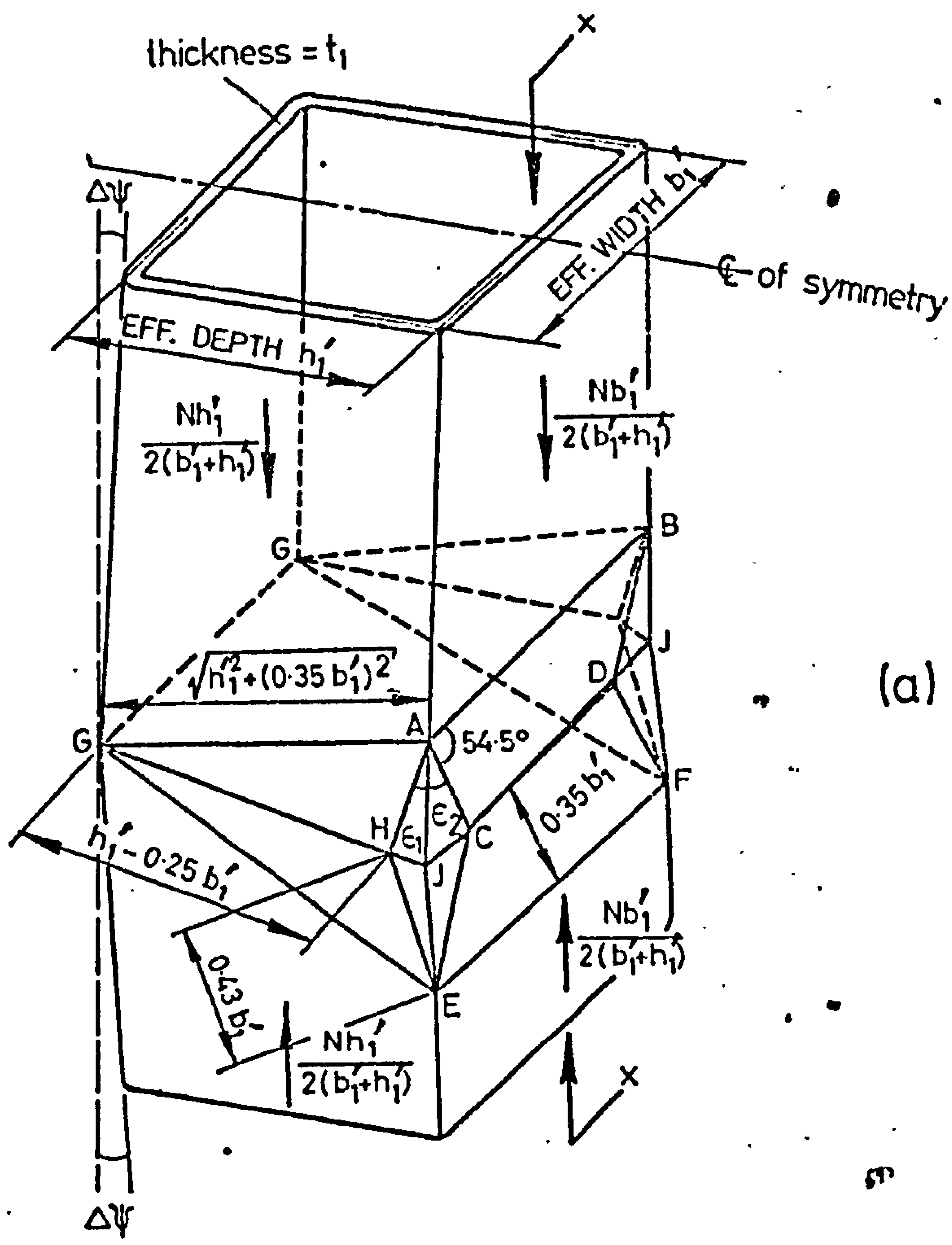

(a)

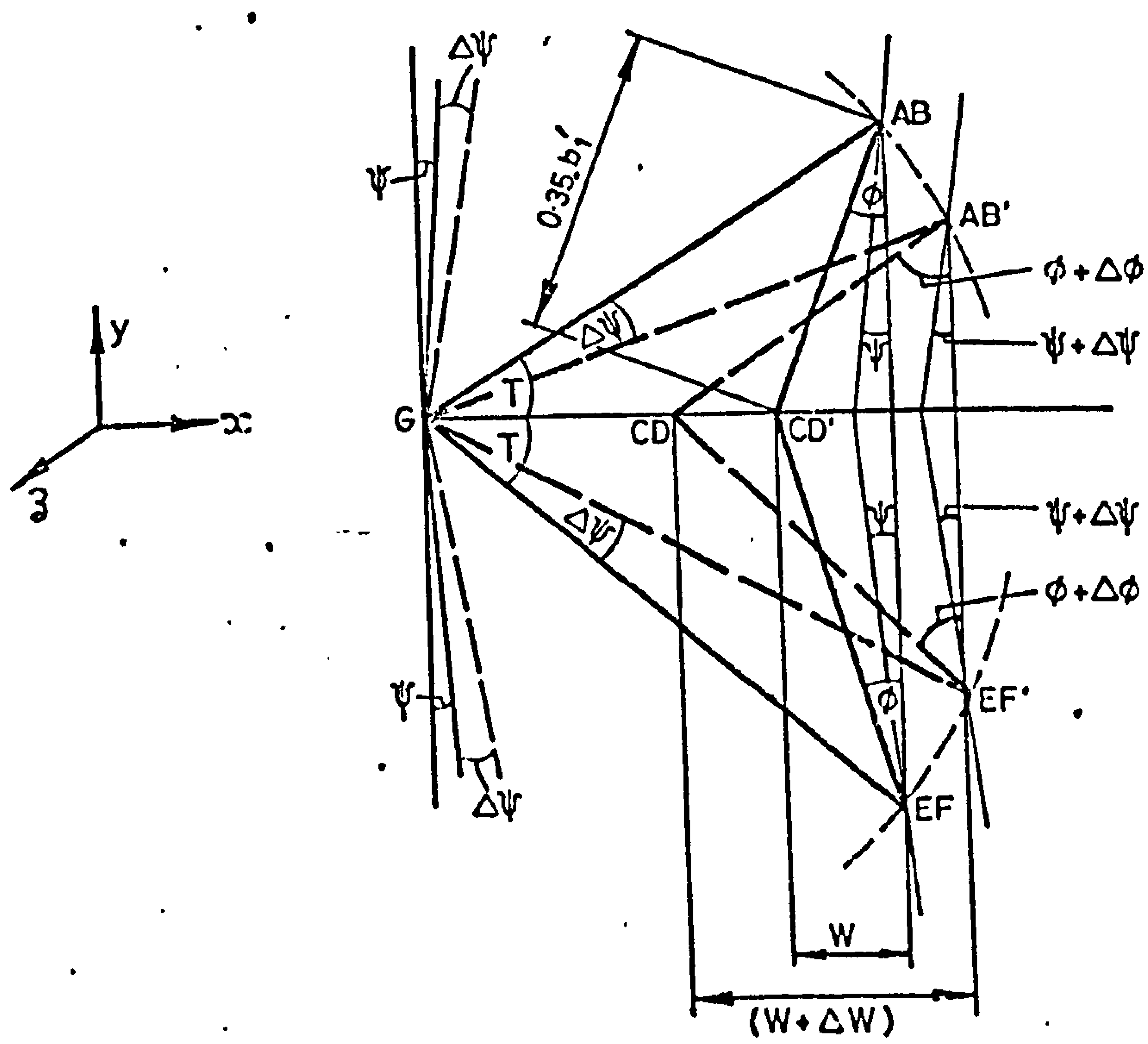

(b)

Section XX

Movement of side of tube in the vertical plane

$GA = \sqrt{h_1'^2 + (0{\cdot}35\,b_1')^2}$

$GH = h_1' - 0{\cdot}25\,b_1'$

$AH = 0{\cdot}4301\,b_1'$

Angles T, ϕ, ψ all change as w increases

Fig.5·8 Yield-line pattern for Strut Buckling Mechanism N°1

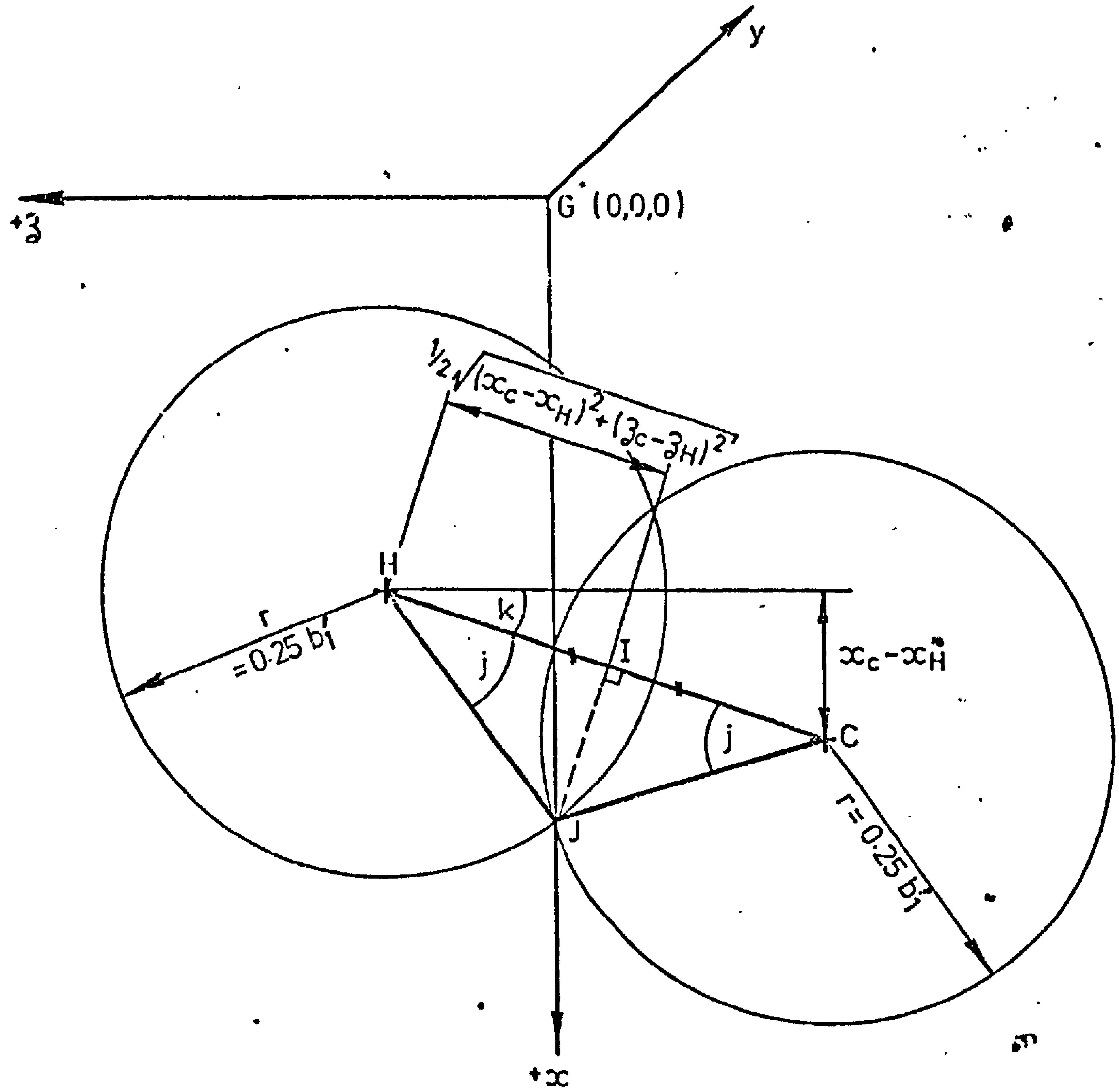

Fig.5·9 Location of point J for Strut Buckling Mech. 1

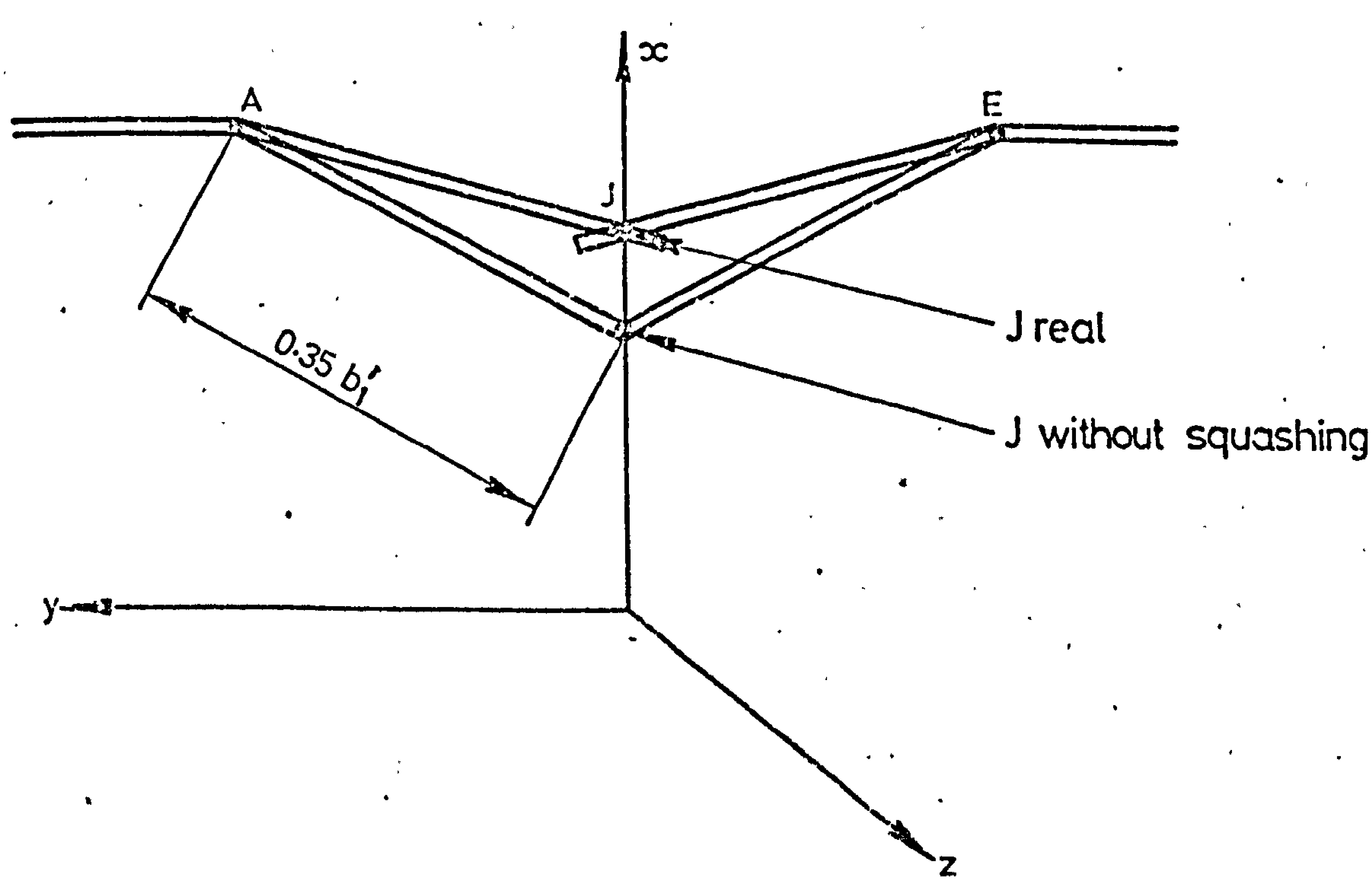

Fig.5·10 Crushing of the tube corners at J

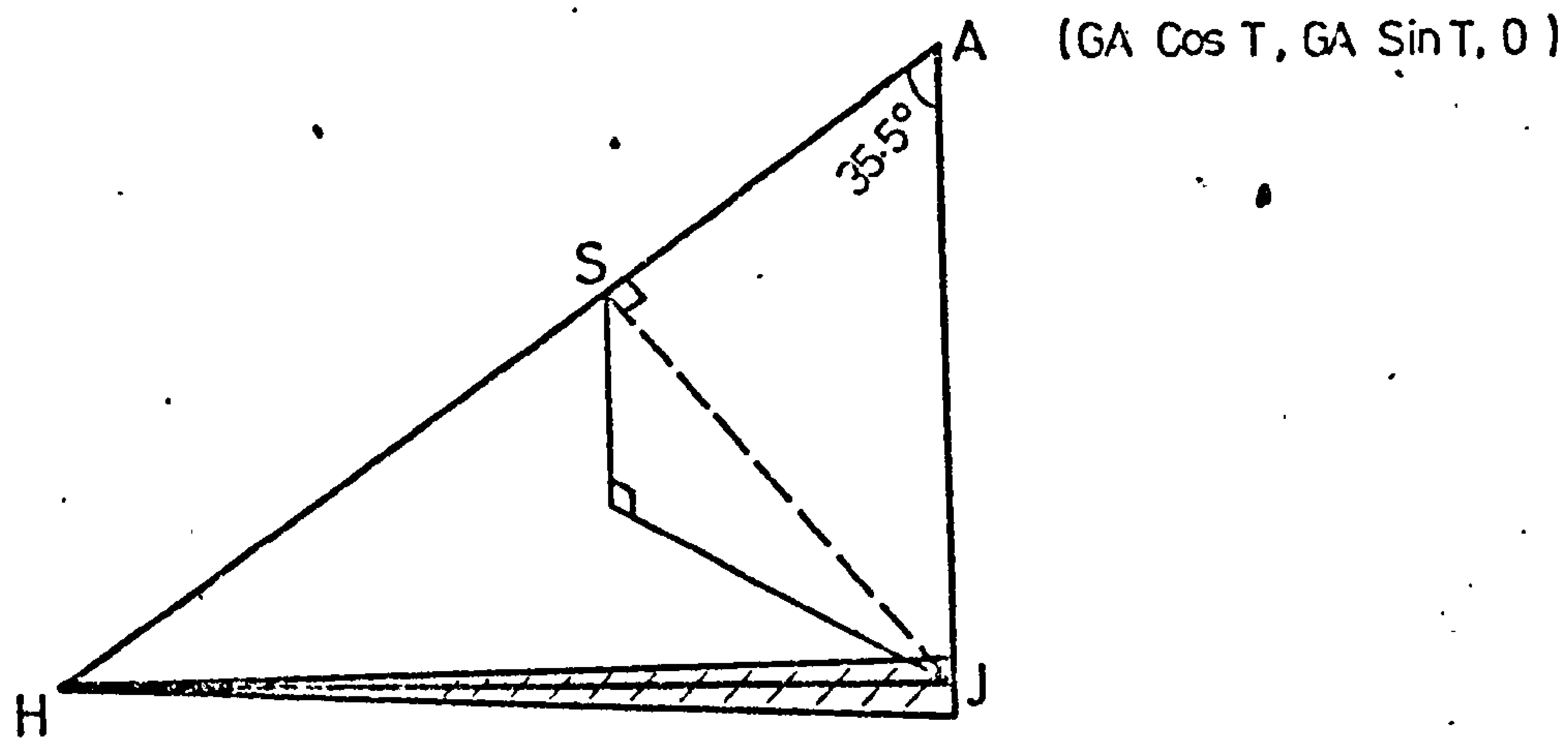

$$H:\left(\frac{GA^2+GH^2-AH^2}{2GA\,\cos T},\,0,\,\sqrt{GH^2-\left[\frac{GA^2+GH^2-AH^2}{2GA\,\cos T}\right]^2}\right)$$

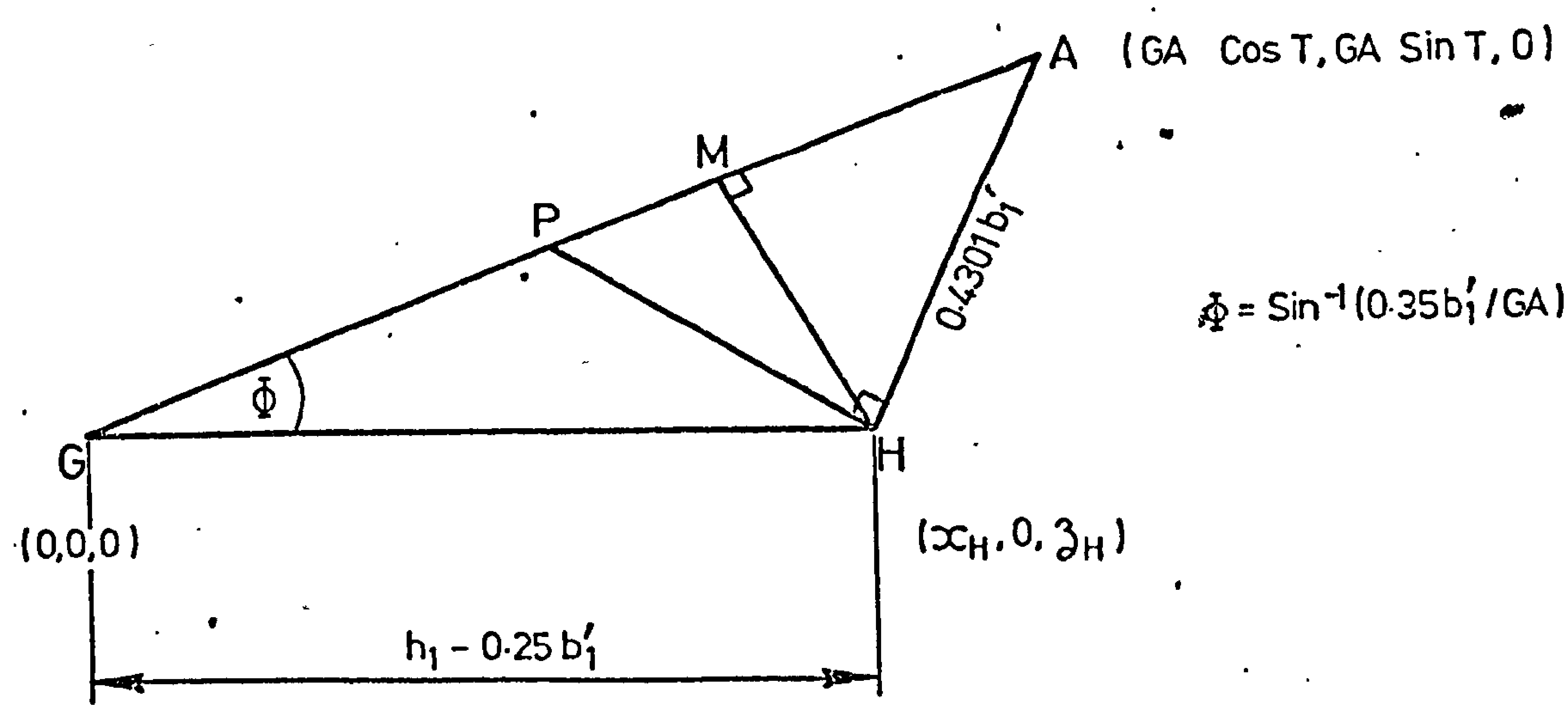

Fig.5·11 Rotation of lines AH and HE

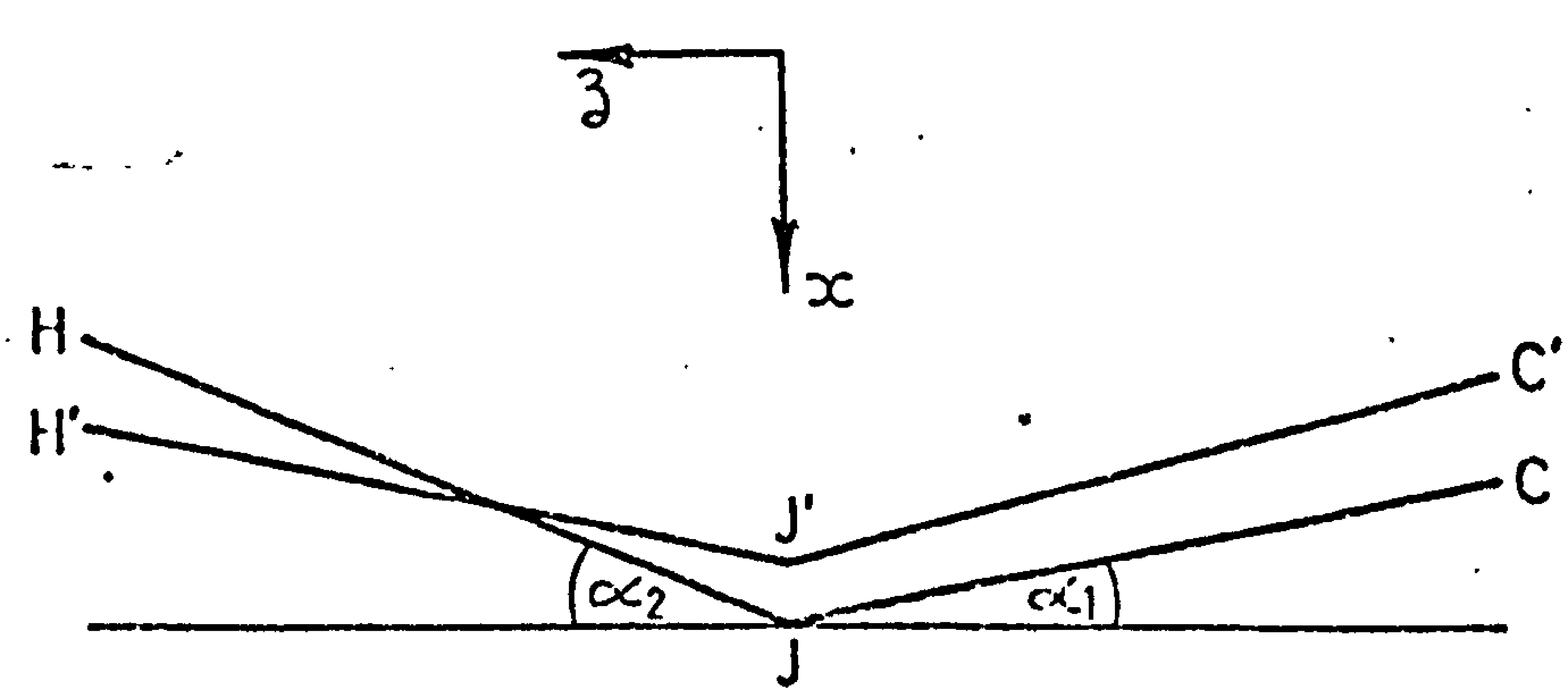

Fig.5·12 HJC viewed in the XZ plane

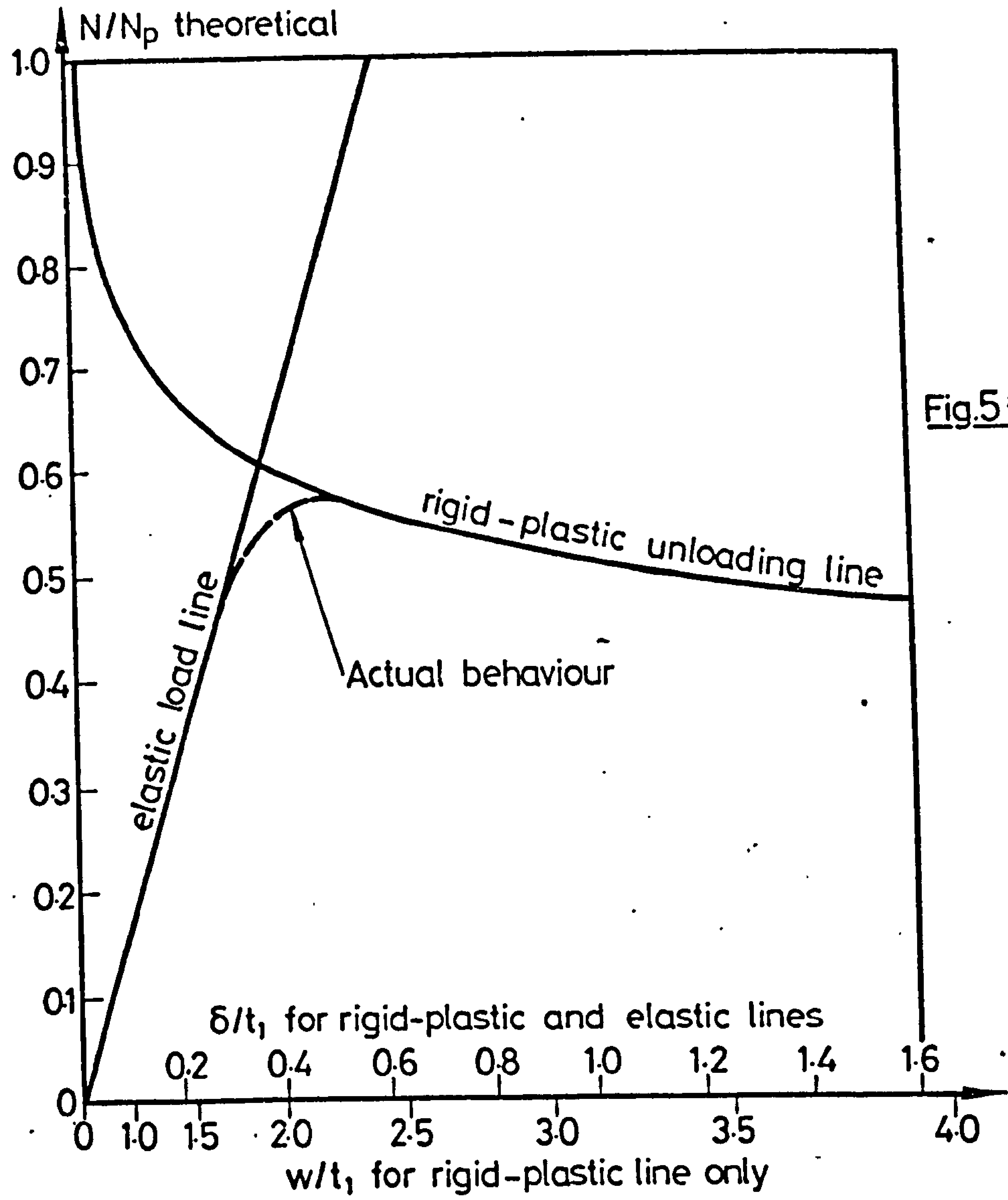

Fig.5·13 Load/deflection behaviour for strut buckling mechanism 1

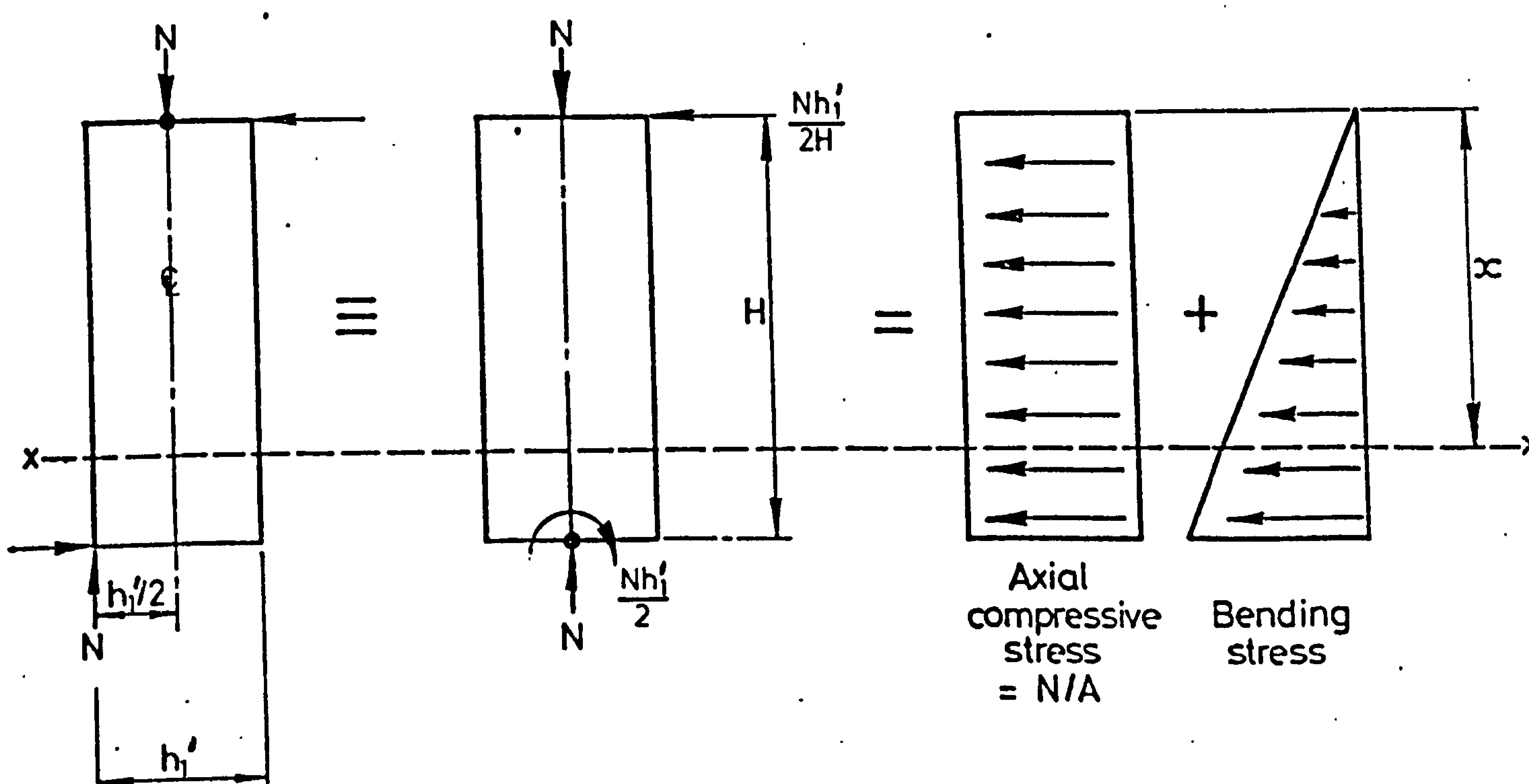

Fig.5·14 Determination of elastic load line for strut buckling mechanism 1

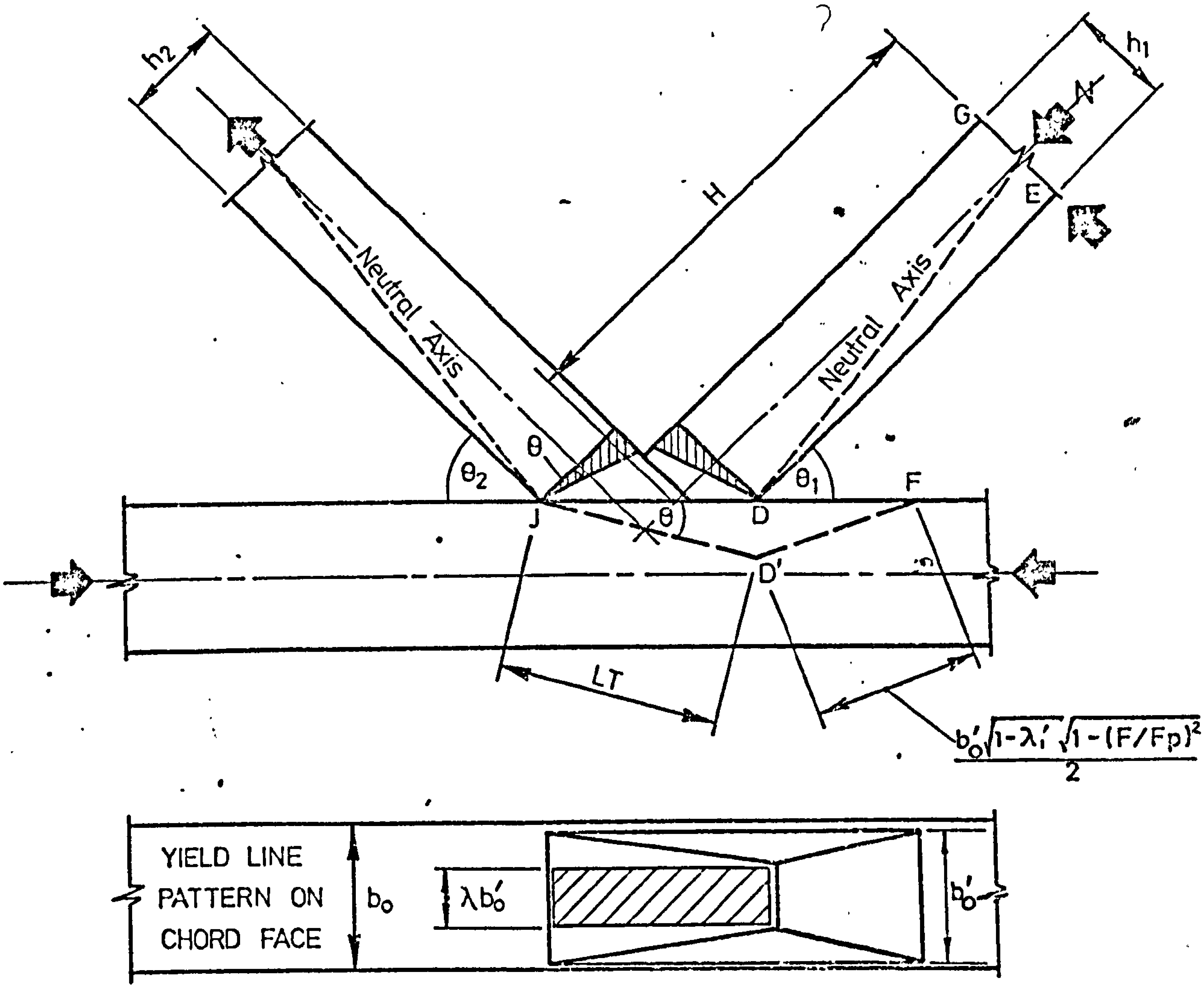

Fig.5·15 Strut local buckling Mechanism N° 2 shown for a Warren truss lapped joint

Fig.5·16 Load v. deflection behaviour of joint P7CI

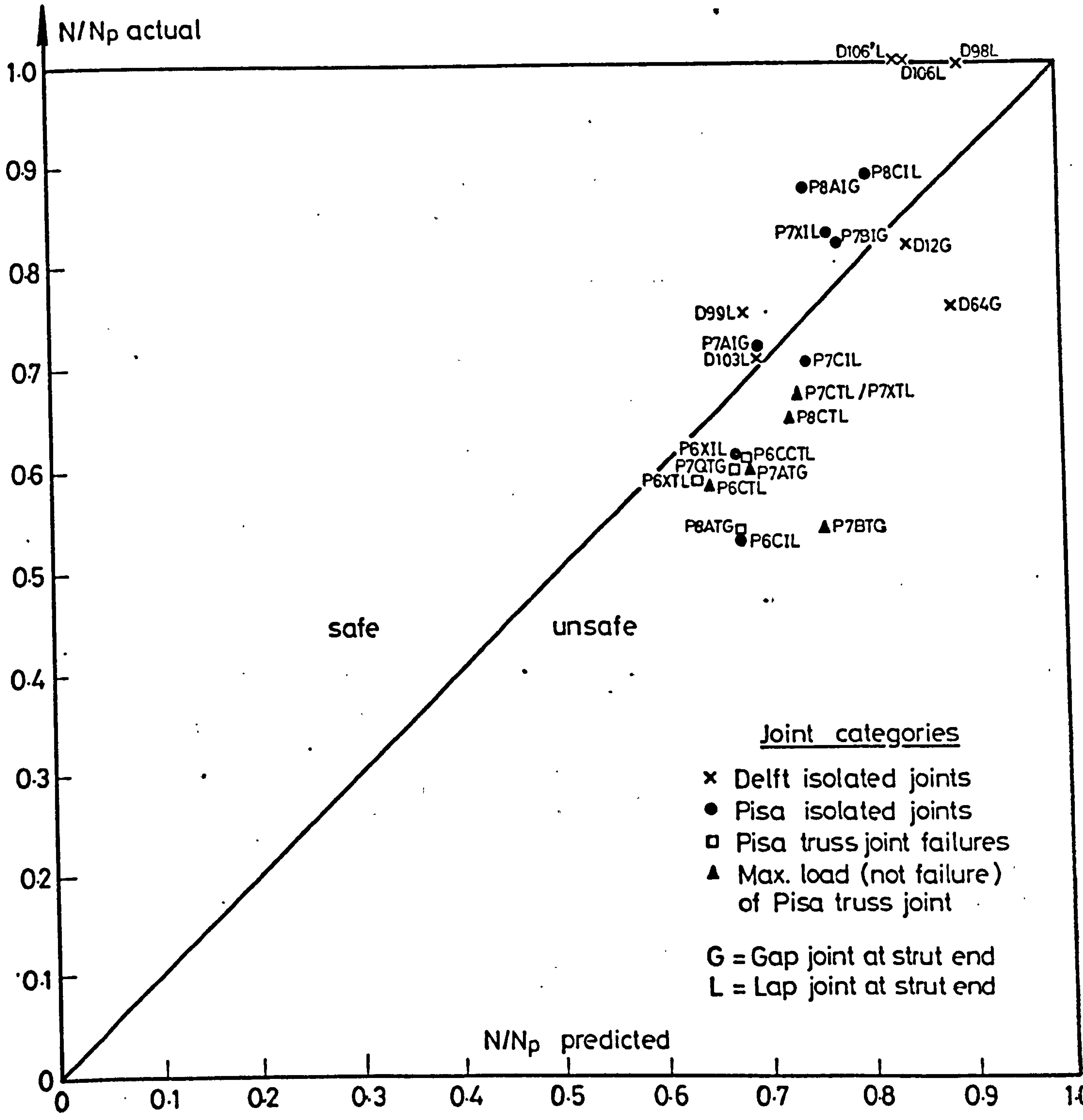

Fig.5.17 Actual v. predicted local buckling loads for struts in RHS gap and lap joints

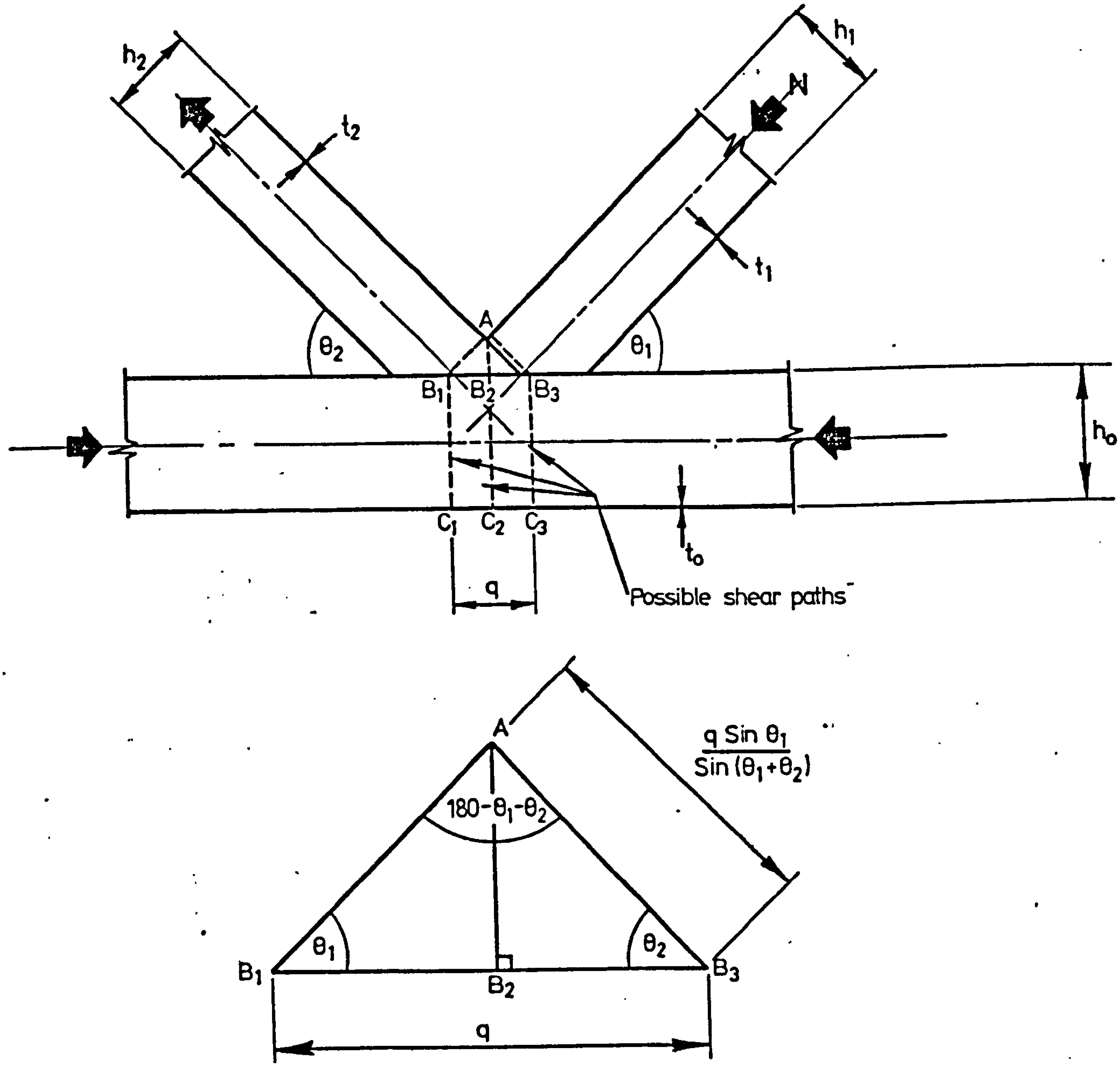

$$AB_2 = \frac{q \sin\theta_1 \sin\theta_2}{\sin(\theta_1+\theta_2)}$$

Fig. 5·18 Chord shear failure for lapped joints

Fig. 5.19 Relationship between Strut buckling and Chord shearing for an N Lap joint

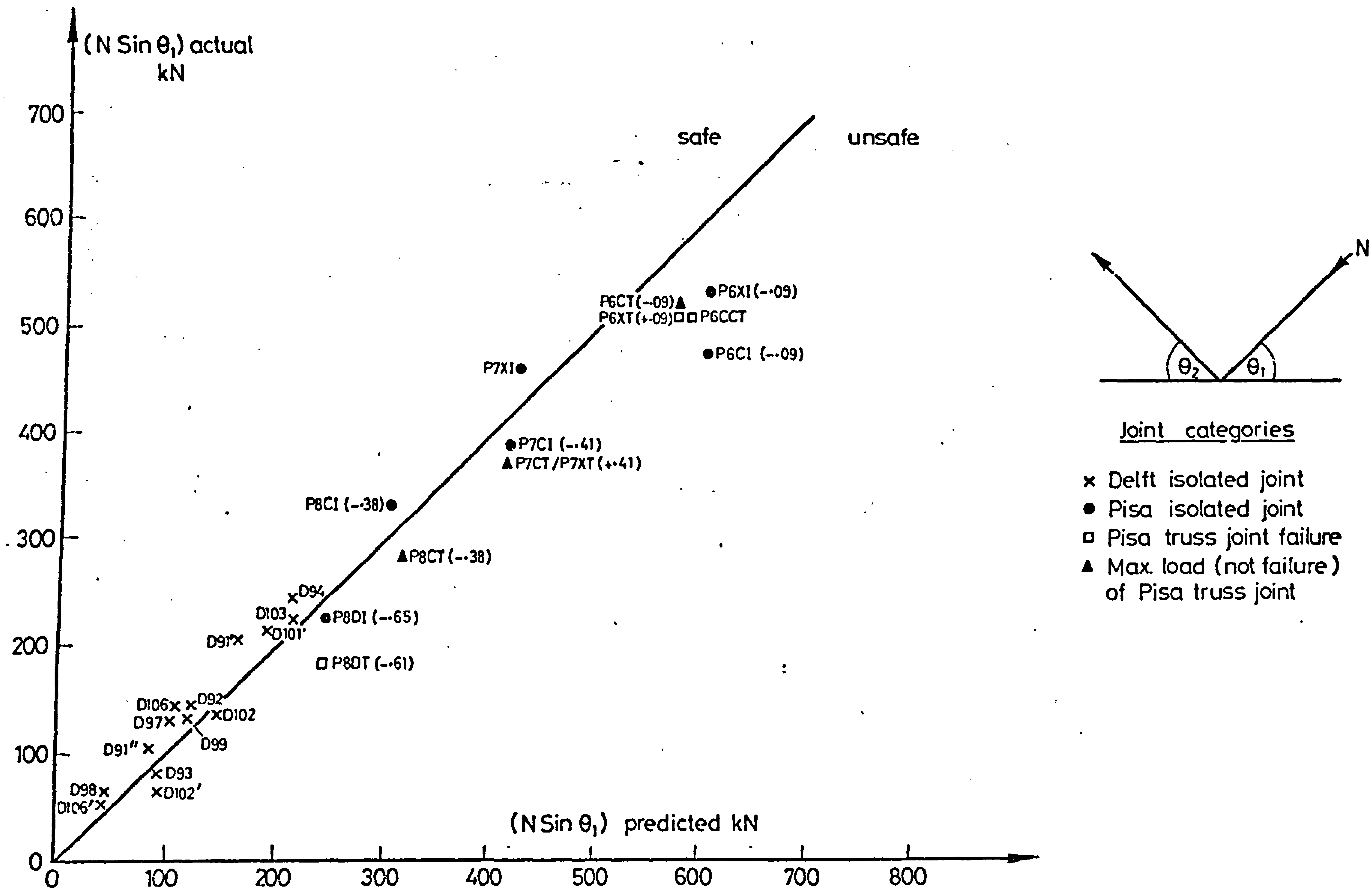

Fig. 5·20 Actual v. predicted ultimate loads for RHS to RHS lap joints

CHAPTER 6

INFLUENCE OF PURLIN LOADS ON ULTIMATE JOINT STRENGTH

The application of a concentrated compressive load, such as a purlin load, at a joint may have two effects:

(a) It may reduce the joint strength, measured as a load in the compression bracing, by means of affecting the joint failure mechanisms which have been presented in Chapters 4 and 5, or

(b) It may cause premature failure of the joint by bringing about failure of the chord side walls (fig. 6.4) or failure of the chord face immediately beneath the purlin load (figs 6.5 and 6.6).

6.1 Reduced joint strength without failure of the chord side walls or the non-connecting face

If the strength of the joint changes due to an applied compressive purlin load it is only of interest if it decreases. If an increase in joint strength were taken into account then the purlin force must be relied upon to always act at its maximum. Consider the joints shown in fig. 6.1 in which the joint strength, (measured, as is common, by a force in the strut), decreases slightly with the addition of a substantial purlin force. If the ultimate strut load decreased as a result of the purlin force then the force in the tension member drops considerably, as does the compression force in the chord member too. Therefore the strut member will tend to push in more than before and the tie will pull out less. For each of the possible joint failure mechanisms previously considered in the joint analysis for both gapped and lapped joints without purlin loading, the following changes will now occur in the theory:

6.1.1 Push-pull Mechanisms

As the strut tends to push in more than the tie, the point of zero displacement of the chord face will move towards the tie member. Hence it is necessary to postulate what the relative displacements would be under each branch member, with strut displacements being greater than tie displacements. If the purlin load is significant the push-pull mechanisms will tend towards the mechanism with $x = 1.0$, but there is usually little difference between the predicted failure loads with $x = 0.5$ or $x = 1.0$ except for large gaps. (If anything the ultimate strength for the mechanisms with $x = 1.0$ will usually be greater than at $x = 0.5$.) If the push-pull mechanism with $x = 0.5$ does occur then the left-hand side of equation (4.17) becomes

$$N\sin\theta_1 \Delta\delta + (N\sin\theta_1 - F_{purl})\Delta\delta = \ldots\ldots , \qquad (6.01)$$

where F_{purl} is the compressive purlin load on the joint.

Therefore for a compressive purlin load applied to the joint, the joint strength, <u>measured as a force in the strut</u>, would increase by $F_{purl}/2\sin\theta_1$. However, if a joint was prone to failure of the chord side walls, (such as a Warren joint with compressive 'preload'), the addition of a compressive purlin force <u>may</u> cause the chord side walls to yield at a lower joint load. So for the push-pull failure mechanisms the joint strength may either show a slight increase, remain unchanged, or possibly show a slight decrease.

6.1.2 Strut Buckling Mechanisms

For the strut buckling mechanism 1 (fig. 5.7), the analysis is such that an extensive yield pattern in the strut, tie and chord face is solved with respect to the force in the strut member regardless of the force in the tie member. The theoretical ultimate load capacity of the strut member will thus remain unchanged with or without a purlin load.

For the strut buckling mechanism 2 (fig. 5.15) there is a change in the local buckling load of the strut because the vertical components of the bracing member forces are no longer equal. As the failure load for this mechanism is generally higher than that for the strut buckling mechanism 1, it may still not be critical. With a purlin force acting, equation (5.34) now becomes:

$$
\begin{aligned}
&N.LTSin\theta_1 \\
&= \frac{b_2'h_2'^2\sigma e_2}{4} - \frac{b_2'\sigma e_2}{4}\left[\frac{NSin\theta_1 - F_{purl}}{Sin\theta_2.b_2'\sigma e_2} + (h_2'-2t_2)(1-2t_2/b_2')\right]^2 \\
&+ \left(\frac{Nsin\theta_1 - F_{purl}}{2Sin\theta_2}\right)\left[\frac{NSin\theta_1 - F_{purl}}{Sin\theta_2.b_2'\sigma e_2} + (h_2'-2t_2)(1-2t_2/b_2')\right] \\
&+ \left[\frac{b_1'h_1'^2\sigma e_1}{4} - \frac{b_1'\sigma e_1}{4}\left[\frac{N}{b_1'\sigma e_1} + (h_1'-2t_1)(1-2t_1/b_1')\right]^2\right].C_2 \qquad (6.02) \\
&+ \frac{N}{2}\left[\frac{N}{b_1'\sigma e_1} + (h_1'-2t_1)(1-2t_1/b_1')\right].C_2 \\
&+ \frac{t_o^2\sigma e_o}{2}\left[b_o'\sqrt{1-(F/Fp)^2} + \frac{4LT}{\sqrt{1-\lambda_1'}} + \frac{4LT(LT+0.5b_o'\sqrt{1-\lambda_1'}\sqrt{1-(F/Fp)^2})}{b_o'(1-\lambda_1')}\right]
\end{aligned}
$$

where $C_2 = (1+LT\cos\theta_1/(H-0.5\tan(\pi/2-\theta_1)h_1'))$

6.1.3 Chord Shearing

When a compressive purlin force acts on a chord member, this load is mainly resisted by compression of the chord side walls, (see §6.2), and so the actual shear force on the joint is only the vertical component of a reduced force in the tension member. Hence the likelihood of chord shear failure decreases with the application of a purlin load, but the shear on the side walls of the chord needs to be considered together with the other local stresses acting, as is discussed in §6.2. Similarly, if a tensile purlin force acts on a chord member at a joint then the same conclusion applies.

6.1.4 Chord Local Buckling

As the total horizontal component of the bracing member forces does not change with the application of a purlin force the chance of failure by chord local buckling remains the same, but if the joint strength is measured as a force in the compression bracing member, then there is a large increase in the strut load which would be required to cause chord local buckling (see fig. 6.1).

6.2 Failure of the chord side walls or the non-connecting chord face

Very little research has hitherto been done on the strength of RHS members loaded transversely to the section causing possible bearing failure in the tube flange or buckling in the tube webs.

6.2.1 Web Buckling Failure

Recently RHS to RHS cross joints, (fig. 6.2(b)), which have a more severe loading of the chord side walls than a truss joint with a purlin loading, (fig. 6.2(a)), have been studied by Czechowski and Brodka[20]. The cross joint loading case in a truss can be avoided by designing the truss such that the support reaction bears directly on to a strut member (fig. 6.3(a)) rather than the chord section (fig. 6.3(b)). Czechowski and Brodka did tests on fabricated square sections in mild steel having b_i/t_i or $h_i/t_i \leq 34$ and used a plastic failure analysis to predict the test failures. They found that for joints with $\lambda_1 = 1.0$, the ultimate bracing load (N) was given by

$$N = (1.06 - 0.021(h_o/t_o))\sigma e_o.A_o, \text{ for } F = 0 \qquad (6.03)$$

For $\lambda_1 < 1.0$, the ultimate bracing load (N) is given by the minimum of:

$$N = 2mp_o\left\{\sqrt{1-(F/Fp)^2}.\left[\pi(2+\gamma+1/\gamma) + \frac{4\lambda_1\gamma}{1-\lambda_1}\right] + \frac{4\eta}{1-\lambda_1}\right\} \qquad (6.04)$$

and $$N = 2mp_o\left\{\sqrt{1-(F/Fp)^2}.\left[\pi(1+\gamma+1/\gamma) + \frac{4\lambda_1\gamma}{1-\lambda_1}\right] + \frac{4\eta}{1-\lambda_1}\right\} \qquad (6.05)$$

where $\eta = h_1/b_o$ and $\gamma = 1/\sqrt{1.273\left(\frac{\lambda_1}{1-\lambda_1}\right) + 1}$.

Equation (6.05) is for an asymmetrical failure mode which might occur if the joint was not given sufficient lateral support, and equation (6.04) is for a symmetrical failure mode. Both of equations (6.04) and (6.05) were based upon the erroneous assumption that the inward deflection of the connecting chord face under the branch members would be the same as the outward deflection of the chord side walls at the mid-depth of the chord. Even the test results from this investigation[20] may not be representative of hot-rolled RHS cross joints because the fabricated sections did not have corner radii.

Morrell[50] found that if a uniform load was applied across the whole flange width, (such as a full width purlin cleat which would be the most common cleat connection), then because of the corner radii involved in hot rolled RHS sections, the load was transmitted eccentrically through the chord side walls or webs of the member. So at failure of the side walls an 'equivalent eccentricity' was derived which corresponded to the position of two point loads acting on the flange of the member. This 'equivalent eccentricity', measured from the outside of the web of the member was approximated to

$$e = 0.021b_o + 0.862t_o \qquad (6.06)$$

This implies that $e > t_o$ whenever $b_o/t_o > 6.57$ which is true for all hot rolled RHS in Britain[12] except 200x100x16 RHS.

Consequently there will always be a small moment on the chord side walls out of the plane of the joint, as well as a moment on the chord side walls in the plane of the joint due to the horizontal components of the bracing member forces. In addition to this loading the axial force in the chord due to 'preload' and the horizontal components of the bracing member forces, the axial compression due to the purlin load and the vertical shear force on the chord walls, make the loading situation on the chord webs extremely complex. Combined with an unknown area of the chord side wall over which these forces and moments are concentrated and unknown boundary restraints for the edges of the chord walls, it is suggested that considerable practical testing on both gapped and lapped joints with purlin loading needs to be done first to provide sufficient information, but empirical rules may be the most reliable solution.

A rigorous analysis of the buckling failure mode for chord side walls has not been attempted as a thorough investigation is now under way in Japan (CIDECT Programme 5Y). However two purlin loaded joint tests have been performed[28,71] in which failure occurred by buckling of the chord side walls. For both of these joints the bracings were full width ($\lambda = 1.0$) and the chord section was relatively stocky. In this case there will be minimal bending moments on the chord side walls and failure of the walls is also likely to be caused by yielding near the mid-depth of the chord. Hence a simplified analysis of the chord side walls is presented in which all bending moments are neglected and failure is caused by yielding of the side walls due to a normal shear load of $N\mathrm{Sin}\theta_1 - F_{purl}$, a normal compression load of F_{purl} and an axial chord force F. It is then hoped that reasonable predictions of the chord side wall failure load can be obtained for these two joints mentioned above (D144 and D145).

If the length of stiff bearing beneath the purlin or purlin cleat is t_p and the length of the bearing beneath the strut member is ℓ_b as shown on fig. 6.4, then an average normal compressive stress on an element in the middle of the chord wall is

$$\sigma_v = F_{purl}/(\ell_b+t_p)t_o$$

The average chord stress,

$$\sigma_H \simeq -F/A_o \tag{6.07}$$

and the normal shear stress

$$\tau_v = \frac{N\sin\theta_1 - F_{purl}}{2(b_o+2t_o)t_o},$$

where the shear area given here is for a gapped joint. Failure under this combination of stresses could then be reached when:

(a) The maximum principal stress reaches the yield stress. (Maximum Principal Stress Theory by Rankine)

i.e.
$$\left(\frac{\sigma_H+\sigma_v}{2}\right) + \sqrt{\tau_v^{\,2} + \left(\frac{\sigma_v-\sigma_H}{2}\right)^2} = \sigma e_o \tag{6.08}$$

or (b) The maximum shear stress reaches the shear yield stress. (Maximum Shear Stress Theory by Tresca)

i.e.
$$\sqrt{\tau_v^{\,2} + \left(\frac{\sigma_v-\sigma_H}{2}\right)^2} = \tau e_o \tag{6.09}$$

or (c) The maximum shear strain energy of distortion is reached. (Von Mises)

i.e.
$$\sigma_H^{\,2} + \sigma_v^{\,2} - \sigma_H\sigma_v + 3\tau_v^{\,2} = \sigma e_o^{\,2} \tag{6.10}$$

Of these three failure theories the two most commonly used for steel are those by Tresca and Von Mises[39]. These failure theories can be applied to the two joints (D144 and D145 having

$\lambda = 1.0$) which failed by buckling of the chord side walls and very good estimates of the side wall yield load, (yielding in the chord side walls would actually produce the appearance of a web buckle), are obtained, as shown on figs 4.12 and 4.13. For both of these joints equation (6.09) gave the lowest predicted failure load.

In all, six tests on purlin loaded joints have been done by Wardenier and De Koning[28,71], all of which were gapped Warren joints with no chord 'preload'. The results of these six tests were compared with six similar tests without purlin loads. Unfortunately one set of six tests with purlin loading did not have the same dimensions and properties as the corresponding set of six tests without purlin loading as there were small differences in measured sizes of the members and in the material yield stress when comparing two 'equivalent' joints. So the effect of the addition of a purlin load to a joint depends upon the particular expression for joint strength which is used, as it will depend upon measured member sizes and the member yield stress. Consequently Dutch (equations 2.04 and 2.07) and British (equations 2.09 to 2.11) joint strength formulae give a different change in joint strength with the addition of purlin loading, for these six tests[28,71].

Apart from two of these joint tests (D144 and D145) discussed previously, all others failed by cracking of the chord connecting face or strut buckling. The ultimate strength of these joints can be predicted by the modified failure mechanism theories of §6.1, with the correlation between the predicted and actual ultimate loads for these joints, (D146, D147, D150 and

D151), being shown in fig. 4.12. The agreement obtained is reasonable but further experimental results from joints with purlin loading is certainly required. The joints in the RHS trusses tested at Pisa[10] which also had applied loads were not representative as they were locally reinforced.

National structural steelwork specifications generally do not give any specific guidance for checking the side walls of RHS members against buckling due to local loading and imply that they can be treated as for buckling of I-section webs. The Australian Institute of Steel Construction[1] actually specifies that the load acting on an RHS member should be dispersed at an angle of 45^{o} to the mid-depth of the member, and then designed as a column of this width and of thickness t_o. The slenderness ratio is given by $b_o''\sqrt{3}/t_o$ where b_o'' is the clear depth between root fillets.

6.2.2 Chord Bearing Failure

This type of failure, as shown in fig. 6.6, has not been observed in any RHS joint tests but the Australian Institute of Steel Construction[1] does give a direct bearing capacity for RHS webs based upon a dispersion of the load at an angle of 30^{o} out to the inside of the flange. For calculation of the bearing capacity of an RHS section the failure mechanism shown in fig. 6.5 is proposed, in which the load is resisted by bending of the tube flange and support from a yielded foundation of web material. A CIRIA research project at the University of Aston uses a similar model for bearing failure in I-sections.

As deflections of this mechanism are small, by equating the internal virtual work done to the external work done by the load gives:

$$F_{purl}.\delta = 4Mp_o'\theta + 2v.\frac{\delta}{2}.w + wt_p\delta$$

where w = upward force from the webs per unit length

$= 2t_o\alpha\sigma e_o$

$\alpha\sigma e_o$ is the upward stress from the chord webs and is determined by a biaxial stress interaction with the axial chord stress.

$$\therefore \qquad F_{purl} = \frac{4Mp_o'}{v} + v.w + wt_p \qquad (6.11)$$

The minimum value of F_{purl} will occur when $\partial F_{purl}/\partial v = 0$;

i.e. when $\qquad v = 2\sqrt{Mp_o'/w}$

It is likely that part of the RHS web just below the flange will also resist the load in bending. Hence the 'effective' plastic moment of resistance of the flange would be increased by this contribution. By trial and error it was found that if the 'effective' plastic moment of resistance of the RHS flange was twice the value of the nominal moment of resistance $(b_o t_o^2 \sigma e_o/4)$ then the final computed bearing strength of the chord was closest to experimental values. An 'effective' flange thickness of $\sqrt{2}t_o$ has thus been used.

$$\therefore \qquad (F_{purl})min = 4\sqrt{Mp_o'.w} + wt_p$$

and

$$Mp_o' = \frac{b_o.2t_o^2}{4}.\sigma e_o(1-(F/Fp)^2)$$

$$\therefore \qquad (F_{purl})\text{min} = 4t_o\sigma e_o(\sqrt{b_o t_o \alpha(1-(F/Fp)^2} + 0.5\alpha t_p) \qquad (6.12)$$

To calculate α consider the stresses acting in the chord webs below the flange of the loaded section. The shear stress due to the vertical components of the branch members will be disseminated and low on the side of the chord where the purlin load acts, and so the dominant stresses will be due to the chord axial force of F/A_o and the upward stress on the purlin load of $\alpha\sigma e_o$. In this biaxial loading situation the yield criterion for the webs may be predicted by the maximum shear strain energy of distortion theory by Von Mises.

$$\text{i.e.} \qquad (F/A_o)^2 + (-\alpha\sigma e_o)^2 - (F/A_o)(-\alpha\sigma e_o) = \sigma e_o^{\,2}$$

$$\therefore \qquad \alpha = \frac{-\sigma e_o . \dfrac{F}{A_o} + \sqrt{\dfrac{\sigma e_o.^2 F^2}{A_o^{\,2}} - 4\sigma e_o^{\,2}.(F^2/A_o^{\,2} - \sigma e_o^{\,2})}}{2\sigma e_o^{\,2}} \qquad (6.13)$$

To test the validity of equations (6.12) and (6.13), a limited number of tests have been done at Nottingham University on RHS specimens such as that in fig. 6.6 which simulate the local bearing failure which could occur under a full-width purlin cleat which has been welded all round. Five tests were done using a 100x100x3.95 RHS with a yield stress of 354 N/mm^2 at different values of axial chord compression load up to $F/Fp = -.72$, (72% of the squash load), and results close to those predicted theoretically were obtained (see fig. 6.7). Further bearing tests on other chord sizes are still required to test the general validity of this model for chord bearing failure.

In concluding this chapter on the influence of a purlin load or external load at a joint, the theoretical and limited experimental evidence which is available indicates that the ultimate joint strength, measured as a force in the compression bracing member, will be changed little by a purlin load, and the purlin loading can probably be ignored in practice providing local failure of the chord side walls, (i.e. buckling or bearing failure of the side walls as described in §6.2.1 or §6.2.2), is not liable to occur.

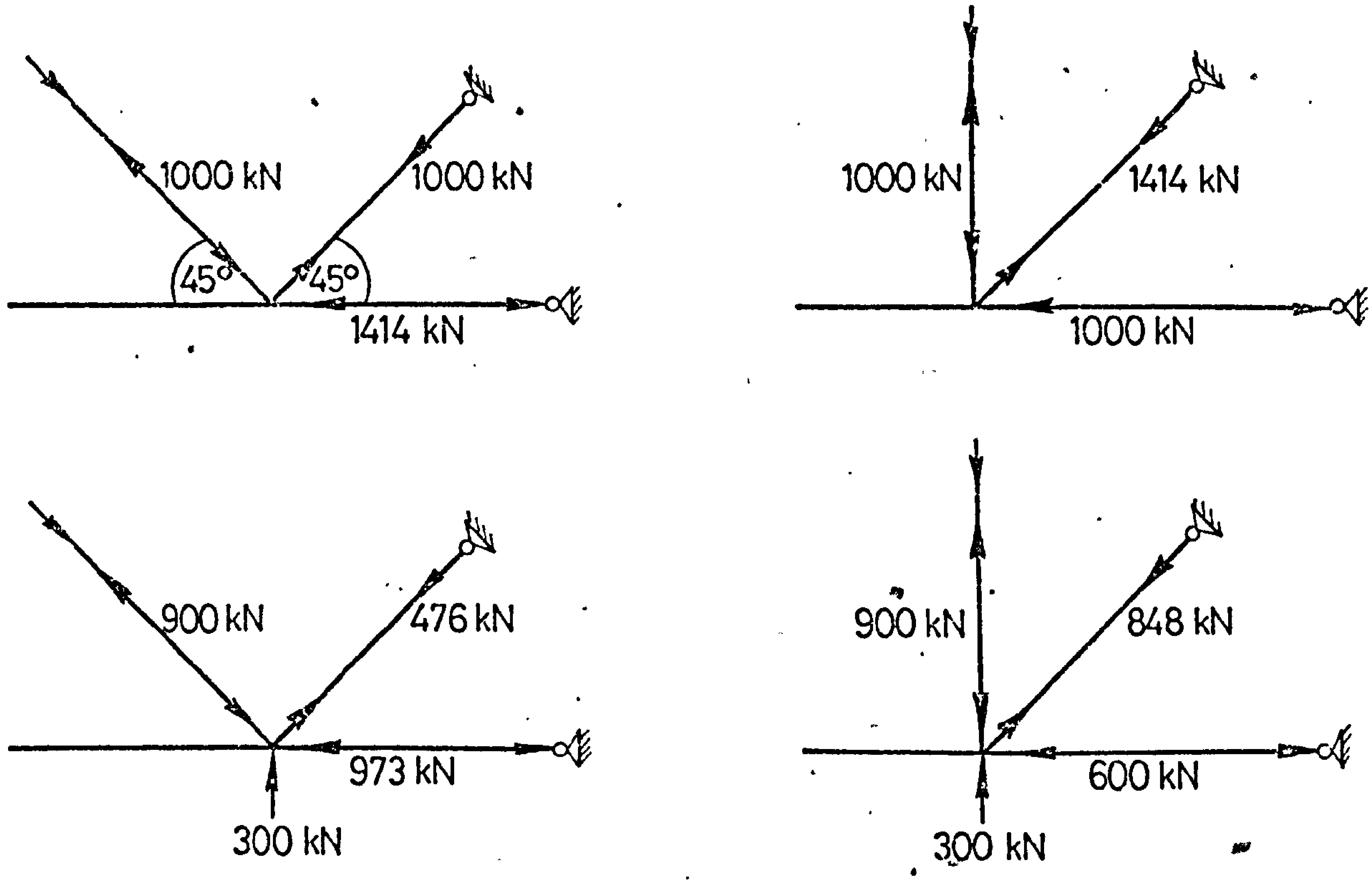

Fig.6·1 45° Pratt and Warren truss joints with and without purlin load

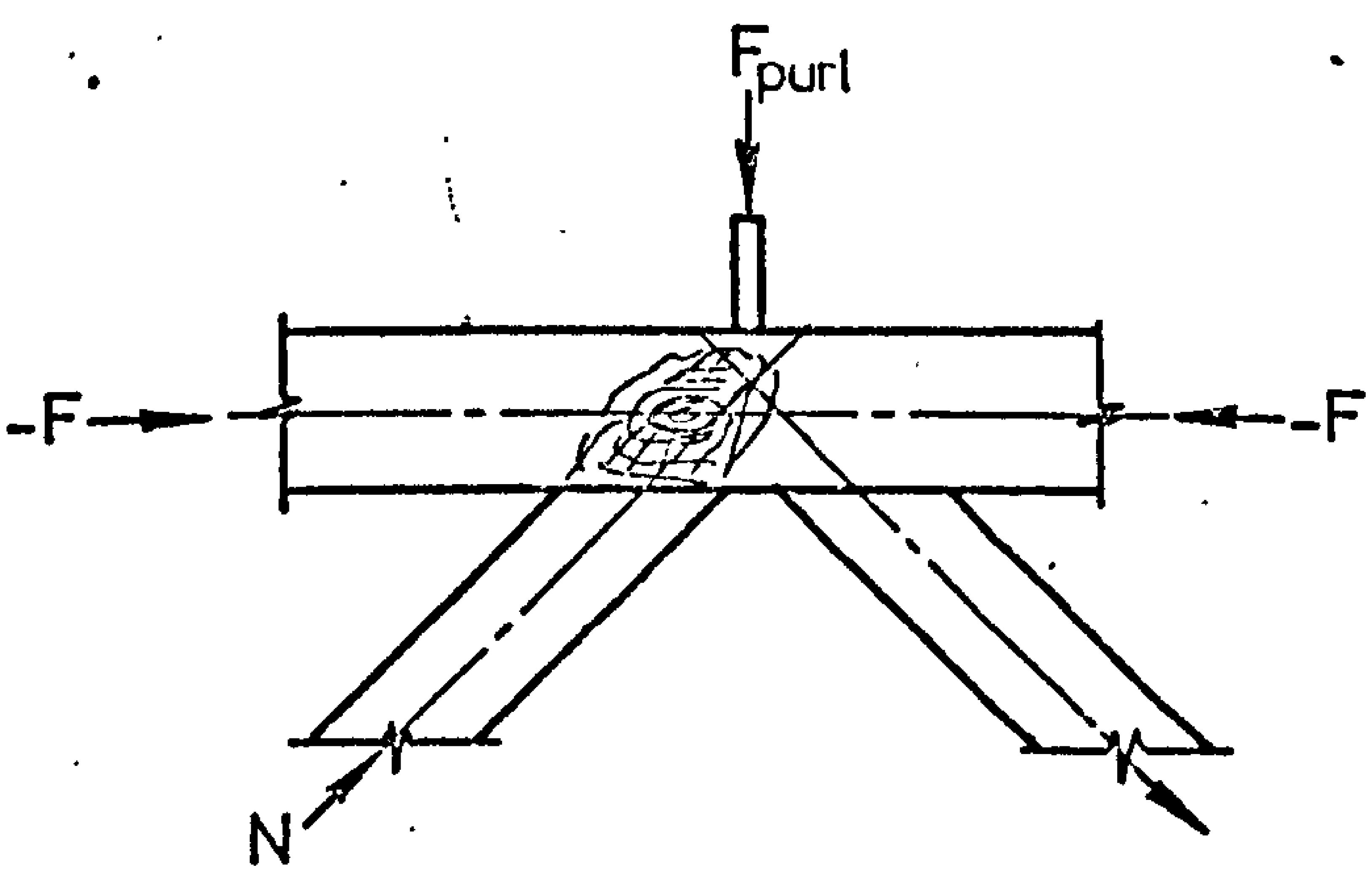

Fig.6·2 (a) Warren truss joint with load from purlin cleat

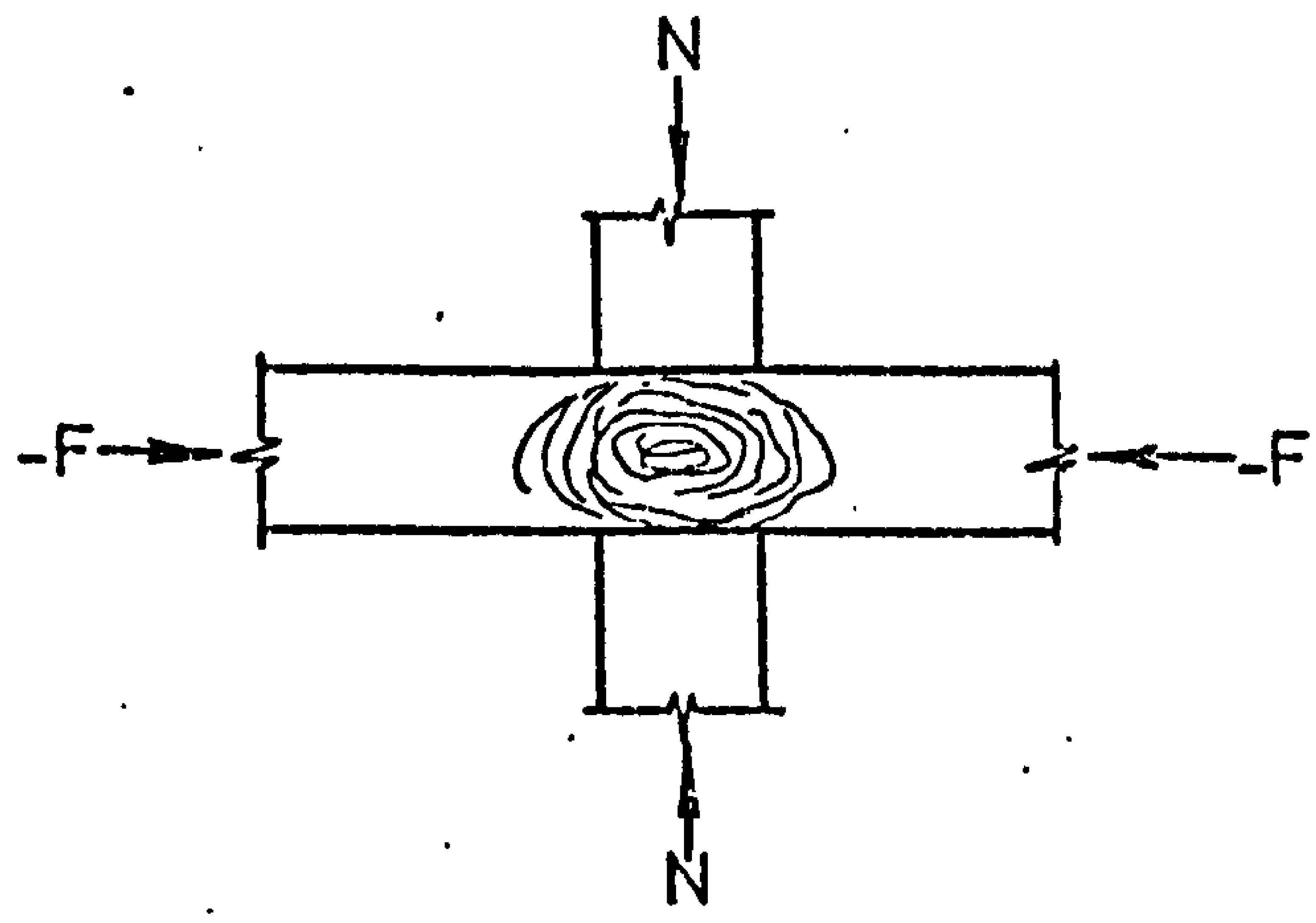

Fig.6·2 (b) Cross joint

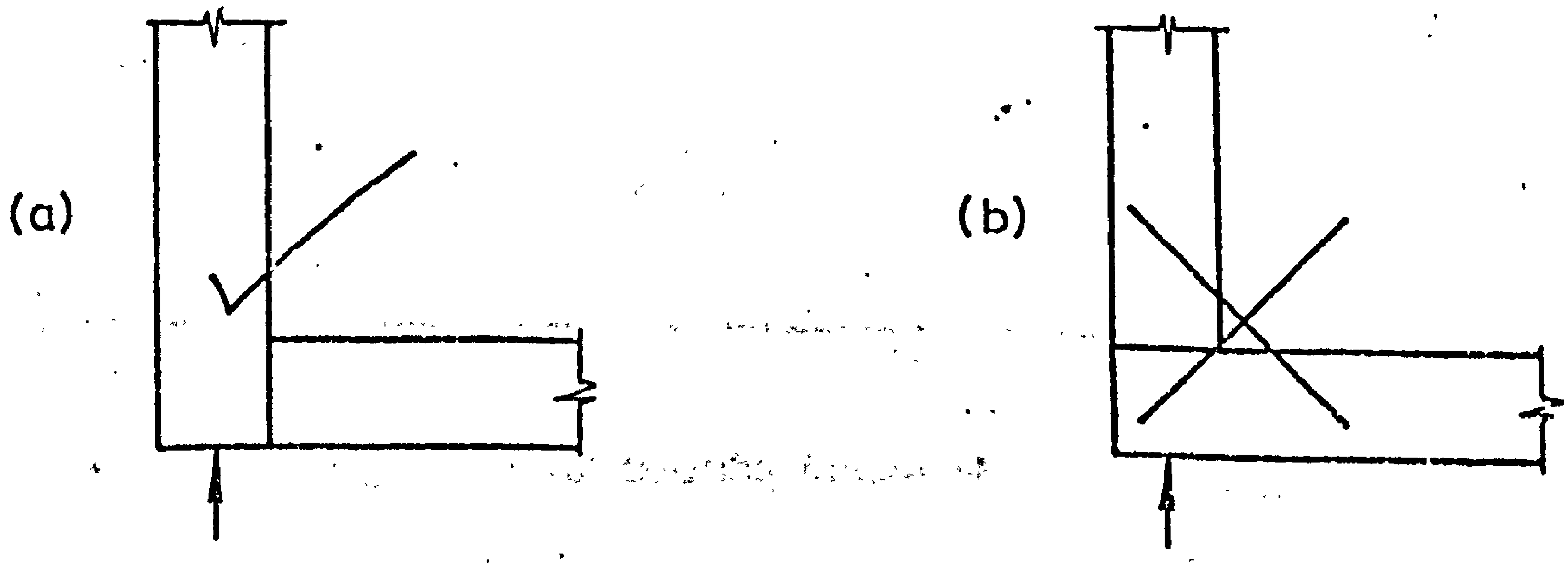

Fig.6·3 Methods of jointing at the end of a truss over a support

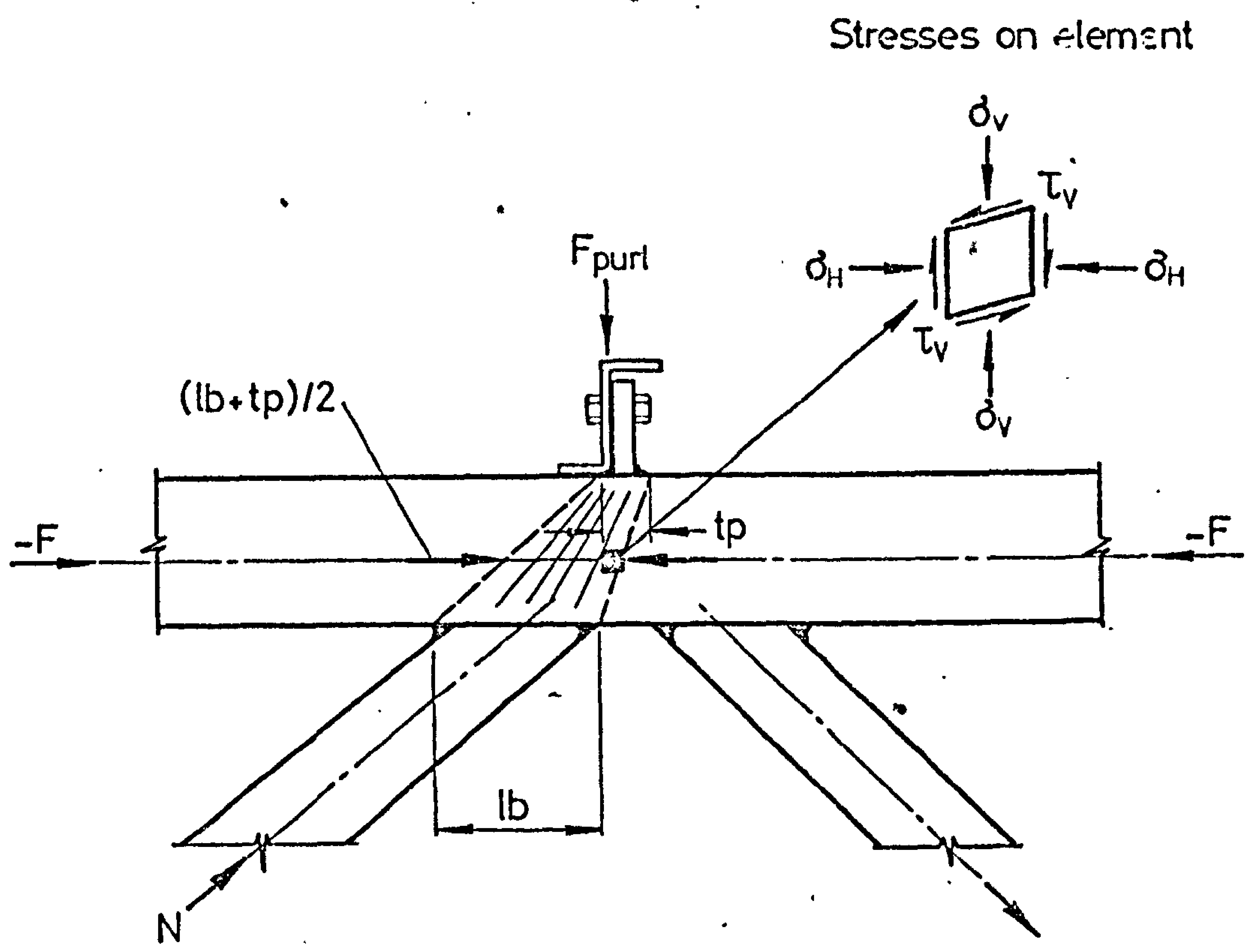

Fig.6·4 Approximation of some of the loads acting on an element in the chord wall

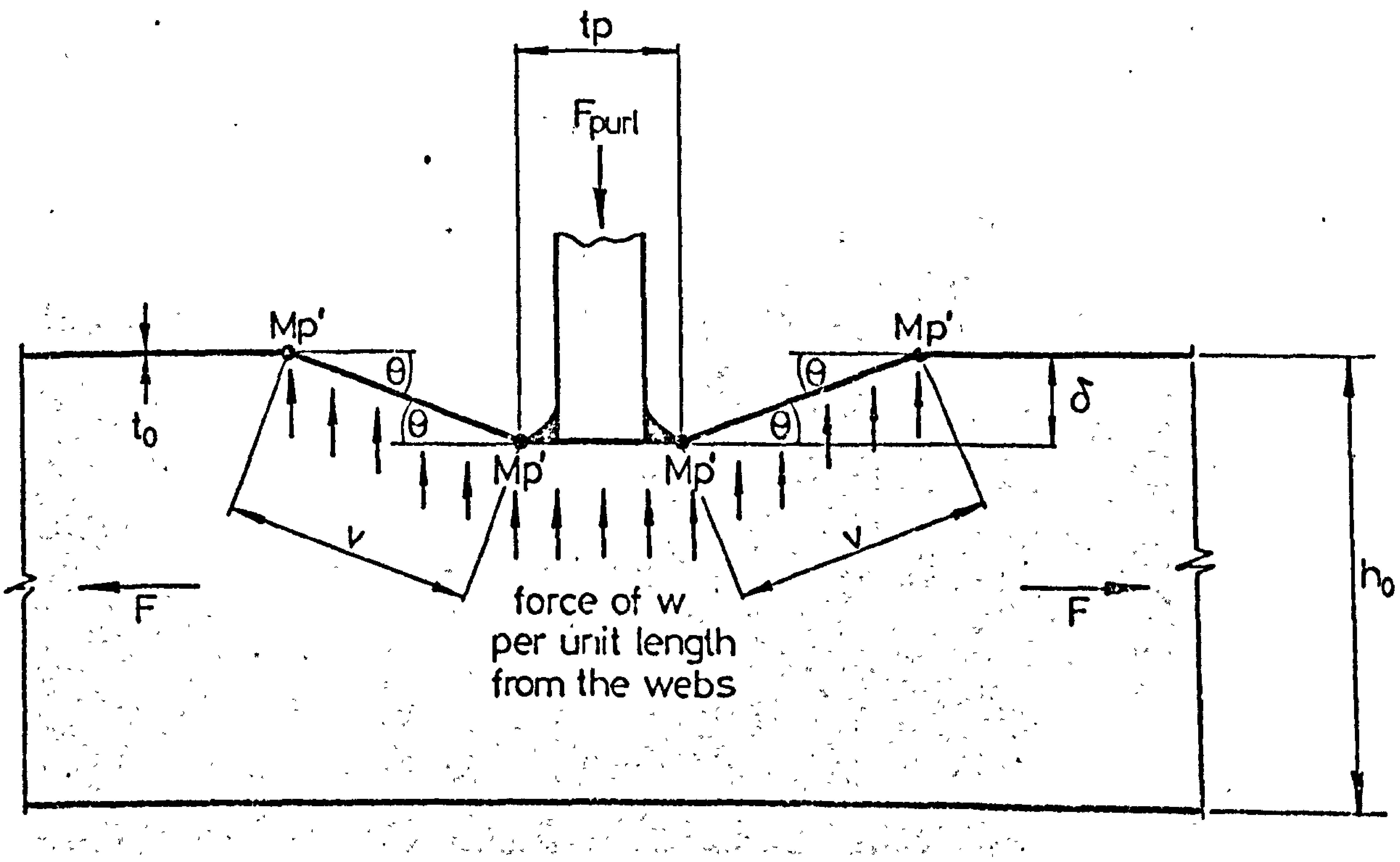

Fig.6·5 Model for bearing failure of an RHS member

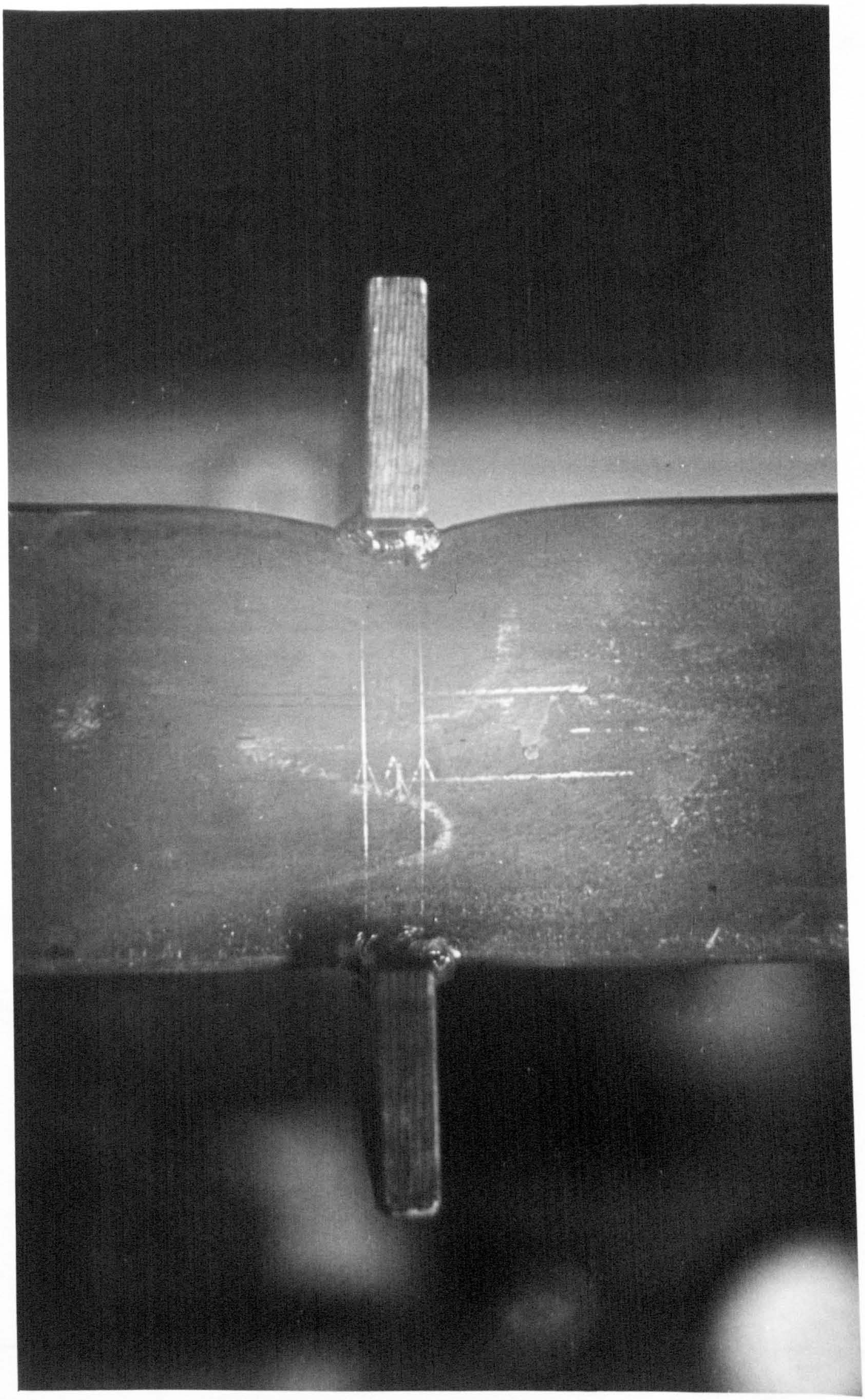

Fig. 6.6 Purlin load test for bearing failure of an RHS member

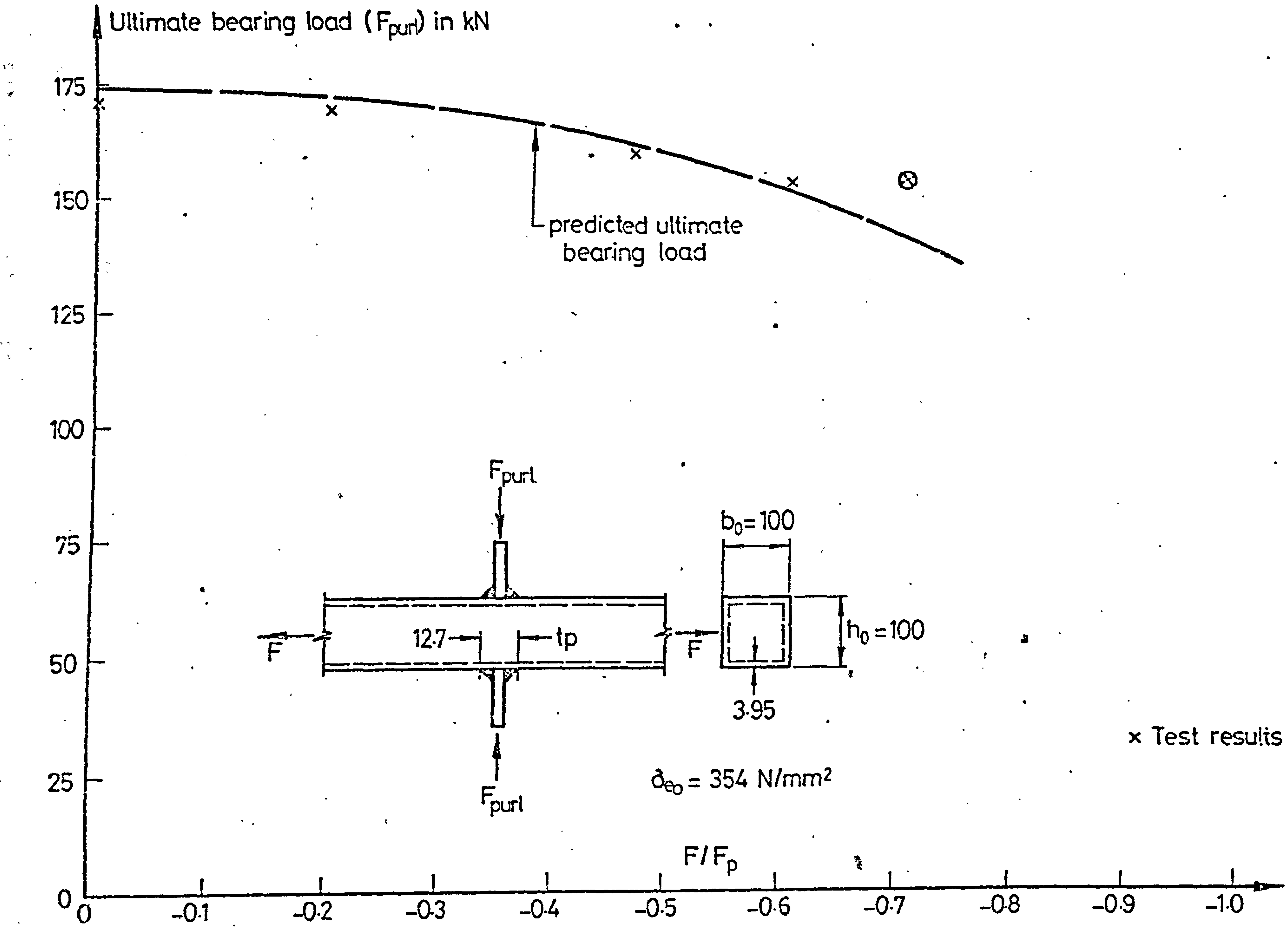

Fig.6·7 Bearing capacity of RHS members – theoretical and experimental comparison

CHAPTER 7

PARAMETER STUDIES ON GAP AND LAPPED JOINTS

The modes of failure which have been identified for gap joints are shown in fig. 3.1 and in Chapter 4 the ultimate strength of gap joints was determined by means of the following failure models:

(i) Push-pull mechanisms, representing the behaviour of the connecting chord face (figs 4.1 and 4.2),

(ii) Strut buckling mechanisms 1 and 2, (figs 5.7 and 5.15), which model a local buckling failure in the compression bracing,

(iii) Local buckling of the chord behind the heel of the tension bracing (fig. 4.10), and

(iv) Chord shear failure (fig. 3.1).

For overlapped joints the identified failure modes are shown in fig. 5.1 and in Chapter 5 their ultimate strength was determined by means of the following failure models:

(i) Strut buckling mechanisms 1 and 2, (figs 5.7 and 5.15), which model a local buckling failure in the compression bracing,

(ii) Local buckling of the chord behind the heel of the tension bracing (fig. 4.10), and

(iii) Chord shear failure (fig. 5.1 and fig. 5.18).

From the research presented in this thesis and from previous research discussed in Chapter 2, it has been decided that the main parameters which influence joint strength and behaviour are as follows: chord width, chord depth and chord wall slenderness, size of bracings relative to the chord member, thickness ratio between the bracings and chord, wall slenderness of the compression bracing member, length of the compression bracing member, amount of overlap or size of gap, angle of the bracings to the chord member, yield stress of the members and chord 'preload'. The effect of these parameters upon the joint strength and behaviour will now be discussed in this chapter by considering the effect of a particular parameter upon the failure models outlined earlier.

7.1 The influence of chord 'preload'

The term 'preload' originates from tests on isolated joints in which it is the axial force in the chord member in addition to the horizontal components of the bracing member forces (i.e. force F in fig. 7.1(a) or -F in fig. 7.1(b)). For a truss joint the chord 'preload' is the force in the chord member on the compression bracing side of the joint.

To illustrate a manner in which the chord 'preload' may influence the ultimate joint strength, consider the joint shown in fig. 7.1(c) without 'preload' and in fig. 7.1(b) with a compression 'preload'. Now let us assume that the mode of joint failure for both with and without 'preload' is attainment of the chord squash load (F_p).

Without 'preload': $N\text{Cos}\theta_1 + T\text{Cos}\theta_2 = F_p$

With 'preload': $N'\text{Cos}\theta_1 + T'\text{Cos}\theta_2 - F = F_p$

$$\therefore \quad N(\cos\theta_1 + \sin\theta_1.\cot\theta_2) = N'(\cos\theta_1 + \sin\theta_1.\cot\theta_2) - F$$

$$\therefore \quad \frac{N'}{N} = 1 + \frac{F}{N(\cos\theta_1 + \sin\theta_1.\cot\theta_2)}$$

$$\text{i.e.} \qquad N' = N(1 + F/Fp) \tag{7.01}$$

So if the joint strength is measured as a force in the compression bracing member it is reduced from N to N' by a factor of (1 + F/Fp) because of the compressive 'preload' and this factor is often called the 'preload reduction factor'. For this case considered the reduction in ultimate joint strength with compressive 'preload' is shown by line a on fig. 7.2. This reduction factor only applies, of course, if yielding of the whole chord section is the failure mode. At the beginning of this chapter many failure modes for gap and lapped joints were listed, so if another failure mode operates a different effect for the influence of the chord 'preload' will almost certainly be obtained, such as line b or line c on fig. 7.2. By means of the failure theories for gap and lapped joints described at the beginning of the chapter the influence of chord 'preload' upon the ultimate strength of joints having different failure modes will now be discussed.

For gap joints which fail by the push-pull mechanism model, (described in §4.1 and shown in figs 4.1 and 4.2), the influence of chord 'preload' upon the ultimate strength is such that an increase or decrease in strength may occur as shown in fig. 7.3. It can be seen that a compressive chord 'preload' may cause a sharp decrease in the joint strength, for this particular Warren joint studied. This reduction occurs because full yielding of the chord section at the gap takes place, (fig. 4.5), which restricts the chord deformation from continuing up to ultimate stress in the crotch membrane, which it may otherwise have done if there were no compressive 'preload' applied. If the gap joint deforms until the ultimate stress in the crotch is reached, both with or without a chord 'preload', then the 'preload' has a less severe influence on the change in joint strength. (For example the curve in fig. 7.3 for $\lambda = 0.2$ between $F/Fp = 0$ and $F/Fp = -0.6$.) As the width ratio of the bracing members (λ) becomes larger, there is a possibility that with compressive 'preloads' the ultimate joint load may be reduced to the joint yield load. Hence in fig. 7.3, for example, the curve for $\lambda = 0.6$ drops suddenly to the joint yield load with only a slight compression 'preload' and the joint yield load is only 53% of the ultimate load attained without any 'preload'. Thereafter this same curve decreases only gradually as this represents the influence of the compression 'preload' upon the joint yield load.

For tension 'preloads' at large width ratios there is the possibility of an apparent increase in joint ultimate strength as shown by the curve for $\lambda = 0.7$ in fig. 7.3. This phenomenon occurs because with zero chord 'preload' the joint may have failed by yielding of the chord section at the gap (fig. 4.5), but when a tensile chord force is applied to the joint the likelihood of this diminishes and the joint is then able to reach the ultimate stress in the membrane, hence producing an increase in joint strength with tensile chord 'preloads'. From tests on isolated joints Wardenier and De Koning[71] have also noticed that a tensile chord 'preload' may increase the joint ultimate strength.

The curves shown in fig. 7.3 apply to the particular Warren joint shown in that figure. If an N joint had been chosen then it is unlikely that the ultimate strength of the joint would have been limited by plasticity of the chord section around the gap, (fig. 4.5), because of the less severe compression force and moment applied to the chord section around the gap. Hence the reduction curves for compressive 'preloads' would then be less severe and generally similar to those for tension 'preloads' in fig. 7.3.

For Warren joints with compressive 'preloads', the predictions for the reduction in ultimate joint strength have been found generally conservative and hence err on the safe side (i.e. reduction in actual joint strength is not as great as predicted).

For gap, or more commonly lapped, joints which fail by strut buckling mechanisms, (described in §5.3 and §5.4 and shown in figs 5.7 and 5.15), the influence of chord 'preload' upon the ultimate strength is shown by fig. 7.4. For the strut buckling mechanisms most of the deformation and hence virtual work is done in the bracing members and so the reduction in joint strength is comparatively small.

For the chord shear mode of failure, (described in §4.3.3 and §5.6), a reduction factor of approximately $\sqrt{1-(F/Fp)^2}$ is applicable to both gap and lapped joints. This factor is a consequence of the Von Mises criterion for yield under combined stresses, which can be expressed[39] by the relationship

$$(F/Fp)^2 + (\tau y'/\tau y)^2 = 1 \ , \qquad (7.02)$$

where τy and $\tau y'$ are the shear yield stress and reduced shear yield stress respectively. This reduction factor of $\sqrt{1-(F/Fp)^2}$ is shown on figs 7.3 and 7.4. For the chord local buckling failure mode, (described in §4.3.2), a compressive chord 'preload' causes a linear reduction in the ultimate joint strength as shown by line a in fig. 7.2 and also in fig. 7.4 for a lapped joint.

From the wide range of reduction effects due to chord 'preload' shown in figs 7.3 and 7.4 it can be appreciated that each failure mode really requires its own 'chord preload reduction factor'. Nevertheless, attempts have been made to give a global reduction factor which represents a lower bound on all the failure modes. A draft of the empirically derived Dutch standard for tubular structures[53] gives the influence of the axial chord force, for the purpose of design rules, as

$$1.3 - \frac{0.4}{\lambda_{av}} \left| \frac{\sigma_{o_{max}}}{\sigma e_o} \right| \text{, but } \nmid 1.0 \qquad (7.03)$$

This reduction factor had been given earlier by $1.0 - |F/Fp|$[71]. Experimental analysis in Britain[18] has proposed a reduction factor of $\sqrt{1-|F/Fp|}$ for both tension and compression 'preloads' as shown in figs 7.3 and 7.4.

7.2 The influence of yield stress

For the strut buckling mechanisms 1 (§5.3 and fig. 5.7) and 2 (§5.4 and fig. 5.15), the joint strength is directly proportionate to the steel yield stress but if hybrid trusses are used, (bracing members having a different yield stress to the chord members), then the joint strength by strut buckling is most dependent upon the yield stress of the bracings and to a much lesser extent on the chord. This has been incorporated into the design proposals of reference 18 for lapped joints which fail by strut buckling.

The chord shearing mode of failure (§4.3.3, §5.6, fig. 3.1, fig. 5.1 and fig. 5.18) and the chord local buckling mode of failure (§4.3.2 and fig. 4.9), providing elastic local buckling does not occur , for both gap and lap joints are dependent upon the chord yield stress and the strength is proportionate to σe_o too. (Except for chord shear failure in lapped joints in which there is a slight dependence upon the yield stress of the bracings as well.) So for gap or lapped joints which fail by either strut buckling, chord local buckling or chord shear, the joint strength is directly dependent upon the yield stress of the members.

For gapped joints which deform according to the push-pull mechanisms, (§4.1, fig. 4.1 and fig. 4.2), the joint strength will depend upon both the yield and ultimate stress of the chord material. Large deformations of the connecting chord face will develop after the yield load, (dependent only upon the chord yield stress), and these will continue until either the ultimate chord stress is reached in the membrane of the crotch or until the whole chord section around the gap reaches plasticity. As almost no experimental testing of gap joints in high yield steel has been done it has been assumed in most empirical formulae to date that the ultimate strength of a gapped joint was proportionate to σe_o.

Consider the three hypothetical Warren joints in Tables 7.1 and 7.2, having b_o/t_o = 20 and 40, which are made of Grade 43C, 50C and 55C steel. According to British Standards Specifications[7] the minimum yield stress for each is 255, 355 and 450 N/mm^2 respectively while the ultimate stresses for each are in the ranges (430-540), (490-620) and (550-700) N/mm^2 respectively. Each of the three joints in Table 7.1 and Table 7.2 is based upon the minimum yield stress and the minimum ultimate stress of each steel grade.

Tables 7.1 and 7.2 show that it is more accurate to consider the ultimate joint strength being proportional to the chord ultimate stress (minimum) rather than the yield stress, providing failure occurs by cracking of the membrane in the crotch, particularly for large b_o/t_o values as in Table 7.2. Cracking of the membrane in the crotch is the likely failure mode for gap joints except when the chord 'preload' is compressive, the joint is Warren and the width ratio (λ) is not low. This problem highlights a vital need for experimental research on joints of high steel grades which has hitherto been neglected.

7.3 The influence of strut wall slenderness and other joint parameters upon the ultimate strength of lap joints.

Strut local buckling failure, (§5.3, §5.4, figs. 5.7 and 5.15), which is the major failure mode for lapped joints and a minor failure mode for gapped joints, may produce an ultimate joint load lower than the strut squash load (or tie yield load) in many cases. This is shown for lapped joints in figs. 7.5 to 7.11. If there is a reduction in the joint ultimate load below the strut squash load, (apart from tie yielding), then the amount of reduction in strength is influenced by:

(i) b_1/t_1

(ii) Width ratio (λ) between bracings and chord

(iii) Thickness ratio (t_1/t_o) between bracings and chord.

(iv) Flexibility or slenderness of chord (b_o/t_o)

(v) Length of the strut member

(vi) Amount of overlap

<u>Parameters (i) to (iv)</u>

It can be seen that the joint ultimate strength is closely linked to the strut squash load in figs. 7.5 and 7.6. From figs. 7.6, 7.7 and 7.8 the greatest reduction in strength below the strut squash load occurs for a width ratio (λ) $\approxeq$ 0.5. The joint strength divided by strut squash load, expressed either in terms of t_1/t_o or b_1/t_1, decreases as the width ratio decreases until $\lambda \approxeq 0.5$, and then increases again for $\lambda < 0.5$ (see figs. 7.7 and 7.8). At the moderate width ratios, the greatest reduction in joint strength is obtained if the strut thickness is about $0.75t_o$, which can be seen on figs. 7.6 and 7.7. At such a strut thickness the b_1/t_1 ratio of the strut will be relatively low as the b_1/t_1 ratio = $\frac{2}{3}$ (b_o/t_o) for this arrangement of parameters. So the greatest reduction in joint ultimate strength relative to the strut squash load is obtained for relatively thick strut members with a width ratio in the order of 0.5. It is also apparent that the parameters b_1/t_1, b_1/b_o, b_o/t_o and t_1/t_o are all inter-related, controlled by the dimensions b_1, t_1, b_o and t_o.

Fig. 7.6 shows that for width ratios of 0.2 or less the strut squash load would determine the strength of a lapped joint. If the strut to chord thickness (t_1/t_o) is small, (that is in the order of 0.25), then the strut squash load again determines the joint strength provided λ is not large enough to induce elastic local buckling in the strut member, (as described in §5.2), which has occurred in fig. 7.6. For joints with a small width ratio in the order of 0.3 to 0.4 and a high t_1/t_o ratio in the order of 1.25, the failure of the joint is governed by the strut buckling mechanism 2 (fig. 5.15) in which both bracing members reach full plasticity at less than both the strut squash load and strut buckling mechanism 1 (fig. 5.7) failure load. This is the reason for the dip in the curve on fig. 7.7 for λ = 0.3 at high t_1/t_o values.

The influence of any one of the parameters b_1/t_1, b_1/b_o, b_o/t_o and t_1/t_o cannot be properly assessed theoretically without affecting another, but the graphs presented in figs. 7.5, 7.6, 7.7 and 7.8 have all the other joint variables common. In discussing the reduction in joint strength below the strut squash load it is assumed that the tie yield load is not the critical failure mode, which may be likely in Pratt truss (N) joints with identical bracing members.

For joints with overlapped rectangular bracing members which are orientated differently, (such as curve B with b_1, b_2 = 60 and h_1, h_2 = 30, and curve D with b_1, b_2 = 30 and h_1, h_2 = 60 in fig. 7.5), and with all other joint variables being the same, it is interesting to note that the joint with the larger strut dimension transverse to the plane of the truss has generally the greater ultimate strength. (i.e. the orientation such that $\lambda = 0.3$ is more likely to induce strut local buckling below the squash load than with $\lambda = 0.6$). This is mainly due to the amount of internal virtual work which is done in the buckle mechanism, this being less for a small strut face adjacent to the crotch.

Parameter (v)

As the length of the strut member decreases the strut local buckling load, (assuming strut buckling mechanism 1 of fig. 5.7 governs), increases until the strut squash load is attained as shown in fig. 7.9 because of the influence upon the elastic loading line of strut buckling mechanism 1. (See § 5.3). If strut buckling mechanism 2 governs, which is not common, then the length of the strut member has no influence upon the joint strength.

Parameter (vi)

By inspection of curves C′ on fig. 7.5, or fig. 7.10, it can be seen that the joint ultimate strength increases as the amount of lap increases for the more common strut buckling mechanism 1 because the amount of tie material which must be yielded, and hence the amount of internal virtual work done, increases, (providing strut buckling takes place at less than the squash load of the strut). The increase in strength with increasing lap is almost linear up to the strut squash load (see fig. 7.10). The amount of lap can also be seen to have no effect on the strut buckling mechanism 2 but causes a linear increase in the chord shear strength (fig. 7.10).

The behaviour of the parameters (i) to (v) affecting strut buckling which have been discussed above will also apply to gapped joints.

Lap joint strength v. Gap joint strength

Could a lapped joint ever have a lower ultimate strength than a joint between the same members which is made gapped? Only if chord local buckling (§ 4.3.2 and fig. 4.9) is the governing failure mode, otherwise the lapped joint will always be as strong or stronger than the gapped joint. The theoretical reasons for this conclusion are as follows. The upper limit on the strength of any joint is the strut squash load and for a lapped joint to fail below the strut squash load it usually fails by strut local buckling, but for the same buckling mechanisms the comparable gapped joint either has the same strut buckling load (strut buckling mechanism 1 in fig. 5.7) with any gap, or has a slightly lower buckling load (strut buckling mechanism 2 in fig. 5.15) with increasing gap. For a gapped joint the 'push-pull' mechanism (figs. 4.1 and 4.2) ultimate load could never exceed the strut local buckling load without the latter then becoming the failure mode. If shear failure of the chord (fig. 3.1 and fig. 5.1) occurs then the shear ultimate load of a gapped joint is always less too because of the smaller shear area at the critical section. So only for the chord local buckling mode, (because lapped joints usually have a negative noding eccentricity and gap joints positive), is it possible, (see §4.3.2 for discussion), that the lap joint strength may be less than the gap joint strength.

A measure of the amount by which the strength of gap joints is generally less than for lap joints can be seen by the curve for strut local buckling mechanism 1 on fig. 7.10. This line shows the rate of decrease in the ultimate joint strength, for this failure mechanism, as the amount of overlap tends towards zero whereupon the joint becomes gapped and the strength of the joint is less than for all amounts of overlap.

7.4 Orientation of bracing members in gap joints.

Figure 7.11 in which the bracing members of a gap joint are rectangular and orientated in different directions, shows that the failure mechanisms proposed for gap joints (Chapter 4) still give reasonable predictions for any orientation of the bracings. Hence several hypothetical gap joints with bracing members of similar dimensions but orientated in different ways on the chord member have been analysed and the change in joint ultimate strength is shown in fig. 7.12.

In order to obtain a simple design formula for the ultimate gap joint strength, the correct parameter relating to the size of the bracing members must be chosen. If the width ratio parameter of $(b_1 + b_2)/2b_o$ is chosen then the joint strength may be sometimes highly overestimated. For example, in fig. 7.12 joint 3 would be expected to have the same strength as joint 11. This severe over-prediction of joint strength when using $(b_1 + b_2)/2b_o$ as the effective width ratio parameter only arises for joints with rectangular bracing members in which both the larger dimensions are transverse to the chord, whereas for most other joints the ultimate strength is approximately dependent upon the factor $(b_1 + b_2)/2b_o$. That is to say that joints 2, 4, 6, 7, 8, and 9 would be expected to have the same ultimate strength as joint 1 in fig. 7.12, which for the worst case (joint 4) would give a 20% overprediction of the joint strength. If the effective width ratio parameter of $(b_1 + b_2 + h_1 + h_2)/4b_o$ was chosen, then the result for the joints in fig. 7.12 would be the same except that joint 3 is estimated to have the strength of joint 1 (rather than joint 11 as before) and joint 5 is estimated to have the strength of joint 1 (rather than joint 10 as before). Hence the tendency for overpredicting the joint strength now occurs when both the larger dimensions of the rectangles are parallel to the chord, but the amount of overestimation is much less than when $(b_1 + b_2)/2b_o$

was the width ratio parameter and is still less than 20%.

The configuration with the larger dimensions of the rectangles parallel to the chord is also generally not practical according to Wardenier and de Koning[71]. Figure 7.12 only shows the ultimate strength variation for the push-pull failure mechanisms (figs. 4.1 and 4.2) and other failure modes such as chord shearing may sometimes operate for other gap joints. Hence if a simple effective width ratio between the bracings and the chord was to be chosen for a joint strength parameter, it would be better to use $(b_1 + b_2 + h_1 + h_2)/4b_o$ rather than $(b_1 + b_2)/2b_o$, as the latter can be more unsafe and would not even distinguish between joints 12 and 3 on fig. 7.12.

The parameter $(b_1 + b_2 + h_1 + h_2)/4$ has been adopted for the 'effective bracing width' in equation (2.09) whereas Wardenier and de Koning[71] concluded that a parameter of $\dfrac{b_1+b_2+\alpha\,(h_1+h_2)}{2(1+\alpha)}$

with $0 \leq \alpha \leq 1$, would be in better agreement with the test results. For most joints a value of $\alpha = 0.33$ gives a better effective width parameter according to theory but for simplicity Wardenier and de Koning[53, 71] have chosen the simple parameter $(b_1 + b_2)/2b_o$ for the effective width ratio. For tests on circular hollow section joints in Japan[76], the width of the compression bracing only is used as the determining parameter (i.e. d_1/d_o), but this would not be satisfactory for rectangular bracing members.

7.5 Influence of the gap size.

The variation in ultimate joint strength, (as predicted by the push-pull mechanisms of figs. 4.1 and 4.2), with increasing gap size for a symmetrical Warren joint is shown in fig. 7.13 (for $b_o/t_o = 20$) and fig. 7.14 (for $b_o/t_o = 40$). These graphs can be compared with the variation in the gap joint yield strength with gap size, (i.e. compare fig. 7.15 with fig. 7.13 and fig. 7.16 with fig. 7.14), which has been illustrated previously by Davies and Roper.[23, 24] For any chord size and width ratio the minimum ultimate joint strength occurs at a gap of approximately $0.1b_o$. For stocky chord sections the ultimate joint strength increases for gap sizes less than $0.1b_o$, particularly at the small width ratios such as $\lambda = 0.2$ (see fig. 7.13). Above this gap size the joint strength again increases, with the increase being greater for large λ and small b_o/t_o values.

Any increase in ultimate joint strength is always subject to whether the joint reaches the limiting strength by another failure mechanism such as chord shearing (fig. 3.1), chord local buckling (fig. 4.10), strut buckling (figs. 5.7 and 5.15) or attainment of a bracing member's yield strength, and so this variation in ultimate gap joint strength (figs. 7.13 and 7.14) is not always found for tests on joints with variable gap. Also, if the gap becomes sufficiently large the joint may behave as two independent T-joints without any interaction between the strut and tie members. In order for two T-joint mechanisms to have sufficient space to both develop on the chord face[23],

$$g > b_o' \sqrt{1 - \lambda_1'}/2 + b_o' \sqrt{1 - \lambda_2'}/2 \qquad (7.04)$$

An experimental investigation of the gap parameter by Wardenier and de Koning[71] found that the ultimate joint strength was practically constant for small λ values at different b_o/t_o, but at greater width ratios the results were inconclusive. Wardenier later proposed[53] an allowable gap range of $0.1 \leq g^*/b_o \leq 1.2 - \lambda_{av}$, the upper limit of which is very close to the gap size of equation (7.04) when $\lambda_1 = \lambda_2$ and weld sizes are insignificant. (i.e. $g/b_o' = \sqrt{1 - \lambda}$). However if the allowable gap size is up to $g^*/b_o = 1.2 - \lambda_{av}$ then very large joint deformations could be incurred before the ultimate load is reached, particularly for small λ values, and the limit state of deflection will then restrict the gap.

There is no agreement on what the limiting local joint deformation should be but Mouty[51] has proposed a working load limit for local deformations of $0.01b_o$ and has shown that this occurs very close to the gap joint yield load. Hence if the ultimate joint strength divided by the load factor is greater than the yield strength, then in practice the ultimate joint capacity should be reduced below the strength limit to a lower limit decided by deflection requirements. The concept of a local deflection limit has been used in recent British joint proposals[18] in which a gap joint is considered to attain its ultimate <u>strength</u> with acceptable deformations if

$$12\text{mm} \leq g^* \leq 1.25\sqrt{b_1 + b_2 + h_1 + h_2} \quad , \qquad (7.05)$$

where all dimensions are in mm. and the lower limit of 12mm is to allow sufficient space for welding.

7.6 Influence of the width ratio between bracings and chord for gap joints.

For a joint which has a constant gap size of $0.1b_o$, the influence of the width ratio (λ_{av}) and b_o/t_o upon the ultimate joint strength is shown in fig. 7.17. The curves for this particular joint consist of three parts. At low to moderate width ratios failure of the joint occurs by fracture of the membrane in the joint crotch, (part a of curve in fig. 7.17), then for higher width ratios the rate of increase in ultimate joint strength decreases as the joint often fails by yielding of the whole chord section (as in fig. 4.5) around the crotch membrane, (part b of curve in fig. 7.17), and then finally for even higher width ratios chord shearing (as in fig. 3.1) is the governing failure mode. The change in ultimate gap joint strength with λ and b_o/t_o is similar to the variation in joint yield strength, which is shown for the same joint in fig. 7.18. This variation of joint yield strength has already been noted by Davies and Roper.[24] It is interesting to note that recent empirically derived proposals[53, 18, 36] for the ultimate strength of gap joints have made the strength proportional to λ_{av} in one case (equation 2.04 when $\sigma_o = 0$), and also a function of

$$\left\{ \frac{b_1 + b_2 + h_1 + h_2}{4(b_o-2t_o)} \right\}^2$$ in another case (equation 2.09)

7.7 Influence of the bracing angle.

The effect of the inclination of the bracing members to the chord member upon the ultimate joint strength is shown in figs. 7.19 and 7.20 for the most likely occurring types of trusses (viz. Pratt or N type trusses or symmetrical Warren trusses). In these figures the joint strength plotted is the force normal to the chord ($N\sin\theta_1$). The smallest angle for the bracings which is considered is 30° as this is thought to be the smallest angle at which a weld under the heel of a bracing member can be properly made. In all cases the chord local buckling load (figs. 4.10) decreases as θ_1 or θ_2 decreases, as would be expected, because the horizontal component of the bracing member forces increases. As the tie angle, or both strut and tie angles, decrease, $N\sin\theta_1$ decreases too for all the strut buckling mechanisms (figs. 5.7 and 5.15) except mechanism 1 (fig. 5.7) when applied to gapped N joints (see figs. 7.19 and 7.20). This apparent decrease in the strut buckling load, (except for gapped N joints failing by strut buckling mechanism 1), occurs because nearly all the joint deformation takes place in the bracing members and consequently the joint strength depends on the axial forces N and T rather than their vertical components.

Strut buckling mechanism 1 (fig. 5.7) is primarily dependent upon the strut force N and the joint strength measured as $N\sin\theta_1$

decreases if $\sin\theta_1$ decreases. Strut buckling mechanism 2 (fig. 5.15) depends both on the strut force N and the tie force T, so the ultimate joint strength measured as $N\sin\theta_1$, (which in this case with no purlin loading equals $T\sin\theta_2$), decreases if $\sin\theta_1$ or $\sin\theta_2$ decrease. If the ultimate load of the strut buckling mechanism 1 is measured by the force N, and the ultimate load of the strut buckling mechanism 2 is measured by the force T, for various values of θ_1 and θ_2, then the curves shown in fig. 7.19(a) and (b) become those of fig. 7.21(a) and (b), and the strut buckling curves in fig. 7.20(a) and (b) become those of fig. 7.21(c) and (d) respectively. Fig. 7.21 thus shows that the ultimate strut buckling load, if measured by an appropriate bracing force, has little variation with changes in the bracing angles θ_1 and θ_2. The failure mode of strut buckling is most prevalent in lapped joints and strut buckling mechanism 1 moreover occurs much more often than strut buckling mechanism 2, so it could be said that lapped joints liable to strut local buckling will practically achieve the same ultimate strut force regardless of the bracing angles (see fig. 7.21(c) and (d)). This deduction has been incorporated into reference 18 for RHS to RHS lapped joints.

The influence of the bracing angles θ_1 and θ_2 upon the push-pull mechanism strength for gapped joints is shown in fig. 7.19(a) and (b). As the bracing angle decreases the push-pull mechanism (figs. 4.1 and 4.2) ultimate strength generally increases, mainly because the yield line pattern on the chord face is enlarged due to the intersection area of the bracings on the chord face being increased. This of course does not apply to the push-pull mechanism with $x = 1.0$ (fig. 4.2) in the case of N joints (see fig. 7.19(b)). However, if the joint is Warren and the bracing angles become small, the horizontal components of the bracing forces may cause the whole chord section to yield around the crotch as in fig. 4.5, (particularly if the chord 'preload' is compressive and λ is large). This type of failure is the reason for the sudden reduction in gap joint strength in fig. 7.19(a) for θ_i less than about 40^o.

From experimental research, Wardenier et al have proposed[53, 71] that the ultimate strut force N is proportional to $(1 + \mathrm{Sin}\theta_1)/2\mathrm{Sin}\theta_1$ for gapped joints, which means that $2N\mathrm{Sin}\theta_1/(1 + \mathrm{Sin}\theta_1)$ at the ultimate load should be constant. Fig. 7.22, however, shows that the variation in joint ultimate strength, (as determined by the push-pull mechanisms of figs. 4.1 and 4.2), with the function of $(1 + \mathrm{Sin}\theta_1)/2\mathrm{Sin}\theta_1$ is even greater than if $1/\mathrm{Sin}\theta_1$ was used (fig. 7.19) and so the latter function is preferable.

The chord shear strength (fig. 3.1) is constant for gapped joints with any angle of the bracing members, but for lapped joints the chord shear strength (fig. 5.18) decreases as the bracing angle decreases (see fig. 7.20) because the shear area through the overlapped bracings is reduced.

7.8 Application to CHS bracings.

The theoretical analysis presented in this thesis has been developed for RHS to RHS truss joints but the computer program resulting from this theory (Appendix 2) has been applied to 40 CHS to RHS gap and lap joints (Appendix 1) which have been tested both in isolation[9] and in trusses.[10] The joints with circular bracing members were treated as square RHS bracing members with a width equal to the outside diameter of the CHS. The correlation between the theoretical ultimate joint loads and the actual test ultimate loads is shown in fig. 7.23 and is very poor with the theoretical predictions erring on the unsafe side consistently.

However, both the circumference and area of a circular and square tube, which are of the same diameter or width, are in the ratio of $\pi : 4$, so the CHS to RHS joints were then analysed by changing the bracing members to square hollow sections with dimensions equal to $\pi/4$ of the original bracing member diameter. The resulting correlation with test results is shown in fig. 7.24 and is now very good. This indicates that CHS to RHS joints can also be analysed by means of the RHS to RHS computer program of Appendix 2 after adjustment of the bracing member dimensions.

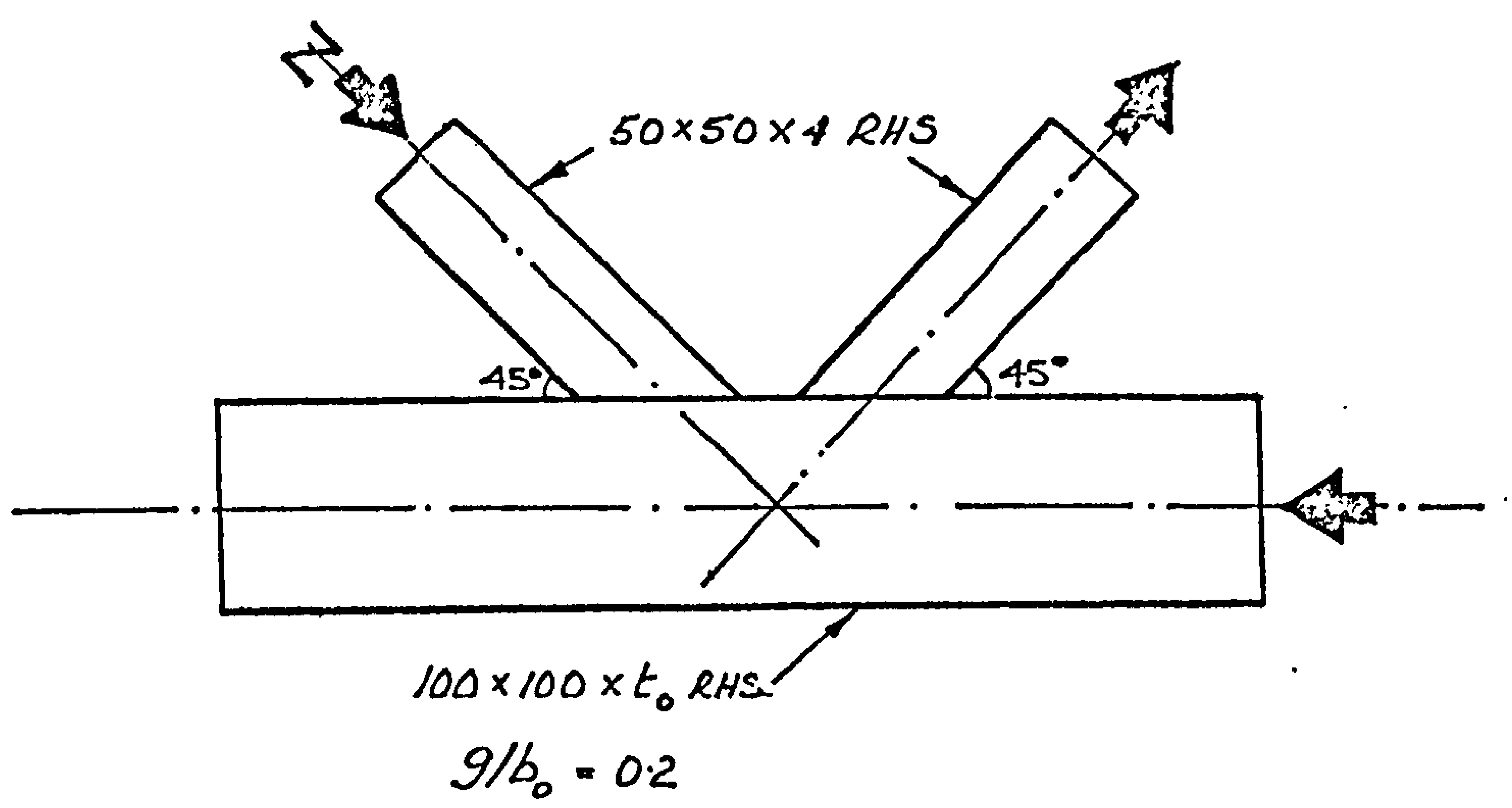

x	$N_{ult.}$ (kN)	$\frac{Nx}{N_{43}}$ ult.	$\frac{\sigma e_o x}{\sigma e_{o43}}$	$\frac{\sigma ult_o x}{\sigma ult_o 43}$	$\frac{\sigma d_o x}{\sigma d_{o43}}$
GRADE 43C	180.0	1.00	1.00	1.00	1.00
GRADE 50C	216.1	1.20	1.39	1.14	1.42
GRADE 55C	246.9	1.37	1.76	1.28	1.67

Table 7.1 Influence of yield and ultimate stress on gap joint strength - b_o/t_o = 20

Same joint as shown above					
x	$N_{ult.}$ (kN)	$\frac{Nx}{N_{43}}$ ult	$\frac{\sigma e_o x}{\sigma e_{o43}}$	$\frac{\sigma ult_o x}{\sigma ult_o 43}$	$\frac{\sigma d_{ox}}{\sigma d_{o43}}$
GRADE 43C	47.2	1.00	1.00	1.00	1.00
GRADE 50C	54.0	1.14	1.39	1.14	1.42
GRADE 55C	59.2	1.25	1.76	1.28	1.67

Table 7.2 Influence of yield and ultimate stress on gap joint strength - b_o/t_o = 40

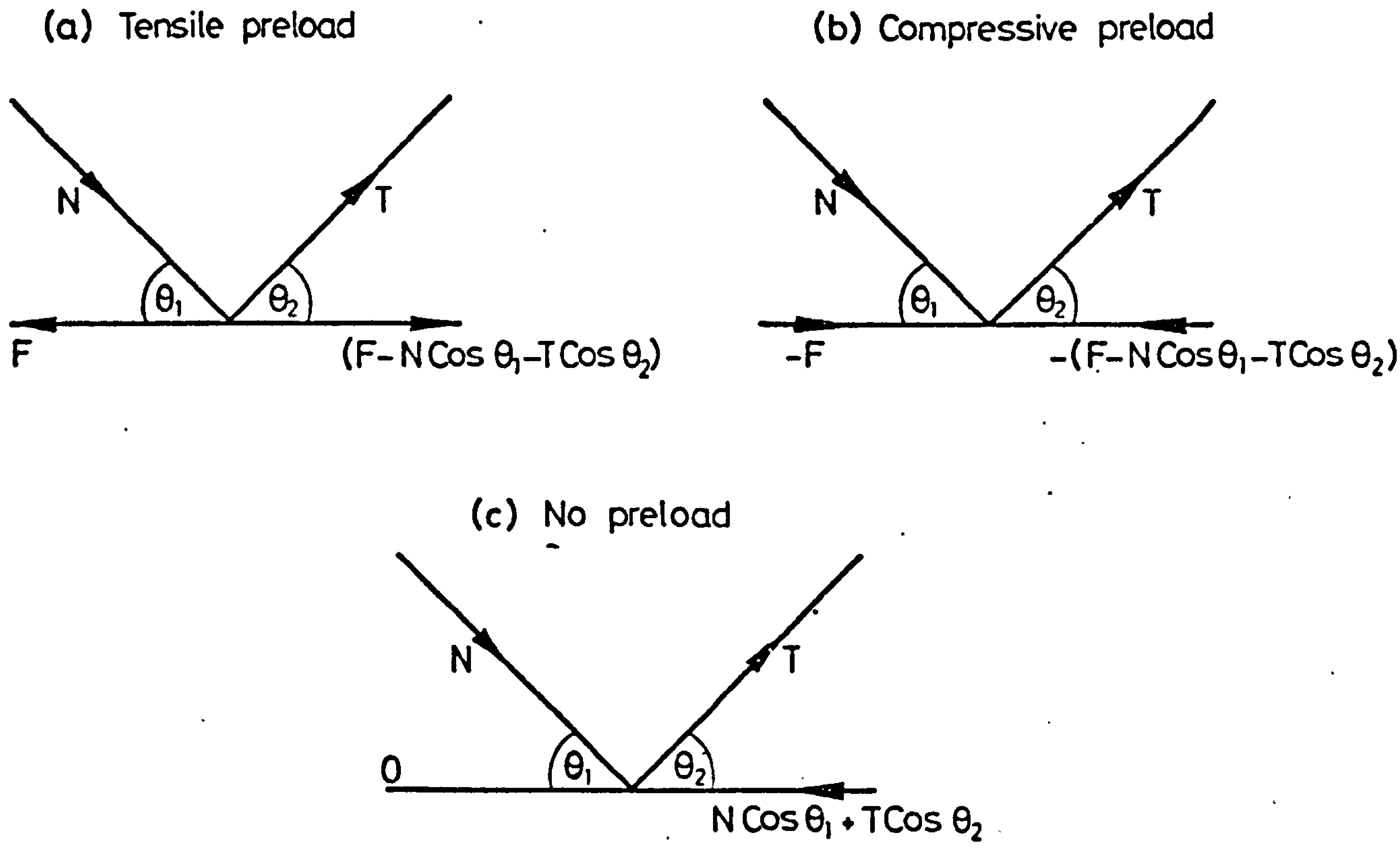

Fig.7·1 Definition of chord 'preload' (+F or −F)

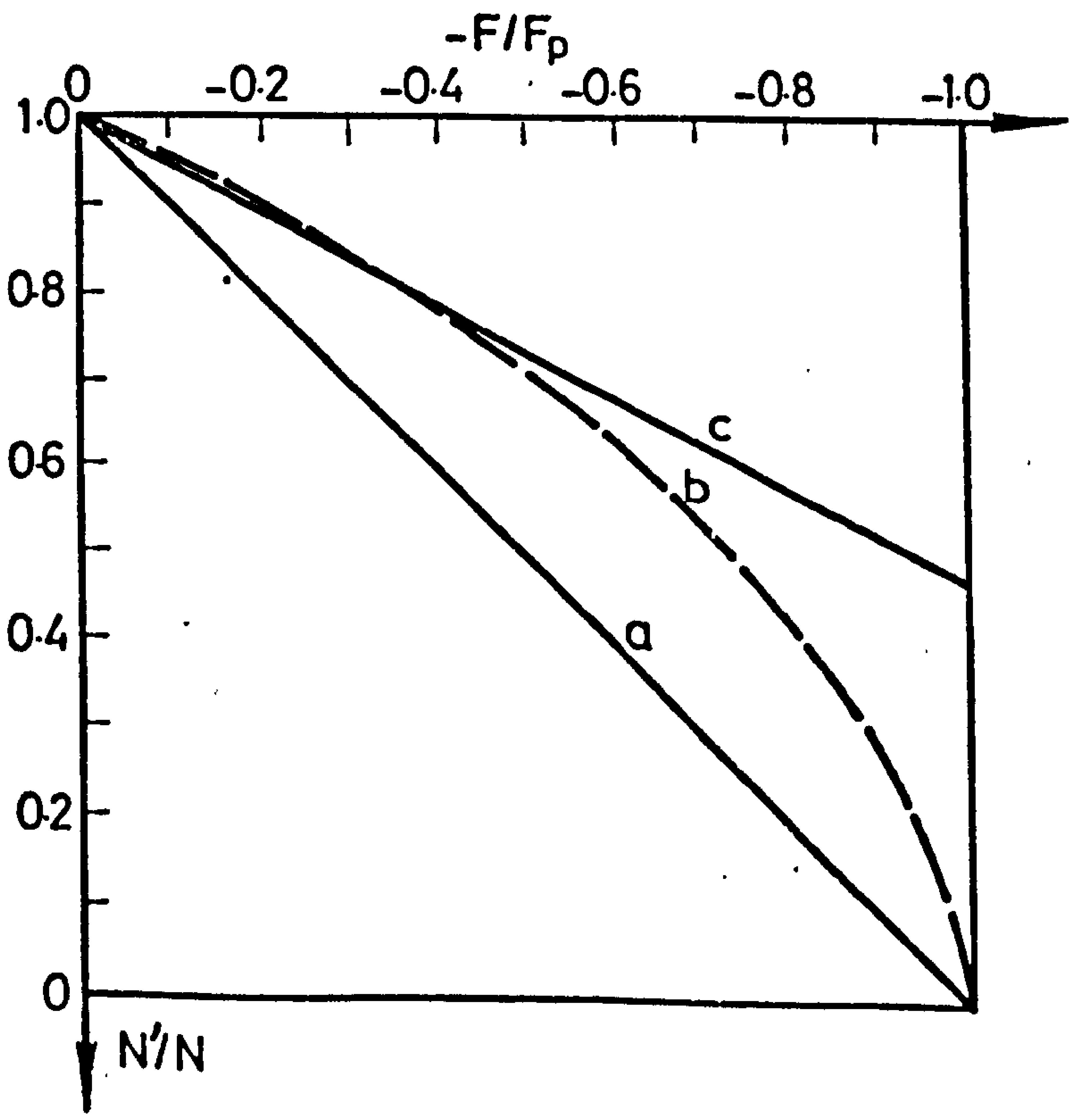

Fig.7·2 Reduction in joint strength caused by compressive 'preload'

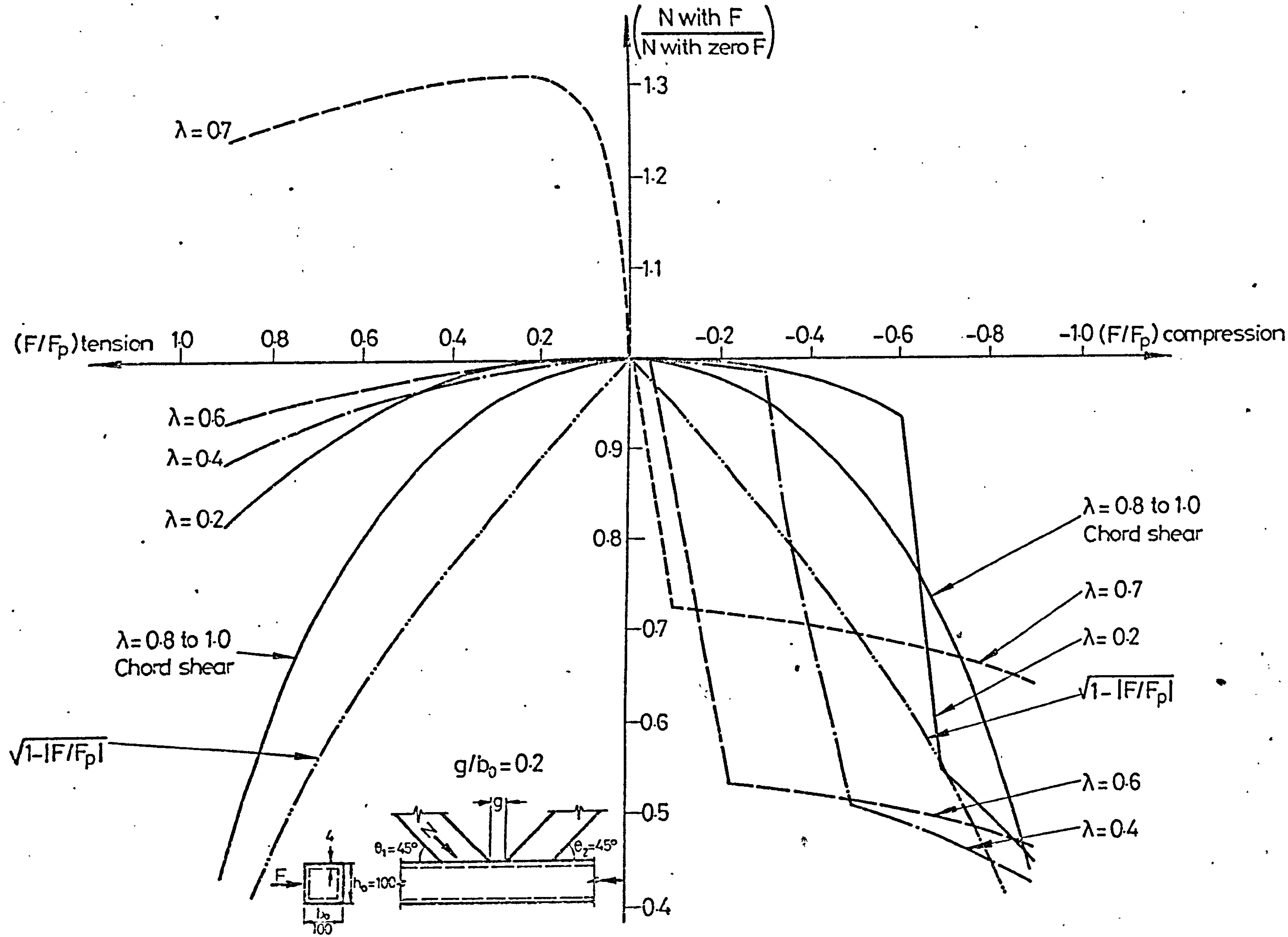

Fig.7.3 The effect of chord load upon the ultimate strength of a gap joint at different width ratios

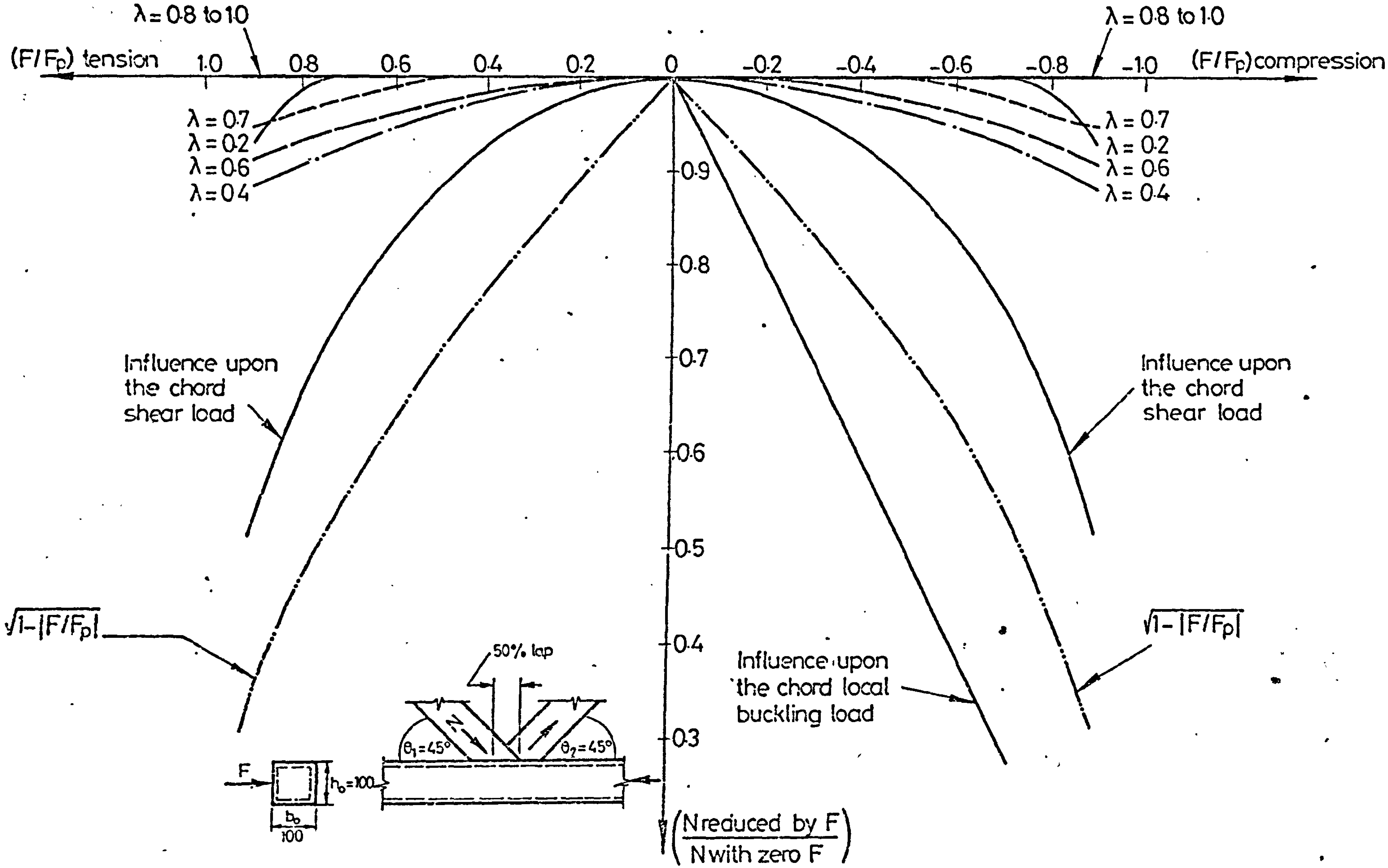

Fig.7·4 The effect of chord load upon the ultimate strength of a lap joint at different width ratios

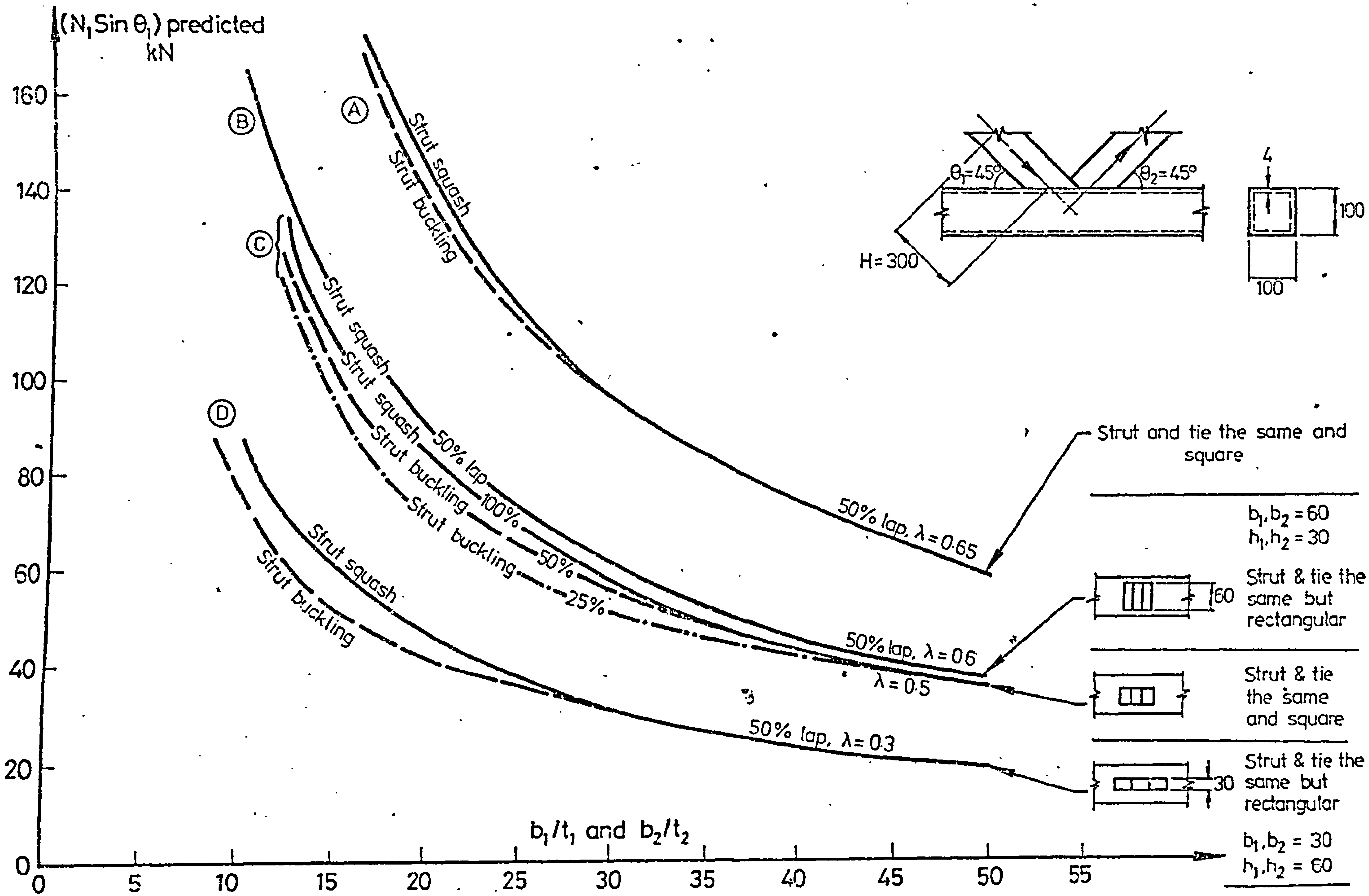

Fig.7·5 The effect of strut slenderness upon the ultimate strength of lap joints

Fig.7·6 The effect of width ratio (λ) on the ultimate strength of lap joints at different t_1/t_0 ratios

Fig.7·7 The effect of t_1/t_0 on the ultimate strength of lap joints at different width ratios (λ)

Fig.7·8 The effect of b_1/t_1 on the ultimate strength of lap joints at different width ratios (λ)

Fig.7·9 Effect of strut length upon the ultimate joint strength

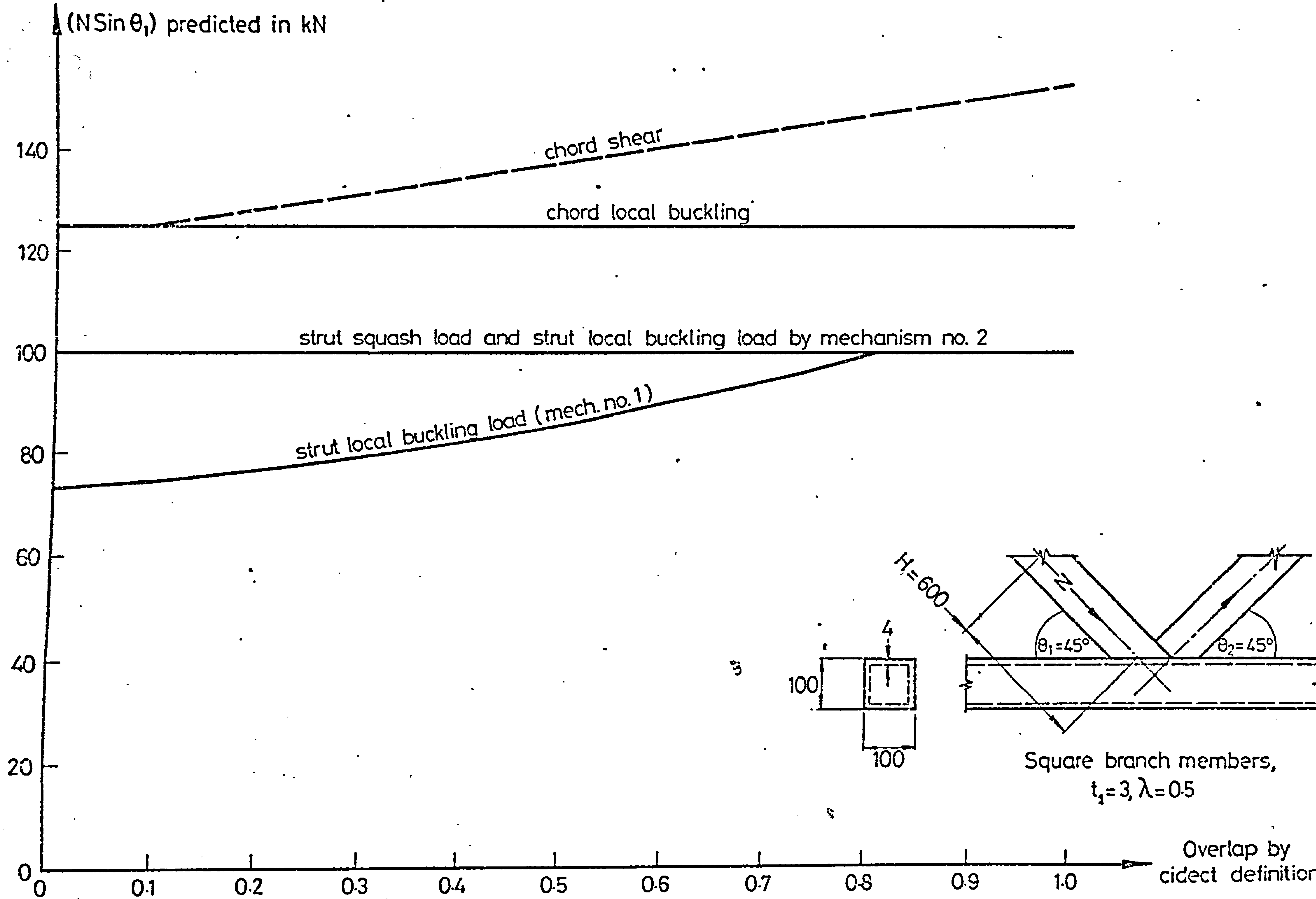

<u>Fig.7·10</u> Effect of overlap upon the ultimate joint strength

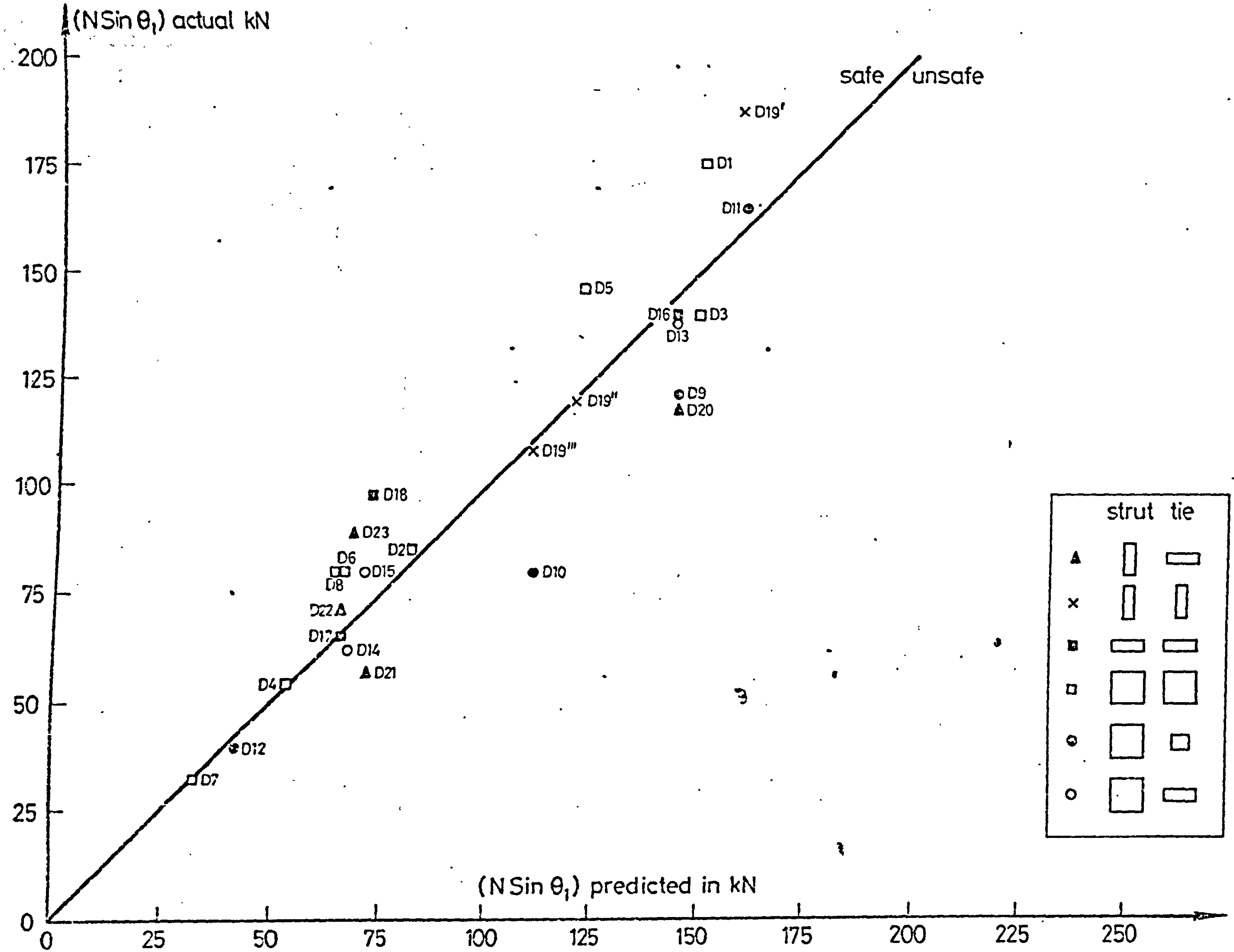

Fig.7·11 Actual v. predicted ultimate loads for RHS to RHS gap joints

Fig.7·12 Effect of orientation of branch members in gap joints

Fig. 7·13 The effect of gap size upon ultimate joint strength at different width ratios (λ) — $b_0/t_0 = 20$

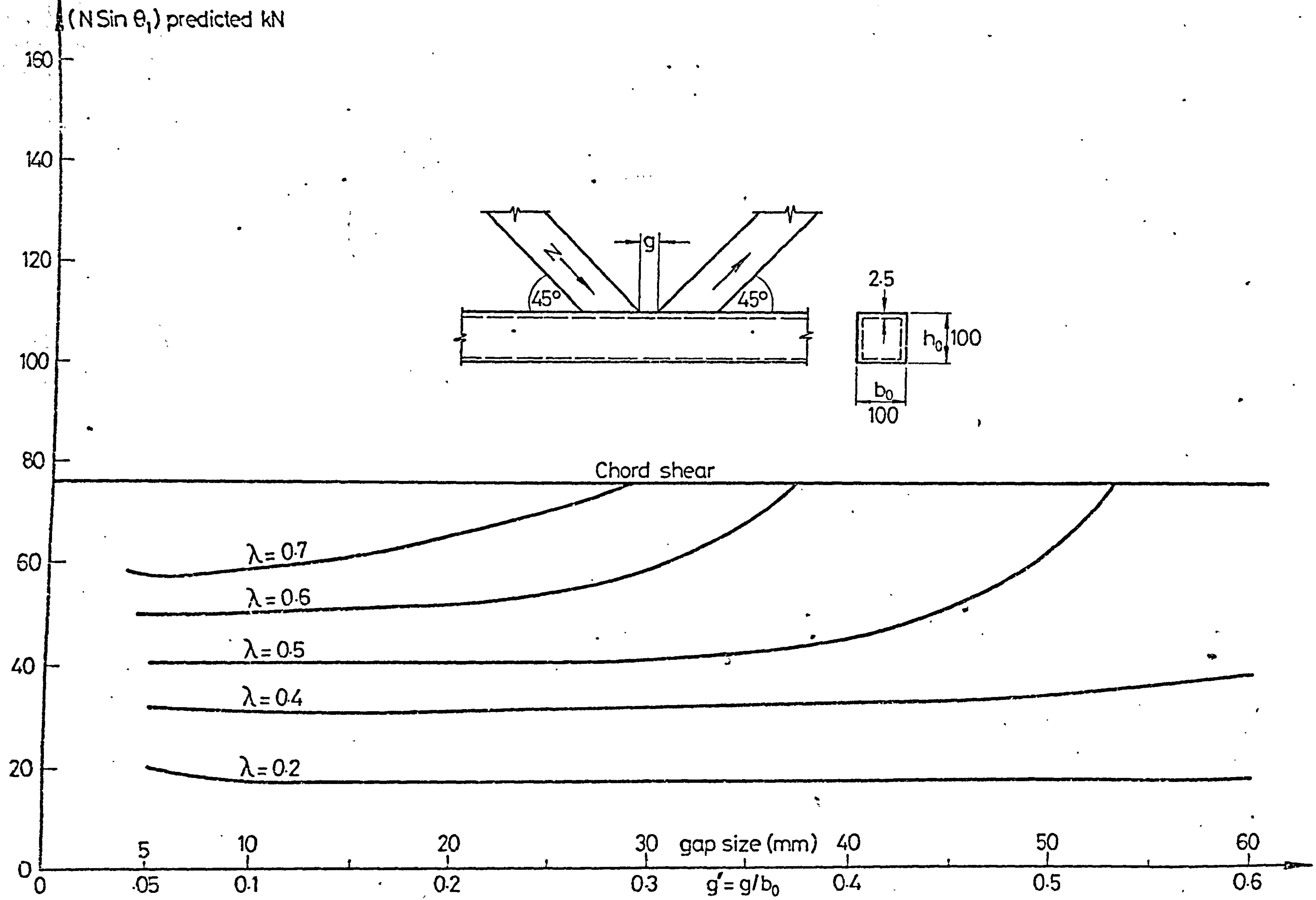

Fig.7.14 The effect of gap size upon ultimate joint strength at different width ratios (λ) — $b_0/t_0 = 40$

Fig. 7·15 The effect of gap size upon joint yield strength at different width ratios (λ) — $b_0/t_0 = 20$

Fig. 7·16 The effect of gap size upon joint yield strength at different width ratios (λ) — $b_0/t_0 = 40$

Fig. 7·17 Influence of λ upon ultimate gap joint strength at different b_0/t_0 values. — $g/b_0 = 0.1$

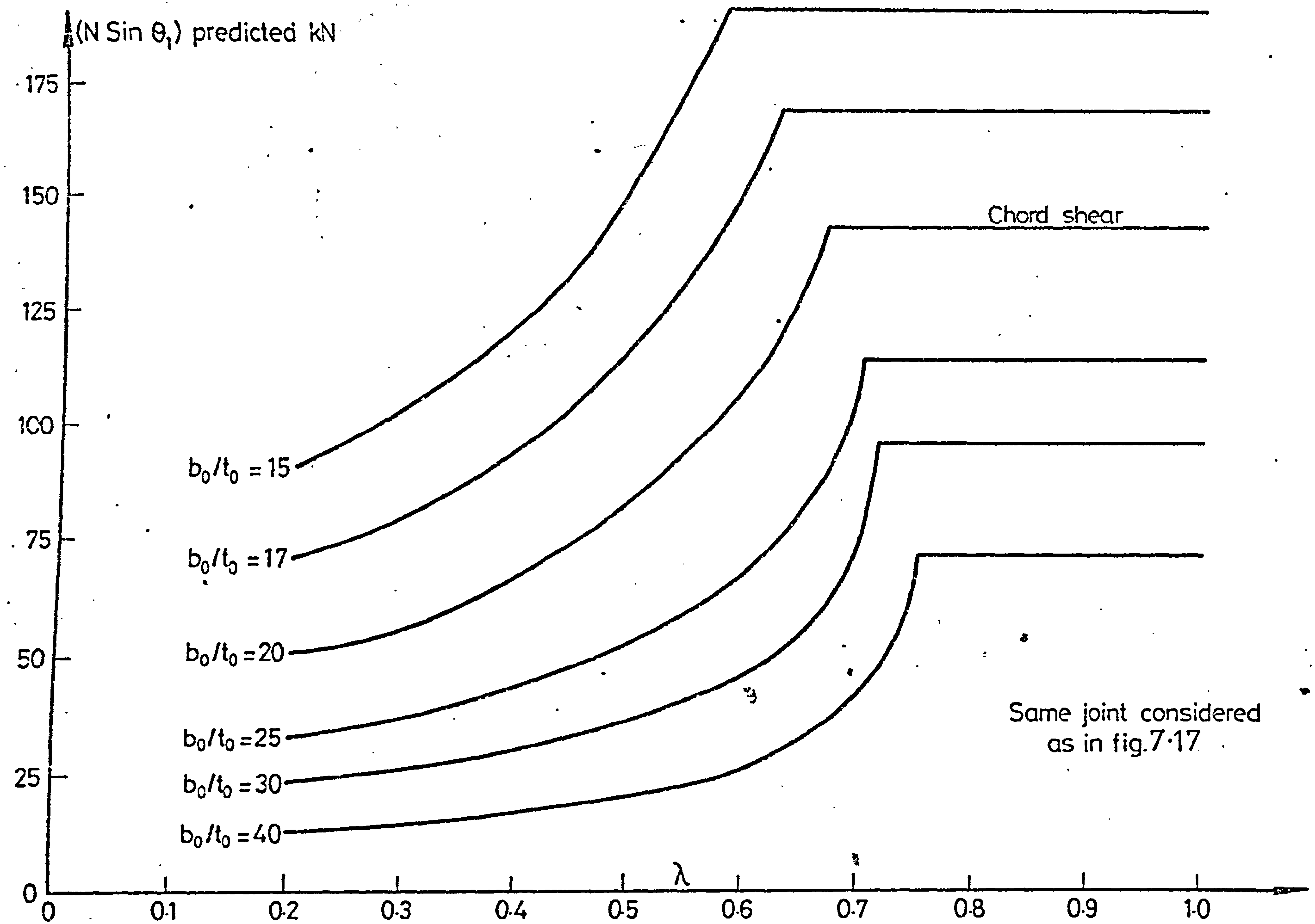

Fig.7·18 Influence of λ upon joint yield strength at different b_0/t_0 values. — $g/b_0 = 0{\cdot}1$

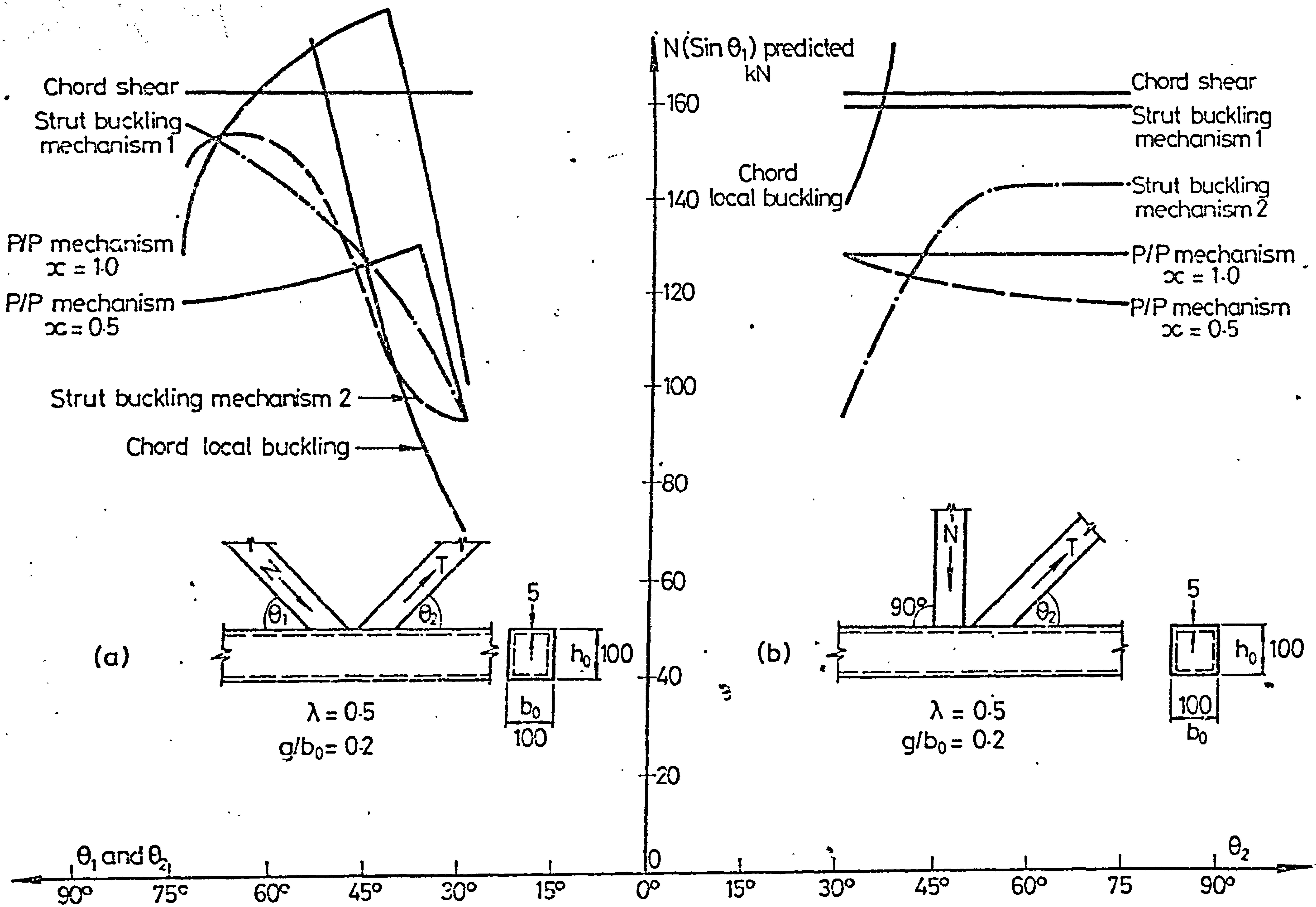

Fig.7·19 Influence of bracing angle upon the ultimate strength of a gapped joint

Fig.7.20 Influence of bracing angle upon the ultimate strength of a lapped joint

Fig.7·21 Influence of bracing angle upon ultimate joint strength, measured as a bracing force

Fig. 7·22 Variation in gap joint strength measured by $2N \sin\theta_1 / (1+\sin\theta_1)$ for various bracing angles

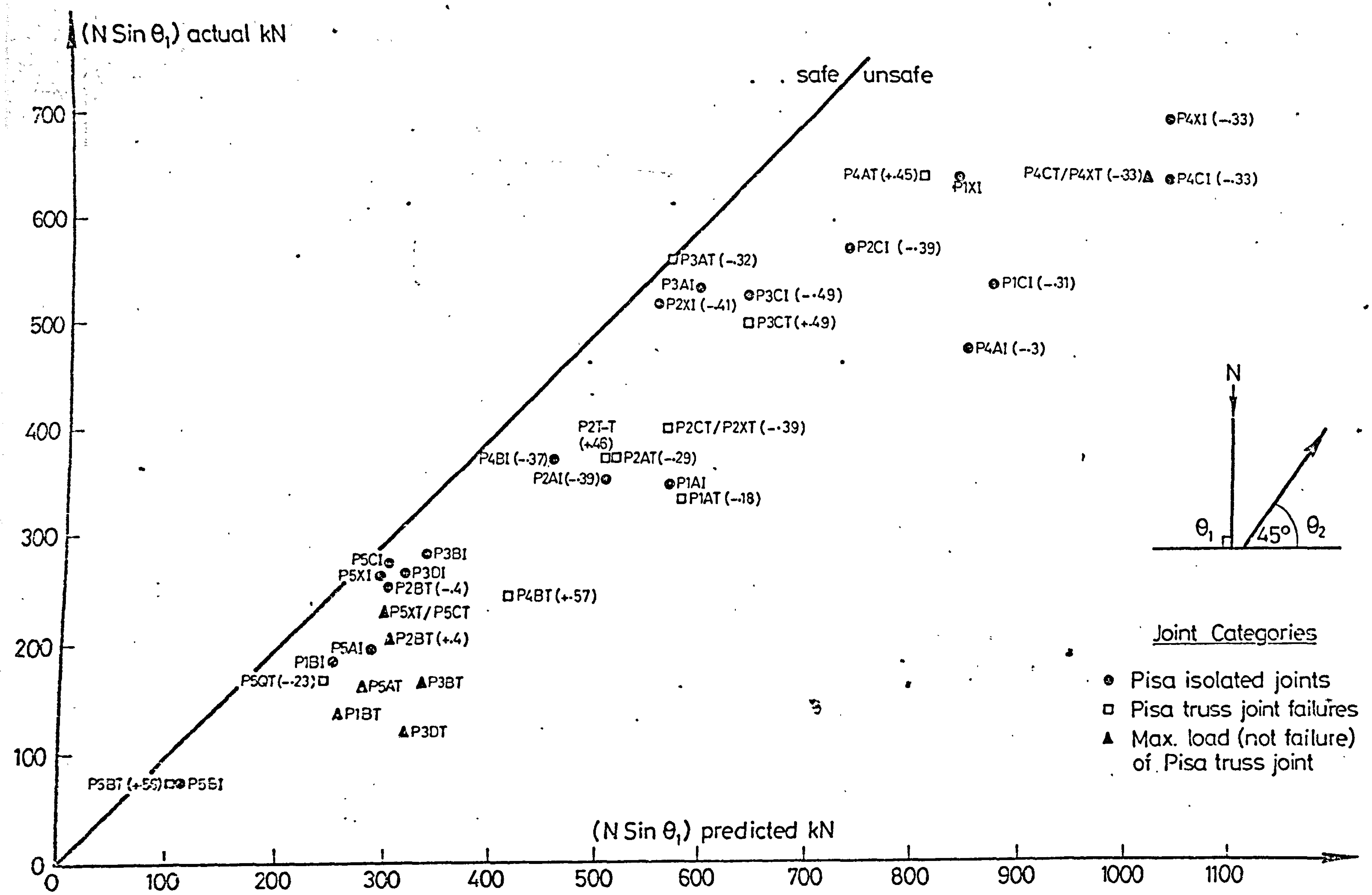

Fig.7·23 Actual v. predicted ultimate loads for CHS to RHS gap and lap joints

Based upon side of square = branch diameter (d), and using RHS to RHS analysis. Bracing member centre lines change to keep gap constant

Fig.7·24 Actual v. predicted ultimate loads for CHS to RHS gap and lap joints

Based upon side of square = 0·7854 x branch diameter = $\pi d/4$ and using RHS to RHS analysis. Branch member centre lines change to keep gap constant.

CHAPTER 8

CONCLUSIONS AND SUGGESTIONS FOR FURTHER RESEARCH

8.1 Conclusions

A theoretical analysis for statically loaded structural hollow section lattice girder joints having one compression bracing member and one tension bracing member welded to an RHS chord member has been undertaken. This analysis is based upon a set of joint failure modes which enable the yield and ultimate strengths of such joints to be assessed and a computer program has been written for this purpose (Appendix 2). The theory has been checked against the results of a total of 150 joint tests conducted both in isolation and in complete girders at testing centres in Corby (England), Delft (Netherlands) and Pisa (Italy).

(i) The push-pull yield line mechanisms which were proposed for modelling the deformations of RHS to RHS gap joints (figs. 3.3, 4.1 and 4.2) gave satisfactory predictions for both the yield load (see fig. 3.7) and ultimate load (see figs. 4.6 and 4.7) of gapped joints which failed in this manner. For these yield line models it was shown that it is permissible to assume that the contact area between the chord and bracings remains rigid during joint deformation and yielding at the toes of the bracing members adjacent to the crotch will have very little influence upon the joint yield line pattern and hence yield load for this failure mode. Due to the linear strain-hardening modulus chosen for the chord material in the joint crotch, the post-yield load v. deflection curve for the chord connecting face, which is produced by the theoretical push-pull models, does not closely represent the actual joint load v. deflection curve.

(ii) The two strut buckling mechanisms proposed in Chapter 5 (figs. 5.7, 5.8 and 5.15) give good agreement between the predicted and actual strut buckling loads of both gap and lapped joints (see fig. 5.17), and strut buckling mechanism 1 also models the actual load v. deflection behaviour of the connecting chord face reasonably well.

(iii) Simple approaches for calculating the ultimate strength of gap or lapped joints which fail by the chord shearing or chord local buckling failure modes have been proposed, and these have been compared with the results of joints which failed by these modes. The overall agreement between the predicted and actual ultimate loads for RHS braced joints, shown in figs. 4.12 and 4.13 for gap joints, and fig. 5.20 for lapped joints, is good.

(iv) The ultimate strength of a joint, measured as a force in the compression bracing member, is changed little by the addition of a compressive purlin load providing local failure of the chord side walls by either side wall buckling or bearing failure does not occur. A yield line mechanism has been proposed for the calculation of the chord bearing failure load (fig. 6.5) and this agrees sufficiently well with the few test results which are available for this mode of failure.

(v) An axial load in the chord member in addition to the horizontal components of the bracing member forces, (i.e. a chord 'preload'), generally causes a reduction in joint ultimate strength. This reduction in joint ultimate strength is different for each of the joint failure mechanisms which may operate and is often severe. (see figs. 7.3 and 7.4).

(vi) The ultimate strength of all joints is directly dependent upon the yield stress of the members, but the strength of some gap joints also depends upon the ultimate stress of the chord member.

(vii) The influence of the parameters b_1/t_1, λ, t_1/t_o, b_o/t_o, length of the strut member and the amount of overlap, upon the ultimate strength of lap joints has been studied (see figs. 7.5 to 7.10). It has been found theoretically that a lapped joint can never have a lower ultimate strength than a joint between the same members which is made gapped providing chord local buckling is not the failure mode.

(viii) It has been found that the failure mechanisms for gapped joints proposed in Chapter 4 cope with any orientation of rectangular bracing members welded to the chord face, and if it is desired to express the joint strength as a function of recognised joint parameters such as the 'width ratio' then a simple appropriate 'width ratio' parameter for RHS bracings would be $(b_1 + b_2 + h_1 + h_2)/4b_o$.

(ix) In the practical range of gap sizes, the ultimate gap joint strength, (providing a joint fails by the push-pull mode of fig. 4.1 or fig. 4.2), tends to theoretically increase with increasing gap providing λ is not small and b_o/t_o is low. For higher b_o/t_o values the tendency is diminished (see figs. 7.13 and 7.14). In practice a different mode of failure may limit the increase in ultimate strength to less than expected at larger gap sizes. Thus the minimum joint strength, which occurs at a gap of about $0.1b_o$, could be safely assumed for all gap sizes. For larger gap sizes the joint deformations increase considerably, particularly if λ is low and b_o/t_o is high.

For gap joints the ultimate strength increases significantly with an increase in the width ratio (λ) in a similar manner to the joint yield strength (see figs. 7.17 and 7.18).

(x) The ultimate strength of joints which fail by strut local buckling, (figs 5.4, 5.7 and 5.15), measured as a force in the bracing members, is virtually independent of the angle of inclination of the bracings to the chord. The ultimate strength of gap joints which fail by the push-pull mode of failure, (figs. 4.1 and 4.2), measured as a force in the compression bracing, is dependent upon the angle of inclination of the compression bracing to the chord and varies approximately with $1/\mathrm{Sin}\theta_1$.

(xi) The theoretical analysis developed for RHS braced joints can be applied successfully to CHS braced joints if the circular bracings of diameter d_i are made into square bracing members with dimensions of $\pi d_i/4$ and the amount of gap or overlap is kept the same.

8.2 Suggestions for further research.

(i) The push-pull failure mechanisms for gapped joints could be modified by incorporating a strain-hardening modulus for the chord material in the crotch which varies with strain, instead of using the existing linear modulus. This might then provide better agreement between the theoretical and actual load v. deflection curves for the connecting chord face in the post-yield range.

(ii) In overlapped joints with bracing members of unequal width the strut member might possibly punch into the tie member. This mode of failure was suggested in Chapter 5 (mode L10 in fig. 5.1) but was not investigated further because no experimental data on such lapped joints was available. Hence testing, and if necessary theoretical work, could be undertaken on joints of this type.

(iii) Experimental evidence on the elastic local buckling of RHS members under axial compression is lacking - particularly for high yield steel rectangular sections rather than square sections.

(iv) More experimental testing of overlapped joints with bracing thicknesses greater than the chord thickness is required over a wide range of overlaps.

(v) Further tests are needed on both gap and lapped joints of all types with purlin loads, ideally comparing them with analagous joints without purlin loads which are made of the same steel sections in order to eliminate the dependency of other joint parameters.

(vi) Further research on web buckling of RHS members loaded transversely to the section is needed, particularly with sections of large depth (h_o) and in high yield steels.

(vii) There is a real deficiency of joint tests of all types in higher grades of steel - especially Grade 55.

REFERENCES

1. AUSTRALIAN INSTITUTE OF STEEL CONSTRUCTION, "Safe load tables for structural steel - Metric units", 3rd edition, Sydney, 1975.

2. BABIKER, D.B., "The fatigue behaviour of welded joints between structural hollow sections", Ph.D. thesis, University of Sheffield, December 1967.

3. BENNETT, C.J., "Research carried out at Sheffield University into the factors affecting the static and dynamic strength of tubular joints (Results)", British Steel Corporation Tubes Division, Corby, CIDECT Report CE 70/7/E, 1970.

4. BENNETT, C.J., COLQUHOUN, I. and MacCORMICK, B., "Design of welded joints in tubular lattice girders - joints between CHS branch members and RHS chord members (Static loading)", British Steel Corporation Tubes Division, Corby, CIDECT Report CE 69/28, November 1969.

5. BLOCKLEY, D.I., "Joints between structural hollow sections in plane frameworks", Ph.D. thesis, University of Sheffield, June 1967.

6. BLOCKLEY, D.I., "Joints between structural hollow sections", Civil Engineering and Public Works Review, November 1972.

7. BRITISH STANDARDS INSTITUTION, "Specification for weldable structural steels", BS4360 : 1972, Table 12, pp. 31.

8. BRITISH STANDARDS INSTITUTION, "Draft standard specification for the structural use of steelwork in building. Part 1:

Simple construction and continuous construction", B/20 Draft, London, November 1977.

9. BRITISH STEEL CORPORATION TUBES DIVISION, "Tests on isolated joints", Report CE73/96/D, Corby, August 1977.

10. BRITISH STEEL CORPORATION TUBES DIVISION, "Tests on complete girders", Draft Report CE73/95, Corby, 1977.

11. BRITISH STEEL CORPORATION TUBES DIVISION, "RHS - Guide to fabrication and design", Corby, March 1977.

12. BRITISH STEEL CORPORATION TUBES DIVISION, "Hot finished structural hollow sections. Sizes and properties. ISO Metric sizes", Corby, 1977.

13. CALLADINE, C.R., "Engineering plasticity", Pergamon Press, Oxford, 1969.

14. CANADIAN INSTITUTE OF STEEL CONSTRUCTION, "Handbook of Steel Construction", 2nd. edition, Willowdale, Ontario, 1970.

15. CANADIAN INSTITUTE OF STEEL CONSTRUCTION, "Limit states design steel manual", 1st. edition, Willowdale, Ontario, January 1977.

16. CHANDRAKEERTHY, S.R. de S., "Structural behaviour related to stress analysis of joints in cold-formed square hollow sections", Ph.D. thesis, University of Sheffield, 1972.

17. CIDECT THEORY WORKING GROUP, Düsseldorf Meeting, 8th March, 1978.

18. COUTIE, M.G., DAVIES, G., PACKER, J.A., et al, Draft recommendations for, "CONSTRADO Design Guide on SHS Connections", CONSTRADO, London, to be published in 1979.

19. CRAN, J.A., "World wide applications of structural hollow sections", Symposium on Tubular Structures, Delft University of Technology, October 1977.

20. CZECHOWSKI, A. and BRODKA, J., "Etude de la résistance statique des assemblages soudés en croix de profils creux rectangulaires", Construction Métallique, No.3, Paris, September 1977.

21. DASGUPTA, A., "The behaviour of joints in tubular trusses", Ph.D. thesis, University of Nottingham, November 1970.

22. DAVIE, J. and GIDDINGS, T.W., "Research into the strength of welded lattice girder joints in structural hollow sections", British Steel Corporation Tubes Division, Corby, CIDECT Report CE 70/3, 1970.

23. DAVIES, G. and ROPER, C.G., "Gap joints with tubular members - A yield line approach", Building Science, Vol. 10, 1975, pp. 199-205.

24. DAVIES, G. and ROPER, C.G., "Gap joints with tubes - A yield line modified by shear approach", Building and Environment, Vol. 12, 1977, pp. 31-38.

25. DAVIES, P., KEMP, K.O. and WALKER, A.C., "An analysis of the failure mechanism of an axially loaded simply supported steel plate", Proceedings of the Institution of Civil Engineers, Part 2, Vol. 59, December 1975.

26. DE KONING, C.H.M. and WARDENIER, J., "Ultimate static strength of welded lattice girder joints in structural hollow sections: Series J - Determination of the influence

of the weld shape", Report No. BI-75-25/05.3.11.270, Delft University of Technology, 1975.

27. DE KONING, C.H.M. and WARDENIER, J., "Ultimate static strength of welded lattice girder joints in rectangular hollow sections: Series K - Scale effects", Report No. BI-75-20/05.3.11.270, Delft University of Technology, 1975.

28. DE KONING, C.H.M. and WARDENIER, J., "Supplement test results of welded joints in structural hollow sections with rectangular boom", CIDECT Report 76/11/5Q, Delft University of Technology, September 1976.

29. DOWLING, P.J., "Some approaches to the non-linear analysis of plated structures", Structural Analysis Non-Linear Behaviour and Techniques Symposium, Transport and Road Research Laboratory, Crowthorne, December 1974.

30. DWIGHT, J.B., "Local buckling in steel hollow sections - State of the art report", Technical Report No. CUED/C - Struct/TR.66, Cambridge University, 1978.

31. EASTWOOD, W. and WOOD, A.A., "Recent research on joints in tubular structures", Canadian Structural Engineering Conference and CIDECT Issue 70/8/E, Toronto, Canada, February 1970.

32. EASTWOOD, W. and WOOD, A.A., "Welded joints in tubular structures involving rectangular sections", Conference on Joints in Structures, Session A Paper 2, University of Sheffield, July 1970.

33. EDWARDS, M. and GIDDINGS, T.W., "The behaviour of welded joints in complete lattice girders with RHS chords (Design and Fabrication)", CIDECT Programme 5F Report 74/3/E, March 1974.

34. EUROPEAN CONVENTION FOR CONSTRUCTIONAL STEELWORK, "Introductory report of the Second International Colloquium on Stability of Steel Structures", Liège, Belgium, April 1977.

35. HALEEM, A.S., "Some aspects of SHS welded joint behaviour", British Steel Corporation Tubes Division, Corby, January 1977.

36. HALEEM, A.S., "Determination of ultimate joint strength for statically loaded SHS welded lattice girder joints with RHS chords", CIDECT Report 77/37, British Steel Corporation Tubes Division, October 1977.

37. HOHL, "Failure load tests on large size RHS Warren joints", Mannesmann Research Institute Report No. 93/74 and CIDECT Report No. 74/15/5M(E), Düsseldorf, West Germany, June 1974.

38. HOHL, "Failure tests on large size RHS Warren type joints", Mannesmann Research Institute Report No. 15/76 and CIDECT Report No. 76/8/5M(E), Düsseldorf, West Germany, February 1976.

39. HORNE, M.R., "Plastic theory of structures", Nelson, London, 1971.

40. JOHANSEN, K.W., "Yield line theory", Cement and Concrete Association, London, 1962.

41. JOHNSTON, B.G., "Guide to stability design criteria for metal structures", 3rd edition, John Wiley and Sons, New York, 1976.

42. JUBB, J.E.M. and REDWOOD, R.G., "Design of joints to box sections", Industrial Building and the Structural Engineer, Institution of Structural Engineers Conference, May 1966.

43. MANG, F., "Report on rectangular hollow sections (RHS) joint study programme - CIDECT Programme 5P", Mannesmann Research Institute, Düsseldorf, West Germany, September 1973.

44. MANG, F., "Tests on Warren joints in large size RHS", CIDECT Programme 5M Interim Report, Mannesmann Research Institute, Düsseldorf, West Germany, September 1975.

45. MANG, F., "Theoretical models for calculating the strength and deformation of welded rectangular hollow section joints", British Steel Corporation Tubes Division Translation No. TD1068 of a University of Karlsruhe research report, Corby, March 1977.

46. MANG, F. and STRIEBEL, A., "Proposals for D1N4116", Normensitzung 24, 11-25, 11, University of Karlsruhe, West Germany, 1978.

47. MANSOUR, M.H., "Theoretical analysis of T-joints in hollow structural sections", M.Eng. thesis, Mc. Master University, Hamilton, Canada, March 1978.

48. MEE, B.L., "The structural behaviour of joints in rectangular hollow section", Ph.D. thesis, University of Sheffield, September 1969.

49. MEHROTRA, L. and REDWOOD, R.G., "Load transfer through connections between box sections", Canadian Engineering Journal C-70-BR & STR 10, August/September 1970, pp. 47-52.

50. MORRELL, P.J.B., "Beams in RHS - The effective line of action of loads applied uniformly over the flanges of RHS beams", Construction Steelwork, March 1972.

51. MOUTY, J., "Calcul des charges ultimes des assemblages soudés de profils creux carrés et rectangulaires", Construction métallique, No.2, Paris, June 1976.

52. MOUTY, J., "Behaviour of welded joints of square and rectangular tubular structures - A theoretical approach based on the method of yield lines", International Institute of Welding Annual Assembly, Document XV-426-78, Dublin, 1978.

53. NETHERLANDS STAALBOUWKUNDIG GENOOTSCHAP, "Richtlijnen voor de berekening van buisconstructies - RB '78", Draft version, October 1977.

54. PACKER, J.A. and DAVIES, G., "Strut local buckling in trusses of rectangular hollow sections", Regional Colloquium on Stability of Steel Structures, Budapest/Balatonfüred, Hungary, October 1977.

55. PACKER, J.A., DAVIES, G. and COUTIE, M.G., "Gap joint strength of rectangular hollow section trusses", International Association for Bridge and Structural Engineering Symposium, Moscow, U.S.S.R., September 1978.

56. PATEL, N.M., "Experimental and analytical investigation of punching shear characteristics of rectangular tubular welded joints", Ph.D. thesis, University of Houston, U.S.A., December 1972.

57. RAWLINGS, B. and SHAPLAND, P., "The behaviour of thin - walled box sections under gross deformation", The Structural Engineer, No.4, Vol. 53, April 1975.

58. ROBINSON, H.C., "Literature survey on tubular steel joints", Part thesis for Ph.D., University of Sheffield, 1969.

59. ROPER, C.G., "An analytical study of the strength and flexibility of tubular joints", M.Phil. Thesis, University of Nottingham, May 1974.

60. ROSE, W., "Data unification - symbols and units", CIDECT Technical Secretariat, Croydon, January 1977.

61. SHINOUDA, M.R., "Stiffened tubular joints", Ph.D. thesis, University of Sheffield, June 1967.

62. STEEL COMPANY OF CANADA LIMITED, "Hollow structural sections welded joint research summaries", Technical Report, Hamilton, Canada, May 1974.

63. STEEL COMPANY OF CANADA LIMITED, "Hollow structural sections - Design manual for connections", 1st. edition, Hamilton, Canada, September 1976.

64. TIMOSHENKO, S., "Theory of elastic stability", Mc.Graw Hill, 1936.

65. WALKER, A.C., "Design and analysis of cold-formed sections", Intertext Books, Bedfordshire, 1975.

66. WARDENIER, J., "General principles for the verification of the safety of predominantly statically loaded tubular joints", Report No. BI-77-16*/35.3.51210, Delft University of Technology, January 1977.

67. WARDENIER, J., "Testing and analyses of truss joints in hollow structural sections", Conference on Structural Hollow Sections, Toronto, Canada, May 1977.

68. WARDENIER, J., "Results of research E.C.S.C.: Welded girder joints in structural hollow sections", Acier - Stahl - Steel, Vol.43, No.1, 1978, pp. 29-33.

69. WARDENIER, J. and DE KONING, C.H.M., "Static tensile tests on T-joints in structural hollow sections - determination of the influence of weld method and type of material", Report No. BI-74-42/05.3.11.270, Delft University of Technology, 1974.

70. WARDENIER, J., DE KONING, C.H.M. and VAN DOUWEN, A.A., "Investigation into the static strength of welded lattice girder joints in structural hollow sections", CIDECT Report 75/29, Delft University of Technology, June 1976.

71. WARDENIER, J. and DE KONING, C.H.M., "Investigation into the static strength of welded lattice girder joints in structural hollow sections. Part 1: Rectangular hollow sections", CIDECT Report 76/12/5Q, Delft University of Technology, June 1976.

72. WARDENIER, J. and DE KONING, C.H.M., "Investigation into the static strength of welded lattice girder joints in structural hollow sections. Part 2: Joints with circular bracings and rectangular boom", CIDECT Report 76/13/5Q, Delft University of Technology, December 1976.

73. WARDENIER, J. and VERHEUL, A., "Bibliography of welded joints in structural hollow sections", Delft University of Technology Report No. BI-77-5/35.3.51210 and I.I.W. Annual Assembly in Copenhagen Document No. XV-403-77, June 1977.

74. WARDENIER, J. and DE KONING, C.H.M., "Investigation into the static strength of welded joints with three bracings made of RHS or CHS", CIDECT Report 77/23/5Q, Delft University of Technology, August 1977.

75. WASHIO, K., TOGO, T. and MITSUI, Y., "Truss joints in tubular structures", Transactions of the Architectural Institute of Japan, October 1966.

76. WASHIO, K., TOGO, T. and MITSUI, Y., "Experimental research on local failure of chord in tubular truss joint", Transactions of the Architectural Institute of Japan, August 1967.

77. WATSON, C. and BABB, A.S., "Box columns: progress report on the determination of stiffening requirements", British Steel Corporation (Swindon Laboratory), Report DTS 68/718/A, October 1969.

78. WOOD, A.A., NETHERCOT, D.A. and CHANDRAKEERTHY, S., "Report on CIDECT Programme 5G - Welded joint tests with cold-formed SHS", University of Sheffield, September 1972.

79. WOOD, R.H., "Plastic and elastic design of slabs and plates", Thames and Hudson, 1961.

APPENDIX 1

JOINT TEST DATA

JOINT NUMBER	Delft 1	Delft 2	Delft 3	Delft 4	Delft 5	Delft 6	Delft 7	Delft 8	Delft 9	Delft 10
λ_1	.99	.99	.63	.60	.63	.38	.40	.38	.76	.69
Strut Tie	□ □	□ □	□ □	□ □	□ □	□ □	□ □	□ □	□ ▫	□ ▫
T1	4.74	2.96	4.00	2.95	4.00	4.00	1.99	4.00	3.85	3.74
T2	4.74	2.96	4.00	2.95	4.00	3.96	1.99	3.96	4.80	3.92
T3	3.74	2.95	3.96	2.93	3.72	3.72	2.93	3.72	3.75	3.35
FY1	.298	.224	.275	.282	.275	.325	.216	.325	.328	.314
FY2	.298	.224	.275	.282	.275	.325	.216	.325	.328	.369
FY3	.322	.230	.334	.232	.317	.317	.232	.314	.310	.292
ULT1	.448	.337	.470	.434	.470	.505	.314	.505	.402	.436
ULT2	.448	.337	.470	.434	.470	.505	.314	.505	.402	.504
ULT3	.460	.335	.478	.337	.455	.455	.337	.455	.447	.438
D	99.8	99.5	99.3	98.9	99.5	99.5	98.4	99.5	99.8	100.2
GAP/LAP	0	0	0	0	0	0	0	0	-.2	-.2
C1	98.9	98.5	62.8	59.8	62.8	38.1	39.7	38.1	75.7	69.3
C2	98.9	98.5	62.8	59.8	62.8	37.8	39.7	37.8	51.0	51.0
E1	98.9	98.5	62.8	59.8	62.8	38.1	39.7	38.1	75.7	69.3
E2	98.9	98.5	62.8	59.8	62.8	37.8	39.7	37.8	51.0	51.0
A1	.7854	.7854	.7854	.7854	0	.7854	.7854	0	.7854	.7854
A2	.7854	.7854	.7854	.7854	.7854	.7854	.7854	.7854	.7854	.7854
E	30.4	30.4	4.6	2.1	46.5	13.2	11.8	15.1	0	0
WS1	6.7	4.19	5.66	4.17	5.66	5.66	2.81	5.66	5.44	5.29
WS2	6.7	4.19	5.66	4.17	5.66	5.66	2.81	5.66	6.79	5.54
F	0	0	0	0	0	0	0	0	0	0
ACH	1420	1110	1470	1092	1420	1420	1092	1420	1420	1275
DEP	99.8	98.5	99.3	98.9	99.5	99.5	98.4	99.5	99.8	100.2
EYS	207	207	207	207	207	207	207	207	207	207
H	300.6	300.8	318.6	320.1	350.0	331.0	330.0	350.0	312.2	315.4
FULT1	253	120	198	78	146	113	46	80	172.5	113.5
BZ	1	1	1	1	1	1	1	1	1	1
FPURL	0	0	0	0	0	0	0	0	0	0
TPURL	0	0	0	0	0	0	0	0	0	0
TR	1	1	1	1	1	1	1	1	1	1
FAILURE MODE REPORTED	G7	G7	G1	G1	G1	G5	G6	G1	G1/G8	G1/G8

JOINT NUMBER	Delft 11	Delft 12	Delft 13	Delft 14	Delft 15	Delft 16	Delft 17	Delft 18	Delft 19'	Delft 19"
λ_1	.76	.50	.76	.71	.51	.64	.61	.38	1.00	1.00
$\boxed{\text{Strut}}$ $\boxed{\text{Tie}}$										
T1	3.85	1.91	3.85	2.99	3.98	4.77	2.97	3.30	4.91	2.98
T2	3.98	1.96	4.91	2.98	3.32	4.77	2.97	3.30	4.91	2.98
T3	3.89	3.35	3.75	2.96	3.75	3.75	2.99	3.75	3.84	3.35
FY1	.322	.192	.322	.337	.305	.321	.211	.325	.314	.221
FY2	.305	.292	.314	.221	.285	.321	.211	.325	.314	.221
FY3	.335	.292	.310	.224	.310	.310	.231	.310	.335	.292
ULT1	.497	.328	.497	.431	.458	.528	.322	.500	.492	.350
ULT2	.458	.438	.492	.350	.458	.528	.322	.500	.492	.350
ULT3	.480	.390	.447	.340	.447	.447	.339	.447	.480	.438
D	99.1	100.2	99.8	98.9	99.8	99.8	98.7	99.8	99.4	100.2
GAP/LAP	-.2	-.2	-.2	-.2	-.2	-.2	-.2	-.2	-.2	-.2
C1	75.7	50.0	75.7	70.3	50.6	63.4	60.3	38.2	101.2	99.9
C2	50.6	35.0	50.6	50.5	25.2	63.4	60.3	38.2	101.2	99.9
E1	75.7	50.0	75.7	70.3	50.6	126.4	99.4	63.0	50.6	50.5
E2	50.6	35.0	101.2	99.9	50.6	126.4	99.4	63.0	50.6	50.5
A1	0	.7854	.7854	.7854	.7854	.7854	.7854	.7854	.7854	.7854
A2	.7854	.7854	.7854	.7854	.7854	.7854	.7854	.7854	.7854	.7854
E	0	0	0	0	0	0	0	0	0	0
WS1	5.44	2.70	5.44	4.23	5.63	6.75	4.2	4.67	6.94	4.21
WS2	5.63	2.77	6.94	4.21	4.70	6.75	4.2	4.67	6.94	4.21
F	0	0	0	0	0	0	0	0	0	0
ACH	1440	1272	1420	1100	1420	1420	1128	1420	1440	1275
DEP	99.1	100.2	99.8	98.9	99.8	99.8	98.7	99.8	99.4	100.2
EYS	207	207	207	207	207	207	207	207	207	207
H	350	325	312.2	314.9	324.7	286.8	300.3	318.5	324.7	324.8
FULT1	165.4	57.5	195	88.5	113	198.6	93	140	266	169
BZ	1	1	1	1	1	1	1	1	1	1
FPURL	0	0	0	0	0	0	0	0	0	0
TPURL	0	0	0	0	0	0	0	0	0	0
TR	1	1	1	1	1	1	1	1	1	1
FAILURE MODE REPORTED	G6	G2	G4	G5	G4/G7	G2/G6	G5	G3/G7	G6	G5

JOINT NUMBER	Delft 19‴	Delft 20	Delft 21	Delft 22	Delft 23	Delft 60	Delft 64	Delft 137 (−.68)	Delft 137″ (−.20)	Delft 137″ (+.60)
λ_1	.63	.89	.81	.51	.51	.63	.37	.64	.99	.99
Strut Tie										
T1	3.31	4.08	2.99	3.30	3.30	4.81	3.89	4.00	4.74	4.74
T2	3.31	4.08	2.99	3.30	3.30	4.81	3.89	4.00	4.74	4.74
T3	3.84	3.75	2.99	3.75	3.75	5.40	5.40	3.72	3.75	3.75
FY1	.325	.281	.225	.285	.285	.284	.335	.275	.298	.298
FY2	.325	.281	.225	.285	.285	.284	.335	.275	.298	.298
FY3	.335	.310	.231	.310	.314	.280	.280	.317	.310	.310
ULT1	.500	.427	.356	.458	.458	.462	.502	.470	.448	.448
ULT2	.500	.427	.356	.458	.458	.462	.502	.470	.448	.448
ULT3	.480	.447	.339	.447	.464	.475	.475	.454	.447	.447
D	99.4	99.8	98.7	99.8	99.8	101.7	101.7	99.5	99.8	99.8
GAP/LAP	−.2	−.2	−.2	−.2	−.2	0	0	0	−.2	−.2
C1	63.0	88.9	79.7	50.5	50.5	63.6	37.8	63.5	98.9	98.9
C2	63.0	37.9	39.6	25.2	25.2	63.6	37.8	62.8	98.9	98.9
E1	38.2	37.9	39.6	25.2	25.2	63.6	37.8	63.5	98.9	98.9
E2	38.2	88.6	79.7	50.5	50.5	63.6	37.8	62.8	98.9	98.9
A1	.7854	.7854	.7854	.7854	0	.7854	.7854	0	.7854	.7854
A2	.7854	.7854	.7854	.7854	.7854	.7854	.7854	.7854	.7854	.7854
E	0	0	0	0	0	3.5	−14.0	46.3	0	0
WS1	4.68	5.77	4.23	4.67	4.67	6.80	5.50	5.66	6.70	6.70
WS2	4.68	5.77	4.23	4.67	4.67	6.80	5.50	5.66	6.70	6.70
F	0	0	0	0	0	0	0	−306	−88	264.6
ACH	1440	1420	1128	1420	1430	1840	1840	1420	1420	1420
DEP	99.4	99.8	98.7	99.8	99.8	101.7	101.7	99.5	99.8	99.8
EYS	207	207	207	207	207	207	207	207	207	207
H	330.9	331.1	330.2	337.4	350	318.2	331.1	350.0	300.6	300.6
FULT1	153	167	80	101.5	92.6	272	122	91	230	350
BZ	1	1	1	1	1	1	1	1	1	1
FPURL	0	0	0	0	0	0	0	0	0	0
TPURL	0	0	0	0	0	0	0	0	0	0
TR	1	1	1	1	1	1	1	1	1	1
FAILURE MODE REPORTED	G8	G8	G5	G5	Tie Yield	G5	G1	G7	G7	G7/G6

JOINT NUMBER	Delft 137''' (-.20)	Delft 137''' (+.59)	Delft 138' (-.20)	Delft 138' (+.60)	Delft 138''' (-.20)	Delft 138''' (+.60)	Delft 139'' (-.20)	Delft 139'' (+.60)	Delft 141' (-.20)	Delft 141' (+.58)
λ_1	1.00	1.00	.63	.63	.61	.61	.63	.63	.37	.37
Strut Tie										
T1	2.95	2.95	4.85	4.85	2.95	2.95	4.00	4.00	4.06	4.06
T2	2.95	2.95	4.85	4.85	2.95	2.95	4.00	4.00	4.06	4.06
T3	3.00	2.95	4.92	4.92	3.00	3.00	3.74	3.74	4.92	4.92
FY1	.230	.230	.330	.330	.282	.282	.275	.275	.314	.314
FY2	.230	.230	.330	.330	.282	.282	.275	.275	.314	.314
FY3	.232	.230	.296	.296	.232	.232	.322	.322	.296	.296
ULT1	.335	.335	.510	.510	.434	.434	.470	.470	.466	.466
ULT2	.335	.335	.510	.510	.434	.434	.470	.470	.466	.466
ULT3	.337	.337	.455	.455	.337	.337	.460	.460	.455	.455
D	98.4	98.6	100.6	100.6	98.3	98.3	99.8	99.8	100.6	100.6
GAP/LAP	-.203	-.203	-.2	-.2	-.2	-.203	-.2	-.2	-.2	-.2
C1	98.5	98.6	63.4	63.4	59.8	59.8	62.8	62.8	37.5	37.5
C2	98.5	98.6	63.4	63.4	59.8	59.8	62.8	62.8	37.5	37.5
E1	98.5	98.6	63.4	63.4	59.8	59.8	62.8	62.8	37.5	37.5
E2	95.5	98.6	63.4	63.4	59.8	59.8	62.8	62.8	37.5	37.5
A1	.7854	.7854	.7854	.7854	.7854	.7854	0	0	.7854	.7854
A2	.7854	.7854	.7854	.7854	.7854	.7854	.7854	.7854	.7854	.7854
E	0	0	0	0	0	0	0	0	0	0
WS1	4.17	4.17	6.8	6.8	4.2	4.17	5.7	5.7	5.7	5.74
WS2	4.17	4.17	6.8	6.8	4.2	4.17	5.7	5.7	5.7	5.74
F	-52	150	-112	325	-48	156	-128	274	-111.6	320
ACH	1116	1110	1880	1880	1116	1116	1420	1420	1880	1880
DEP	98.4	98.6	100.6	100.6	98.3	98.3	99.8	99.8	100.6	100.6
EYS	207	207	207	207	207	207	207	207	207	207
H	300.8	300.7	318.3	318.3	320.1	320	350	350	331.3	331.3
FULT1	110	146	227	290	61	119	130	150	125	137
BZ	1	1	1	1	1	1	1	1	1	1
FPURL	0	0	0	0	0	0	0	0	0	0
TPURL	0	0	0	0	0	0	0	0	0	0
TR	1	1	1	1	1	1	1	1	1	1
FAILURE MODE REPORTED	G7	G6	G5	G5	G2	G6	G5	G5	G5	G6

JOINT NUMBER	Delft 141" (-0.2)	Delft 141" (-0.5)	Delft 141" (+0.6)	Delft 141"' (+0.6)	Delft 142" (-.2)	Delft 142" (-.5)	Delft 142" (-.7)	Delft 142" (+.6)	Delft 140 (-.8)	Delft 142"' (-.2)
λ_1	.38	.38	.38	.41	.37	.37	.37	.37	.38	.38
Strut Tie	☐ ☐	☐ ☐	☐ ☐	☐ ☐	☐ ☐	☐ ☐	☐ ☐	☐ ☐	☐ ☐	☐ ☐
T1	3.89	4.06	3.93	2.06	4.06	4.06	4.06	4.06	4.00	4.00
T2	3.93	4.06	3.93	1.93	4.06	4.06	4.06	4.06	3.89	4.00
T3	3.75	3.75	3.75	2.96	4.92	4.92	4.92	4.92	3.96	3.74
FY1	.335	.314	.345	.240	.314	.314	.314	.314	.335	.310
FY2	.345	.314	.345	.232	.314	.314	.314	.314	.335	.310
FY3	.314	.314	.314	.224	.296	.296	.296	.296	.334	.322
ULT1	.502	.466	.520	.368	.466	.466	.466	.466	.502	.483
ULT2	.520	.466	.520	.360	.466	.466	.466	.466	.502	.483
ULT3	.454	.454	.454	.337	.455	.455	.455	.455	.478	.460
D	99	99	99	97.9	100.6	100.6	100.6	100.6	99.4	99.8
GAP/LAP	-.2	-.2	-.2	-.204	-.2	-.2	-.2	-.2	-.2	-.2
C1	37.8	37.8	37.9	40.3	37.5	37.5	37.5	37.5	38.1	37.9
C2	37.9	37.5	37.9	40.0	37.5	37.5	37.5	37.5	37.8	37.9
E1	37.8	37.8	37.9	40.3	37.5	37.5	37.5	37.5	38.1	37.9
E2	37.9	37.5	37.9	40.0	37.5	37.5	37.5	37.5	37.8	37.9
A1	.7854	.7854	.7854	.7854	0	0	0	0	0	0
A2	.7854	.7854	.7854	.7854	.7854	.7854	.7854	.7854	.7854	.7854
E	0	0	0	0	0	0	0	0	0	0
WS1	5.5	5.7	5.5	2.91	5.7	5.7	5.7	5.7	5.7	5.7
WS2	5.5	5.7	5.5	2.73	5.7	5.7	5.7	5.7	5.7	5.7
F	-89.8	-200	270	148	-110	-267	-320	324	-400	-89
ACH	1430	1430	1430	1100	1880	1880	1880	1880	1470	1420
DEP	99	99	99	97.9	100.6	100.6	100.6	100.6	99.4	99.8
EYS	207	207	207	207	207	207	207	207	207	207
H	331.1	331.3	331.1	329.9	350	350	350	350	350	350
FULT1	101	62	125	50	96	92.5	87.5	123	35	82
BZ	1	1	1	1	1	1	1	1	1	1
FPURL	0	0	0	0	0	0	0	0	0	0
TPURL	0	0	0	0	0	0	0	0	0	0
TR	1	1	1	1	1	1	1	1	1	1
FAILURE MODE REPORTED	G5	G7/G2	G5	G6	G5	G5	G5	G5	G5/G7	G5

JOINT NUMBER	Delft 142"' (−.5)	Delft 142"' (−.7)	Delft 142"' (+.6)	Delft 142"" (−.7)	Delft 142"" (+.6)	Delft 139 (−.67)	Delft 142	Delft 142'	Delft 7CF	Delft 174'
λ_1	.38	.38	.38	.41	.41	.38	.37	.41	.41	1.00
Strut Tie	☐☐	☐☐	☐☐	☐☐	☐☐	☐☐	☐☐	☐☐	☐☐	☐☐
T1	3.93	4.00	3.93	1.93	1.93	4.00	4.06	1.93	1.90	1.87
T2	3.93	4.00	3.93	1.93	1.93	3.89	4.06	1.93	1.90	1.87
T3	3.75	3.74	3.75	3.00	2.95	3.96	4.92	3.00	2.95	1.87
FY1	.325	.310	.325	.232	.232	.335	.314	.232	.384	.228
FY2	.345	.310	.345	.232	.232	.335	.314	.232	.384	.228
FY3	.314	.322	.314	.206	.230	.334	.296	.206	.308	.228
ULT1	.505	.483	.505	.360	.360	.502	.466	.360	.505	.354
ULT2	.520	.483	.520	.360	.360	.502	.466	.360	.505	.354
ULT3	.454	.460	.454	.329	.335	.478	.455	.329	.405	.354
D	99	99.8	99	98.6	98.1	99.4	100.6	98.6	98.3	50.1
GAP/LAP	−.2	−.2	−.2	−.2	−.2	0	0	−.2	−.2	−.4
C1	37.8	37.9	37.8	40.0	40.0	38.1	37.5	40.0	40.15	50.1
C2	37.8	37.9	37.8	40.0	40.0	37.8	37.5	40.0	40.15	50.1
E1	37.8	37.9	37.8	40.0	40.0	38.1	37.5	40.0	40.15	50.1
E2	37.8	37.9	37.8	40.0	40.0	37.8	37.5	40.0	40.15	50.1
A1	0	0	0	0	0	.7854	0	0	.7854	.7854
A2	.7854	.7854	.7854	.7854	.7854	.7854	.7854	.7854	.7854	.7854
E	0	0	0	0	0	−13.2	15.1	0	0	0
WS1	5.6	5.7	5.6	2.7	2.73	5.66	5.74	2.73	2.69	2.64
WS2	5.6	5.7	5.6	2.7	2.73	5.66	5.74	2.73	2.69	2.64
F	−218	−200	268	−100	153	−330	0	0	0	0
ACH	1430	1420	1430	1120	1110	1470	1880	1120	1060	351
DEP	99	99.8	99	98.6	98.1	99.4	100.6	98.6	98.3	50.1
EYS	207	207	207	207	207	207	207	207	207	207
H	350	350	350	350	350	331	350	350	329.9	325
FULT1	69	65	68	27.2	46	54	100	44	68	48
BZ	1	1	1	1	1	1	1	1	1	1
FPURL	0	0	0	0	0	0	0	0	0	0
TPURL	0	0	0	0	0	0	0	0	0	0
TR	1	1	1	1	1	1	1	1	1	1
FAILURE MODE REPORTED	G5	G5	G5	G4	G6	G7	G1	G6	G6	G3

JOINT NUMBER	Delft 178	Delft 183	Delft 184	Delft 185	Delft 144	Delft 145	Delft 146	Delft 147	Delft 150	Delft 151
λ_1	.63	1.00	.60	.40	1.00	1.00	.64	.60	.39	.40
$\boxed{\text{Strut}}$ $\boxed{\text{Tie}}$										
T1	6.50	4.96	3.95	4.40	4.87	3.35	4.25	3.00	4.10	1.90
T2	6.50	4.96	3.95	4.40	4.87	3.35	4.25	3.00	4.10	1.90
T3	8.05	4.05	4.05	4.05	3.87	3.35	3.87	3.35	3.87	3.35
FY1	.292	.335	.374	.420	.338	.292	.321	.379	.342	.384
FY2	.292	.335	.374	.420	.338	.292	.321	.379	.342	.384
FY3	.312	.330	.330	.330	.331	.292	.331	.292	.331	.292
ULT1	.490	.405	.410	.462	.480	.390	.495	.443	.477	.428
ULT2	.490	.405	.410	.462	.480	.390	.495	.443	.477	.428
ULT3	.473	.403	.403	.403	.372	.390	.372	.390	.372	.390
D	197.5	100.2	100.0	100	99.4	100.1	99.4	100.1	99.4	100.1
GAP/LAP	0	-.2	0	0	-.2	-.2	-.2	-.2	-.2	-.2
C1	125.0	99.8	59.7	40.1	99	100.1	63.2	59.8	38.5	40.15
C2	125.0	99.8	59.7	40.1	99	100.1	63.2	59.8	38.5	40.15
E1	125.0	99.8	59.7	40.1	99	100.1	63.2	59.8	38.5	40.15
E2	125.0	99.8	59.7	40.1	99	100.1	63.2	59.8	38.5	40.15
A1	.7854	.7854	.7854	.7854	.7854	.7854	.7854	.7854	.7854	.7854
A2	.7854	.7854	.7854	.7854	.7854	.7854	.7854	.7854	.7854	.7854
E	-.5	0	2.4	-11.8	0	0	0	0	0	0
WS1	9.19	7.01	5.59	6.22	6.89	4.74	6.00	4.24	5.80	2.69
WS2	9.19	7.01	5.59	6.22	6.89	4.74	6.00	4.24	5.80	2.69
F	0	0	0	0	0	0	0	0	0	0
ACH	6140	1450	1450	1450	1415	1277	1415	1277	1415	1277
DEP	197.5	100.2	100.0	100	99.4	100.1	99.4	100.1	99.4	100.1
EYS	207	207	207	207	207	207	207	207	207	207
H	287.5	300.1	320.2	330	300.3	300	318.4	320.1	330.8	329.9
FULT1	710	272	180	107	270	214	164	105	136	58
BZ	1	1	1	1	1	1	1	1	1	1
FPURL	0	0	0	0	91.6	57.5	63.8	29.7	50.0	14.4
TPURL	0	0	0	0	70	70	70	70	70	70
TR	1	1	1	1	1	1	1	1	1	1
FAILURE MODE REPORTED	-	G7	G1	G1	G9	G9	G2/G3	G1/G6	G2	G6

JOINT NUMBER	Pisa 6AI	Pisa 6AT	Pisa 6BI	Pisa 6BT	Pisa 7AI	Pisa 7AT	Pisa 7BI	Pisa 7BT	Pisa 8AI	Pisa 8AT
λ_1	.60	.60	.30	.30	.67	.67	.33	.33	.58	.58
$\boxed{\text{Strut}}$ $\boxed{\text{Tie}}$										
T1	4.90	4.90	4.00	4.00	4.00	4.00	3.20	3.20	3.60	3.60
T2	9.50	9.50	4.90	4.90	6.30	6.30	4.00	4.00	6.30	6.30
T3	6.30	6.30	6.30	6.30	6.30	6.30	6.30	6.30	6.30	6.30
FY1	.296	.296	.292	.292	.339	.339	.332	.332	.289	.333
FY2	.354	.354	.416	.416	.287	.287	.323	.323	.279	.279
FY3	.358	.358	.405	.405	.383	.383	.383	.383	.405	.408
ULT1	.472	.472	.494	.494	.513	.513	.522	.522	.481	.496
ULT2	.481	.481	.580	.580	.457	.457	.503	.503	.460	.460
ULT3	.496	.496	.516	.516	.496	.496	.496	.496	.499	.510
D	254.0	254.0	254.0	254.0	152.4	152.4	152.4	152.4	152.4	152.4
GAP/LAP	-.098	-.098	-.098	-.098	-.164	-.164	-.164	-.164	-.164	-.164
C1	152.4	152.4	76.2	76.2	101.6	101.6	50.8	50.8	88.9	88.9
C2	152.4	152.4	76.2	76.2	101.6	101.6	50.8	50.8	88.9	88.9
E1	152.4	152.4	76.2	76.2	101.6	101.6	50.8	50.8	88.9	88.9
E2	152.4	152.4	76.2	76.2	101.6	101.6	50.8	50.8	88.9	88.9
A1	0	0	0	0	0	0	0	0	0	0
A2	.7854	.7854	.7854	.7854	.7854	.7854	.7854	.7854	.7854	.7854
E	0	0	0	0	0	0	0	0	0	0
WS1	6.3	6.3	6.3	6.3	6.3	6.3	6.3	6.3	6.3	6.3
WS2	6.3	6.3	6.3	6.3	6.3	6.3	6.3	6.3	6.3	6.3
F	-604	-604	-731	731	0	0	0	0	0	-225.4
ACH	6270	6270	6270	6270	3690	3690	3690	3690	3690	3690
DEP	254.0	254.0	254.0	254.0	152.4	152.4	152.4	152.4	152.4	152.4
EYS	207	207	207	207	207	207	207	207	207	207
H	573	798	573	798	623.8	748.8	623.8	748.8	623.8	748.8
FULT1	242.2	291	194.2	104	380.5	318	166.7	109.8	310.9	221.6
BZ	1	1	1	1	1	1	1	1	1	1
FPURL	0	0	0	0	0	0	0	0	0	0
TPURL	0	0	0	0	0	0	0	0	0	0
TR	1	2	1	2	1	2	1	2	1	2
FAILURE MODE REPORTED	G1	Did not fail	G1	Did not fail	G6	Did not fail	G6	Did not fail	G6	G1

JOINT NUMBER	Pisa 8BI	Pisa 8BT	Pisa 6NT	Pisa 7QT						
λ_1	.50	.50	.60	.67						
Strut Tie	☐ ☐	☐ ☐	☐ ☐	☐ ☐						
T1	3.20	3.20	4.90	4.00						
T2	4.00	4.00	9.50	6.30						
T3	6.30	6.30	6.30	6.30						
FY1	.491	.491	.322	.339						
FY2	.322	.312	.354	.287						
FY3	.405	.408	.405	.387						
ULT1	.652	.652	.508	.513						
ULT2	.486	.467	.481	.457						
ULT3	.499	.510	.516	.500						
D	152.4	152.4	254	152.4						
GAP/LAP	-.164	-.164	-.098	-.164						
C1	76.2	76.2	152.4	101.6						
C2	76.2	76.2	152.4	101.6						
E1	76.2	76.2	152.4	101.6						
E2	76.2	76.2	152.4	101.6						
A1	0	0	0	0						
A2	.7854	.7854	.7854	.7854						
E	0	0	0	0						
WS1	6.3	6.3	6.3	6.3						
WS2	6.3	6.3	6.3	6.3						
F	0	-918.4	832.6	-361.9						
ACH	3690	3690	5872	3690						
DEP	152.4	152.4	254	152.4						
EYS	207	207	207	207						
H	623.8	748.8	798	748.8						
FULT1	248.1	155.0	294	316.8						
BZ	1	1	1	1						
FPURL	0	0	0	0						
TPURL	0	0	0	0						
TR	1	2	2	2						
FAILURE MODE REPORTED	G1	G1	G1	G1						

JOINT NUMBER	Pisa 1AI	Pisa 1AT	Pisa 1BI	Pisa 1BT	Pisa 2AI	Pisa 2AT	Pisa 2BI	Pisa 2BT	Pisa 3AI	Pisa 3AT
λ_1	.76	.76	.45	.45	.55	.55	.35	.35	.75	.75
Strut Tie	OO	OO	OO	OO	OO	OO	OO	OO	OO	OO
T1	4.90	4.90	3.60	3.60	4.50	4.50	4.00	4.00	5.40	5.40
T2	6.30	6.30	5.40	5.40	6.30	6.30	5.40	5.40	6.30	6.30
T3	6.30	6.30	6.30	6.30	9.50	9.50	9.50	9.50	9.50	9.50
FY1	.354	.354	.374	.374	.329	.329	.312	.312	.368	.368
FY2	.314	.314	.357	.357	.277	.277	.377	.377	.329	.329
FY3	.346	.346	.315	.315	.300	.300	.287	.287	.314	.314
ULT1	.443	.443	.522	.522	.578	.578	.422	.422	.518	.518
ULT2	.428	.428	.497	.497	.463	.463	.499	.499	.463	.463
ULT3	.479	.479	.440	.440	.478	.478	.465	.465	.471	.471
D	254	254	254	254	254	254	254	254	152.4	152.4
GAP/LAP	-.098	-.098	-.098	-.098	-.098	-.098	-.098	-.098	-.164	-.164
C1	193.7	193.7	114.3	114.3	139.7	139.7	88.9	88.9	114.3	114.3
C2	193.7	193.7	114.3	114.3	139.7	139.7	88.9	88.9	114.3	114.3
E1	193.7	193.7	114.3	114.3	139.7	139.7	88.9	88.9	114.3	114.3
E2	193.7	193.7	114.3	114.3	139.7	139.7	88.9	88.9	114.3	114.3
A1	0	0	0	0	0	0	0	0	0	0
A2	.7854	.7854	.7854	.7854	.7854	.7854	.7854	.7854	.7854	.7854
E	0	0	0	0	0	0	0	0	0	0
WS1	6.3	6.3	6.3	6.3	6.3	6.3	6.3	6.3	6.3	6.3
WS2	6.3	6.3	6.3	6.3	6.3	6.3	6.3	6.3	6.3	6.3
F	0	-396.2	0	0	-1098.4	-804.2	-1078.8	1078.8	0	-535.5
ACH	6270	6270	6270	6270	9290	9290	9290	9290	5400	5400
DEP	254	254	254	254	254	254	254	254	152.4	152.4
EYS	207	207	207	207	207	207	207	207	207	207
H	573	798	573	798	573	561.5	573	561.5	623.8	748.8
FULT1	347.2	339	189.3	137	355	370.7	254	203	539.4	564.9
BZ	2	2	2	2	2	2	2	2	2	2
FPURL	0	0	0	0	0	0	0	0	0	0
TPURL	0	0	0	0	0	0	0	0	0	0
TR	1	2	1	2	1	2	1	2	1	2
FAILURE MODE REPORTED	G1	G1	G1	Did not fail	G1	G1	G1	Did not fail	G1	G1

JOINT NUMBER	Pisa 3BI	Pisa 3BT	Pisa 4AI	Pisa 4AT	Pisa 4BI	Pisa 4BT	Pisa 5AI	Pisa 5AT	Pisa 5BI	Pisa 5BT
λ_1	.50	.50	.76	.76	.45	.45	.70	.70	.38	.38
Strut Tie										
T1	3.20	3.20	4.90	4.90	4.50	4.50	3.20	3.20	3.20	3.20
T2	4.50	4.50	6.30	6.30	6.30	6.30	4.00	4.00	3.20	3.20
T3	9.50	9.50	9.50	9.50	9.50	9.50	4.90	4.90	4.90	4.90
FY1	.368	.368	.317	.317	.363	.363	.405	.405	.440	.440
FY2	.381	.381	.366	.366	.358	.358	.383	.383	.448	.448
FY3	.379	.379	.304	.304	.304	.304	.394	.394	.329	.329
ULT1	.514	.514	.456	.456	.505	.505	.532	.532	.572	.572
ULT2	.505	.505	.428	.428	.462	.462	.525	.525	.586	.586
ULT3	.516	.516	.471	.471	.471	.471	.539	.539	.489	.489
D	152.4	152.4	254	254	254	254	127	127	127	127
GAP/LAP	-.164	-.164	-.098	-.098	-.098	-.098	-.197	-.197	-.197	-.197
C1	76.1	76.1	193.7	193.7	114.3	114.3	88.9	88.9	48.3	48.3
C2	76.1	76.1	193.7	193.7	114.3	114.3	88.9	88.9	42.4	42.4
E1	76.1	76.1	193.7	193.7	114.3	114.3	88.9	88.9	48.3	48.3
E2	76.1	76.1	193.7	193.7	114.3	114.3	88.9	88.9	42.4	42.4
A1	0	0	0	0	0	0	0	0	0	0
A2	.7854	.7854	.7854	.7854	.7854	.7854	.7854	.7854	.7854	.7854
E	0	0	0	0	0	0	0	0	0	0
WS1	6.3	6.3	6.3	6.3	6.3	6.3	6.3	6.3	6.3	6.3
WS2	6.3	6.3	6.3	6.3	6.3	6.3	6.3	6.3	6.3	6.3
F	0	0	-843.4	1284.7	-1048.4	1618.2	0	0	0	438.4
ACH	5400	5400	9290	9290	9290	9290	2370	2370	2370	2370
DEP	152.4	152.4	254	254	254	254	127	127	127	127
EYS	207	207	207	207	207	207	207	207	207	207
H	623.8	748.8	573	798	573	798	636.5	761.5	536.5	761.5
FULT1	284.4	160.8	479.6	642.4	371.7	245.2	195,2	161.8	71.6	71.6
BZ	2	2	2	2	2	2	2	2	2	2
FPURL	0	0	0	0	0	0	0	0	0	0
TPURL	0	0	0	0	0	0	0	0	0	0
TR	1	2	1	2	1	2	1	2	1	2
FAILURE MODE REPORTED	G6	Did not fail	G1	G1	G1	G1	G1	Did not fail	G1	G1

JOINT NUMBER	Pisa 2T.T	Pisa 5QT								
λ_1	.55	.70								
Strut Tie	OO	OO								
T1	4.50	3.20								
T2	6.30	4.00								
T3	9.50	4.90								
FY1	.329	.405								
FY2	.277	.383								
FY3	.287	.326								
ULT1	.578	.533								
ULT2	.463	.525								
ULT3	.465	.508								
D	254	127								
GAP/LAP	-.098	-.197								
C1	139.7	88.9								
C2	139.7	88.9								
E1	139.7	88.9								
E2	139.7	88.9								
A1	0	0								
A2	.7854	.7854								
E	0	0								
WS1	6.3	6.3								
WS2	6.3	6.3								
F	1235	-172.6								
ACH	9290	2273								
DEP	254	127								
EYS	207	207								
H	498	761.5								
FULT1	370.7	161.8								
BZ	2	2								
FPURL	0	0								
TPURL	0	0								
TR	2	2								
FAILURE MODE REPORTED	G1	G1								

JOINT NUMBER	Delft 92	Delft 93	Delft 94	Delft 97	Delft 98	Delft 99	Delft 102	Delft 102'	Delft 103	Delft 106
λ_1	.63	.62	.63	.39	.40	.38	.63	.61	.39	.41
Strut Tie										
T1	4.25	3.00	4.00	4.10	2.06	3.96	4.00	3.00	4.03	4.10
T2	4.03	3.00	4.00	4.10	1.95	3.96	4.00	3.00	4.03	4.10
T3	3.74	2.94	3.74	3.74	3.35	3.74	3.72	2.95	3.72	3.72
FY1	.321	.262	.350	.342	.240	.325	.275	.262	.330	.325
FY2	.272	.262	.350	.342	.230	.325	.275	.262	.330	.325
FY3	.321	.325	.321	.321	.292	.321	.319	.300	.319	.319
ULT1	.495	.414	.470	.477	.368	.505	.470	.414	.452	.495
ULT2	.452	.414	.470	.477	.262	.505	.470	.414	.452	.495
ULT3	.453	.471	.453	.453	.372	.453	.447	.435	.447	.447
D	99.8	97.1	99.8	99.8	100.2	99.8	99.7	97.4	99.7	99.7
GAP/LAP	.499	.496	.599	.496	.494	.599	.261	.261	.315	.261
C1	62.7	60.0	62.8	38.7	40.3	37.7	62.9	59.8	62.7	38.7
C2	63.3	60.0	62.8	38.7	40.0	37.7	62.9	49.8	62.7	38.7
E1	62.7	60.0	62.8	38.7	40.3	37.7	62.9	59.8	62.7	38.7
E2	63.3	60.0	62.8	38.7	40.0	37.7	62.9	59.8	62.7	38.7
A1	.7854	.7854	0	.7854	.7854	0	.7854	.7854	0	.7854
A2	.7854	.7854	.7854	.7854	.7854	.7854	.7854	.7854	.7854	.7854
E	0	0	0	0	0	0	0	0	0	0
WS1	6.01	4.24	5.66	5.80	2.91	5.60	5.66	4.24	5.7	5.8
WS2	5.70	4.24	5.66	5.80	2.76	5.60	5.66	4.24	5.7	5.8
F	0	0	0	0	0	0	0	0	0	0
ACH	1420	1100	1420	1420	1260	1420	1420	1110	1420	1420
DEP	99.8	97.1	99.8	99.8	100.2	99.8	99.7	97.4	99.7	99.7
EYS	207	207	207	207	207	207	207	207	207	207
H	317.7	320.0	350.0	330.7	329.9	350	318.8	320.1	350	330.7
FULT1	208.5	115	243.3	184	67.5	131.4	192.5	95	223	198
BZ	1	1	1	1	1	1	1	1	1	1
FPURL	0	0	0	0	0	0	0	0	0	0
TPURL	0	0	0	0	0	0	0	0	0	0
TR	1	1	1	1	1	1	1	1	1	1
FAILURE MODE REPORTED	L7	L7	Yield in tie	Yield in strut	L4	L4	L7	L7	Yield in tie	L4

JOINT NUMBER	Delft 106'	Delft 91'	Delft 91"	Delft 101'	Pisa 6CI	Pisa 6CT	Pisa 6XI	Pisa 6XT	Pisa 7CI	Pisa 7CT 7XT
λ_1	.41	1.00	.96	1.00	.60	.60	.60	.60	.67	.67
Strut Tie										
T1	2.06	3.84	2.98	3.84	5.10	5.10	5.10	5.10	4.20	4.20
T2	1.95	3.84	2.98	3.84	9.40	9.40	9.40	9.40	6.20	6.20
T3	2.95	3.84	3.00	3.96	6.20	6.20	6.00	6.00	5.90	5.90
FY1	.240	.335	.231	.335	.292	.292	.292	.296	.339	.339
FY2	.230	.335	.231	.335	.362	.362	.362	.362	.311	.311
FY3	.300	.335	.224	.334	.363	.363	.387	.387	.395	.395
ULT1	.368	.480	.339	.480	.473	.473	.473	.473	.513	.513
ULT2	.362	.480	.339	.480	.496	.496	.496	.496	.463	.463
ULT3	.436	.480	.344	.478	.483	.483	.483	.486	.508	.508
D	97.4	99.4	100.6	99.4	254.0	254.0	254.0	254.0	152.4	152.4
GAP/LAP	.260	.496	.496	.261	.334	.334	.334	.334	.434	.434
C1	40.3	99.4	97.0	99.4	152.4	152.4	152.4	152.4	101.6	101.6
C2	40.0	99.4	97.0	99.4	152.4	152.4	152.4	152.4	101.6	101.6
E1	40.3	99.4	97.0	99.4	152.4	152.4	152.4	152.4	101.6	101.6
E2	40.0	99.4	97.0	99.4	152.4	152.4	152.4	152.4	101.6	101.6
A1	.7854	.7854	.7854	.7854	0	0	0	0	0	0
A2	.7854	.7854	.7854	.7854	.7854	.7854	.7854	.7854	.7854	.7854
E	0	0	0	0	0	0	0	0	0	0
WS1	2.91	5.43	4.21	5.43	6.3	6.3	6.3	6.3	6.3	6.3
WS2	2.76	5.43	4.21	5.43	6.3	6.3	6.3	6.3	6.3	6.3
F	0	0	0	0	-200.0	-200.0	-225	+225	-598	+598
ACH	1110	1440	1120	1430	6270	6270	6270	6270	3690	3690
DEP	97.4	99.4	100.6	99.4	254.0	254.0	254.0	254.0	152.4	152.4
EYS	207	207	207	207	207	207	207	207	207	207
H	329.9	300.3	301.5	300.3	573	798	573	798	623.8	748.8
FULT1	78	289	149	300	473.7	519.8	529.6	519.8	389.3	372
BZ	1	1	1	1	1	1	1	1	1	1
FPURL	0	0	0	0	0	0	0	0	0	0
TPURL	0	0	0	0	0	0	0	0	0	0
TR	1	1	1	1	1	2	1	2	1	2
FAILURE MODE REPORTED	L6	L7	L7	L7	L6	Did not fail	L6	L6	L6	Did not fail

JOINT NUMBER	Pisa 7XI	Pisa 8CI	Pisa 8CT	Pisa 8DI	Pisa 8DT	Pisa 6CCT				
λ_1	.67	.58	.58	.50	.50	.60				
Strut Tie										
T1	4.20	3.80	3.80	3.60	3.60	4.90				
T2	6.20	6.00	6.00	3.80	3.80	9.50				
T3	5.90	6.40	6.40	6.40	6.40	6.30				
FY1	.339	.289	.333	.491	.491	.296				
FY2	.311	.344	.344	.322	.312	.362				
FY3	.395	.384	.384	.384	.408	.387				
ULT1	.513	.481	.496	.652	.652	.473				
ULT2	.463	.530	.530	.485	.467	.496				
ULT3	.508	.496	.496	.496	.510	.486				
D	152.4	152.4	152.4	152.4	152.4	254				
GAP/LAP	.434	.319	.319	.142	.142	0				
C1	101.6	88.9	88.9	76.2	76.2	152.4				
C2	101.6	88.9	88.9	76.2	76.2	152.4				
E1	101.6	88.9	88.9	76.2	76.2	152.4				
E2	101.6	88.9	88.9	76.2	76.2	152.4				
A1	0	0	0	0	0	0				
A2	.7854	.7854	.7854	.7854	.7854	.7854				
E	0	0	0	0	0	0				
WS1	6.3	6.3	6.3	6.3	6.3	6.3				
WS2	6.3	6.3	6.3	6.3	6.3	6.3				
F	0	-541	-541	-922	-922	0				
ACH	3690	3690	3690	3690	3690	6270				
DEP	152.4	152.4	152.4	152.4	152.4	254				
EYS	207	207	207	207	207	207				
H	623.8	623.8	748.8	623.8	748.8	798				
FULT1	460.9	331.5	279.5	226.5	181	519.8				
BZ	1	1	1	1	1	1				
FPURL	0	0	0	0	0	0				
TPURL	0	0	0	0	0	0				
TR	1	1	2	1	2	2				
FAILURE MODE REPORTED	L6	L6	Did not fail	L7	-	-				

JOINT NUMBER	Pisa 1CI	Pisa 1CT	Pisa 1XI	Pisa 1XT	Pisa 2CI	Pisa 2CT 2XT	Pisa 2XI	Pisa 3CI	Pisa 3CT	Pisa 3DI
λ_1	.76	.76	.76	.76	.55	.55	.55	.75	.75	.50
Strut Tie										
T1	4.90	4.90	4.90	4.90	4.50	4.50	4.50	5.40	5.40	3.20
T2	6.30	6.30	6.30	6.30	6.30	6.30	6.30	6.30	6.30	4.50
T3	6.30	6.30	6.30	6.30	9.50	9.50	9.50	9.50	9.50	9.50
FY1	.344	.344	.354	.354	.329	.343	.329	.368	.368	.368
FY2	.314	.314	.314	.314	.360	.277	.360	.329	.329	.346
FY3	.377	.377	.325	.325	.303	.303	.289	.389	.389	.389
ULT1	.454	.454	.443	.443	.578	.525	.578	.518	.518	.514
ULT2	.428	.428	.428	.428	.522	.463	.522	.463	.463	.502
ULT3	.483	.483	.452	.452	.481	.481	.485	.527	.527	.527
D	254	254	254	254	254	254	254	152.4	152.4	152.4
GAP/LAP	0	0	0	0	0	0	0	0	0	0
C1	193.7	193.7	193.7	193.7	139.7	139.7	139.7	114.3	114.3	76.1
C2	193.7	193.7	193.7	193.7	139.7	139.7	139.7	114.3	114.3	76.1
E1	193.7	193.7	193.7	193.7	139.7	139.7	139.7	114.3	114.3	76.1
E2	193.7	193.7	193.7	193.7	139.7	139.7	139.7	114.3	114.3	76.1
A1	0	0	0	0	0	0	0	0	0	0
A2	.7854	.7854	.7854	.7854	.7854	.7854	.7854	.7854	.7854	.7854
E	0	0	0	0	0	0	0	0	0	0
WS1	6.3	6.3	6.3	6.3	6.3	6.3	6.3	6.3	6.3	6.3
WS2	6.3	6.3	6.3	6.3	6.3	6.3	6.3	6.3	6.3	6.3
F	-743.4	-743.4	0	0	-1098.4	-1098.4	-1098.4	-1027.8	1027.8	0
ACH	6270	6270	6270	6270	9290	9290	9290	5400	5400	5400
DEP	254	254	254	254	254	254	254	152.4	152.4	152.4
EYS	207	207	207	207	207	207	207	207	207	207
H	573	798	573	798	573	561.5	573	623.8	748.8	623.8
FULT1	539.4	0	644.3	0	573.7	397.2	519.8	529.6	504.1	262.8
BZ	2	2	2	2	2	2	2	2	2	2
FPURL	0	0	0	0	0	0	0	0	0	0
TPURL	0	0	0	0	0	0	0	0	0	0
TR	1	2	1	2	1	2	1	1	2	1
FAILURE MODE REPORTED	L6 L7	Did not fail	L6	Did not fail	L6	Did not fail	L6	L6	Did not fail	Strut lateral failure

JOINT NUMBER	Pisa 3DT	Pisa 4CI	Pisa 4CT 4XT	Pisa 4XI	Pisa 5CI	Pisa 5CT	Pisa 5XI	Pisa 5XT		
λ_1	.50	.76	.76	.76	.70	.70	.70	.70		
Strut Tie										
T1	3.20	4.90	4.90	4.90	3.20	3.20	3.20	3.20		
T2	4.50	6.30	6.30	6.30	4.00	4.00	4.00	4.00		
T3	9.50	9.50	9.50	9.50	4.90	4.90	4.90	4.90		
FY1	.368	.317	.317	.317	.377	.377	.377	.377		
FY2	.346	.366	.366	.366	.368	.368	.312	.368		
FY3	.389	.322	.322	.322	.329	.329	.329	.326		
ULT1	.514	.456	.456	.456	.502	.502	.502	.502		
ULT2	.502	.428	.428	.428	.518	.518	.422	.518		
ULT3	.527	.478	.478	.478	.508	.508	.508	.508		
D	152.4	254	254	254	127	127	127	127		
GAP/LAP	0	0	0	0	0	0	0	0		
C1	76.1	193.7	193.7	193.7	88.9	88.9	88.9	88.9		
C2	76.1	193.7	193.7	193.7	88.9	88.9	88.9	88.9		
E1	76.1	193.7	193.7	193.7	88.9	88.9	88.9	88.9		
E2	76.1	193.7	193.7	193.7	88.9	88.9	88.9	88.9		
A1	0	0	0	0	0	0	0	0		
A2	.7854	.7854	.7854	.7854	.7854	.7854	.7854	.7854		
E	0	0	0	0	0	0	0	0		
WS1	6.3	6.3	6.3	6.3	6.3	6.3	6.3	6.3		
WS2	6.3	6.3	6.3	6.3	6.3	6.3	6.3	6.3		
F	0	-998.4	-998.4	-1000.3	0	0	0	0		
ACH	5400	9290	9290	9290	2370	2370	2370	2370		
DEP	152.4	254	254	254	127	127	127	127		
EYS	207	207	207	207	207	207	207	207		
H	748.8	573	798	573	636.5	761.5	636.5	761.5		
FULT1	166.7	640.4	647.3	699.2	275.6	232.4	261.8	232.4		
BZ	2	2	2	2	2	2	2	2		
FPURL	0	0	0	0	0	0	0	0		
TTURL	0	0	0	0	0	0	0	0		
TR	2	1	2	1	1	2	1	2		
FAILURE MODE REPORTED	Did not fail	L6	Did not fail	L6	L6	Did not fail	L6	Did not fail		

APPENDIX 2

COMPUTER PROGRAM FOR RHS CHORD JOINT ANALYSIS

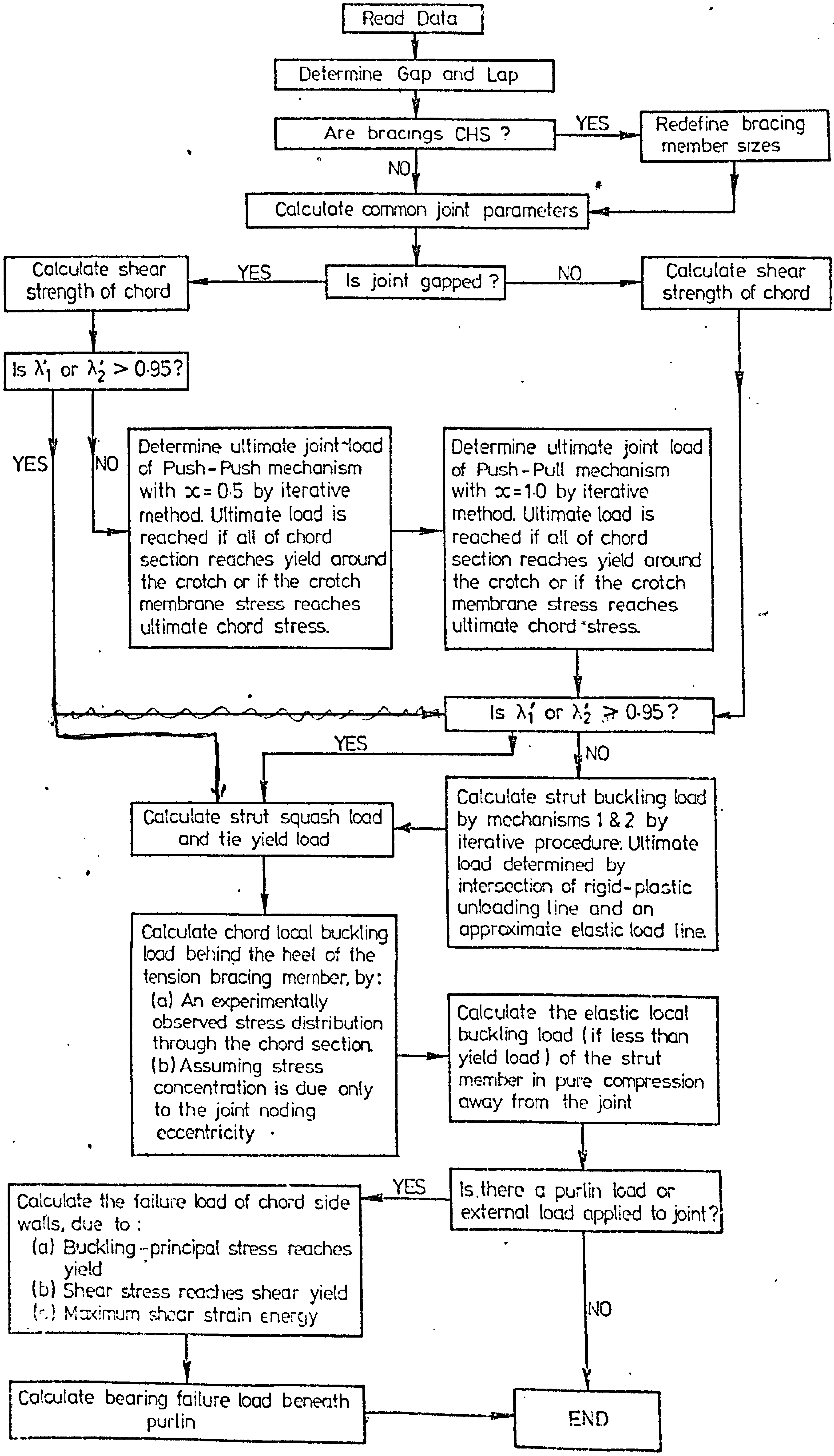

Appendix 2·1 Flow diagram for computer program analysis of a joint between CHS or RHS bracing members and RHS chord

JOINT:			
	30 Joint Parameters in this order	Symbol	Units
1.	Thickness of compression bracing member	T1	mm
2.	Thickness of tension bracing member	T2	mm
3.	Thickness of chord member	T3	mm
4.	Yield stress of the compression bracing member	FY1	kN/mm^2
5.	Yield stress of the tension bracing member	FY2	kN/mm^2
6.	Yield stress of the chord member	FY3	kN/mm^2
7.	Ultimate stress of the compression bracing member	ULT1	kN/mm^2
8.	Ultimate stress of the tension bracing member	ULT2	kN/mm^2
9.	Ultimate stress of the chord member	ULT3	kN/mm^2
10.	Width of chord member (90° to plane of truss)	D	mm
11.	For a gapped joint: Nominal gap (neglecting welds) between bracings divided by the width of the chord member, and expressed as a <u>negative</u> number. Insert 0.0 if gap is not known but joint eccentricity is known.	GAP	None
	For a lapped joint: Express the lap as a decimal fraction (<u>positive</u> number) by CIDECT definition of the lapped length of bracings, measured along the chord face, divided by the strut depth measured along the chord face. Insert 0.0 if lap is not known but eccentricity is known.	LAP	None
12.	Width of compression bracing (90° to plane of truss)	C1	mm
13.	Width of tension bracing (90° to plane of truss)	C2	mm
14.	Depth of compression bracing (in plane of truss)	E1	mm
15.	Depth of tension bracing (in plane of truss)	E2	mm
16.	Angle of the compression bracing to the VERTICAL	A1	radians
17.	Angle of the tension bracing to the VERTICAL	A2	radians
18.	Eccentricity of Noding - positive is towards the outside of the girder - insert 0.0 if gap or lap was given in item 11.	E	mm
19.	Nominal weld LEG LENGTH on compression bracing *	WS1	mm
20.	Nominal weld LEG LENGTH on tension bracing*	WS2	mm
21.	Axial load (preload) in chord <u>in addition to</u> the horizontal reaction from bracings - tension is positive and compression negative.	F	kN
22.	Cross - sectional area of chord member	ACH	mm^2
23.	Depth of chord member (in plane of truss)	DEP	mm
24.	Modulus of elasticity**	EYS	kN/mm^2
25.	The length of the strut member, measured along its centre-line, from the chord face. In the case of a truss the length is half the centre-line distance between the inside faces of the two chord members.	H	mm
26.	Ultimate (or maximum if the joint did not fail) load in the compression bracing member. Insert 0 if this is not known	FULT1	kN
27.	Insert 1 if bracings are RHS, or 2 if bracings are CHS.	BZ	None
28.	Compression load applied by purlin cleat at the joint	FPURL	kN
29.	Width of purlin bearing (including welds to the chord), measured along the length of the chord member	TPURL	mm
30.	Insert 2 for a joint with chord member continuous on either side, or 1 for chord member continued on one side only.	TR	None

* Weld leg length can be assumed to be $\sqrt{2}$ x thickness of the bracing member connected, unless otherwise specified.

** British Standards recommend a value of 206 kN/mm^2 (8), and the ECCS (34) recommend a value of 210 kN/mm^2.

<u>Appendix 2.2</u> Data required for computer program input

Appendix 2.3 Listing of computer program

```
      MASTER VERSION
      REAL MH,JK1,JK2,NUM,L1,L,LAP,LTOT,L2,N1,N2,LM,MP,J,K,MSTR,LB,L3
C***************************************************************************
C
C
C     YIELD AND ULTIMATE LOAD ANALYSIS FOR GAP AND LAP RHS CHORD JOINTS
C                            WITH PURLIN LOADING
C
C                            BY :  J.A.PACKER
C
C                          OCTOBER 1978
C
C
C***************************************************************************
C     T1=THICKNESS OF COMP. MEM.,T2 OF TENS. MEM.,T3 OF CHORD MEM.
C     A1=ANGLE(RADIANS) OF COMP. MEMBER TO VERTICAL
C     A2=ANGLE(RADIANS) OF TENS. MEMBER TO VERTICAL
C     FY1=YIELD STRESS OF COMP. MEM.,FY2 OF TENS. MEM.,FY3 OF CHORD MEM.
C     ULT1,ULT2,ULT3=ULTIMATE TENSILE STRESS OF STRUT,TIE AND CHORD RESPECTIVELY
C     G*D=Z2=ACTUAL WELD GAP , D=WIDTH OF CHORD MEMBER , DEP=DEPTH OF CHORD.
C     C1=WIDTH OF COMP. MEM.,C2=WIDTH OF TENS. MEM.
C     E1=DEPTH OF COMP. MEM.,E2=DEPTH OF TENS. MEM.
C     LENGTH OF WELD LEG ON COMP. MEMBER = WS1
C     LENGTH OF WELD LEG ON TENS. MEMBER = WS2
C     EYS=YOUNG'S MODULUS OF ELASTICITY
C     F=CHORD AXIAL TENSION PRELOAD . FP=CHORD SQUASH LOAD . ACH=AREA OF CHORD .
C     LAP IS DEFINED BY BSC TERMINOLOGY: OVERLAPPED LENGTH/DEPTH OF STRUT PROJ.
C     ONTO CHORD FACE.IF JOINT IS LAPPED,THEN 'GAP' IS ACTUALLY THE LAP VALUE
C     BUT WRITTEN POSITIVE INSTEAD OF NEGATIVE.
C     E=NODING ECCENTRICITY IN MM. WITH POSITIVE BEING TOWARDS THE OUTSIDE OF
C     THE GIRDER.
C     H=THE LENGTH(IN MM.) OF THE STRUT MEMBER,MEASURED ALONG ITS CENTRE-LINE,
C     FROM THE CHORD  FACE. IN THE CASE OF A TRUSS THE LENGTH IS HALF THE CENTRE
C     -LINE DISTANCE BETWEEN THE INSIDE FACES OF THE TWO CHORD MEMBERS.
C     BZ=1 FOR RHS,=2 FOR CHS BRACINGS.
C     FULT1=ULTIMATE LOAD IN STRUT
C     FPURL=VERTICAL PURLIN LOADING, AND TPURL=THICKNESS OF PURLIN LOAD AREA.
C     TR=2 FOR A JOINT WITH CHORD MEMBER CONTINUOUS ON EITHER SIDE.
C     TR=1 FOR CHORD MEMBER CONTINUED ON ONE SIDE ONLY.
C***************************************************************************
      WRITE(6,17)
   17 FORMAT(1H7,1X,'ALL VALUES OF LOADS (P) ARE THE VERTICAL COMPONENTS
     1 OF THE BRACING MEMBER FORCES.')
      WRITE(6,18)
   18 FORMAT(2X,'IF PURLIN LOAD ACTS ON JOINT THEN THE LOADS (P) GIVEN A
     1RE FOR THE VERTICAL COMPONENT OF THE STRUT MEMBER')
      WRITE(6,51)
      DO 10 I=1,500
      READ(5,180)T1,T2,T3,FY1,FY2,FY3,ULT1,ULT2,ULT3,D,GAP,C1,C2,E1,E2,
     1A1,A2,E,WS1,WS2,F,ACH,DEP,EYS,H,FULT1,BZ,FPURL,TPURL,TR
  180 FORMAT(30F0.0)
      IF(T1.LE.0.01)STOP
      IF(GAP.LT.0.0)LAP=0.0
      IF(GAP.GT.0.0)LAP=GAP
      IF(GAP.LT.0.0)GAP=ABS(GAP)
      IF(GAP.EQ.0.0)CALL ECC(E,D,A1,A2,E1,E2,GAP,LAP)
      IF(BZ.EQ.1.0)GO TO 19
      C1=0.7854*C1
      E1=C1
      C2=0.7854*C2
      E2=C2
C     IF BRACING MEMBERS ARE CHS THEN DIAMETER IS MADE INTO A SQUARE H.S. WITH
C     SIDES EQUAL TO 0.7854*DIAMETER.
   19 D=D-T3
C     FOR CALCULATIONS HINGES ARE IN THE MIDDLE OF THE CHORD WALLS.
      Z1=GAP*(D+T3)
      Z8=GAP*(D+T3)
      Z2=Z1-WS1
      IF(A1.GT.0.5)Z2=Z1
      G=Z2/D
      FX=ABS(F)
      FP=ACH*FY3
      RATIO=F/FP
      CON1=1.0-(F/FP)**2
      L1=(C1+2.0*WS1)/D
      ZQ=(C1+2.0*WS1)/(D+T3)
      IF(ZQ.GT.1.00)ZQ=1.00
      L2=(C2+2.0*WS2)/D
      N1=(2*WS1+E1/COS(A1))/D
      IF(A1.GT.0.5)N1=(WS1+E1/COS(A1))/D
      N2=(WS2+E2/COS(A2))/D
      WRITE(6,15)I,ZQ,RATIO
   15 FORMAT(2X,'JOINT NUMBER=',I3,10X,'L1(INCL. WELDS)=',F4.2,5X,
     1'F/FP=',F5.2)
      IF(LAP.EQ.0.0)GO TO 20
      CALL SHEARLAP(LAP,E1,A1,A2,T1,T2,T3,FY1,FY2,FY3,DEP,CON1,FPURL)
      GO TO 22
   20 CALL SHEARGAP(DEP,T3,FY3,CON1,FPURL)
```

```
      IF(L1.GT.0.95.OR.L2.GT.0.95)GO TO 22
      CALL PP05(L1,L2,D,FY3,T3,G,CON1,EYS,F,ULT3,FX,FP,Z2,N1,N2,PY5,PU5,
     1PSHF1,PCHB,PSBK,FPURL,A1,A2,DEP,WS1,E1,C1,C2)
C     IF PURLIN LOAD ACTS ON A GAP JOINT AND THE GAP IS 'RELATIVELY SMALL', THE
C     PP10 MECHANISM IS MORE LIKELY TO OCCUR THAN THE PP05 MECHANISM.
   44 CALL PP10(L1,L2,D,FY3,T3,G,CON1,EYS,F,ULT3,FX,FP,Z2,N1,N2,PY10,
     1PU10,PSHF1,PCHB,PSBK,FPURL,A1,A2,DEP,WS1,E1,C1,C2)
   22 CALL BUCKLE3(T1,T2,T3,FY1,FY2,FY3,D,LAP,C1,C2,E1,E2,A1,A2,L1,CON1,
     1ACH,FYS,H,GAP,Z1,PSQASH,PYEELD,PBUCK3,PBUCK4,L2,FPURL)
   26 CALL CHORD(L1,A1,A2,F,ACH,EYS,T3,D,FY3,PCHB,FPURL,E1,E2,Z8,GAP,
     1LAP,DEP,TR)
      CALL STRUT(C1,E1,EYS,T1,FY1,A1,PSBK)
      CALL PURLIN(D,F,ACH,FPURL,TPURL,T3,FY3,DEP,E1,N1,LAP,A1,A2,T1)
      CALL PURLIN2(FY3,F,ACH,T3,D,TPURL,FPURL)
   10 WRITE(6,51)
   51 FORMAT(2X,'*******************************************************
     1***************************************************************')
      STOP
      END
      SUBROUTINE SHEARLAP(LAP,E1,A1,A2,T1,T2,T3,FY1,FY2,FY3,DEP,CON1,
     1FPURL)
      REAL LAP,L
      IF(FPURL.NE.0.0)GO TO 20
      L=E1*LAP/COS(A1)
      CUV=2.0*L*COS(A1)*COS(A2)/SIN(A1+A2)
      CTV=2.0*(DEP+T3)*T3*FY3*SQRT(CON1)/SQRT(3.0)
      PSH1=(CUV+2.0*T1)*T1*FY1/SQRT(3.0)+CTV
      PSH2=(CUV+2.0*T2)*T2*FY2/SQRT(3.0)+CTV
      PSHLAP=AMIN1(PSH1,PSH2)
      WRITE(6,10)PSHLAP
   10 FORMAT(/,2X,'JOINT IS LAPPED - CHORD SHEAR(ULTIMATE) OCCURS AT P='
     1,F8.2,' KNS.')
   20 RETURN
      END
      SUBROUTINE SHEARGAP(DEP,T3,FY3,CON1,FPURL)
      IF(FPURL.NE.0.0)GO TO 20
      PSHF1=2*DEP*T3*FY3*SQRT(CON1)/SQRT(3.0)
      PSHF2=2*(DEP+2.0*T3)*FY3*SQRT(CON1)*T3/SQRT(3.0)
      WRITE(6,10)PSHF1,PSHF2
   10 FORMAT(/,2X,'JOINT IS GAPPED - CHORD SHEAR YIELD OCCURS AT P=',
     1F8.2,' KNS. AND ULTIMATE AT P=',F8.2,' KNS.')
   20 RETURN
      END
      SUBROUTINE STRUT(C1,E1,EYS,T1,FY1,A1,PSBK)
C     SUBROUTINE STRUT CALCULATES THE MINIMUM LOCAL BUCKLING LOAD OF ANY FACE
C     FOR RHS BY MODE 1,EFFECTIVE STRUT WIDTH=(C1-T1)OR(E1-T1). PMAX IS THE
C     LOCAL BUCKLING LOAD FOR ALL OF STRUT.
      PCRIT=3.55*EYS*T1**3/(C1-T1)
      PYSTR=(C1-T1)*T1*FY1
      IF(PYSTR.LE.PCRIT)GO TO 620
      CZ=(0.36*PYSTR*PCRIT+0.83*PCRIT**2)*0.76
      PMAX=(SQRT(CZ+PCRIT**2)-PCRIT)/0.38
      PMAX=(PMAX*2.0*((C1-T1)+(E1-T1)))/(C1-T1)
      GO TO 621
  620 PMAX=((C1-T1)*2.0+(E1-T1)*2.0)*T1*FY1
  621 PSTR1=PMAX*COS(A1)
      PCRIT=3.55*EYS*T1**3/(E1-T1)
      PYSTR=(E1-T1)*T1*FY1
      IF(PYSTR.LE.PCRIT)GO TO 654
      CZ=(0.36*PYSTR*PCRIT+0.83*PCRIT**2)*0.76
      PMAX=(SQRT(CZ+PCRIT**2)-PCRIT)/0.38
      PMAX=(PMAX*2.0*((C1-T1)+(E1-T1)))/(E1-T1)
      GO TO 655
  654 PMAX=((C1-T1)*2.0+(E1-T1)*2.0)*T1*FY1
  655 PSTR2=PMAX*COS(A1)
      PSBK=AMIN1(PSTR1,PSTR2)
      WRITE(6,932)PSBK
  932 FORMAT(/,2X,'STRUT LOCAL BUCKLING DUE TO AXIAL LOAD ONLY OCCURS AT
     1 P=',F8.2,' KNS.')
      RETURN
      END
      SUBROUTINE PP05(L1,L2,D,FY3,T3,G,CON1,EYS,F,ULT3,FX,FP,Z2,N1,N2,
     1PY5,PU5,PSHF1,PCHB,PSBK,FPURL,A1,A2,DEP,WS1,E1,C1,C2)
      REAL L1,L2,N1,N2,LM,MP,J,K,MSTR,L3
C     SUBROUTINE PP05 CALCULATES THE LOAD/DEFLECTION BEHAVIOR OF THE CHORD TOP
C     FACE SUBJECT TO BRANCH MEMBER FORCES,USING AN INCREMENTAL DEFLECTION
C     ANALYSIS. RIGID-PLASTIC BEHAVIOUR IS ASSUMED AND MEMBRANE ACTION TAKES
C     PLACE IN THE CROTCH ONLY. THE DISTANCES K AND J ARE CONSTANT AT THE
C     VALUES OF THE SMALL DEFLECTION ANALYSIS. X IS ALSO SET AT 0.5
C     STRAIN HARDENING MODULUS FOR CROTCH IS EYS/300
C     ULTIMATE LOAD IS REACHED BY ULTIMATE STRESS IN CROTCH OR THE
C     WHOLE CHORD CROSS-SECTION REACHING PLASTICITY AT THE CROTCH.
C***************************************************************************
      K=D*SQRT(1-L1)*0.5
      J=D*SQRT(1-L2)*0.5
      IF((J+K).LT.Z2)WRITE(6,50)
   50 FORMAT(/,2X,'CLEAR WELD GAP IS LARGE ENOUGH FOR SEPARATE T-JOINT A
```

```
     1CTION')
      LM=SQRT((D*(1-L1)/2.0)**2+K**2)
      EF=SQRT((G*D/2.0)**2+(D*(1-L1)/2.0)**2)
      QR=SQRT((D*(1-L2)/2.0)**2+J**2)
      FG=SQRT((G*D/2.0)**2+(D*(1-L2)/2.0)**2)
      CO21=1.0-(FX/FP)*(FX/FP)*(0.5*D*(1-L1)/LM)**4
      CO22=1.0-(FX/FP)*(FX/FP)*(0.5*D*(1-L2)/QR)**4
      CO31=1.0-(FX/FP)*(FX/FP)*(0.5*D*(1-L1)/EF)**4
      CO32=1.0-(FX/FP)*(FX/FP)*(0.5*D*(1-L2)/FG)**4
      MP=(FY3*T3**2)/4.0
      PY5=0.0
      ZZA=0.0
      DEFM=0.01*(D+T3)
      TH=0.0
      DEL=0.0
      DTH=ATAN(0.0001*(D+T3)/Z2)
      IF(DTH.LT.0.0005)DTH=0.0005
      DO 100 N=1,2000
      ARG1=G*TAN(TH+DTH)/(1-L1)
      ARG2=G*TAN(TH+DTH)/(1-L2)
      IF(ARG1.LT.1.0.AND.ARG2.LT.1.0)GO TO 500
      WRITE(6,54)
   54 FORMAT(/,2X,'FOR P/P MODEL WITH X=0.5,THERE IS NO MATH. SOLUTION')
      WRITE(6,55)TH,DEL
   55 FORMAT(2X,'AND MAX. ROTATION IS REACHED AT THETA=',F6.2,
     1'  RADIANS, AND DELTA=',F8.2,' MM.')
      GO TO 543
  500 DL=G*D/COS(TH+DTH)-G*D/COS(TH)
      DDEL=(G*D/2.0)*(TAN(TH+DTH)-TAN(TH))
      DFH1=ATAN(G*D*TAN(TH+DTH)/(2.0*K))-ATAN(G*D*TAN(TH)/(2.0*K))
      DFH2=ATAN(G*D*TAN(TH+DTH)/(2.0*J))-ATAN(G*D*TAN(TH)/(2.0*J))
      DGA1=ASIN(ARG1)-ASIN(G*TAN(TH)/(1-L1))
      DGA2=ASIN(ARG2)-ASIN(G*TAN(TH)/(1-L2))
      DBETA=(G*TAN(TH+DTH)*K)/((1-L1)*LM)
      DBETB=(G*TAN(TH+DTH)*J)/((1-L2)*QR)
      DBET1=ASIN(DBETA)
      DBET5=ASIN(DBETB)
      DBET2=ASIN(G*TAN(TH)*K/((1-L1)*LM))
      DBET6=ASIN(G*TAN(TH)*J/((1-L2)*QR))
      DBET3=ATAN((G*D*TAN(TH+DTH)*D*(1-L1))/(4.0*K*LM))
      DBET7=ATAN((G*D*TAN(TH+DTH)*D*(1-L2))/(4.0*J*QR))
      DBET4=ATAN(G*D*TAN(TH)*D*(1-L1)/(4.0*K*LM))
      DBET8=ATAN(G*D*TAN(TH)*D*(1-L2)/(4.0*J*QR))
      DBE1=DBET1-DBET2+DBET3-DBET4
      DBE2=DBET5-DBET6+DBET7-DBET8
      DALF1=ASIN((G*TAN(TH+DTH)*G*D)/(2.0*EF*(1-L1)))
      DALF5=ASIN((G*TAN(TH+DTH)*G*D)/(2.0*FG*(1-L2)))
      DALF2=ASIN((G*TAN(TH)*G*D)/(2.0*EF*(1-L1)))
      DALF6=ASIN((G*TAN(TH)*G*D)/(2.0*FG*(1-L2)))
      DALF3=ATAN(TAN(TH+DTH)*D*(1-L1)/(2.0*EF))
      DALF7=ATAN(TAN(TH+DTH)*D*(1-L2)/(2.0*FG))
      DALF4=ATAN(TAN(TH)*D*(1-L1)/(2.0*EF))
      DALF8=ATAN(TAN(TH)*D*(1-L2)/(2.0*FG))
      DAL1=DALF1-DALF2+DALF3-DALF4
      DAL2=DALF5-DALF6+DALF7-DALF8
      P1=((1+L1)*D*MP*DFH1*CON1+(1+L2)*D*MP*DFH2*CON1)/(2.0*DDEL)
      EY=FY3/EYS
      L3=(C1+C2)/(D*2.0)
      SP=L3*D*T3*FY3
      S=EYS*L3*D*T3*((1.0/COS(TH))-1.0)
      SZ=L3*D*T3*(1.0/COS(TH)-1.0-EY)*EYS/300.0
      IF((1.0/COS(TH)-1.0).GT.EY)S=SP+SZ
      P2=L1*D*MP*(1.0-(S/SP)**2)*DTH/DDEL
      P8=L2*D*MP*(1.0-(S/SP)**2)*DTH/DDEL
      P2=(P2+P8)/2.0
      IF(S.GT.SP)P2=0.0
      P3=D*MP*DGA1*(4.0*N1+G+2.0*K/D)
      P9=D*MP*DGA2*(4.0*N2+G+2.0*J/D)
      P3=(P3+P9)/(DDEL*2.0)
      P4=2.0*LM*MP*DBE1*CO21
      P10=2.0*QR*MP*DBE2*CO22
      P4=(P4+P10)/(DDEL*2.0)
      P5=2.0*EF*MP*DAL1*CO31
      P11=2.0*FG*MP*DAL2*CO32
      P5=(P5+P11)/(DDEL*2.0)
      P6=(S*DL)/(2.0*DDEL)
      P7=0.0
      P=P1+P2+P3+P4+P5+P6+P7+FPURL/2.0
   10 IF(N.GT.1)GO TO 42
      PY5=P
   42 IF(ZZA.NE.0.0)GO TO 99
      IF(P.LT.PY5)P=PY5
      IF(DEL.GT.DEFM)WRITE(6,72)P
   72 FORMAT(/,2X,'LIMIT OF 1 PER CENT OF CHORD WIDTH FOR DEFORMATION EX
     1CEEDED AT P=',F8.2,' KNS.')
      IF(DEL.GT.DEFM)ZZA=1.0
C*****************************************************************************
```

```
 99 MSTR=1000.0*S/(L3*D*T3)
    CALL SIDEWALL2(FY3,ULT3,D,T3,DEP,A1,WS1,Z2,TH,MSTR,F,E1,
   1L1,L2,PALLOW,C1,C2,P)
    ULT4=ULT3*1000.0
 98 DEL=DEL+DDEL
    THMAX=TH
    TH=TH+DTH
    IF(P.LT.PY5)P=PY5
    PU5=P
    IF(MSTR.GE.ULT4)GO TO 544
    IF(PALLOW.LT.PU5)GO TO 517
100 CONTINUE
544 WRITE(6,515)PY5,PU5,THMAX
515 FORMAT(/,2X,'FOR P/P MODEL WITH X=0.5,YIELD LOAD(P)=',F8.2,
   1' KNS. AND ULTIMATE LOAD(P)=',F8.2,' KNS & THETA =',F5.3)
    WRITE(6,516)P6,PALLOW
516 FORMAT(/,2X,'P6=',F8.2,' KNS. & P-ALLOWANCE FOR HORIZ. COMPS.=',
   1F8.2,' KNS.')
    GO TO 543
517 IF(PALLOW.LT.PY5)PALLOW=PY5
    WRITE(6,518)PY5,PALLOW
518 FORMAT(/,2X,'FOR P/P MODEL WITH X=0.5,YIELD LOAD(P)=',F8.2,
   1' KNS. AND ULT. LOAD(DUE TO HORIZ. COMPS.)=',F8.2,' KNS.')
543 RETURN
    END
    SUBROUTINE PP10(L1,L2,D,FY3,T3,G,CON1,EYS,F,ULT3,FX,FP,Z2,N1,N2,
   1PY10,PU10,PSHF1,PCHB,PSBK,FPURL,A1,A2,DEP,WS1,E1,C1,C2)
    REAL L1,L2,N1,N2,LM,MP,J,K,MSTR,L3
C     SUBROUTINE PP10 CALCULATES THE LOAD/DEFLECTION BEHAVIOR OF THE CHORD TOP
C     FACE SUBJECT TO BRANCH MEMBER FORCES,USING AN INCREMENTAL DEFLECTION
C     ANALYSIS. RIGID-PLASTIC BEHAVIOUR IS ASSUMED AND MEMBRANE ACTION TAKES
C     PLACE IN THE CROTCH ONLY. THE DISTANCE K IS TAKEN TO BE CONSTANT AT THE
C     VALUE FOR THE SMALL DEFLECTION ANALYSIS. X IS ALSO SET AT 1.0
C     STRAIN HARDENING MODULUS FOR CROTCH IS EYS/300
C     ULTIMATE LOAD IS REACHED BY ULTIMATE STRESS IN CROTCH OR THE
C     WHOLE CHORD CROSS-SECTION REACHING PLASTICITY AT THE CROTCH.
C*****************************************************************************
    K=D*SQRT(1-L1)*0.5
    LM=SQRT((D*(1-L1)/2.0)**2+K**2)
    EF=SQRT((G*D)**2+(D*(1-L1)/2.0)**2)
    CON2=1.0-(FX/FP)*(FX/FP)*(0.5*D*(1-L1)/LM)**4
    CON3=1.0-(FX/FP)*(FX/FP)*(0.5*D*(1-L1)/EF)**4
    CON4=1.0-(FX/FP)*(FX/FP)*COS(0.5*D*(1-L1)/EF)**4
    MP=(FY3*T3**2)/4.0
    PY10=0.0
    ZZA=0.0
    DEFM=0.01*(D+T3)
    TH=0.0
    DEL=0.0
    DTH=ATAN(0.0001*(D+T3)/Z2)
    IF(DTH.LT.0.0005)DTH=0.0005
    DO 100 N=1,2000
    ARG1=2.0*G*TAN(TH+DTH)/(1-L1)
    IF(ARG1.LT.1.0)GO TO 500
    WRITE(6,54)
 54 FORMAT(/,2X,'FOR P/P MODEL WITH X=1.0,THERE IS NO MATH. SOLUTION')
    WRITE(6,55)TH,DEL
 55 FORMAT(2X,'AND MAX. ROTATION IS REACHED AT THETA=',F6.2,
   1'  RADIANS, AND DELTA=',F8.2,' MM.')
    GO TO 543
500 DL=G*D/COS(TH+DTH)-G*D/COS(TH)
    DDEL=G*D*TAN(TH+DTH)-G*D*TAN(TH)
    DDELTA=SQRT(K**2-(DEL**2)/4.0)-SQRT(K**2-((DEL+DDEL)**2)/4.0)
    DFHI=ATAN(G*D*TAN(TH+DTH)/K)-ATAN(G*D*TAN(TH)/K)
    DGAM=ASIN(ARG1)-ASIN(2.0*G*TAN(TH)/(1-L1))
    DBET1=ASIN((2.0*G*TAN(TH+DTH)*K)/((1-L1)*LM))
    DBET2=ASIN(2.0*G*TAN(TH)*K/((1-L1)*LM))
    DBET3=ATAN(G*D*TAN(TH+DTH)*D*(1-L1)/(K*2.0*LM))
    DBET4=ATAN(G*D*TAN(TH)*D*(1-L1)/(K*2.0*LM))
    DBET=DBET1-DBET2+DBET3-DBET4
    DALF1=ASIN(2.0*G*TAN(TH+DTH)*G*D/((1-L1)*EF))
    DALF2=ASIN(2.0*G*TAN(TH)*G*D/((1-L1)*EF))
    DALF3=ATAN(TAN(TH+DTH)*D*(1-L1)/(2.0*EF))
    DALF4=ATAN(TAN(TH)*D*(1-L1)/(2.0*EF))
    DALF=DALF1-DALF2+DALF3-DALF4
    P1=(1+L1)*D*MP*CON1*DFHI/DDEL
    EY=FY3/EYS
    L3=(C1+C2)/(D*2.0)
    SP=L3*D*T3*FY3
    S=EYS*L3*D*T3*((1.0/COS(TH))-1.0)
    SZ=L3*D*T3*(1.0/COS(TH)-1.0-EY)*EYS/300.0
    IF((1.0/COS(TH)-1.0).GT.EY)S=SP+SZ
    P2=(1+L1)*D*MP*(1.0-(S/SP)**2)*DTH/DDEL
    IF(S.GT.SP)P2=0.0
    P3=2.0*D*(2.0*N1+G+K/D)*MP*DGAM/DDEL
    P4=2.0*LM*MP*DBET*CON2/DDEL
    P5=2.0*EF*MP*DALF*CON4/DDEL
```

```
      P6=S*DL/DDEL
      P7=0.0
      P=P1+P2+P3+P4+P5+P6+P7
      IF(N.GT.1)GO TO 42
      PY10=P
   42 IF(ZZA.NE.0.0)GO TO 99
      IF(P.LT.PY10)P=PY10
      IF(DEL.GT.DEFM)WRITE(6,72)P
   72 FORMAT(/,2X,'LIMIT OF 1 PER CENT OF CHORD WIDTH FOR DEFORMATION EX
     1CEEDED AT P=',F8.2,' KNS.')
      IF(DEL.GT.DEFM)ZZA=1.0
C************************************************************ ****************
   99 MSTR=1000.0*S/(L3*D*T3)
      Z2=Z2*2.0
      CALL SIDEWALL2(FY3,ULT3,D,T3,DEP,A1,US1,Z2,TH,MSTR,F,E1,L1,L2,
     1PALLOW,C1,C2,P)
      Z2=Z2/2.0
      ULT4=ULT3*1000.0
   98 DEL=DEL+DDEL
      THMAX=TH
      TH=TH+DTH
      IF(P.LT.PY10)P=PY10
      PU10=P
      IF(MSTR.GE.ULT4)GO TO 544
      IF(PALLOW.LT.PU10)GO TO 517
  100 CONTINUE
  544 WRITE(6,616)PY10,PU10,THMAX
  616 FORMAT(/,2X,'FOR P/P MODEL WITH X=1.0,YIELD LOAD(P)=',F8.2,
     1' KNS. AND ULTIMATE LOAD(P)=',F8.2,' KNS. & THETA=',F5.3)
      WRITE(6,516)P6,PALLOW
  516 FORMAT(/,2X,'P6=',F8.2,' KNS. & P-ALLOWANCE FOR HORIZ. COMPS.=',
     1F8.2,' KNS.')
      GO TO 543
  517 IF(PALLOW.LT.PY10)PALLOW=PY10
      WRITE(6,518)PY10,PALLOW
  518 FORMAT(/,2X,'FOR P/P MODEL WITH X=1.0,YIELD LOAD(P)=',F8.2,
     1' KNS. AND ULT. LOAD(DUE TO HORIZ. COMPS.)=',F8.2,' KNS.')
  543 RETURN
      END
      SUBROUTINE BUCKLE3(T1,T2,T3,FY1,FY2,FY3,D,LAP,C1,C2,E1,E2,A1,A2,
     1L1,CON1,ACH,EYS,H,GAP,Z1,PSQASH,PYEELD,PBUCK3,PBUCK4,L2,FPURL)
      REAL MH,JK1,JK2,NUM,L1,L,LAP,LTOT,L2
C     THIS ROUTINE PREDICTS STRUT LOCAL BUCKLING LOADS FOR GAP OR LAP JOINTS,
C     BY TWO DIFFERENT MECHANISMS INVOLVING CHORD ROTATION.
C****************************************************************************
      IF(LAP.LE.0.0)GAP=ABS(LAP)
      IF(LAP.LT.0.0)LAP=0.0
      T=T1
      C=C1-T1
      E=E1-T1
      L=F1+LAP/COS(A1)
      LTOT=E2/COS(A2)+E1/COS(A1)-L
      IF(LAP.EQ.0.0)LTOT=E2/COS(A2)+E1/COS(A1)+Z1
      DW=0.02*T
C     C=EFFECTIVE STRUT WIDTH OF (C1-T1)
C     E=EFFECTIVE STRUT DEPTH OF (E1-T1)
      W=0.0
      THETA=0.0
   22 IF(L1.GT.0.95.OR.L2.GT.0.95)GO TO 26
      DO 20 N=1,201
      Z=W/T
      GA=SQRT(E*E+(0.35*C)**2)
      GH=E-0.25*C
      MH=0.35*C*(E-0.25*C)/GA
      AH=SQRT((0.25*C)**2+(0.35*C)**2)
      IF(((W+DW)**2).GE.((0.35*C)**2))GO TO 17
      ROE=ASIN(SQRT((0.35*C)**2-W**2)/GA)
      DROE=ROE-ASIN(SQRT((0.35*C)**2-(W+DW)**2)/GA)
      XA1=GA*COS(ROE)
      XA2=GA*COS(ROE-DROE)
      YA1=GA*SIN(ROE)
      YA2=GA*SIN(ROE-DROE)
      NUM=GA*GA+GH*GH-AH*AH
      XH1=NUM/(2.0*GA*COS(ROE))
      XH2=NUM/(2.0*GA*COS(ROE-DROE))
      ARG1=GH*GH-(NUM/(2.0*GA*COS(ROE)))**2
      IF(ARG1.LT.0.0)ARG1=0.0
      ZH1=SQRT(ARG1)
      ZH2=SQRT(GH*GH-(NUM/(2.0*GA*COS(ROE-DROE)))**2)
      DSPR=ASIN(ZH2/MH)-ASIN(ZH1/MH)
      DTOR=2.0*ASIN(ZH2*E/(MH*GA))-2.0*ASIN(ZH1*E/(MH*GA))
      FHI=ASIN(W/(0.35*C))
      DFHI=ASIN((W+DW)/(0.35*C))-ASIN(W/(0.35*C))
      XC1=GA*COS(ROE)-0.35*C*SIN(FHI)
      XC2=GA*COS(ROE-DROE)-0.35*C*SIN(FHI+DFHI)
      ZC1=-0.25*C
      ZC2=ZC1
```

```
      R=0.25*C
      ANJ1=ACOS(SQRT((XC1-XH1)**2+(ZH1-ZC1)**2)/(2.0*R))
      ANJ2=ATAN(ABS((XC1-XH1)/(ZH1-ZC1)))
      ANJK1=ANJ1+ANJ2
      ANK1=ACOS(SQRT((XC2-XH2)**2+(ZH2-ZC2)**2)/(2.0*R))
      ANK2=ATAN(ABS((XC2-XH2)/(ZH2-ZC2)))
      ANJK2=ANK1+ANK2
      XJ1=XH1+R*SIN(ANJK1)
      XJ2=XH2+R*SIN(ANJK2)
      ZJ1=ZH1-R*COS(ANJK1)
      ZJ2=ZH2-R*COS(ANJK2)
      AJ1=SQRT((XA1-XJ1)**2+YA1*YA1+ZJ1*ZJ1)
      AJ2=SQRT((XA2-XJ2)**2+YA2*YA2+ZJ2*ZJ2)
      SQL1=0.7*C-2.0*AJ1
      SQL2=0.7*C-2.0*AJ2
      DSQL=SQL2-SQL1
      SJ1=0.58*SQRT((XA1-XJ1)**2+YA1*YA1+ZJ1*ZJ1)
      SJ2=0.58*SQRT((XA2-XJ2)**2+YA2*YA2+ZJ2*ZJ2)
      AS1=0.314*SQRT((XA1-XJ1)**2+YA1*YA1+ZJ1*ZJ1)
      AS2=0.314*SQRT((XA2-XJ2)**2+YA2*YA2+ZJ2*ZJ2)
      XS1=XA1+(AS1/AH)*(XH1-XA1)
      XS2=XA2+(AS2/AH)*(XH2-XA2)
      YS1=YA1-(AS1/AH)*YA1
      YS2=YA2-(AS2/AH)*YA2
      ZS1=(AS1/AH)*ZH1
      ZS2=(AS2/AH)*ZH2
      CHI=ASIN(0.35*C/GA)
      PH=0.35*C*(E-0.25*C)/GA
      SIG=ASIN(ABS(ZS1-ZJ1)/SJ1)+ASIN(ABS(ZH1)/PH)
      DSIG=ASIN(ABS(ZS2-ZJ2)/SJ2)+ASIN(ABS(ZH2)/PH)-SIG
      ARG2=ZH1-ZJ1
      IF(ARG2.EQ.0.0)GO TO 52
      HI=ATAN((XJ1-XC1)/(ZC1-ZJ1))+ATAN((XH1-XJ1)/(ZH1-ZJ1))
      GO TO 53
   52 HI=-1.5707963
   53 DHI=ATAN((XJ2-XC2)/(ZC2-ZJ2))+ATAN((XH2-XJ2)/(ZH2-ZJ2))-HI
      DHI=ABS(DHI)
      JK1=SIN(0.619591884)*AJ1
      JK2=SIN(0.619591884)*AJ2
      AK1=0.314*AJ1
      AK2=0.314*AJ2
      AC=AH
      XK1=XA1+(AK1/AC)*(XC1-XA1)
      XK2=XA2+(AK2/AC)*(XC2-XA2)
      ETA=ASIN(ABS(XJ1-XK1)/JK1)+ASIN(1.659151302*W/C)
      DETA=ASIN(ABS(XJ2-XK2)/JK2)+ASIN(1.659151302*(W+DW)/C)-ETA
      AA1=0.5*GA*DSPR*(COS(CHI))**4+0.25*GH*DTOR
      AA2=0.02446*C*DSIG
      AA3=0.05635*AC*DETA
      AA=(AA1+AA2+AA3)*T/(C+E)
      ROTN=DROE*2.0
      B=E*SIN(ROTN)
C     MOVEMENT OF P IS MEASURED ALONG DIRECTION OF STRUT FOR CALCULATION OF
C     EXTERNAL VIRTUAL WORK DONE.
      CC1=0.375*DFHI*C+0.5*GA*DSPR+0.25*GH*DTOR
      CC2=0.215*C*DSIG+0.5*AJ1*DHI
      CC3=0.5*AC*DETA+0.25*C*(DSQL)/T
      CC4=FY2*T2*ROTN*(C2*(L*COS(A2)-0.5*T2)+(L*COS(A2)-T2)**2)
      CC4=CC4/(T*T*FY1*2.0)
      IF(LAP.EQ.0.0)CC4=0.0
      CC5=(4.0*E1/COS(A1))*(2.0*E1/(COS(A1)*D*(1-L1))+1/SQRT(1-L1))
      CC5=CC5+(2.0*D+4.0*E1/(COS(A1)*SQRT(1-L1)))*CON1
      CC5=CC5*ROTN*0.125*T3*T3*FY3/(T*T*FY1)
      V=(CC1+CC2+CC3+CC4+CC5)*T/(C+E)
      XX1=(SQRT(B*B+4*AA*V)-B)/(2.0*AA)
  161 PP=2.0*(C+E)*T*FY1
      IF(XX1.GT.1.00)XX1=1.00
      PBUCK3=XX1*PP*COS(A1)
   12 DEFLN=E1*SIN(ASIN(0.35*C/GA)-ROE)/COS(A1)
C     DEFLN=VERTICAL DISPLACEMENT OF HEEL OF STRUT MEMBER.
      DELTAP=(0.35*C-YA1)*2.0
C     DELTA=TOTAL VERTICAL CLOSURE OF OUTSIDE EDGE OF BUCKLE, WITH P FOR
C     PLASTIC AND E FOR ELASTIC.
      ZNA=(T*(E+T)**2/3)+T*(C-T)*(E*E+T*T/3)/(E+T)
      AREA=2.0*(C+E)*T
      DELTAE=2.0*(C+E)*T*FY1*H*XX1*((1/AREA)+(.25*E/ZNA))/EYS
      IF(DELTAP.GE.DELTAE)GO TO 17
C     DELTA=ROTATION OF CHORD FACE UNDER STRUT.
      THETA=THETA+ROTN
   20 W=W+DW
C     CALCULATIONS FOR MECHANISM NO.2 FOLLOW:
   17 ZV1=C2*E2*E2*FY2/4.0
      ZV2=C2*FY2/4.0
      ZV3=COS(A1)/(COS(A2)*C2*FY2)
      ZV4=(E2-2.0*T2)*(1.0-2.0*T2/C2)
      ZV5=COS(A1)/(2.0*COS(A2))
      ZV6=C1*E1*E1*FY1/4.0
```

```
      ZV7=C1*FY1/4.0
      ZV8=1.0/(C1*FY1)
      ZV9=(E1-2.0*T1)*(1.0-2.0*T1/C1)
      ZV10=CON1*(D+2.0*LTOT/SQRT(1-L1))
      ZV11=4.0*LTOT*(LTOT+0.5*D*SQRT(1-L1))/(D*(1-L1))
      ZV12=0.5*T3*T3*FY3
      ZV13=LTOT*COS(A1)
      ZV17=1.0+LTOT*SIN(A1)/(H-0.5*TAN(A1)*E1)
      ZV14=ZV2*ZV3**2-ZV5*ZV3+ZV7*ZV17*ZV8**2-0.5*ZV8*ZV17
      ZV20=FPURL/(COS(A2)*C2*FY2)
      ZV21=FPURL/(2.0*COS(A2))
      ZV15=ZV13+2.0*ZV2*ZV3*(ZV4-ZV20)+ZV21*ZV3-ZV5*(ZV4-ZV20)
      ZV15=ZV15+2.0*ZV7*ZV17*ZV8*ZV9-0.5*ZV17*ZV9
      ZV16=ZV1-ZV2*(ZV4-ZV20)**2-ZV21*(ZV4-ZV20)+ZV6*ZV17
      ZV16=ZV16-ZV9*ZV9*ZV7*ZV17+ZV12*(ZV10+ZV11)
      P=(SQRT(ZV15**2+4.0*ZV14*ZV16)-ZV15)/(2.0*ZV14)
      IF(P.GT.PP)P=PP
      PBUCK4=P*COS(A1)
      PSQASH=PP*COS(A1)
      PYEELD=2.0*(C2+E2-2.0*T2)*T2*FY2*COS(A2)
      IF(PBUCK4.GT.PYEELD)PBUCK4=PYEELD
      WRITE(6,13)PBUCK3,PBUCK4
   13 FORMAT(/,2X,'STRUT LOCAL BUCKLING LOAD BY MECH.1=',F7.2,
     1' KNS. AND BY MECH.2=',F7.2,' KNS.')
   26 PSQASH=2.0*(C+E)*T*FY1*COS(A1)
      PYEELD=2.0*(C2+E2-2.0*T2)*T2*FY2*COS(A2)
      WRITE(6,14)PSQASH,PYEELD
   14 FORMAT(/,2X,'STRUT SQUASH LOAD=',F7.2,' KNS. AND TIE YIELD LOAD=',
     1F7.2,' KNS.')
      RETURN
      END
      SUBROUTINE ECC(E,D,A1,A2,E1,E2,GAP,LAP)
      REAL L1,L2,LAP
C     SUBROUTINE ECC CALCULATES THE REAL VALUE OF GAP IF DIFFERENT TO ASSUMED
      TP1=(E+D/2.)*TAN(A1)-E1/(COS(A1)*2.0)
      TP2=(E+D/2.)*TAN(A2)-E2/(COS(A2)*2.0)
      TP3=TP1+TP2
      GAP=0.0
      IF(TP3.GT.0.0)GAP=TP3/D
      LAP=0.0
      IF(TP3.LE.0.0)LAP=TP3*COS(A1)/E1
      LAP=ABS(LAP)
      RETURN
      END
      SUBROUTINE CHORD(L1,A1,A2,F,ACH,EYS,T3,D,FY3,PCHB,FPURL,
     1E1,E2,Z8,GAP,LAP,DEP,TR)
      REAL L1,LAP
C     SUBROUTINE CHORD CALCULATES THE LOCAL BUCKLING LOAD OF THE CHORD TOP FACE
C     FOR RHS,FOR AN EFFECTIVE CHORD WIDTH OF (D-T3).
C     POSITIVE CHORD PRELOAD (F) IS TENSION.
      PCRIT=3.55*EYS*T3**3/D
      PYSTR=D*T3*FY3
      IF(PYSTR.LE.PCRIT)GO TO 720
      CZ=(0.36*PYSTR*PCRIT+0.83*PCRIT**2)*0.76
      PMAX=(SQRT(CZ+PCRIT**2)-PCRIT)/0.38
      GO TO 721
  720 PMAX=PYSTR
C     PMAX=BUCKLING LOAD OF CHORD CONNECTING FACE ONLY.
  721 BST=PMAX/(D*T3)
      IF(L1.LE.0.7)FACT=2.0
      IF(L1.GT.0.7)FACT=1.0
      PCHB=(BST*ACH+F+FPURL*TAN(A2)*FACT)
      PCHB=PCHB/((TAN(A1)+TAN(A2))*FACT)
      WRITE(6,722)PCHB
  722 FORMAT(/,2X,'CHORD LOCAL BUCKLING OCCURS AT P=',F8.2,' KNS.')
      CALL CHORD2(E1,E2,A1,A2,Z8,D,GAP,LAP,DEP,FPURL,TR,T3,
     1F,ACH,BST)
      RETURN
      END
      SUBROUTINE CHORD2(E1,E2,A1,A2,Z8,D,GAP,LAP,DEP,FPURL,TR,
     1T3,F,ACH,BST)
      REAL LAP
      IF(LAP.NE.0.0)EXTRA=-LAP*E1/COS(A1)
      IF(LAP.EQ.0.0)EXTRA=Z8
      ZEL=((D+T3)*DEP**3-(D-T3)*(DEP-2.0*T3)**3)/12.0
      ZEL=ZEL/(DEP/2.0)
      E=(E2/(2.0*COS(A2))+E1/(2.0*COS(A1))+EXTRA)/(TAN(A1)+TAN(A2))
      E=E-DEP/2.0
      WRITE(6,20)E
   20 FORMAT(/,2X,'ECCENTRICITY=',F7.2,' MM.')
      E=ABS(E)
      P=(BST+F/ACH)/(1.0/ACH+E/(TR*ZEL))+FPURL*TAN(A2)
      P=P/(TAN(A1)+TAN(A2))
      WRITE(6,10)P
   10 FORMAT(/,2X,'CHORD LOCAL BUCK. BY ECC. METHOD AT P=',F8.2,
     1' KNS. - IGNORE THIS IF ECCENTRICITY IS POSITIVE.')
      RETURN
```

```
      END
      SUBROUTINE PURLIN(D,F,ACH,FPURL,TPURL,T3,FY3,DEP,E1,N1,LAP,A1,A2,
     1T1)
      REAL N1,LB,LAP,L
C     SUBROUTINE PURLIN CALCULATES THE FAILURE LOAD OF THE CHORD SIDE WALLS DUE
C     TO AN APPLIED COMPRESSIVE PURLIN LOAD AT THE JOINT.
      LB=N1*D
      PART=FPURL/((LB+TPURL)*T3*2.0)+F/(2.0*ACH)
      WALL=2.0*T3*(DEP+2.0*T3)
      L=E1*LAP/COS(A1)
      CUV=(2.0*L*COS(A1)*COS(A2)/SIN(A1+A2)+2.0*T1)*T1
      IF(LAP.NE.0.0)WALL=CUV+2.0*T3*(DEP+T3)
      SPQR=(FY3-PART+F/ACH)**2-PART**2
      IF(SPQR.LT.0.0)GO TO 20
      PPURL1=SQRT(SPQR)*WALL+FPURL
      GO TO 21
   20 PPURL1=FPURL
   21 PSQR=(FY3/2.0)**2-PART**2
      IF(PSQR.LT.0.0)GO TO 22
      PPURL2=SQRT(PSQR)*WALL+FPURL
      GO TO 23
   22 PPURL2=FPURL
   23 IF(FPURL.EQ.0.0)GO TO 14
      WRITE(6,13)FPURL,PPURL1,PPURL2
   13 FORMAT(/,2X,'PURLIN LOAD ON JOINTS IS',F8.2,' KNS. - CHORD WALL BU
     1CKLING LOAD=',F8.2,' KNS.,AND CHORD WALL SHEAR LOAD=',F8.2,' KNS')
      PPURL3=FY3*FY3-(F/ACH)**2-(FPURL/((LB+TPURL)*T3))**2
      DOG=(PPURL3-(F/ACH)*(FPURL/((LB+TPURL)*T3)))/3.0
      IF(DOG.LT.0.0)GO TO 30
      PPURL4=(SQRT(DOG))*WALL+FPURL
      GO TO 31
   30 PPURL4=FPURL
   31 WRITE(6,12)PPURL4
   12 FORMAT(2X,'AND MAX. SHEAR STRAIN ENERGY EXCEEDED AT ',F8.2,' KNS')
      GO TO 16
   14 WRITE(6,15)
   15 FORMAT(/,2X,'NO PURLIN LOAD APPLIED TO JOINT')
   16 RETURN
      END
      SUBROUTINE PURLIN2(FY3,F,ACH,T3,D,TPURL,FPURL)
C     SUBROUTINE PURLIN2 CALCULATES THE BEARING FAILURE LOAD OF A CHORD
C     FACE DIRECTLY BENEATH A PURLIN LOAD.
      IF(FPURL.EQ.0.0)GO TO 14
      R=F/ACH
      S=F/(ACH*FY3)
      ALPHA=SQRT(FY3*FY3*R*R-4.0*FY3*FY3*(R*R-FY3*FY3))
      ALPHA=(ALPHA-FY3*R)/(2.0*FY3*FY3)
      IF(ALPHA.GT.1.0)ALPHA=1.0
      FMAX=SQRT((D+T3)*T3*ALPHA*(1.0-S*S))*4.000+2.0*ALPHA*TPURL
      FMAX=FMAX*FY3*T3
      WRITE(6,10)FMAX
   10 FORMAT(/,2X,'CHORD WILL FAIL IN BEARING IF PURLIN FORCE REACHES',
     1F8.2,' KNS.')
   14 RETURN
      END
      SUBROUTINE SIDEWALL(FY3,ULT3,D,T3,DEP,A1,WS1,Z2,
     1TH,MSTR,F,E1,PALLOW)
      REAL MSTR
C     SUBROUTINE SIDEWALL CALCULATES THE MAXIMUM BRACING MEMBER
C     LOAD WHICH THE CHORD SIDEWALLS CAN SUPPORT BEFORE HORIZONTAL
C     COMPONENTS CAUSE PLASTICITY IN THEM.
      BT=D+T3
      AB=FY3*BT*(0.5+BT/(4.0*T3))
      AC=FY3*BT*(0.5*DEP-(DEP*BT/(4.0*T3)))
      AC=AC-FY3*BT*DEP*(0.5+BT/(4.0*T3))
      DIS=(E1/(2.0*COS(A1)))+WS1+Z2/2.0
      IF(A1.GT.0.5)DIS=DIS-WS1
      S=(MSTR/1000.0)*D*T3
      X=(2.0*DEP-2.0*T3+BT)/4.0
      AD=COS(A1)*DIS-SIN(A1)*X
      AE=FY3*BT*DEP*(DEP/2.0-DEP*BT/(4.0*T3))-S*COS(TH)*X
      AE=AE+F*(X-DEP/2.0)
      AF=2.0*FY3*BT
      AG=(DEP*T3-T3*T3-BT*DEP+0.5*BT*T3)/BT
      AH=(S*COS(TH)-F)/AF-AG
      AJ=SIN(A1)*SIN(A1)*AB/(AF*AF)
      AK=(2.0*SIN(A1)*AH*AB)/AF+(AC*SIN(A1))/AF-AD
      AL=AH*AH*AB+AC*AH-AE
      PALLOW=((SQRT(AK*AK-4.0*AJ*AL)-AK)/(2.0*AJ))*COS(A1)
      RETURN
      END
      SUBROUTINE SIDEWALL2(FY3,ULT3,D,T3,DEP,A1,WS1,Z2,TH,MSTR,
     1F,E1,L1,L2,PALLOW,C1,C2,P)
      REAL L1,L2,MSTR,L
      L=(C1+C2)/(D*2.0)
C     SUBROUTINE SIDEWALL2 IS SIMILAR TO SUBROUTINE SIDEWALL
C     EXCEPT ONLY A PART OF THE TOP CHORD FACE IS REMOVED BY
```

```
C     MEMBRANE ACTION.
      V=0.0
      PALLOW=0.0
      Y=9000.0
      BT=D+T3
      X=(2.0*DEP+L*D)/4.0
      S=(HSTR/1000.0)*L*D*T3
      IF(A1.EQ.0.0)GO TO 20
      AB=FY3*BT/2.0+FY3*BT*BT/(2.0*(BT-L*D))
      AC=FY3*BT*BT*DEP/(BT-L*D)
      AD=FY3*BT*DEP*DEP/2.0-FY3*BT*BT*DEP*DEP/(2.0*(BT-L*D))
   60 AE=2.0*FY3*BT
      AF=(DEP*T3-DEP*BT+BT*T3-2.0*T3*T3-L*D*T3/2.0)/BT
      DIS=(E1/(2.0*COS(A1)))+WS1+Z2/2.0
      IF(A1.GT.0.5)DIS=DIS-WS1
      AG=S*COS(TH)*X-F*(X-DEP/2.0)
      AH=SIN(A1)*X-COS(A1)*DIS
      AJ=((S*COS(TH)-F)/AE)-AF
      AK=SIN(A1)/AE
      AL=AB*AK*AK
      AM=AH+2.0*AJ*AK*AB-AC*AK
      AN=AG+AJ*AJ*AB-AC*AJ-AD
      IF((AM*AM-4.0*AL*AN).LT.0.0)GO TO 10
      PALLOW=((SQRT(AM*AM-4.0*AL*AN)-AM)/(2.0*AL))*COS(A1)
   10 Y=(PALLOW*TAN(A1)-F+S*COS(TH))/(2.0*FY3*BT)
      Y=Y-(DEP*T3-DEP*BT+BT*T3-2.0*T3*T3-L*D*T3/2.0)/BT
      IF(V.NE.0.0)GO TO 50
      V=((DEP-Y)*BT)/(BT-L*D)
      IF(V.GT.T3)GO TO 40
      GO TO 50
   40 AB=FY3*BT/2.0+FY3*BT*BT/(4.0*T3)
      AC=FY3*BT*(DEP*BT/(2.0*T3)-(BT-L*D)/2.0+T3)
      AD=BT*DEP*DEP/2.0-BT*DEP*X+T3*(X-T3/2.0)*(BT-L*D)
      AZ=(DEP*BT-T3*(BT-L*D))*(4.0*T3*X-DEP*BT+T3*(BT-L*D)-4.0*T3*T3)
      AD=((AZ/(4.0*T3))+AD)*FY3
      GO TO 60
   20 IF(A1.GT.0.0)GO TO 100
      PALLOW=9999999.0
      SQ=FY3*T3*2.0*(BT+DEP-L*D/2.0-2.0*T3)
      SMAX=(SQ+F)/COS(TH)
      IF(S.GT.SMAX)PALLOW=P-0.001
      IF(A1.EQ.0.0)GO TO 100
   50 IF(Y.GT.(DEP-T3))GO TO 100
      BF=4.0*FY3*T3
      BG=(L*D+2.0*DEP)/4.0
      BC1=2.0*T3**3-BT*T3*T3+L*D*T3*T3/2.0+BT*DEP*T3
      BC2=BT*DEP*DEP-2.0*T3*DEP-T3*DEP*DEP
      BC3=-T3*DEP*L*D-T3*L*L*D*D/4.0
      BC=(BC1+BC2+BC3)*FY3
      BD=2.0*FY3*T3
      BE=(2.0*T3*DEP+T3*L*D)*FY3
      BH=AG-BC
      BJ=SIN(A1)/BF
      BK=(S*COS(TH)-F)/BF+BG
      BL=AH
      BM=BD*BJ*BJ
      BN=BD*BJ*BK-BE*BJ+BL
      BP=BH+BE*BK-BD*BK*BK
      PALLOW=((SQRT(BN*BN-4.0*BM*BP)-BN)/(2.0*BM))*COS(A1)
  100 RETURN
      END
```

****

APPENDIX 3

Detailed example of yield line method applied to an RHS to RHS T joint

The proposed deformation model, based on a pattern of yield lines, for an RHS to RHS T joint with a width ratio less than 1.0 is shown in fig. A3.1. The plastic moment of each yield line, per unit length, is $\frac{t_o^2\sigma e_o}{4}$ where the assumption is made that the chord connecting face is of uniform thickness and that the material is homogeneous and isotropic. The work carried out by any yield hinge is therefore

$$\frac{t_o^2\sigma e_o}{4} \cdot \theta_i \ell_i \qquad \text{(A3.01)}$$

where θ_i and ℓ_i are the rotation and length of the yield hinge respectively. Consequently for a whole set of hinges the total work done is

$$\frac{t_o^2\sigma e_o}{4} \Sigma\theta_i \ell_i \qquad \text{(A3.02)}$$

The length of the yield lines in fig. A3.1 are as follows:

$$\begin{aligned}
AB &= GH = \eta_1 b_o' + b_o'(1-\lambda_1')/\mathrm{Tan}\alpha, \\
AG &= BH = b_o', \\
CE &= DF = \lambda_1' b_o', \qquad \text{(A3.03)} \\
CD &= EF = \eta_1 b_o', \\
AC &= GE = BD = FH = b_o'(1-\lambda_1')/(2\mathrm{Sin}\alpha),
\end{aligned}$$

and the angular rotations of the hinges are:

$$AB,\ CD,\ EF \text{ and } GH \rightarrow \theta_o \text{ where } \mathrm{Tan}\theta_o = \frac{2\delta}{b_o'(1-\lambda_1')}$$

$$AG,\ CE,\ DF \text{ and } BH \rightarrow \theta_1 \text{ where } \mathrm{Tan}\theta_1 = \frac{2\delta\mathrm{Tan}\alpha}{b_o'(1-\lambda_1')} \qquad \text{(A3.04)}$$

$$AC,\ GE,\ DB \text{ and } FH \rightarrow \theta_2 \text{ where } \theta_2 = \theta_o\mathrm{Cos}\alpha + \theta_1\mathrm{Sin}\alpha$$

For small deflections, δ, $\mathrm{Tan}\theta \cong \theta$, and so for the hinges having undergone an angular rotation of θ_o (AB, CD, EF and GH),

$$\Sigma\theta_i\ell_i = \frac{4\delta}{b_o'(1-\lambda_1')}\left\{2\eta_1 b_o' + \frac{b_o'(1-\lambda_1')}{\mathrm{Tan}\alpha}\right\}. \qquad \text{(A3.05)}$$

For the hinges having undergone an angular rotation of θ_1 (AG, CE, DF and BH),

$$\Sigma\theta_i\ell_i = \frac{4\delta\mathrm{Tan}\alpha}{b_o'(1-\lambda_1')}\left\{b_o' + \lambda_1'b_o'\right\}. \qquad \text{(A3.06)}$$

For the hinges having undergone an angular rotation of θ_2 (AC, GE, DB and FH),

$$\Sigma\theta_i\ell_i = \left\{\frac{2\delta\mathrm{Cos}\alpha}{b_o'(1-\lambda_1')} + \frac{2\delta\mathrm{Tan}\alpha\mathrm{Sin}\alpha}{b_o'(1-\lambda_1')}\right\}\cdot\left\{\frac{4b_o'(1-\lambda_1')}{2\mathrm{Sin}\alpha}\right\} \qquad \text{(A3.07)}$$

Hence the total work done by the hinges is

$$\frac{t_o^2\sigma e_o}{4}\Sigma\theta_i\ell_i = \frac{t_o^2\sigma e_o}{4}\left\{\frac{8\delta\eta_1}{(1-\lambda_1')} + \frac{8\delta}{\mathrm{Tan}\alpha} + \frac{8\delta\mathrm{Tan}\alpha}{(1-\lambda_1')}\right\} \qquad \text{(A3.08)}$$

This represents the total internal virtual work done by the yield lines which can then be equated to the total external work done by the applied load of $N\delta$.

Hence

$$N = \sigma e_o t_o^2\left\{\frac{2\eta_1}{(1-\lambda_1')} + \frac{2}{\mathrm{Tan}\alpha} + \frac{2\mathrm{Tan}\alpha}{(1-\lambda_1')}\right\} \qquad \text{(A3.09)}$$

With yield line patterns such as fig. A3.1 in which the inclined yield lines AC, BD, GE and FH are bounded by yield lines at right angles to each other, (for example AB and AG), equation (A3.08) may be obtained more easily by using a component vector method for the inclined yield lines.

i.e. $$\frac{t_o^2 \sigma e_o}{4} \Sigma \theta_i \ell_i = \frac{t_o^2 \sigma e_o}{4} \left\{ 4AB\theta_o + 4AG\theta_1 \right\} \qquad (A3.10)$$

The value N given by equation (A3.09) is an upper bound to the yield load but the minimum value of N will occur when $\frac{\partial N}{\partial \alpha} = 0$.

i.e. $$-2\text{Cosec}^2\alpha + \frac{2\text{Sec}^2\alpha}{(1-\lambda_1')} = 0$$

i.e. $$\text{Tan}\alpha = \sqrt{1-\lambda_1'} \qquad (A3.11)$$

By substitution,

$$N = \sigma e_o t_o^2 \left(\frac{2\eta_1}{1-\lambda_1'} + \frac{4}{\sqrt{1-\lambda_1'}} \right) \qquad (A3.12)$$

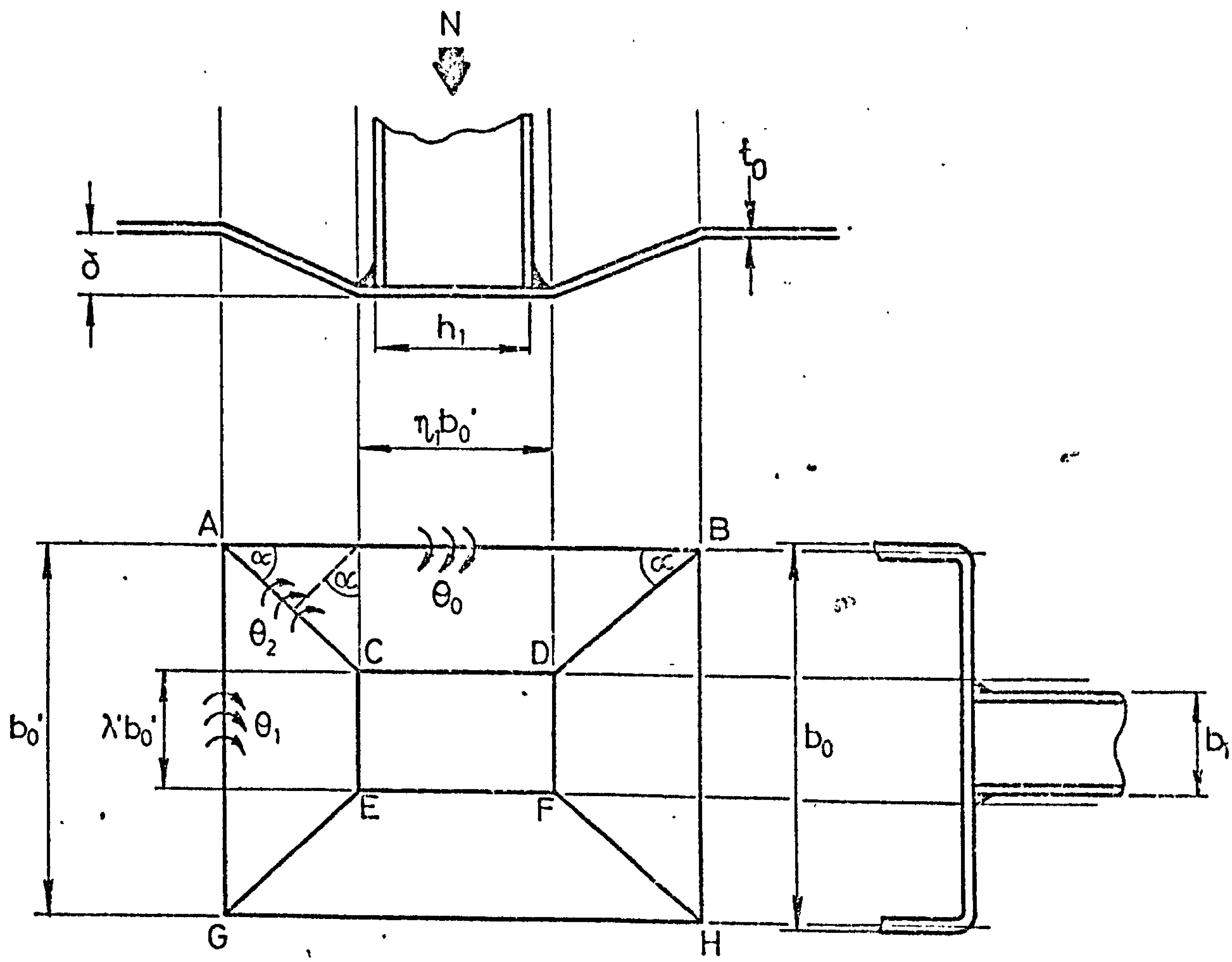

Fig.A3·1 Yield line pattern for RHS to RHS T joint